



<https://theses.gla.ac.uk/>

Theses Digitisation:

<https://www.gla.ac.uk/myglasgow/research/enlighten/theses/digitisation/>

This is a digitised version of the original print thesis.

Copyright and moral rights for this work are retained by the author

A copy can be downloaded for personal non-commercial research or study,
without prior permission or charge

This work cannot be reproduced or quoted extensively from without first
obtaining permission in writing from the author

The content must not be changed in any way or sold commercially in any
format or medium without the formal permission of the author

When referring to this work, full bibliographic details including the author,
title, awarding institution and date of the thesis must be given

Enlighten: Theses

<https://theses.gla.ac.uk/>
research-enlighten@glasgow.ac.uk

LOW REYNOLDS NUMBER PERFORMANCE OF A

NACA 0015 AND A GA(W)-1 AEROFOIL

by

George Kokkodis, B.Sc.

Thesis presented for the degree of M.Sc.

to the Faculty of Engineering,

The University of Glasgow

Department of Aeronautics and
Fluid Mechanics

February 1987

ProQuest Number: 10948147

All rights reserved

INFORMATION TO ALL USERS

The quality of this reproduction is dependent upon the quality of the copy submitted.

In the unlikely event that the author did not send a complete manuscript and there are missing pages, these will be noted. Also, if material had to be removed, a note will indicate the deletion.



ProQuest 10948147

Published by ProQuest LLC (2018). Copyright of the Dissertation is held by the Author.

All rights reserved.

This work is protected against unauthorized copying under Title 17, United States Code
Microform Edition © ProQuest LLC.

ProQuest LLC.
789 East Eisenhower Parkway
P.O. Box 1346
Ann Arbor, MI 48106 – 1346

ACKNOWLEDGEMENTS

The work described in this dissertation was carried out by the author in the Department of Aeronautics and Fluid Mechanics of the University of Glasgow. This dissertation is original in content except where otherwise stated.

The author wishes to acknowledge, with sincere gratitude, the valuable suggestions and constant encouragement and advice he received from his supervisor, Dr. R. Galbraith, during the course of his work.

The author wishes to express his gratitude to Professor B. Richards, Mr. A. Kokkalis and Mr. F. Coton for their valuable discussions and suggestions during this work.

To the many members of the technical and computing staff of the Engineering Faculty who have worked or otherwise helped the author, with special mention to Mr. J. Kitching, Mr. D. Perrins and Mrs. E. Smith, the author expresses his thanks.

To Miss L. Cullen for her immaculate typing of the manuscript the author expresses his thanks.

Finally, the author expresses his loving gratitude to his parents for their support and understanding given to him during this work.

SUMMARY

Due to the recent interest in a wide variety of low Reynolds number applications such as mini RPV's, wind turbine fans, sailplanes etc., attention has been focused on the evaluation of efficient airfoil sections at chord Reynolds numbers from about 50,000 to about 1,000,00. In this experimental study, the low Reynolds number aerodynamic characteristics of two airfoil sections, namely the NASA GA(W)-1 and NACA-0015 were examined. These were compared to the ones obtained from previous investigations for the GU25-5(11)8 airfoil section. The airfoils were tested in the Reynolds number range from about 50,000 to about 500,000 and for incidences of 0° to 22°.

An automated pressure measuring system was developed to improve the speed and facilitate the measurements of pressures around the airfoil sections. The pressure measurements were converted to pressure coefficients and these were in turn integrated to provide normal force and pitching moment coefficients.

Oil flow visualisation was used to obtain a better picture of the different flow phenomena around the airfoil sections. It proved to be an essential tool for obtaining information about the different flow fields which occur around the airfoil models when these were not apparent by pressure distributions.

Many of the significant aerodynamic problems which occur in this low Reynolds number regime such as the creation and behaviour of laminar separation bubbles and the extreme sensitivity of the boundary layer to the test environment (i.e. free stream turbulence level, mechanical vibrations and noise levels) were highlighted.

Significant differences were found in the behaviour of the boundary layer and subsequently in the aerodynamic characteristics of the three airfoil sections. This resulted in marginal differences as far as the Reynolds number operational range is concerned.

NOMENCLATURE

c	Airfoil chord length
C_D	Profile drag coefficient
C_L	Lift coefficient corrected for streamline curvature and solid blocking
C_{Lu}	Lift coefficient
$C_{M_{\frac{1}{4}}}$	Pitching moment coefficient about the quarter chord corrected for streamline curvature and solid blockage
$C_{M_{\frac{1}{4}u}}$	Pitching moment coefficient
C_N	Normal force coefficient
C_p	Pressure coefficient corrected for streamline curvature and solid blockage
h	Tunnel height
Re	Chord Reynolds number corrected for streamline curvature and solid blockage
Re_u	Chord Reynolds number

t	Airfoil thickness
U	Free stream velocity corrected for streamline curvature and solid blockage
U_u	Free stream velocity
x	Airfoil abscissa
z	Airfoil ordinate
α	Angle of attack of airfoil, angle between chord line and airstream axis, corrected for streamline curvature and solid blockage
α_{geom}	Airfoil geometric incidence
α_u	Angle of attack

CONTENTS

	SUMMARY	I
	NOMENCLATURE	III
CHAPTER 1	INTRODUCTION	1
CHAPTER 2	DETAILS OF TEST FACILITY & EXPERIMENTAL PROCEDURE	
2.1	INTRODUCTION	7
2.2	EXPERIMENTAL APPARATUS	8
2.2.1	WIND TUNNEL	8
2.2.2	20-SIGNAL AUTO-SELECTOR BOXES	9
2.2.3	DIGITAL MICROMANOMETER	9
2.2.4	COMPUTATIONAL SYSTEM FOR DATA PROCESSING	10
2.3	AIRFOIL MODELS	11
2.4	EXPERIMENTAL SET-UP	14
2.5	EXPERIMENTAL CONSIDERATIONS	15
2.6	TEST PROCEDURE	18
2.7	FLOW VISUALISATION	19
2.8	DATA ACQUISITION AND SOFTWARE	22
2.9	DISCUSSION	24
CHAPTER 3	RESULTS AND DATA REDUCTION	
3.1	INTRODUCTION	26
3.2	DATA CORRECTIONS	26
3.3	FLOW VISUALISATION	28
3.3.1	NASA GA(W)-1	28
3.3.2	NACA-0015	31
3.4	PRESSURE MEASUREMENTS	33
3.4.1	NASA GA(W)-1	34
3.4.2	NACA-0015	41

	3.5	NORMAL FORCE AND PITCHING MOMENT	45
	3.5.1	NASA GA(W)-1	45
	3.5.2	NACA-0015	48
	3.6	CONCLUSIONS	50
CHAPTER	4	DISCUSSION OF RESULTS	
	4.1	PRELIMINARY DISCUSSION	52
	4.2	FLOW VISUALISATION	55
	4.2.1	NASA GA(W)-1	56
	4.2.2	NACA-0015	58
	4.3	PRESSURE MEASUREMENTS	59
	4.3.1	NASA GA(W)-1	59
	4.3.2	NACA-0015	61
	4.4.	NORMAL FORCE AND PITCHING MOMENT	62
	4.4.1	NASA GA(W)-1	63
	4.4.2	NACA-0015	65
	4.5	TUNNEL EFFECTS	67
	4.6	COMPARISON OF NASA GA(W)-1 AIRFOIL SECTION CHARACTERISTICS WITH EXISTING DATA	69
	4.7	COMPARISON OF NACA-0015 AIRFOIL SECTION CHARACTERISTICS WITH EXISTING DATA	71
	4.8	COMPARISON OF GU25-5(11)8, NASA GA(W)-1 AND NACA-0015 AIRFOIL SECTION CHARACTERISTICS	72
	4.9	CONCLUSIONS	76
CHAPTER	5	CONCLUSIONS AND SUGGESTIONS FOR FUTURE WORK	
	5.1	SUMMARY OF CONCLUSIONS	78
	5.2	SUGGESTIONS FOR FUTURE WORK	80
	5.3	CONCLUDING DISCUSSION	83
REFERENCES			85-89
TABLES			90-96
FIGURES			97-176

CHAPTER 1

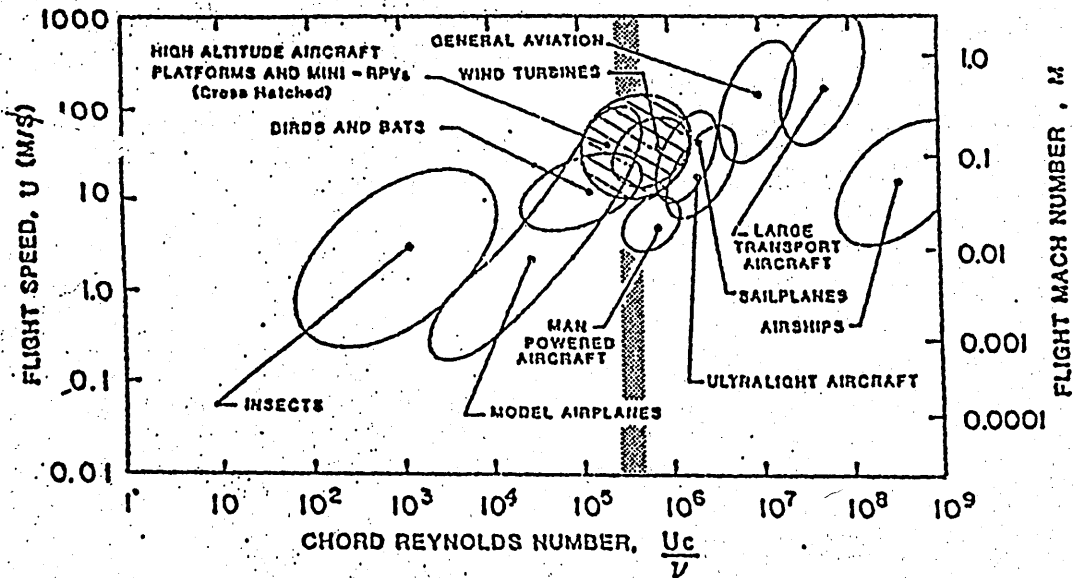
INTRODUCTION

The airfoil section is the basic element of a wing or lifting surface. It, therefore, occupies a central position in any design discipline relating to fluid mechanics, from animal flight through marine propellers to aircraft. The proper functioning of the airfoil is the prerequisite to the satisfactory performance of the lifting surface itself, and thus the airfoil is of fundamental technical importance [ref (1)]. The aerofoil work to be described, relates only to incompressible flow.

Since the early work of Eiffel and Joukowsky at the turn of the century, fluid dynamicists have recognised the importance of the airfoil shape and have developed a variety of airfoil designs and "families". The ideal shape of an airfoil however depends profoundly upon the size and speed of the wing of which it is the core. This dependence is called scale effect.

In the thirties, the significance of the scale effect was first recognised. This relates to the phenomenon that an airfoil that has most excellent qualities on an insect or bird may not exhibit these advantages when scaled up for an airplane wing and vice versa. Different sizes of airfoils require different shapes. This scale effect is partly characterized by the chord Reynolds number, R , defined by $R = \frac{Uc}{\nu}$ where U is the flight speed, c is the chord and ν is the kinematic viscosity of the fluid in which the airfoil is operating. The Reynolds number quantifies the relative importance of the inertial effects on the airfoil behaviour compared with the viscous effects. It is the latter effects that essentially control the airfoil performance since they dictate the drag or streamwise resistance as well as limiting and controlling the maximum lift of the airfoil.

A broad perspective on the range of chord Reynolds numbers versus flight velocity and Mach number for a variety of natural and man-made flying objects is shown in Fig 1.1.



(TAKEN FROM REF (1))

The performance of airfoils operating in low Reynolds number incompressible flow has been of increasing interest in the past decade. This interest has been a result of the desire to improve the low speed performance of general aviation aircraft and high aspect ratio sailplane wings, and to improve the design of remotely piloted vehicles (RPVs), jet engine fan blades and propellers at high altitudes. The inboard sections of helicopter rotors, wind turbine rotors and free flying model aircraft also represent applications where low Reynolds number performance is very important. These systems require efficient airfoil sections in the chord Reynolds number range from about 100,000 to about 1,000,000 [ref (3)].

Many significant aerodynamic problems occur below chord Reynolds numbers of about 500,000 [ref (4)]. These problems are associated with the behaviour of the airfoil boundary layer and the difficulties related in making accurate wind tunnel and free flight measurements. Although some progress has been made, these problems require more study if further improvements are to be realised.

In relation to the airfoil boundary layer, three Reynolds number bands, with brief descriptions of the changing flow regimes will be discussed below.

(a) Reynolds numbers between 30,000 and 70,000

This regime is of most interest to the technically oriented model aircraft builders and flyers. Both the Nordic A-2, tow-line launched model sailplanes and the Wakefield rubber powered models operate in this region. These models are judged on endurance and must have as high as possible a ratio of $\frac{(\text{lift})^{3/2}}{\text{drag}}$. Induced drag considerations call for a high aspect ratio wing but this reduces the Reynolds number, so great care must be taken in the choice of the airfoil section-aspect ratio combination. Six percent thick airfoils can become supercritical near the upper end of this regime and the critical Re can be decreased toward the lower end by artificially tripping the boundary layer. Under natural laminar separation conditions, the distance from separation to reattachment can be expressed as $Re_R - Re_S \approx 50,000$. Thus in the lower chord Re regime there is simply insufficient distance to the trailing edge for reattachment to occur. Nevertheless excellent performing wing sections have been developed for this regime.

b) Reynolds numbers between 70,000 and 200,000

At the lower end of this regime we find the bat in nature and small radio controlled model sailplanes and model power planes as man-made devices. Extensive laminar flow is easy to obtain and airfoil performance improves markedly in this regime. At the upper end, boundary layer tripping devices are no longer needed for sections as thick as 12%. There is a small data base for this regime but more work is justified in view of high altitude RPV and low altitude mini-RPV interest. The laminar separation bubble degrades significantly the performance in this region of flight.

c) Reynolds numbers between 200,000 and 700,000

In this regime we find large soaring birds of quite remarkable performance, large radio controlled model aircraft, foot launched ultra-light man-carrying hang gliders and the human powered aircraft. Again extensive laminar flow is easy to obtain and airfoil performance continues to rapidly improve compared to that at lower Reynolds numbers. However the laminar separation bubble is still of significant relative length and, to some extent, degrades the performance of the airfoil. One must still be careful in choice of the thickness-camber combination.

The amount of experimental data in the above mentioned regimes is limited [ref (5)]. Airfoil testing involves an intrinsic difficulty in that

the two quantities to be correlated - the lift and the drag - differ in magnitude by a factor of about 100. It is possible to measure these forces either directly using a balance or to calculate them by measuring the pressures on the airfoil and the velocity and pressure in the wake. Pressure measuring techniques however have the advantage of providing information on the details of the chordwise pressure distribution.

In wind tunnel testing it is important to consider the incoming turbulence in the test flow and any perturbations due to mechanical or acoustic disturbances [ref (1)]. This is because changes in any of these disturbances can trigger large effects on the boundary layer which in turn affects the overall performance of the airfoil. Furthermore, there are frequently difficulties with wall effects. These are both inviscid, where the confined potential flow must be taken into account, and viscous, where boundary layers originating from the walls or the support system can influence the boundary layer behaviour of the test airfoil section.

For all the above reasons, test data in the low-Reynolds number range have long been regarded with scepticism, especially earlier test results, and there is indeed a substantial record of nonrepeatability of data from tests in different facilities. Sometimes this can simply be attributed to inaccurate measurement techniques, but more often it can be because the model and the environment are actually different from one test section to another.

The aim of the present investigation is to carry out an experimental investigation into the aerodynamic characteristics of two airfoil sections, namely the NASA GA(W)-1 and the NACA-0015, proposed for low Reynolds number applications. Furthermore, it is to compare these with the results obtained for the GU25-5(11)8 which has been extensively tested in the past at Glasgow University. In order to be able to directly compare the experimental data the tests were carried out in the same wind tunnel and using the same size models.

The sensitivity of the boundary layer of the airfoil sections to the disturbance environment, especially close to the stalling incidence was demonstrated. The two airfoil sections tested presently gave a greater low Reynolds number operational range than the GU25-5(11)8 but they also produced much lower lift. Thus one has to look very closely on the requirements for a particular application of interest before deciding which of the three sections would be more suitable.

Further discussion regarding the experimental set-up, procedure and the results and conclusions of the present investigation will be given in subsequent chapters.

CHAPTER 2

DETAILS OF TEST FACILITY

Although existing airfoil sections are efficient for chord Reynolds numbers greater than about 500,000, their performance generally deteriorates for lower values. This is because many interesting aerodynamic problems occur in that area, which are related to the boundary layer behaviour. Important areas of concern are the separated regions which occur near the leading and/or trailing edges, the creation of laminar separation bubbles (i.e. their length and location) and transition from laminar to turbulent flow. It is well known [ref (6)] that separation and transition are highly sensitive to Reynolds number, pressure gradient and disturbance environment. Transition and separation play a critical role in the development of the boundary layer which in turn, affects the overall performance of the airfoil [ref(7)].

To evaluate airfoil section performance and improve existing design procedures, accurate wind tunnel data are needed. These data include lift, drag and pitching moment measurements and a knowledge of the location of transition and separation on two-dimensional airfoil sections. Although it is not the purpose of the present work to try to add further understanding to the flow phenomena of the boundary layer, it is important to obtain these as accurate as possible so that they can be related to the aerodynamic characteristics of the airfoil sections.

The experimental arrangement and test procedures as, well as the data acquisition used in the present experimental studies, will be discussed in the following sections.

2.2 EXPERIMENTAL APPARATUS

2.2.1 Wind Tunnel

In the present investigation, Glasgow University's low speed closed return tunnel was used. This tunnel has a rectangular shaped working section of the following dimensions:

Length	1.70m
Width	1.15m
Height	0.84m

The lower limit of air flow velocity in the working section is approximately 2.5m/s and the maximum is 30+0.3m/s. The longitudinal turbulence intensity component of the flow is 0.4% while the lateral one is 0.6% both components measured at the position of centre axes of the working section at a speed of 10 m/s [ref (8)].

The airfoil models which contained 60 static pressure tappings (see section 2.3) were mounted vertically in the tunnel working section and attached to circular steel plates - forming the top and lower tunnel walls. These plates could be rotated around the graduated scale, so that the centre of rotation was at 0.25c on the model's chord lines and thus facilitated changes to the model's angle-of-attack.

2.2.2 20-Signal Auto-Selector Boxes

The function of these pressure selector boxes was to enable the automatic sequential selection of one static pressure tube so that the respective pressure measurement could be carried out. A total of three selector boxes were used in the current investigation. These selector boxes were made by Furness Controls Limited and were customised for this experiment with the addition of an IEEE-488 instrumentation bus controller. This addition was made, so that the selection of a particular pressure port could be carried out remotely by the data acquisition programs. A maximum of twenty pressure tubes can be mounted at the rear pressure ports of a selector box. The output is attached to the input of a digital micromanometer. When a particular pressure port is selected a small light in the front of the selector box marked by the same number confirms that only this particular port is connected to the output and hence the micromanometer.

2.2.3 Digital Micromanometer

A digital micromanometer was used to convert the pressure into an electrical Analogue. It was made by FURNESS CONTROLS LTD. type MDC-FC002 and had a range of 0→199.9mm H₂O.

A feature of this micromanometer is the equalizing valve. Pressure to the two sides of the measuring head is taken, via this valve, from two fittings at the rear of the instrument. The equalizing valve is controlled by a push-pull knob on the front panel of the unit, marked IN=;OUT≠. When the knob is pushed in, the atmospheric pressure is applied to both sides of the transducer diaphragm permitting the zero to be set on the unit and protects the measuring head from accidental overloads. During operation the differential mode is set and the appropriate pressure difference measured.

The accuracy of this micromanometer is $\pm 1\%$ and its linearity $\pm 0.5\%$. The output voltage varies from 0-2 V D.C.. Two such micromanometers were used in the present investigation. One for measuring free stream velocity and the other for taking pressure measurements, via a tube connecting it to the three selector boxes.

2.2.4 Computational system for data processing

The computer system used for the data acquisition and analysis of the measured data was a DEC 11/23 (MINC). The CPU (central processing unit) was a PDP 11/23 processor with a 128K bytes RAM memory. Its associated peripherals included a two disc storage system (1.024M bytes of storage capacity), a 17Mb magnetic real tape system, printer, plotter and a VDU terminal. An IBM PC VT125 configured as a terminal was used in conjunction with the MINC for the production of

graphic displays. The availability of this computer system to the user, as well as its portability, were the prime reasons for its use in the logging and analysis of the measured data.

The A/D converter used was an integral part of the MINC system (DEC type MNCAD) and was used in conjunction with a programmable digital clock (DEC type MNCKW), both of which were controlled by the MINC through the Q-Bus.

The operating languages used on the MINC were BASIC and FORTRAN IV.

2.3 AIRFOIL MODELS

Two different airfoil sections were used in the present experimental investigation, namely the NASA GA(W)-1 and the NACA-0015. A schematic of the airfoil sections is shown in Figs 2.2 and 2.3. Major differences between the airfoils are:

- a) Leading edge,
- b) Position of max thickness,
- c) Trailing edge.

The NASA GA(W)-1 profile was chosen for two main reasons. First, because it has never been tested before in the low Reynolds number region of 50,000 to 500,000 and, second, because it has been shown that

thick airfoils with some supercritical characteristics have increased performance over conventional airfoil sections at subcritical conditions [ref (9)]. The NACA-0015 was tested because it is a typical low speed profile in the NACA-00 series and has been used in root rotor parts of helicopter blades and in wind turbine generators. A further reason for testing this profile is that it is used currently on a research programme for the study of blade/vortex interaction at low Reynolds number and therefore its behaviour in this flow region is of interest to that program.

The GA(W)-1 airfoil section has a maximum thickness of 17% occurring at 40% chord. It has a blunt nose and a cusped lower surface near the trailing edge which has 2% thickness. The NACA-0015 is one of the NACA's symmetrical airfoil sections, having a max thickness of 15% occurring at 30% chord. A complete set of coordinate data for both airfoil sections are shown in Tables 1 and 2.

From the above mentioned coordinates, accurate steel templates were made. Their accuracy was in the order of 0.5%. These templates were then used to make the model moulds on a wax block which was resting securely on a level table.

A gell-coat type CW 240 2A mixed with hardener type HY 2402 [both manufactured by CIBA-GEIGY] was laid on these moulds. On top

of this coat, several layers of glass fibre cloth [Woven Roving] type ECK8 were placed. A special mixture consisting of resin type CY219, hardener type HY219 and accelerator type DY219 was stippled onto the glass fibre mapping and allowed to solidify. The external shape of the airfoil was thus achieved. Care was taken so that the resin chosen for the above applications did not contract and thus alter the shape of the airfoil's profiles when solidified.

Pressure measuring tubes made of copper were then accurately positioned at mid-span. For reasons of torsional stiffness foam consisting of casting resin type CW2215 mixed with HM hardener was placed inside the two halves which were then glued together to form an integral airfoil section. Finally each model was polished to give smooth surfaces.

Each model had a chord of 30cm and a span of 0.84m. These dimensions were chosen so that they would match those of the GU25-5(11)8 model (previously tested ref 35) and the test results could thus be directly comparable.

There was a total of 60 pressure tappings on each model. Twenty of these were located on the lower surface while the remaining forty were on the upper surface. These tappings were staggered at the first 10% of chord from the leading edge on the upper and lower surfaces and at 20% of chord from the trailing edge on the upper surface for reasons explained in section 2.5. The positions of these were measured using a vernier scale. This was done by placing the model on a level

table so that its chord line would be perpendicular to the table and parallel to the vernier scale. The coordinates of the tappings for the two models are shown in Tables 3 and 4. The reason for using so many pressure tappings was so that a good assessment of the C_p profile could be inferred from the pressure measurements.

2.4 EXPERIMENTAL SET-UP

The model was mounted securely in the tunnel. Pressure tubes were run out the bottom of the wing and were connected securely at the rear of the selector boxes so that there would be no pressure leaks. There was a total of three selector boxes used and each had twenty pressure tubes attached at its rear. The order in which these tubes were connected was such that tube number 1 in Selector Box 1 corresponded to the tap closest to the trailing edge on the upper surface of the airfoil and tube number 60 in Selector Box 3 corresponded to the tap closest to the trailing edge on the airfoil's lower surface. Boxes two and three were connected through special cabling to box one which in turn was connected to the MINC's IEEE-BUS, so that all three boxes would be automatically controlled by the MINC. The output of each box was also connected through tri-star junctions to a common tube which was attached at the rear of the micromanometer. The output voltage of the micromanometer was fed to the A/D converter. Care was taken so that the MINC and the manometer had the same zero volt reference.

The minimum Reynolds number at which Glasgow University's low speed tunnel can produce steady air flow conditions is approximately 50,000. No tests were carried out above an Re of 500,000 because the pressures involved were above the micromanometer's operational range and it was believed that the possible severe lift degradation occurred below 500,000.

Pressure tubes were used in both models instead of pressure transducers and this was mainly due to cost and complexity of equipment reasons. The pressure tapings were staggered where appropriate to avoid interference in a downstream measurement due to an upstream tap [see figure 2.4] [ref (10)].

Normal force and pitching moment forces were obtained by integrating the static pressure distribution around the airfoil. However, the measurement of drag at low Reynolds numbers is very difficult. A method of determining drag which has been used successfully at high Reynolds numbers is the wake traverse method. There would appear to be no reason why this method should not produce good results at low Reynolds numbers if the static and total pressure can be measured accurately. However at low Re and especially below 100,000 most airfoil wakes are composed of large scale vortices which produce an unsteady or oscillating wake somewhat similar to the one behind a circular cylinder. A fixed static and total pressure rake, as shown in Fig 2.5, is

related to the changing flow direction [ref (11)]. The velocity distribution obtained from the wake traverse is used in the momentum equation written in the direction parallel to the test section centreline. The airfoil drag is then assumed to be equal to the decrease in momentum in this direction. Since these low Reynolds number airfoil flows are dominated by large scale vortices, accurate measurement of the velocity component parallel to the test section centreline is very difficult, if possible at all, using a rake wake. Additionally at these low Reynolds numbers, laminar separation and transition, very often produce large scale spanwise flow structures, usually on the upper surface of the airfoil [ref (11)]. The measurement of static and total pressures with a rake in such an oscillating wake can be subject to considerable errors. This problem is compounded when a significant spanwise flow structure is present. Due to the above mentioned reasons and due to time limitations it was decided that no drag measurements would be made.

A further consideration was, that the tunnel was stopped before each test. This was done in order to eliminate any possible "hysteresis" effects which might occur. Some airfoils exhibit a phenomena near stall in which the aerodynamic forces developed depend on the direction in which the angle of attack was reached. As the angle of attack increases the lift and drag forces increase. At stall an abrupt decrease in lift and increase in drag occurs. A small reduction in the angle of attack, however, does not restore the forces to their former values. Instead, the angle may have to be reduced several degrees before the lift and drag suddenly revert to the values obtained under conditions of increasing

angle of attack. This behaviour is known as "high-lift" or "clockwise" hysteresis and is attributed to the development and bursting of a short bubble [ref (12)].

The reverse situation may also occur in which an abrupt increase in lift and decrease in drag takes place at high angles of attack. The forces do not revert to the values obtained under conditions of increasing angle of attack until a sufficiently low angle is achieved. This is known as the "moderate-lift" or a "counterclockwise" hysteresis [ref (13)]. This type of hysteresis appears to result from the growth of a long bubble and its sudden collapse into a short bubble. The two different types of hysteresis are shown in Fig 2.6.

The effect of free stream turbulence (velocity fluctuation) acoustic phenomena (pressure fluctuations) and mechanical vibrations have been shown to be very considerable on the airfoil's performance, especially at an $Re \ll 200,000$ [ref (14)]. The above mentioned influences vary considerably from one wind tunnel to another and have been attributed to a large extent for the differences observed in the results of similar tests in different tunnels. However they will not be examined presently since this study is mainly comparative and the GU-25 airfoil with which the behaviour and aerodynamic characteristics of the current airfoil models will be compared with, has been tested in the same wind tunnel.

The experimental set-up used has already been described in Section 2.4. Since this was the first time that this particular configuration was used for data acquisition, an initial check was made to assess if there was any drift in the signal received by the A/D converter from the micromanometer. A signal source producing known voltages was plugged in the input of the A/D while a voltmeter was attached to the output. The D.C. voltage fed in the A/D varied from 0-2V which is the same as the output voltage from the micromanometer. Fig 2.7 shows the relationship between input and output voltages of the A/D converter and linearity is in the order of $\pm 1\%$. Random checks were also carried out throughout the tests by comparing the pressure readings displayed on the micromanometer and the readings recorded on the MINC's terminal. The difference of the two values varied from 0% in the region of 0-15mm H₂O to a max of $\pm 2\%$ in the region of 15-199.9mm H₂O.

The tests were carried out in the Reynolds number region of 50,000 to 500,000 at intervals of 50,000 and in the angle of attack range of 0° to 22° in steps of various degrees. The combination of Reynolds numbers and incidences tested in the current investigation for the NASA GA(W)-1 and NACA-0015 airfoil sections are presented in Tables 5 and 6.

Before each series of tests a warm up time of 15-30 minutes was allowed so that the electronics of the micromanometer, the A/D converter and the selector boxes would be brought up to operational temperatures.

For each Reynolds number tested the following experimental procedure (as illustrated in Fig 2.8) was adopted. The model was mounted securely in the tunnel working section. The tunnel was then started and was brought up to the desired speed. Once the speed was stabilized the program GEOR.BAS was run.

The auto-logging sequence of taking the pressure measurements was thus initiated. Boxes 1, 2 and 3 were selected in turn and once all the pressure readings were carried out and recorded on the MINC the program was automatically stopped. The tunnel speed was brought down to zero. The 'equalizing' mode of the micromanometer was then checked and the micromanometer was zeroed if necessary [refer to section 2.2.3]. The angle of attack of the model was then changed and the speed brought up to the desired level.

2.7 FLOW VISUALISATION

Two major flow visualisation techniques were considered for application in the current investigation.

- a) The "china clay" method whereby a Kaolin (china clay) solution is initially sprayed onto the clean airfoil profile and is allowed to dry forming a uniform white dust. Then before each test the coating is sprayed with an oil of the same refractive index which results in a transparent coating. The relative rates of evaporation between the different flow fields produces contrasting shades on the

airfoil, hence points of laminar separation and turbulent reattachment can be obtained. There are two main advantages of the above method:

- i) The china clay can be obtained as very fine particles so that a very smooth film can be applied to the surface of the airfoil. The film is therefore unlikely to upset transition at low Reynolds numbers [ref (15)].
- ii) The china clay is sprayed on once then used repeatedly. There is no rubbing down of the model between each investigation.

However, major difficulties arose when this method was applied. The initial white coating that covered the airfoil was not uniform because the spraying device available did not emit the china clay solution uniformly. Furthermore when the oil was sprayed onto this white coating it was seen to somehow disturb the position of the white dust filaments. The above two mentioned problems caused considerable change in the rate of evaporation of the oil irrespective of the air flow, and yielded poor quality results. This quality was due to the current procedures of applying the coatings and could have been improved with additional modifications. Since the surface oil film technique seemed reasonably satisfactory this became the preferred method.

b) The surface oil flow method consisted of a mixed solution of Odina oil and Saturn Yellow "Dayglo" pigments which was then applied to the airfoil by carefully stippling using a sponge so as to produce a uniform layer. The uniform layer was then distributed by the flow producing different patterns which correspond to the different flow regions. Once the oil was applied to the airfoil sections and the wind tunnel operating at its test speed, the oil moves by the action of the shear stresses at the wall in the boundary layer. The oil moved over the airfoil in the form of light streaks and, with the vertically mounted aerofoil a gravitational component of force induced a downward bias to the pattern. As the oil approached the point of laminar separation the oil flow fell vertically in a thin light band at the point of separation due to the very small wall stresses in that region.

When a bubble occurs, the boundary layer trips into a turbulent one. Long bubbles are characterized by a separation line followed by a "dead-air" region where the oil is stationary. Reattachment is noted as a dark band where the flow is moving the oil apart. The advantage of this method is that the various flow fields which occur on the airfoil's surface are relatively easy to distinguish.

A shortcoming of this method however is that the airfoil models can not be tested below a Reynolds number of 150,000. Visual observations below this Reynolds number indicated that the

oil film was adversely altering the boundary layer characteristics of the airfoils. Care must also be taken when interpreting the various flow patterns, since the extent to which the viscosity and the thickness of the oil film would alter boundary layer characteristics such as laminar separation, transition and turbulent reattachment is not well known.

Before each test the tunnel was stopped and the model wiped clean and a new coat of oil mix applied. Special care was taken to ensure that this coat of oil was uniformly distributed. A very extensive set of tests was carried out using this technique in the Reynolds number region of 150,000 to 500,000 and for various incidences. The combination of Reynolds numbers and angles of attack tested for both models is shown in Table 7.

The different flow patterns obtained were illuminated by an ultra-violet light and photographed by an FE-NIKON camera using a polarizing filter to cut out unwanted reflections.

2.8 DATA ACQUISITION AND SOFTWARE

Because of the amount of data needed to be analysed, the desirability of using of a high speed digital computer became apparent. In this respect, the MINC 11/23 digital computer was made available. Although it is not the most suitable computer to use because of its limited processing capacity (64K RAM memory) its comprehensive configuration makes it a suitable choice. In particular, its ability to convert analog signals into digital data.

A schematic of the instrumentation used for the data acquisition and processing of the pressure measurements is shown in Fig 2.9.

The static pressure of different points on the airfoil's surface was acquired through pressure tubes and was measured on the digital micromanometer, via the selector boxes. The micromanometer converted each pressure reading into an electrical signal which was then fed to the A/D converter. The latter then translated this signal into a 12-bit binary value that was supplied to the computer. The MINC converted this value to a standard arithmetical format which was then stored on a floppy disc. Further analysis of these data will be discussed in section 3.4.

A flow chart diagram of the logging sequence is shown in Fig 2.10. For each pressure measurement, 100 values of the electrical signal from the micromanometer were taken in a period of 1 second. After the first average of these values was computed a second set of 100 values in 1 second was obtained. If the difference between the two average values was below or equal to $\pm 2\%$ of the first average then this value was stored on the system disc and the next tube was selected for the respective pressure measurement. In case that the above mentioned convergence criterion was not satisfied, then the whole process of taking new values would be repeated up to a maximum of twenty times. If no convergence was obtained after the twenty cycles then the last average value was recorded together with a warning that this particular tube did not converge. It can thus be deduced, that the test time varied in the

present investigation and depended upon the time response of the pressure tube and micromanometer to each measurement. It was observed that the time at any tube varied from a minimum of 3 seconds to a maximum of 12 seconds.

The plotting of the results was carried out using a Gould (type DS7 COLOURWRITER) digital plotter in parallel with the MINC.

2.9 DISCUSSION

So far, an important assumption regarding the flow around the airfoil sections has been made, i.e., the flow is assumed to be two-dimensional. That is the velocity component of the flow along the z-axis is assumed to be negligible. However, in real situations of air flow around an airfoil this may not be true. Two-dimensional flow can only exist around infinitely spanned airfoils. The models used had a finite span and therefore all three co-ordinate velocity components can exist. It has been shown [ref (11)] that three-dimensional effects become apparent in general at Re below about 100,000 and large spanwise flow structures are usually observed in that chord Reynolds number region.

Regarding the method used for the data acquisition of the measured data, it can be said that it has two main advantages:

- i) It was automated.
- ii) At any time during the experiment, the recorded pressure value on the computer system can be checked with the value displayed on the digital micromanometer.

However the recorded measurements on the MINC were subject up to a maximum variance of $\pm 2\%$ of the actual values read by the micromanometer. This was due to the 'convergence criterion' as well as possible noise drifts in the electrical signal from the micromanometer to the A/D converter.

Although every possible precaution was taken in order to eliminate sources of experimental error, there were errors present which were unavoidable such as:

- a) The tunnel flow velocity can only be maintained to within $+0.1$ m/s.
- b) The variation of ambient temperature during the test runs which had to be conducted over a period of several days.
- c) Steady state conditions can not be fully maintained during a test run.
- d) Errors as high as $\pm 1\%$ can be introduced due to the accuracy of the digital micromanometer used.

CHAPTER 3

RESULTS AND DATA REDUCTION

This chapter presents the results obtained from oil flow visualisation and pressure measurements for each airfoil section considered.

The oil film technique was used to study the behaviour of the boundary layer and to ascertain the location and breadth of possible separation bubbles on the upper surface of the airfoils. The oil flow experiments were particularly useful for obtaining reattachment locations when long bubbles formed on the airfoils.

Analysis of the pressure data was performed in two steps. First plots of the pressure distributions were analyzed for separation and bubble formation in the airfoil boundary layer and, second the pressure distributions were integrated to obtain normal force and $\frac{1}{4}$ chord pitching moment. All results presented are corrected for solid blockage (2 - D) and streamline curvature (2 - D) in the manner of [ref (16)]. Although wake blocking contributes considerably to blockage effects, it was not taken into account since no wake measurements were made.

Data were reduced using a specialised computer programme. Pressure measurements were converted to pressure co-efficients and these were in turn integrated using the trapezoidal rule to provide normal force and pitching moment coefficients (about $\frac{1}{4}$ chord).

Corrections were made to C_p , C_N , $C_{M\frac{1}{4}}$ for wind tunnel blockage effects, namely solid body blockage and streamline curvature (2-Dimensions). The presence of the airfoil within a closed test section alters the flow field so that corrections are necessary to predict the behaviour of the airfoil in a free environment. Solid body blockage occurs because the airfoil model reduces the cross-sectional area of the test section, hence the free stream velocity increases to maintain a constant mass flow through the section. Streamline curvature results because the test section walls prevent the streamlines from assuming their normal curvature in the vicinity of the airfoil. A summary of these wind tunnel corrections follows [ref (16)].

Corrections

Free stream velocity	$U = U_u(1 + \epsilon b)$
Chord Reynolds Number	$Re = Re_u(1 + \epsilon b)$
Lift coefficient	$C_L = C_{L_u}(1 - \sigma - 2\epsilon)$
Pitching moment coefficient	$C_{M\frac{1}{4}} = C_{M\frac{1}{4}_u}(1 - 2\epsilon) + \frac{\sigma C_L}{4}$

where $\sigma = \frac{\pi^2 c^2}{48h^2}$ and $c =$ chord length

$h =$ test section height

and $\epsilon b = \frac{k_1 x V}{C^{3/2}}$

$k_1 = 0.52$ for a model spanning the tunnel height

$V =$ airfoil volume

$C =$ tunnel test section area

(Taken from ref. 16)

Incidence

It was found [ref (17)] that the flow in the tunnel working section is yawed by 0.6 degrees in the same plane as the test incidence is measured. Hence the actual incidence was obtained by adding 0.6 to the geometric incidence i.e.

$$\alpha_u = \alpha_{geom} + 0.6$$

and the correct incidence $\alpha = \alpha_u + \frac{57.3\sigma}{2\pi} (C_{Lu} + 4C_{M\frac{1}{4}})$

3.3 FLOW VISUALISATION

Photographic records were made of some of the ensuing flow patterns occurring on the upper surface of the two airfoil sections. Due to the large number of pictures taken only a representative few are presented here. The full set, however, can be seen in [ref (18)].

3.3.1 NASA GA(W)-1

The flow around the airfoil's upper surface at various Reynolds numbers and for 0.6° angle of attack is shown in Figs 3.1a,b & c. For a Reynolds number of 150,000 a long bubble forms after the mid-chord of the airfoil. The laminar flow separates at approx 0.65 x/c, it transits and the turbulent flow reattaches at approx 0.9 x/c. The turbulent

boundary layer then separates at approx 2% of the chord from the trailing edge. The bubble is present throughout the Re number range tested, but its length reduces from about 25% of the chord at 150,000 to approx 20% at 500,000. This is mainly because the reattachment location of the turbulent boundary layer moves towards the mid-chord position of the airfoil. However, the turbulent flow separates from the airfoils surface very close to the trailing edge for all Reynolds numbers tested. Increasing the Reynolds number appears to have no effect on the position of laminar flow separation.

The behaviour of the flow at 3.6° angle of attack and at a Reynolds number of 150,000, 300,000 and 350,000 is shown in Figs 3.2a,b & c respectively. It is observed that a long bubble also forms after mid-chord at this angle of attack. This bubble has a length of approx 25% of the chord at a Reynolds number of 150,000 which is similar in length as that observed for the 0.6° case. Its length diminishes with increasing Reynolds number and the bubble disappears at an Re of approx 300,000. Above this value the laminar flow remains attached to the airfoils surface followed by natural transition to turbulent flow with eventual separation close to the trailing edge.

At 6.6°, and for all the Reynolds numbers tested, the location of laminar flow separation from the airfoil's surface moves forward close to the leading edge (at approx 0.15 x/c) as shown in Figs 3.3a,b & c. A long bubble of approx 20% chord forms at a Reynolds number of 150,000 and this reduces to a short bubble of approx 10% chord at a

Re number of 250,000. Also, the location of turbulent boundary layer separation shifts from approx $0.8 x/c$ to $0.9 x/c$ respectively. For Reynolds numbers above 250,000 the length of the short bubble and the position of turbulent separation appears to be constant.

As the angle of attack increases (in particular at 12.6°) and for all the Re tested a bubble forms close to the leading edge of the airfoil as shown in Figs 3.4a,b & c. of the separation location. The bubble's length is approx 12% of the chord at a Reynolds number of 150,000 but decreases with increasing Reynolds number. The turbulent flow separates from the airfoil at approx $0.6 x/c$ (at a $Re \approx 150,000$) and there is a movement of the separation line towards the trailing edge as the Re number increases up to 300,000. For larger Re tested it remains constant at approx $0.7 x/c$.

The flow characteristics at an angle of attack of 16.6° and for various Reynolds numbers is shown in Figs 3.5a,b & c. Laminar separation occurs close to the leading edge without subsequent reattachment and the airfoil has stalled. Flow reversal close to the trailing edge is observed and increases in prominence with increasing the Reynolds number.

Figs 3.33 to 3.40 shows, for various incidences and Reynolds numbers, the location of separation and reattachment of the flow when long bubbles are formed. These were all deduced from the oil flow visualisation data described.

Nominal two-dimensionality of the flow over the airfoil section was established since laminar and turbulent separation locations appeared in the form of vertical straight lines. However the turbulent separation line had a scalloped wave pattern for Re above 350,000 and at high incidences as shown in Fig 3.4c. This small three-dimensional effect will be discussed in section 4.2.1.

3.3.2 NACA 0015

A long bubble forms before the mid-chord of the airfoil (at approx $0.25 x/c$) and has a length of approx 65% of the chord at a Reynolds number of 150,000 and an angle of attack of 0.6° , as shown in Figs 3.6a,b & c. However, it substantially reduces in length as the Reynolds number increases and the bubble may have disappeared above an Re of 400,000 dependent on the subjective interpretation of the oil flow pattern. The location at which laminar flow separates, shifts from approx $0.25 x/c$ to $0.5 x/c$ as the Reynolds number increases whilst the turbulent reattachment location moves towards the mid-chord position. At sufficiently high Reynolds numbers ($>400,000$) the present interpretation of the patterns is that the laminar flow does not separate from the airfoil's surface and it transits to a turbulent one. The turbulent boundary layer then separates from the airfoil at approx 96% of the chord.

As the angle of attack is increased to 3.6° , a long bubble of length approx 35% of the chord forms before the mid-chord position on

the airfoil's surface, at a Reynolds number of 150,000, as shown in Figs 3.7a,b & c. As the Reynolds number increases the length of this bubble reduces considerably until at a $Re \approx 500,000$ the bubble has a length of approx 8% chord. The position at which the laminar flow separates appears to shift from approx $0.2 x/c$ to approx $0.3 x/c$ for Reynolds number of 150,000 and 500,000 respectively. Also the position that the turbulent boundary layer separates shifts from $0.85 x/c$ to $0.98 x/c$.

At 6.6° and for various Re the laminar flow separates very close to the leading edge as shown in Figs 3.8a,b & c. A bubble approx 20% of the chord in length forms at an $Re \approx 150,000$ and reduces to a short bubble of approx 8% of the chord above an $Re \approx 350,000$. The turbulent flow separates at approx $0.7x/c$ for the 150,000 case but as the Reynolds number increases the separation location moves very close to the trailing edge.

A bubble of approx 10% of the chord forms close to the leading edge of the airfoil at 9° and for a Re of 150,000. However, its length decreases slightly with an increase in the Reynolds number as shown in Figs 3.9 a,b & c. The turbulent boundary layer separates at approx $0.5 x/c$ and at approx $0.9 x/c$ for Reynolds numbers of 150,000 and 500,000 respectively.

The flow around the airfoil at an incidence of 13.6° and for various Re is shown in Figs 3.10a,b & c. Laminar separation occurs very close to the leading edge and the flow does not reattach. Flow reversal is observed close to the trailing edge and increases in prominence with increasing the Reynolds number.

Figs 3.43 to 3.50 show the location of separation and reattachment when long bubbles form on the upper surface of the airfoil for all incidences and Reynolds numbers tested taken from oil flow visualisation data.

At low incidences, a long bubble forms on this airfoil section before the mid-chord position extending well beyond it provided the Re is sufficiently low, as opposed to the after mid-chord position observed for the NASA GA(W)-1 airfoil. However the long bubble shows similar trends in its behaviour, that is, decreasing in length with increasing incidence and Reynolds number.

Two-Dimensional flow was also confirmed for this airfoil section, i.e. laminar and turbulent separation locations were in the form of straight lines. The scalloped wave pattern which was observed for the NASA GA(W)-1 airfoil section was present once more at high Reynolds numbers ($>350,000$) and high incidences [see Fig 3.10d]. It is interesting to note that the patterns observed were almost identical for both airfoil models.

3.4 PRESSURE MEASUREMENTS

Due to the large volume of data in the present thesis, three-dimensional plots showing the static pressure distribution along the upper surface of the airfoil for all incidences tested, are presented for each Reynolds number. Figures 3.11 to 3.20 relate to the NASA

GA(W)-1 section whilst Figs 3.21 to 3.30 are for the NACA-0015. The complete static pressure distributions for angles of attack of 0.6° to 22.6° and Reynolds numbers of 50,000 to 500,000 for both models are presented in [ref (19)].

Analysis of the pressure distributions themselves, provides a better understanding of the boundary layer behaviour.

3.4.1 NASA GA(W)-1

The static pressure distribution for a Reynolds number of 100,000 is shown in Fig 3.12. From 0.6° to 4.7° the airfoil exhibits a pressure distribution which infers the existence of a separation bubble on the upper surface after the mid-chord position. This is indicated by the value of the pressure coefficient which remains constant after approximately $0.6 x/c$, suggesting that the laminar boundary layer has separated from the airfoil's surface, followed by an increase in pressure which is characteristic of the turbulent mixing region between the approximate end of transition and reattachment [ref (20)]. The total bubble length is taken to be the distance between the separation and the reattachment point. Although no accurate prediction of the length of this bubble can be inferred from these pressure measurements [ref to section 4.1], it appears that it decreases in length as the angle of the attack increases in this Re range. This is so, because the position of the pressure recovery region moves toward the mid-chord with increasing incidence, thus suggesting that reattachment occurs further away from

the trailing edge. From 6.79° to 8.8° there is no clear indication of a bubble formation but this does not imply non existence. At 8.8° the pressure coefficient has a constant value from approx $0.87 x/c$ onwards which implies that the boundary layer separates from the airfoil at that point. As the incidence is further increased from 10.8° to 12.9° a typical short bubble is evident close to the leading edge of the airfoil. Its length appears to increase from 17% of the chord at 10.6° to 18% at 12.9° . As the angle of attack is increased from 8.8° to 12.9° the boundary layer separation location is shifted by 12% of the chord towards the mid-chord position. Above 12.9° laminar separation occurs very close to the leading edge (approx $0.05 x/c$) and the flow never reattaches. This is shown by the collapse of the pressure distribution into a constant pressure line.

The static pressure distribution for a Reynolds number of 150,000 is shown in Fig 3.13. For 0.6° to 2.6° it is very similar to the one obtained for the 100,000 case. However the pressure coefficient exhibits slightly higher values for both incidences, than previously. A separation bubble forms after the mid-chord which appears to decrease in length as the incidence increases from 0.6° to 2.6° . This bubble has smaller length than the one formed for the respective incidence range at a Re of 100,000 and this is indicated by the fact that the pressure recovery region is shifted to an earlier position by approx 5% of the chord for both angles of attack. From 4.7° to 8.8° the pressure distributions give no clear evidence of a bubble being present. At 8.8° the boundary layer separates at approx $0.87 x/c$. A bubble forms very close to the leading

edge between 10.8° and 13.6° and its length decreases from 19% to 12% of the chord respectively. Also the turbulent boundary layer separates at approx $0.84 x/c$ and $0.65 x/c$ in the respective incidence range.

It is interesting to note the decrease in the value of the pressure coefficient after apparent separation of the turbulent boundary layer has occurred at 13.6° . This pressure distribution will be discussed in more detail in section 4.3.1. Above 13.6° laminar separation occurs very close to the leading edge of the airfoil and stall occurs.

The pressure distribution for a Reynolds number of 200,000 is shown in Fig 3.14. For angles of attack of 0.6° and 2.7° the pressure distribution is very similar to the 150,000 case, the pressure coefficient, however, has slightly higher values. Once again a bubble forms at these incidences and appears to decrease in length with increasing angle of attack. The bubble also seems to be smaller in length compared to the 150,000 case for 0.6° and this is because the laminar separation point appears to have shifted towards the trailing edge by approx 4% of the chord while the position of the pressure recovery region remained constant. Between 4.7° and 8.8° no clear evidence of a bubble formation is obtained from the pressure distributions. At 10.8° , 12.8° and 13.6° a bubble forms close to the leading edge and the bubble length is 8%, 10% and 12% of the chord respectively. The turbulent boundary layer separates at approx $0.89 x/c$ and at $0.74 x/c$ at angles of attack of 10.8° and 13.6° respectively. It is worthwhile to notice that the turbulent boundary layer appears to separate from the airfoil's surface at

10.8° as opposed to 8.6° which is the case for Reynolds numbers of 100,000 and 150,000. Laminar separation very close to the leading edge of the airfoil occurs for angles of attack above 13.6° and is delayed by 1° compared to the 100,000 case.

Fig 3.15 shows the pressure distribution at a Reynolds number of 250,000. At 0.6° and 2.7° a bubble forms which appears to be smaller in length than the one formed at a Reynolds number of 200,000. Also the bubble decreases in length as the incidence increases from 0.6° to 2.7°. From 4.7° to 8.8° again no bubble appears to form and the pressure distributions are almost identical to the ones obtained at a Reynolds number of 200,000. A bubble forms close to the leading edge at incidences of 10.8°, 12.8° and 14.9° and its length is 8%, 8% and 10% of the chord respectively. The turbulent boundary layer separates at 0.86 x/c and 0.72 x/c for incidences of 10.8° and 14.9° respectively. Stall is delayed by 1.3° from the 200,000 case and laminar separation of the leading edge occurs above 14.9°.

For a Reynolds number of 300,000 the pressure coefficient plots are shown in Fig 3.16. The bubble appears to have further decreased in length at 0.6° and 2.7° than the 250,000 case but the location of separation of the laminar boundary layer as well as the beginning of the pressure recovery region is not as clearly defined as in the lower Reynolds numbers. The general trend from 4.7° to 8.8° is the same as in the 250,000 case and there is no apparent indication of a bubble forming. At incidences of 10.8°, 12.8° and 14.9° a bubble forms close to

the leading edge with length of 8%, 7% and 5% of the chord respectively. Again at this Reynolds number the turbulent boundary layer separates at approx $0.85 x/c$ and $0.68 x/c$ for incidences of 10.8° and 14.9° . Above 15.7° laminar separation at the leading edge occurs.

For a Reynolds number of 350,000 the bubble appears to be present and smaller in length than at 300,000 only for an angle of attack of 0.6° as shown in Fig 3.17. Between 2.7° and 8.8° no bubble is indicated by the pressure distribution. However for angles of attack of 10.8° to 14.9° a bubble forms close to the leading edge whose length varies from 9% to 5% of the chord respectively. The turbulent boundary layer separates at approx $0.9 x/c$ and $0.81 x/c$ for incidences of 10.8° and 14.9° respectively. Laminar separation at the leading edge takes place at 15.7° .

The static pressure distribution for a Reynolds number of 400,000 is shown in Fig 3.18. The pressure coefficient plot at 0.6° suggests once more the presence of a bubble but it is very difficult to comment on the length of this bubble because no accurate positioning of the laminar separation point as well as the pressure recovery region can be made. From 2.7° to 8.2° the trend of the pressure distribution is pretty much the same as in the 350,000 case, exhibiting however slightly higher values of C_p . Above 8.8° a slight kink is observed at approx mid-chord for all incidences. As no other reason is apparent this is likely to be attributed to the blockage of a pressure measuring tube in that region. A bubble forms close to the leading edge between 10.6° and 14.6° whose

length varies from 7% to 4% of the chord respectively. The turbulent boundary layer separation location varies from $0.87 x/c$ to $0.66 x/c$ for angles of attack of 10.8° and 14.9° . At 15.7° the pressure coefficient shows a large negative suction peak downstream of which there is very small plateau (approx 1% of the chord) of constant pressure followed by a large and rapid increase in pressure. The value of the pressure coefficient is constant from approx $0.08 x/c$ onwards, indicating separation of the boundary layer. This pressure distribution is of particular importance and will be discussed in section 4.3.1.

At a Reynolds number of 450,000 the bubble appears to be present at an incidence of 0.6° but no deduction can be made about its length [see Fig 3.19]. Between 2.6° and 10.6° there is no clear indication of a bubble being present on the airfoil's upper surface. However the boundary layer separates at 10.6° at approx $0.85 x/c$. From 12.6° to 15.6° a bubble forms close to the leading edge whose length is approx 4% of the chord for all incidences. Also there is a separation of the turbulent boundary layer at $0.76 x/c$, $0.66 x/c$ and $0.6 x/c$ for incidences of 12.6° , 14.6° and 15.6° respectively. At 16.6° laminar separation at the leading edge occurs.

The pressure distribution at a Reynolds number of 500,000 is shown in Fig 3.20. In this case the bubble appears to be present at 0.6° . From 2.6° to 12.6° there is no indication of a bubble formation. The boundary layer separates at $0.85 x/c$ at 10.6° and the separation point moves forwards by approx 10% of the chord at 12.6° . A bubble forms

close to the leading edge for incidences of 14.6° , 15.6° and 16.6° . Its length for all three angles of attack is approx 4% of the chord. The separation point of the turbulent boundary layer shifts from $0.65 x/c$ to $0.55 x/c$ for incidences of 14.6° and 16.6° respectively. At 17.6° laminar separation at the leading edge occurs.

At low incidences pressure measurements suggested the existence of a bubble after the mid-chord position of the airfoil. Although no accurate prediction of the length of these bubbles can be made, it was indicated that they reduced in length as Reynolds number and incidence was increased.

For high incidences and at Reynolds numbers less than 300,000, a bubble was observed to form close to the leading edge. Its length varied from about 18% to 10% chord for Reynolds numbers of 100,000 and 250,000 respectively.

For Reynolds numbers of 300,000 and above a bubble formed close to the leading edge of the airfoil. Its length varied from 8% of the chord at 300,000 to approx 4% of the chord at 500,000.

Stall is delayed to a higher incidence as the Reynolds number increases. At 50,000 it occurs above 12.9° while at 500,000 it occurs above 16.6° .

The pressure distribution at a Reynolds number of 50,000 is shown in Fig 3.21. The value of the pressure coefficient fluctuates violently along the chord and for all incidences tested. Unfortunately, from this pressure distribution, little can be deduced concerning the boundary layer behaviour.

For a Reynolds number of 100,000 the pressure distribution is shown in Fig 3.22. No clear evidence of a bubble is shown by the pressure distribution at the lower incidences. At 8.6°, however, an obvious separation bubble of approx 16% of the chord forms very close to the leading edge (approx 0.09 x/c). From 9.6° to 11° the bubble decreases in length to approx 13% of the chord and its location moves by 2% closer to the leading edge (i.e. 0.07 x/c). Laminar separation at the leading edge occurs at 11.6° and stall occurs.

The pressure distribution at a Reynolds number of 150,000 is shown in Fig 3.23. In the incidence range of 0.6° to 7.6° the trends of the pressure distribution are very similar to the 100,000 case. At 8.6° a bubble of approx 11% of the chord forms very close to the leading edge (approx 0.09 x/c). Between 8.6° and 11.6° the bubble's length decreases to approx 9% and there is a gradual movement of the location at which the bubble begins to form towards the leading edge. The turbulent boundary layer separates at 0.9 x/c and 0.83 x/c at angles of attack of 9.6° and 11.6° respectively. At 12.6° laminar separation at the leading edge occurs and stall is delayed by 1° compared to the 100,000 case.

At a Reynolds number of 200,000 the pressure distribution is shown in Fig 3.24. Again, at the lower incidences the pressure profiles are very similar to the ones obtained at 150,000. For incidences of 8.6° to 11.6° an obvious bubble is present close to the leading edge and its length is approximately 8% of the chord. Its position also moves closer to the leading edge as the incidence increases. The first indication that the turbulent boundary layer separates is given at 10.6° when it does so at approx 0.87 x/c . As the incidence increases to 11.6° the separation point moves to 0.81 x/c . At 12.6° laminar separation at the leading edge occurs.

The pressure distribution at a Reynolds number of 250,000 is shown in Fig 3.25. The trends are very similar to the ones observed at 200,000, for angles of attack of 0.6° to 7.6° the pressure coefficient however exhibiting slightly higher values than before. A separation bubble is clearly defined at 8.6°, being located very close to the leading edge (approx 0.09 x/c). Its length is approx 7% of the chord and it remains constant as the incidence increases to 12.6°. However as the incidence increases the location that the bubble forms shifts towards the leading edge and at 12.6° the bubble is located at 0.05 x/c . Turbulent separation occurs at approx 0.85 x/c and 0.77 x/c for incidences of 10.6° and 11.6° respectively. At 13.6° laminar separation occurs due to the bursting of the leading edge bubble and stall occurs.

For a Reynolds number of 300,000 the pressure distribution is shown in Fig 3.26. In the incidence range of 0.6° to 8.6° no bubble is

clearly visible from the pressure distribution and the trends are very similar to the 250,000 case. Between 9.6° and 13.1° a bubble forms close to the leading edge. The bubble's length is approx 6% of the chord and it is located at approx $0.05 x/c$ in this incidence range. The turbulent boundary separation location shifts from approx $0.89 x/c$ to $0.76 x/c$ for incidences of 10.6° and 13.1° respectively. Laminar separation at the leading edge occurs at 13.6° and is attributed to the bursting of the separation bubble formed very close to the leading edge.

The pressure distribution at a Reynolds number of 350,000 is shown in Fig 3.27. The trends of the pressure coefficient plots in the incidence range of 0.6° to 7.6° are very similar to the ones obtained at 300,000. However the values of C_p are slightly higher than before. A separation bubble forms very close to the leading edge for angles of attack of 8.6° to 13.1° . The bubble's length is approx 6% of the chord (for all incidences) and its location shifts from $0.06 x/c$ at 8.6° to $0.04 x/c$ at 13.1° . Turbulent separation takes place at $0.86 x/c$ at 11.6° and this position moves to $0.77 x/c$ as the incidence is increased to 13.1° . At 13.6° laminar separation at the leading edge occurs due to the bursting of the leading edge bubble.

For a Reynolds number of 400,000 the pressure distribution is shown in Fig 3.28. At low incidences the pressure distribution does not indicate clearly the presence of a bubble. From 9.6° to 13.1° a clear bubble forms very close to the leading edge and its length is approx 7% and 5% of the chord at incidences of 9.6° and 13.1° respectively. The

turbulent separation location moves from $0.88 x/c$ to $0.78 x/c$ as the incidence increases from 11.1° to 13.1° . Also the location that the bubble forms shifts from $0.05 x/c$ at 9.6° to $0.04 x/c$ at 12.6° . At 13.6° laminar separation at the leading edge occurs.

The pressure distribution at a Reynolds number of 450,000 is shown in Fig 3.29. In the incidence range of 0.6° to 8.6° the trends are very similar to the ones obtained at 400,000 and no bubble is clearly indicated. A bubble forms very close to the leading edge for angles of attack of 9.6° to 13.6° . Its length is approx 7% of the chord at 9.6° and 10.6° , however it decreases to approx 4% in the incidence range of 11.6° to 13.6° . The separation location of the turbulent boundary layer moves from $0.88 x/c$ at 11.6° to $0.75 x/c$ at 13.6° . At 14.6° laminar separation at the leading edge occurs due to the bursting of the leading edge bubble and stall is delayed by 1° compared to the 400,000 case.

At a Reynolds number of 500,000 the pressure distribution is shown in Fig 3.30. Between 0.6° and 8.6° there is no clear indication of a bubble forming on the airfoil surface. However between 9.6° and 13.6° a bubble forms very close to the leading edge and its length varies from approx 6% to 4% of the chord respectively. The pressure distribution at 14.1° shows a separation bubble of approx 3% of the chord forming close to the leading edge and the turbulent flow to separate at approx $0.45 x/c$; this particular pressure distribution will be discussed in section 4.3.2. The turbulent boundary layer separation location shifts from approx $0.9 x/c$ at 10.6° to approx $0.82 x/c$ at 13.6° . At an incidence of 14.6° laminar separation at the leading edge occurs.

At high incidences the pressure distribution indicated that a bubble forms close to the leading edge of the airfoil whose length varied from 16% to 9% of the chord for Reynolds numbers of 100,000 and 150,000 respectively. Above 200,000 the bubble's length decreased from 8% to 4% of the chord with increasing Reynolds number.

The position that the turbulent boundary layer separated moved forward from the trailing edge with decreasing Reynolds number and increasing incidence. The angle of attack above which stall occurs was increased from 11.6° at 100,000 to 13.6° at 500,000.

3.5 NORMAL FORCE AND PITCHING MOMENT

The normal force and pitching moment characteristics for Reynolds numbers of 50,000 to 500,000 are shown for both models in Figs 3.31 to 3.50. Also included in these Figures are the position of laminar separation, transition and reattachment for separation bubbles deduced from pressure measurements. This was done so that the effect of the boundary layer behaviour can be directly linked to the changes observed in the aerodynamic characteristics of the airfoils.

3.5.1 NASA GA(W)-1

The aerodynamic characteristics of the airfoil at a Reynolds number of 50,000 are shown in Fig 3.31. The performance of the airfoil is very poor as indicated by the C_N and C_M versus angle of attack graphs. In

particular the normal force coefficient curve approximates a certain type of behaviour [see Fig 4.9b] which has been observed in the past at low Reynolds numbers and is indicative of poor performance [ref (21)].

At a Reynolds number of 100,000 there are changes observed in the lift curve slope (as shown in Fig 3.32) which are associated mainly with the location of the separation bubble on the airfoil's surface and that of turbulent separation. There is a sudden and large drop in lift after 12.9° which suggests leading edge type of stall [ref(22)]. The pitching moment coefficient curve shows a small nose down pitching moment between 0.6° to 2.6° is constant from 2.6° to 6.6°, this is followed by a small increase until stall at 6.6°.

The aerodynamic characteristics at Reynolds numbers of 150,000 and 200,000 are very similar and are shown in Figs 3.33 and 3.34. As the incidence increases above 4.6° there is a gradual reduction in the C_N slope. At 12.9° the max value of C_N is 1.17 and is obtained for both Reynolds numbers. The airfoil exhibits a gradual loss of lift and stall occurs above 12.9°. The zero normal force angle of attack is approximately -3° for both cases. The pitching moment coefficient is very similar for both Reynolds numbers and is nearly constant from 0.6° to 4.6°. As the incidence is further increased the value increases slightly (presumably due to trailing edge separation) until the stall.

For Reynolds numbers of 250,000, 300,000 and 350,000 the aerodynamic characteristics are shown in Fig 3.35, 3.36 and 3.37

respectively. The value of the max normal force coefficient has increased to approx 1.23 for all cases but the trends in $\frac{dC_N}{d\alpha}$ are very similar to the ones described for the 200,000 case. The zero normal force coefficient angle of attack lies between -3° and -4° for both Reynolds numbers. Stall occurs after 14.9° . The value of the pitching moment coefficient is nearly constant from 0.6° to 4.6° and increases until it is close to zero, as stall is approached.

The aerodynamic characteristics at Reynolds numbers of 400,000, 450,000 and 500,000 are shown in Figs 3.38, 3.39 and 3.40 respectively. The max value of C_N obtained is 1.25, 1.29 and 1.28 at an angle of attack of 15.6° , 15.6° and 16.6° respectively. The trends in $\frac{dC_N}{d\alpha}$ are very similar for all three cases and there is a gradual decrease as stall is approached. Zero normal force coefficient is very close to -4° for all three cases. Also the pitching moment coefficient is nearly constant from 0.6° to 4.6° and increases as stall is approached (nose up pitching moment).

The aerodynamic characteristics at a Reynolds number of 2×10^6 taken from [ref (9)] are shown in Fig 4.13. Although C_L rather than C_N is presented in the above mentioned figure; comparison with present experimental data at a Reynolds number of 500,000 reveals good agreement in the trends of the behaviour of both the normal force and pitching moment coefficient.

The aerodynamic characteristics at a Reynolds number of 100,000 are shown in Fig 3.42. The normal force coefficient versus angle of attack plot is non-linear. There are various kinks observed that cause changes in the normal force curve slope $\frac{dC_N}{d\alpha}$ and are associated with the location and type of separation bubble present on the airfoil's surface, as well as the behaviour of the turbulent boundary layer (i.e. whether or not, it separates and at which point along the chord it does so). The maximum value of C_N is approx 0.84 and stall occurs above 11.1° . Each change in the normal force curve slope is accompanied by a corresponding one in the value of the pitching moment coefficient, as a result of which it fluctuates closely to the zero value line. Stall causes a large nose down pitching moment.

The aerodynamic characteristics at a Reynolds number of 150,000 and 200,000 are shown in Figs 3.43 and 3.44 respectively. The normal coefficient versus angle of attack plots are non-linear. The value of the max C_N increases from 0.84 to 0.9 respectively. Stall occurs at 11.6° for the 150,000 case and at 12.1° for 200,000. At stall there is a small nose up pitching moment followed by a large nose down for both cases. For incidences before stall the pitching moment coefficient value changes in a manner similar to the one described for the 100,000 case. As the incidence increases from 0.6° to 5.6° , the bubble that forms on the airfoil's surface reduces in length for both Reynolds numbers, the effect of which is an increase in $\frac{dC_N}{d\alpha}$. However, as the incidence is further increased the turbulent boundary layer separates forwards from the trailing edge of the airfoil resulting in a reduction of $\frac{dC_N}{d\alpha}$.

For a Reynolds number of 250,000 the normal force coefficient versus angle of attack plot is non-linear, mainly in the mid- C_N range, as shown in Fig 3.45. This agrees well with one type of behaviour observed to occur in the C_L versus α curves at higher Reynolds numbers [ref (5)]. The max value of C_N is 0.94 and it occurs at an angle of attack of 12.6° above which stall takes place. The pitching moment coefficient is nearly constant over an angle of attack range of 0.6° to 9.6° . Above that incidence there is a small nose up pitching moment followed by a large nose down at stall.

The aerodynamic characteristics for Reynolds numbers of 300,000, 350,000 and 400,000 are shown in Figs 3.46, 3.47 and 3.48 respectively. The C_N versus α curves are non-linear mainly in the mid- C_N range. Stall takes place above an angle of 13.1° and the max value of C_N increases to approx 0.98 for all three cases. The pitching moment coefficient values are almost identical for all three cases and are nearly constant at an angle of attack range of 0.6° to 9.6° . As the incidence is further increased there is a small nose up pitching moment followed by a large nose down at stall.

At a Reynolds number of 450,000 and 500,000 stall occurs at angles of attack above 13.6° as shown in Figs 3.49 and 3.50 respectively. The value of the max C_N has increased to approx 1.05 and the C_N versus α curves are observed to be non-linear in the mid- C_N range. For the 500,000 case and for an angle of attack of 14.1° the value of C_N lies well beyond the normal force curve slope of the latter part of the

graph. This large increase in the value of C_N is explained in section 4.3.2. However in the present analysis it will be ignored. The pitching moment coefficient behaves in a similar fashion for both Reynolds numbers and is nearly constant in the incidence range of 0.6° to 10.6° .

The normal force coefficients versus angle of attack plot for Reynolds numbers of 200,000, 300,000, 400,000 and 500,000 obtained from [ref (23)] are shown in Fig 4.14. For Reynolds numbers of 200,000, 300,000 and 400,000 the trends in the normal force curve slope are very similar to the ones obtained in the present investigation. However the max C_N coefficient obtained for all these cases is smaller than the one obtained presently. For a Reynolds number of 200,000 the max C_N had a value of approx 0.76 as opposed to 0.9 and at Reynolds numbers of 300,000 and 400,000 it had a value of approx 0.83 compared to 0.98 which was obtained currently. Good agreement in the value of C_{Nmax} occurs for a Reynolds number of 500,000. Present investigation revealed a value of 1.05 while from Fig 4.14 this is obtained to be approx 1.02.

3.6 CONCLUSIONS

The following conclusions can be drawn from the present results:

- i) Flow visualisation confirmed the initial assumption of two-dimensional flow over the major part of both airfoil models. However, the bubble forming on the NACA-0015 airfoil section forms before the mid-chord position as opposed to the after

mid-chord position which is the case for the NASA GA(W)-1 airfoil. Its length however decreases considerably for both airfoil sections with increasing Reynolds number and angle of attack.

- ii) Maximum normal force coefficients varied non-uniformly with increasing the Reynolds number from 50,000 to 500,000 for both sections. The value of the max normal force coefficients was 1.26 and 1.02 for the NASA GA(W)-1 and NACA-0015 respectively.

CHAPTER 4

DISCUSSION OF RESULTS

In the following sections we shall often refer to the type (i.e. short or long), effect and behaviour of laminar separation bubbles. The structure of such a bubble is shown in Figs 4.1 and 4.2a. It consists of an initial "dead-air" region of almost constant pressure followed by a reverse flow vortex associated with a marked pressure rise to the reattachment point. The fluid in the laminar region of the bubble moves very slowly while in the turbulent region it moves in a vigorous recirculating manner. The total bubble length is taken to be the distance between the separation and reattachment point [ref (24)].

The classification of the separation bubbles into 'long' and 'short' ones is made merely on their length rather than their effect on the pressure distribution. Bubbles with more than 10% of the chord length will be referred as 'long' while those with less than that will be considered 'short'.

When a short bubble forms, there is very little effect on the overall pressure distribution as shown in Fig 4.2b [ref (22)]. In other words, the pressure distribution is much the same as that if the bubble were not present. The high peak suction at the nose is maintained and will increase with increase in incidence. The laminar boundary layer separates from the airfoil as a result of a strong adverse pressure gradient downwards of the point of minimum pressure. This is clearly indicated by the small region where the pressure coefficient has a constant value. The separated shear layer is very unstable and transition usually begins a short distance downstream of separation. After complete

transition, shear stresses energize the shear layer by entraining fluid from the external stream so that it grows rapidly, causing pressure to rise (pressure recovery region). Reattachment occurs when the pressure is nearly equal to the value for the boundary layer over the airfoil with no separation bubble present [ref (20)].

Since no such data were available in the present investigation, a good approximation was used for the location of the reattachment point. It was taken to be the point where the pressure gradient changes downwards of the pressure recovery region [ref (25)]. Gault [ref (26)] has shown that the length of the region of constant pressure is 0.75 to 0.85 of the total length of the bubble. Because the bubble hardly affects the overall pressure distribution the position of laminar separation does not vary much with changes in Reynolds number but moves forward with increase in incidence.

The presence of a long bubble greatly alters the pressure distribution from its theoretical form and causes a collapse of the leading edge suction peak as shown in Fig 4.2b. For this case, although the separated shear layer goes turbulent at much the same position after separation as does the shear layer of a short bubble, the turbulent mixing and entrainment process can no longer increase the pressure high enough for reattachment to occur at a short distance downstream of separation. Thus the turbulent shear layer reattaches much further downstream to form a long bubble. The peak velocity decreases which reduces the pressure gradient over the bubble. Long separation bubbles

exhibit a surface pressure distribution that has a smoother recovery to the unseparated boundary layer value. The region of constant pressure in a long bubble may be an appreciably smaller proportion of the total bubble length than in short bubbles and the reattaching flow may fluctuate noticeably [ref (26)].

In the present investigation it was observed that bubbles forming close to the leading edge of the airfoils for Reynolds numbers less than 200,000 and at high incidences, had length much greater than 10% of the chord but their effect on the pressure distribution was similar to that of short bubbles.

It was mentioned in section 3.1 that reattachment points were obtained from oil flow visualisation data as opposed to pressure measurements, when long bubbles formed at low incidences on the airfoil's upper surfaces. This is because, many empirical methods for obtaining reattachment points are valid only for short bubbles where the pressure distribution is not greatly altered from the unseparated boundary layer case. However, since this is not the case when long bubbles form, these methods are no longer valid. Flow visualisation produced a well defined dark zone or band where reattachment was deemed to have occurred. The actual reattachment location was assumed to occur at the centre of this band. This was because the turbulent reattachment region of the long bubble appears as a dark area and the extent of this region cannot be defined accurately. It should be noted, however, that reattachment points from oil flow visualisation data were read with an estimated accuracy of $\pm 2\%$ of the chord.

4.2 FLOW VISUALISATION

Doubts of the validity of the oil flow technique used in the present investigation are associated with the possibility of the paint film interfering with the flow in the boundary layer, and, also, that the streaks do not necessarily lie in the local flow direction because of gravitational and pressure gradient effects. Although there is undoubtedly, some substance to such objections, experience [ref (27)] has shown that the effects are small, and that the method gives reliable information in many complex conditions. Also analysis by Maltby [ref (27)] has led to the following conclusions:

- (a) As far as the motion of the oil relative to the boundary layer is concerned, the oil follows the boundary layer surface streamlines, except near separation where it tends to form an envelope upstream of the true separation envelope. This early indication of separation is less marked for turbulent than laminar boundary layers. The distance by which separation is apparently altered, depends on the oil thickness and the model size, but is independent of the oil viscosity as shown in Fig 4.3. Extrapolating from Fig 4.3 which shows the reduction in separation distance as percentage of the chord for an oil sheet with thickness 0.002" against speed, it would appear that in our case separation occurs less than 2% of the chord earlier, for all the Reynolds numbers tested.

(b) The effect of the oil flow on the motion of the boundary is very small in most practical cases.

(c) Special care was taken in interpreting the oil pattern at the lower Reynolds number tested because transition can be erroneously interpreted as separation. This is because at the lower Reynolds number, the skin friction at transition is quite low, whereas the pressure gradient is quite large and thus x-component of the oil velocity could tend to zero.

The fact that the addition of the oil sheet changes the roughness over the airfoil section and its subsequent effects such as tripping of the laminar boundary layer into a turbulent one has not been examined.

Flow visualisation gave a very good indication of the flow around both airfoil sections.

4.2.1 NASA GA(W)-1

For the NASA GA(W)-1 airfoil section, flow visualisation confirmed the indications given by the pressure distribution, for the existence and behaviour of the long bubble formed at an incidence range of 0.6° to 3.6° , for all the Reynolds numbers tested. That is, its length decreases with increasing incidence and Reynolds number. Increasing the Reynolds number decreases the length of the laminar shear layer, transition takes place earlier and as a consequence the turbulent shear layer reattaches at

an earlier position, thus reducing the bubble's length [ref (28)]. McGregor [ref (29)] noted that the length of a long bubble increases with increasing incidence. This is because reattachment occurs further downstream due to the nature of the pressure gradient although, the laminar portion of the separated shear layer decreases with increasing incidence and transition takes place slightly earlier. In the present case, however, the pressure gradient is such so that it permits earlier reattachment and thus reducing the length of the bubble. It is worth noticing that at 3.6° and for Reynolds numbers greater than 300,000 (see Figs 3.2a,b, and c), the long bubble disappears due to transition taking place before the laminar boundary layer separates, and so the flow remains fully attached. At 6.6° pressure measurements show no clear indication of a bubble being present on the airfoil section for all the Reynolds numbers tested. However flow visualisation indicated the existence of a long bubble close to the leading edge having length of approx 20% of the chord at an Re of 150,000. This reduced to a short one above an Re of 250,000 with length 10% of the chord.

At 12.6° and 16.6° , flow visualisation results agreed very closely with those obtained from the pressure measurements, for all the Reynolds numbers tested.

It was mentioned in section 3.3.1, that the turbulent separation line had a slight scalloped wave pattern which was observed at an incidence of 12.6° and for Reynolds numbers $\geq 350,000$. The mode of this pattern did not change with increasing Reynolds number. This 3-D spanwise flow

structure has been observed in the past by other investigators [ref (30)] as shown in Fig 4.4. It is attributed to the formation of streamwise vortices at separation due to an instability mechanism of the shear layer at high incidences. The effect of this structure is very important because of its potential influence on the near wake. For example, as shown in Fig 4.5, Althaus [ref (31)] gives evidence that such spanwise variations in flow properties can significantly influence drag determination by the near wake momentum-defect survey method.

4.2.2 NACA-0015

Flow visualisation was very useful in the examination of the flow at low to moderate incidences, where it clearly showed the formation of separation bubbles when these were not too apparent from the pressure distribution. For 0.6° and 3.6° a long bubble forms on the airfoil's upper surface which decreases in length with increasing incidence and Reynolds number, for the same reasons as those described for the GA(W)-1 airfoil. However, the pressure distribution gave no clear-cut indication of a bubble being present in this incidence range. The long bubble disappears above a Reynolds number of 400,000 for the 0.6° case while at 3.6° it decreases to a short bubble with length 8% of the chord at a Reynolds number of 500,000. At 6.6° , although no clear evidence could be inferred from the pressure distribution which would suggest the formation of a separation bubble, flow visualisation showed the existence of a long bubble close to the leading edge. As the Reynolds number was increased however the bubble reduced to a short

one above an Re of 300,000. For incidences of 9° and above flow visualisation agreed very closely with the indications given by the pressure distribution and gave a good picture of the different flow phenomena around the airfoil section.

The scalloped wave pattern observed in the turbulent separation line on the NASA GA(W)-1 model was seen again at an incidence of 13.1° and for Reynolds numbers above 350,000. The mode of the pattern was almost identical as the one observed for the NASA GA(W)-1 section and its existence is attributed to the same reasons as the ones discussed previously in this section.

4.3 PRESSURE MEASUREMENTS

4.3.1 NASA GA(W)-1

Two of the pressure distributions demonstrated the sensitivity of the boundary layer at low Re and at an angle of attack close to the stalling incidence. In particular at a Reynolds number of 150,000 and an incidence of 13.6° [see Fig 4.6b] the pressure distribution indicates the formation of a short bubble close to the leading edge. The turbulent boundary layer reattaches at approx 0.16 x/c and the pressure increases steadily till approx 0.65 x/c. After that there is a sudden decrease in the value of the pressure coefficient which remains more or less constant from that point onwards, and is almost identical to the one obtained in the respective chord range at an incidence of 14.67°, where the airfoil

was stalled [see Fig 4.6c]. Bearing in mind that the order in which the pressure measurements were made was from the last tapping on the upper surface to the leading edge and then back along the lower surface, the most likely explanation is, that although the airfoil was initially stalled, some sort of disturbance caused the boundary layer to "flick-on" the airfoil surface. The second pressure distribution which could be explained in a similar fashion is the one obtained at a Reynolds number of 400,000 and an angle of attack of 15.6° (see Fig 4.7b). This pressure distribution indicates the existence of a short bubble very close to the leading edge and has an almost constant pressure coefficient value from approx $0.06 x/c$ onwards indicating separation of the turbulent boundary layer. Initially one could explain the behaviour of this pressure distribution by the suggestion made by Hurley, Ward and Wallis [ref (22)] that turbulent separation can occur shortly downstream of reattachment.

However, the fact that the pressure distribution of the upper surface is almost identical, from approx $0.06 x/c$ onwards, to the one obtained at 16.6° [see Fig 4.7c] and the value of the lift coefficient equals the one obtained at an angle of attack of 14.6° [see Fig 3.38] indicates that this is not the case. Again this pressure distribution shows that the separated boundary layer is very sensitive at this critical angle of attack and can reattach onto the airfoil's surface at any time, due to influences in the tunnel environment such as free stream disturbances, mechanical vibrations and noise levels (refer to section 4.5). The above mentioned pressure distributions are very important since they

demonstrate how susceptible the boundary layer is close to the stalling incidence at low Reynolds numbers. It must be pointed out, however, that this behaviour is strongly pronounced only at low Re and shows that the results of the tests must be treated very cautiously near the critical angle of attack at which the airfoil stalls.

NACA 0015

The pressure distribution at a Reynolds number of 50,000 is shown in Fig 3.11. Nothing can be deduced about the behaviour of the boundary layer because the value of the pressure coefficient fluctuates violently along the chord and for all the incidences tested. This is likely to be attributed to either the sensitivity of the micromanometer since pressures corresponding to below 0.5mm H₂O had to be measured accurately or steady air flow conditions not being sustained since 50,000 is approx the minimum Reynolds number at which such conditions can be attained by the Glasgow University's low speed wind tunnel.

The sensitivity of the boundary layer close to the critical angle of attack at which stall occurs was once more demonstrated with this airfoil section at a Reynolds number of 500,000 and an angle of attack of 14.1° [see Fig 4.8b]. The value of the pressure coefficient indicates that the turbulent boundary layer separates at approx 0.45 x/c which is much earlier than it does at 13.6° where it separates at approx 0.8 x/c. The leading edge suction peak is slightly increased and the pressure measurements on the lower surface have identical values as at 13.6° [see

Fig 4.8a]. An abrupt increase in the value of the normal force coefficient is observed to occur from 13.6° to 14.1° [see Fig 3.41] which should not normally take place. However it is seen that the value of the pressure coefficient from $0.45 x/c$ is identical to the value obtained in the respective chord range when the airfoil section is fully stalled at 14.6° [see Fig 4.8c]. Its value has also considerably decreased compared to the one obtained when the turbulent boundary layer separates at 13.6° and accounts for the large increase in the normal force coefficient between the two cases. This leads us to believe that the initial pressure readings were made while the boundary layer was separated from the airfoil's surface. The boundary layer however reattached when the pressure tubes were measuring the reading at approx $0.45 x/c$ and produced the subsequent pressure distribution.

4.4 NORMAL FORCE AND PITCHING MOMENT

The investigations of Gault (32), together with McCullough (32) and of Peterson (33) on thin symmetrical NACA low-drag airfoils showed that the stalling characteristics were dependent on the behaviour and kind of laminar separation bubble present. McCullough and Gault have classified different stalling phenomena into three principal types as shown in Fig 4.9a:

- (i) Trailing edge stall where there is a gradual loss of lift at high lift coefficient values as the turbulent separation point moves forward from the trailing edge.

- (ii) Leading edge stall where there is a sudden loss of lift due to the breakdown of a short bubble at the leading edge.
- (iii) Thin airfoil stall with gradual loss of lift at low lift coefficient values due to the lengthening of a long bubble.

Also Carmichael (5) notes that the lift versus angle of attack curves undergo distortions relative to the forms to which we are accustomed at high Reynolds numbers. He classifies the forms into five categories as shown in Fig 4.9b.

- A: Linear well behaved as at high Reynolds numbers.
- B: Non-linear in the mid- C_L range.
- C: Hysteresis loop in the mid- C_L range.
- D: Hysteresis loop at or beyond C_{Lmax} .
- E: Very limited C_{Lmax} .

An attempt will be made in the following sections to relate some of the changes observed in the aerodynamic characteristics of the airfoils with the location and breadth of laminar separation bubbles and that of turbulent separation.

4.4.1 NASA GA(W)-1

At a Reynolds number of 100,000 there is a sudden and large drop in the normal force after 12.9° as shown in Fig 3.32 which suggests leading edge type of stall. In the Reynolds number region of 150,000 to

500,000 there is a gradual loss of the normal force (and subsequently of lift) as stall is approached as shown in Fig 3.33 to 3.40 which suggests trailing edge type of stall.

The maximum value of the normal force coefficient C_{Nmax} is 1.21 at a Reynolds number of 100,000 and is higher than the one obtained for Reynolds numbers of 150,000 and 200,000 which is 1.14 as shown in Fig 4.10b. This shows the somehow "irregular" behaviour of the boundary layer at low Reynolds numbers since one would expect the value of C_{Nmax} to increase steadily with increasing Reynolds number.

The C_N versus α curves are almost identical for Reynolds numbers of 150,000 and 200,000 as shown in Fig 4.10a. The existence of a long bubble which is located after the mid-chord position does not seem to significantly affect the performance of the airfoil section in the low incidence range of 0.6° to 4.6° . On the contrary, the highest $\frac{dC_N}{d\alpha}$ is obtained in that region. As the incidence is increased flow visualisation indicated the formation of a long bubble close to the leading edge of the airfoil and turbulent separation to occur near the trailing edge. This causes a decrease in the $\frac{dC_N}{d\alpha}$ slope. Further increases in the incidence cause the bubble to decrease in length but the turbulent separation point moves forwards from its previous position thus resulting in new reductions in the $\frac{dC_N}{d\alpha}$ slope until stall is reached.

For Reynolds numbers of 250,000 to 500,000 (see Fig 4.10a) the behaviour of the $\frac{dC_N}{d\alpha}$ slope is explained in a similar manner. In

these cases however the long bubble is present only in the lowest angles of attack tested and for a smaller incidence range than previously which decreases as the Reynolds number is increased. A short bubble is formed for incidences above 6.6° which should theoretically increase $\frac{dC_N}{d\alpha}$, but it appears that the major factor for the reduction in the $\frac{dC_N}{d\alpha}$ slope, is the forward movement of the turbulent separation point from the trailing edge. There are certain anomalies observed in the value of C_{Nmax} as shown in Fig 4.10b. It has a value of approx 1.20 for Re of 250,000 and 300,000 while its value is 1.22, 1.23, 1.25 and 1.22 for Re of 350,000, 400,000, 450,000 and 500,000 respectively.

4.4.2 NACA-0015

At a Reynolds number of 100,000 the airfoil appears to exhibit leading edge type of stall since there is a sudden loss of the normal force above 11.1° as shown in Fig 4.11a. Unfortunately no oil flow visualisation data exists for this Reynolds number and the pressure distributions do not give a clear picture of the boundary layer behaviour in the low to moderate incidence range. As the Reynolds number is increased to 150,000 and 200,000 the airfoil appears to undergo a combination of leading and trailing edge type of stall since there is a gradual loss of the normal force followed by a rapid one at stall. This type of stall has also been observed by other investigators [ref (25)] but in a non-symmetrical airfoil section. There is an increase in the $\frac{dC_N}{d\alpha}$ slope as the incidence is increased from 3.6° to 4.6° for both Reynolds numbers. This is due to the considerable shortening of the long

bubble which forms approx $0.3 x/c$ for both cases and covers a large part of the airfoil's upper surface. As the incidence increases the bubble length decreases further but turbulent separation occurs forwards from the trailing edge thus reducing the $\frac{dC_N}{d\alpha}$ slope. In general it can be seen that the amount by which the $\frac{dC_N}{d\alpha}$ slope changes is strongly dependant on the length and location of the separation bubble present and the location of turbulent separation. The value of the C_{Nmax} behaves as at high Reynolds numbers, that is it increases from 0.87 to 0.92 for Re of 150,000 and 200,000 respectively as shown in Fig 4.11b.

For Reynolds numbers between 250,000 and 500,000 the airfoil appears to exhibit leading edge type of stall as shown in Fig 4.11a. The normal force coefficient versus angle of attack curves are non-linear in the mid- C_N range and fall well within one of the types of behaviour observed by other investigators [ref (5)] [see Fig 4.9b]. This discontinuity in the $\frac{dC_N}{d\alpha}$ slope is due to the formation of a short laminar separation bubble close to the leading edge as opposed to the long bubble which forms at lower incidences and covers most of the central part of the airfoil section. The reduction of the $\frac{dC_N}{d\alpha}$ slope after the point of discontinuity is due to the forward movement of the turbulent separation point from the trailing edge. The particular sensitivity of the boundary layer is once more demonstrated by the value of the max normal force coefficient as shown in Fig 4.11b. In the Reynolds number range from 250,000 to 300,000 it increases from 0.95 to 1.00, it then decreases and remains constant between 350,000 and 400,000 with a value of 0.96. Finally its value decreases from 1.02 to 0.97 for Reynolds numbers of 450,000 and 500,000 respectively.

The effect of the formation of a long bubble in the central part of the airfoil section has a significant effect on the aerodynamic characteristics of this airfoil section, particularly for Re below 250,000 and increases the value of C_N at low incidences, as shown in Fig 4.11a. At sufficiently high Reynolds numbers (above 300,000) the long bubble disappears at low incidences but it appears that this produces lower values of C_N in this incidence range.

4.5 TUNNEL EFFECTS

The effect of free stream disturbances on the aerodynamic characteristics of the airfoils varies with magnitude, frequency content and source of disturbance [ref (14)]. The disturbance environment present in the test section is usually determined by free stream turbulence (velocity fluctuations), acoustic phenomena (pressure fluctuations) and mechanical vibrations. The free stream turbulence level depends on the history of the flow in the settling chamber, flow straighteners or screens and inlet leading to the test section. Acoustic phenomena are related to the noise emitted from turbulent boundary layers on the side walls, unsteady separated flow regions and the fan and its associated drive system. Mechanical vibrations may be caused by rigid coupling of the fan and the drive system of the wind tunnel.

The lift and drag performance of a smooth Lissaman airfoil, taken from [ref (14)], in the lowest turbulence, quietest wind tunnel configuration that could be attained in that facility is shown in Fig

4.12a. It was found that a significant hysteresis region existed in the lift and drag forces. the presence and extend of this hysteresis was determined by the location of separation and/or transition in the boundary layer. The location of transition from laminar to turbulent flow in the boundary layer has been known to be affected by the level and type of free stream disturbances for a long time [ref (6)]. The result of changing the acoustical environment by adding one flow restrictor at the end of the test section is shown in Fig 4.12b. The addition of one restrictor increases both the free stream turbulence level and sound pressure level for a fixed value of the tunnel velocity. This test section environment reduced the size of the hysteresis region and produced a slightly higher C_{Lmax} of almost 1.4. Increasing the free stream turbulence level to about 0.3% by adding one 7.09 meshes/cm screen at the upstream end of the test section with no flow restrictor produced the lift and drag coefficients presented in Fig 4.12e. This test section environment completely eliminated the hysteresis region and yielded values of C_{Lmax} between those of Fig 4.11a and 4.11b. It is apparent that, in general, each wind tunnel has a different disturbance environment which is a function of its design and method of fabrication. It is not surprising therefore, that similar experiments on the same geometry model at low Reynolds numbers often produce results which may differ considerably from one wind tunnel to the next.

The layout at Glasgow University's low speed tunnel (see Fig 2.1) makes it inevitable that the motor and the fan will be the main contributors to the tunnel noise and mechanical vibrations and little

could be done to eliminate this, given the proximity of the motor to the working section. A turbulence intensity of 0.5% in the working section is quoted by Kelling [ref (17)] but it should be noted that his investigation was concerned with Reynolds numbers of approx 400,000 and above.

The extreme sensitivity of the boundary layers of the two airfoil models to the free stream disturbance environment would be pronounced in the present investigation for all the Re tested, and particularly close to the stalling incidence. This was shown by the non-uniform variation of the max C_N value as the Reynolds number increased [see Figs 4.10b and 4.11b] and also by the fact that each airfoil section appeared to exhibit two different types of stall.

Free stream disturbances, mechanical vibrations and noise levels are a major source of disparity in experimental data at low Reynolds numbers. However model imperfections or surface roughness can produce results identical to those achieved due to the above mentioned influences [ref (33)].

4.6 COMPARISON OF GA(W)-1 AIRFOIL SECTION CHARACTERISTICS WITH EXISTING DATA

Published data on the GA(W)-1 airfoil section exist in the Reynolds number range from about 2×10^6 to 12×10^6 [ref (9)]. However, these data are not corrected for any blockage effects of the tunnel. Although presently the airfoil was tested for Reynolds numbers of about 500,000

and below, a brief comparison of the aerodynamic characteristics will be made. For this purpose the normal force and pitching moment coefficient at 500,000 is displaced together with the aerodynamic characteristics obtained from [ref (9)] at $\approx 2 \times 10^6$ in Fig 4.13. The GA(W)-1 airfoil section encounters trailing edge type of stall for both Reynolds numbers and the angle at which stall takes place is approx 16° . However there is a considerable difference of approx 0.37 between the max section lift coefficient C_{Lmax} at 2×10^6 and the max normal force coefficient at 500,000. In the previous experimental investigation [ref (9)] it was found that the value of the C_{Lmax} was 1.6, 1.8 and 2.0 for Reynolds numbers of 2×10^6 , 4×10^6 and 6×10^6 respectively. There is an increase of 0.2 in the value of C_{Lmax} as the Re is raised successively by 2×10^6 . The difference in Reynolds number between the two curves compared in Fig is 1.5×10^6 which could account if taken proportionally for almost half of the difference obtained in the values of C_{Lmax} and C_{Nmax} . Bearing in mind, however, that the boundary layer behaviour changes dramatically for Re numbers below 1.0×10^6 , i.e. thickens appreciably thus reducing the lift by a large amount, the above mentioned difference may be expected. Also the present results are corrected for blockage effects while those obtained at 2×10^6 are not. Finally there is a big difference in turbulent intensity levels between the two wind tunnels where the experiments were carried out of approx 0.4%. It is very difficult to state in which way this considerable difference in the test environment would influence the results on that particular airfoil section, but undoubtedly it contributes to the difference observed in the values of C_{Lmax} and C_{Nmax} .

The pitching moment coefficient data indicated more negative values of C_M at 2×10^6 since the boundary layer thickens decreases as the Reynolds number increases as shown in Fig 4.13. The trends however in both curves are the same up to the stalling incidence. That is the value of C_M is nearly constant up to 4° which above that incidence it increases steadily.

It is interesting to note that the addition of roughness at $0.08c$ on the GA(W)-1 airfoil model in the previous investigation produces values of C_L and C_M which lie closely to the ones obtained presently in the low-angle of attack range of 0° to 4° as shown in Fig 4.13. This is likely to be the result of a thicker boundary layer induced by the addition of roughness.

4.7 COMPARISON OF NACA-0015 AIRFOIL SECTION CHARACTERISTICS WITH EXISTING DATA

Normal force coefficient versus angle of attack plots obtained from present and other experimental investigations [ref(23)] on the NACA-0015 section and for various Reynolds numbers are shown in Fig 4.14. For Reynolds numbers of 200,000, 300,000 and 400,000 the trends in the normal force coefficient curve are more or less the same but the present experimental values of C_N have slightly higher values. Also stall is delayed by about 2° and there is a difference of approx 0.1 in the value of C_{Nmax} for all three cases. The delay in the angle at which stall occurs and the higher values of C_{Nmax} obtained in the current

tests could be attributed to the different turbulent intensity levels of the two wind tunnels. Glasgow University's tunnel has a turbulence level of approx 0.5% while the previous test facility had a turbulence level of approx 0.1%. This difference is quite considerable and as already mentioned in section 4.5 a higher turbulence level tunnel can produce similar results. Additionally there is the effect of noise levels and mechanical vibrations, the magnitude of which changes with Reynolds number. The combined effect of all these three determining factors of the test environment at various Reynolds numbers can have different influences on the boundary layer and consequently on the results of the tests. This could be a possible explanation for the fact that the values of C_N at an Re of 500,000 in the present investigation are lower than the ones obtained from [ref (23)] as shown in Fig 4.14. The maximum value of C_N was approx 1.00 and the values of C_N are exactly the same in the incidence range of 0° to 4° for both cases.

4.8 COMPARISON OF THE GU25-5(11)8, NASA GA(W)-1 AND NACA-0015 AIRFOIL SECTION CHARACTERISTICS

The GU25-5(11)8 is a 'low-drag' airfoil section and was designed by T. Nonweller at Glasgow University. Extensive tests on this airfoil section have been carried out at GU low speed wind tunnel in the period from 1968 to 1985 [ref (17,34,35,36)]. The results of these tests are too voluminous to be included in this thesis. However the important features of the results are summarised in Figs 4.15 to 4.18. The lift curves in Fig 4.15 show quite clearly how laminar separation affects the

lift coefficient at a given Reynolds number. In this case the laminar boundary layer separates from the upper surface of the airfoil before the mid-chord position and never reattaches, as a result of which the value of the lift coefficient and of the lift curve slope is very low. As the incidence is increased however a laminar separation bubble forms close to the mid-chord position and the flow reattaches. This increases by a large amount the value of C_L and there is an abrupt change in the lift curve slope for Reynolds numbers between 100,000 and 300,000, the intensity of which decreases with increasing Re. Also the angle at which this large increase in the lift curve slope takes place decreases with increasing the Reynolds number. The increase in lift curve slope is accompanied by a large decrease in the value of the pitching moment coefficient as shown in Fig 4.15.

An interesting observation is made concerning the angle at which the airfoil stalls as the Reynolds number increases. Contrary to what was observed in the current investigation, that is, the angle at which stall occurs increases as the Re increases, the GU25-5(11)8 airfoil stalling angle decreases with increasing Re (see Fig 4.15). This could be explained by the fact that the unstable bubble observed to form at approx mid-chord [ref (35)] became more stable as the Re increased. This in turn would imply that trailing edge separation would start earlier as a result of which stall takes place at a lower angle of attack.

The variation of the maximum lift coefficient with Reynolds number for the GU25-5(11)8, GA(W)-1 and NACA-0015 airfoil sections

are shown in Figs 4.10b, 4.11b and 4.19. The GU25-5(11)8 has a much higher value of C_{Lmax} at each Reynolds number than the value of C_{Nmax} of the other two sections. Also the GA(W)-1 has higher values of C_{Nmax} than the NACA-0015. These differences however could be attributed to the fact that the GU25-5(11)8 airfoil section is 3% and 5% thicker than the GA(W)-1 and NACA-0015 respectively. A thicker section implies more camber as shown in Figs 2.1,2 and 3 therefore more lift.

In order to obtain a better overall picture of the performance and of the operational range of each airfoil section, contours of constant C_L and C_N are plotted against a base of incidence and Reynolds number. These are shown in Fig 4.17, 4.20 and 4.21. Care must be taken in interpreting the word performance since in the current investigation no drag measurements were made and therefore the overall aerodynamic characteristics of the airfoil sections are not available. The context in which this word is used merely refers to the normal force and pitching moment characteristics.

The GU25-5(11)8 airfoil section has been found to suffer badly from laminar separation at two 'critical' Reynolds numbers namely at 320,000 and 75,000 as shown in Fig 4.17 and 4.18 [ref (36)]. These are 'critical' since with the contour lines close together a small change in either Reynolds number or incidence will result in a large change in C_L and $C_{M\frac{1}{4}}$. It can also be seen from the contour that there is a critical incidence for each Reynolds number between these limits. These results clearly show that there are operating limits which would apply to any

practical application for which a GU25-5(11)8 airfoil might be used, namely at Reynolds numbers above 350,000 and at incidences below the stalling incidence [see Fig 4.17] [ref (35,36)].

The C_N contour for the NASA GA(W)-1 airfoil section as shown in Fig 4.20 indicates a more gradual drop of lift in the Reynolds number region of 50,000 to 200,000 than the one obtained for the GU25-5(11)8 airfoil at 72,000 and 320,000. For Reynolds numbers greater than 200,000 the contour lines are almost straight lines spaced widely apart, showing that the airfoil can be safely operated in this region and up to a maximum normal force coefficient of 1.17. Although this airfoil section gives an additional lower Reynolds number operating range, it has a maximum normal force coefficient which is approx 0.3 lower than the C_{Lmax} obtained for the GU25-5(11)8 section. So the advantage of a greater Reynolds number operational range is counterbalanced by the fact that it produces much lower lift.

The C_N contour for the NACA-0015 section is shown in Fig 4.21 and indicates an insensitivity of the value of C_N with Reynolds number. The contour lines are almost straight lines from a Reynolds number of 100,000 onwards. This implies that this airfoil section can be operated down to that Reynolds number range. The lowest Re operational limit is increased by 250,000 and 100,000 compared to the GU25-5(11)8 and GA(W)-1 airfoil sections respectively. The value of the max C_N coefficient is decreased however by approx 0.2 compared to the GA(W)-1 section and by 0.6 compared to the GU25-5(11)8 section.

From the C_N and C_L contours it can be seen that the stalling incidence for all three airfoil sections lies close to 12° . This therefore doesn't infer any differences in the incidence range at which the three airfoil sections can operate. Although the GU25-5(11)8 section suffers badly from laminar separation for Re below 350,000, above that Re it proves to have by far the best performance compared to the other two sections. However in the Reynolds numbers between 350,000 to 200,000 and 200,000 to 100,000 the NASA GA(W)-1 and the NACA-0015 show to have the best performance respectively.

4.9 CONCLUSIONS

- i) Flow visualisation gave a good indication of the flow around the airfoil models. It was particularly useful for obtaining flow characteristics when these were not apparent from the pressure distributions. Close agreement was obtained in areas where the pressure measurements clearly indicated the behaviour of the flow around the airfoil sections.

- ii) The aerodynamic characteristics showed that the NACA-0015 section exhibits mainly leading edge type of stall with an exception at a Reynolds number of 150,000 and 200,000 where it shows a combination of leading and trailing edge type of stall. The NASA GA(W)-1 section exhibits trailing edge type of stall with an exception at a Reynolds number of 100,000 where it appears to undergo leading edge type of stall.

- iii) Comparison of the aerodynamic characteristics of the GU25-5(11)8, NASA GA(W)-1 and the NACA-0015 sections revealed that the operational ranges of these airfoils would be above a Reynolds number of 350,000, 200,000 and 100,000 respectively. However the max operational lift coefficient obtained for the GU25-5(11)8 airfoil section is 1.5 and is higher than the ones obtained for the NASA GA(W)-1 and the NACA-0015 by approximately 0.33 and 0.6 respectively.

- iv) The sensitivity of the boundary layer in the Reynolds number range of 50,000 to 500,000 to the test environment was shown by the behaviour of a few pressure distributions, the non-uniform variation of C_{Nmax} and the two different types of stall exhibited by each airfoil section.

- v) The existence of a long bubble in the low incidence range of 0° to 4° on the upper surface of the NACA-0015 airfoil section and for Reynolds numbers smaller than 300,000 proved to induce values of normal force coefficient which were higher than the ones obtained at higher Re in the respective incidence range where the flow was fully attached.

CHAPTER 5
CONCLUSIONS AND SUGGESTIONS FOR FUTURE WORK

I)

Oil flow visualisation provided essential information concerning the different flow regimes which occur on the airfoil's upper surfaces in the Reynolds number range of 150,000 to 500,000 and for all the incidences tested. It confirmed the initial assumption for nominal two-dimensional flow over the major part of both airfoil sections. It also, indicated the formation of long bubbles on the airfoil's upper surfaces in the low incidence range of 0.6° to 4.6° . In doing so, it was particularly useful, since no accurate deduction could be inferred from the pressure measurements with respect to the existence and behaviour of such separation bubbles. The formation of this bubble takes place a distance after the point of max thickness of both airfoil sections, namely at about $0.30c$ and $0.55c$ for the NACA-0015 and NASA-GA(W)-1 respectively. However the behaviour of this bubble is similar for both cases, that is, its length decreases considerably with increasing the Reynolds number and angle of attack.

In areas, where the pressure measurements gave a clear indication of the behaviour of the flow, close agreement was obtained with the flow characteristics observed using the oil flow visualisation technique.

- II) Maximum normal force coefficients varied non-uniformly with increasing the Reynolds number from about 100,000 to 500,000 for both airfoil sections. The value of the max normal force coefficients was 1.26 and 1.02 for the NASA GA(W)-1 and NACA-0015 respectively.
- III) The NACA-0015 airfoil section was found to exhibit leading edge type of stall with an exception at a Reynolds number of 150,000 and 200,000 where it appears to undergo a combination of leading and trailing edge type of stall. The NASA GA(W)-1 section exhibits a gradual or trailing edge type of stall with an exception at a Reynolds number of 100,000 where it shows stalling characteristics of the leading edge type.
- IV) The extreme sensitivity of the boundary layer to disturbances in the test environment was shown by the behaviour of some pressure distributions, the non-uniform variation of C_{Nmax} and the two different types of stall exhibited by each airfoil section.
- V) The somewhat "irregular" behaviour of the boundary layer at low Reynolds numbers was demonstrated by the fact that the existence of the long bubble in the low incidence range of 2.6° to 5.6° on the upper surface of the NACA-0015 section and for Re smaller than 300,000, proved

to induce values of normal force coefficient which were higher than the ones obtained at higher Re in the respective incidence range where the flow was fully attached.

VI) Finally, comparison between the GU25-5(11)8, NASA GA(W)-1 and NACA-0015 sections revealed that the operational ranges of these airfoils to be above a Reynolds number of 350,000, 200,000 and 100,000 respectively. However the max operational lift coefficient obtained for the GU25-5(11)8 airfoil section is 1.5 and is higher than those obtained for the NASA GA(W)-1 and NACA-001 by approx 0.33 and 0.6 respectively.

5.2 SUGGESTIONS FOR FUTURE WORK

The prime objective of the present investigation was to compare the aerodynamic characteristics of the GU25-5(11)8 airfoil section with those of the NASA GA(W)-1 and the NACA-0015 in the low Reynolds number range of 50,000 to 500,000. By using models of the same size and testing them in the same wind tunnel, all three airfoil sections are subjected to the same free stream turbulence, noise levels and mechanical vibrations. Therefore, the results of these tests are directly comparable. However, as mentioned in section 4.5, it is well known that the above mentioned influences vary from one wind tunnel to another and are a major source of discrepancy in experimental data obtained on similar tests. In order for the present data to be useful and meaningful to other experimental

investigators, it is very important that in future, an accurate recording of each of these disturbances is made for all Reynolds numbers tested. Furthermore, although it appears that little can be done to eliminate noise levels and mechanical vibrations due to the layout of Glasgow University's low speed wind tunnel, free stream turbulence can be reduced. This can be done by installing a number of anti-turbulence screens and it would be very interesting to see the effect of these on the results of the tests.

As far as the computer system used for the data acquisition and reduction is concerned, it is suggested that the IBM PC or compatible is employed. This is because it has a greater memory, faster processing capability and better graphics display than the MINC 11/23. Also it is suggested that a new computer program is developed which will enable the automatic processing of data immediately after each test run. That was not done currently since the program used for data acquisition was written in Basic while the program used for data reduction was in Fortran IV. The immediate processing and displaying of the experimental data enables the investigator to check the data from a test run and if necessary to repeat the run. In the present investigation, a considerable amount of time was spent confirming the validity of certain experimental data, especially at the lowest Reynolds numbers tested, by repeating a number of test runs after each series of tests had been concluded.

Another time consuming procedure proved to be the spalling manual change of angle of attack of the model. It is estimated that at least 3 to 4 minutes were spent between each test run to ensure the accurate change in incidence. It is advisable that in future, a mechanism is installed which will permit the remote control change in angle of attack and thus the whole process will be facilitated.

It would be interesting to see the difference (if any) in the results of testing the same type of airfoil sections using the direct force balance of Glasgow University's low speed tunnel, namely the lift and pitching moment. Although this measuring technique does not provide any information for the chordwise pressure distribution it appears that it is the most suitable for measuring the very small drag forces which occur in the low Reynolds number range of 50,000 to 500,000. This is because as mentioned in section 2.5, there are large errors induced when measuring the drag using a wake rake arrangement.

As far as flow visualisation is concerned, it is suggested that smoke visualisation should also be used in the future to give valuable information about the behaviour of the boundary layer for Reynolds numbers smaller than 150,000, since this was not possible by applying the oil flow visualisation technique. Also, provided a very fine atomizer is used, the china clay method [refer to section 2.7] can be applied for obtaining the different flow regimes which occur around an airfoil section as an alternative to oil flow visualisation.

Finally the use of a micromanometer with a greater operational range of 0 - 199.9mm H₂O is advised if pressures are to be recorded above a Reynolds number of about 500,000. This is because in the present investigation the micromanometer went out of its maximum range when testing the airfoil sections at a Re of about 550,000.

5.3 CONCLUDING DISCUSSION

The validity of the present results could be put under some criticism, since the test facility used has a relatively high free stream turbulence and noise levels etc.. Most of the modern test facilities used for low Reynolds number airfoil testing have a very low level of these disturbances. This is because it appears that the aerodynamic characteristics of an airfoil section are favourably influenced, especially close to the stalling incidence, by a high level of free stream turbulence or noise. Therefore, in real flight, and under conditions where both of these disturbances are minimal, the airfoil section won't perform in the predicted manner. However there are several practical applications such as mini-RPVs flying at low altitude, root rotor parts of helicopter blades and wind turbine generators where there is a considerable amount of noise emitting from the engine as well as a high level of free stream turbulence due to wind and gusts. Thus it seems that the practical applicability of the current results for such purposes should be valid.

From the results discussed in the previous sections, it is evident that what was originally thought as very poor performance for the

GU25-5(11)8 airfoil section is not totally justified. Comparison with the two airfoil sections tested presently, namely the NASA GA(W)-1 and NACA-0015, revealed that, although they have much lower Reynolds number operational ranges, the GU25-5(11)8 has a significantly higher lift coefficient. The GU25-5(11)8, NASA GA(W)-1 and NACA-0015 have a Reynolds number operational range above 350,000, 200,000 and 100,000 and a max C_L of about 1.5, 1.17 and 0.9 respectively. The choice therefore between one of these airfoil sections for a particular application depends on the specific requirements, that is whether it is important to have an efficient airfoil section operating in a lower Reynolds number range, irrespective of the fact that this would cost in lift performance or vice-versa.

References

1. LISSAMAN, P.B.S. "Low Reynolds Number Airfoils", Annual Review of Fluid Mechanics, 15, pp 223-239, 1983.
2. McMASTERS, J.H. and HENDERSON, M.L. "Low Speed Single Element Airfoil Synthesis", NASA CP 2085, Part I, pp 1-31, March 1979.
3. JANSEN, B.J. and MUELLER, T.J. "Experimental Studies of the Boundary Layer on an Airfoil at Low Reynolds Numbers", AIAA paper 83-1671.
4. POHLEN, L.J. and MUELLER, T.J. "Boundary Layer Characteristics of the Miley Airfoil at Low Reynolds Numbers", AIAA paper 83-1795.
5. CARMICHAEL, B.H. "Low Reynolds Number Airfoil Survey", NASA-CR-165803, Vol. 1, November 1981
6. SCHLICHTING, H. "Boundary Layer Theory", Seventh Edition, McGraw-Hill Book Company, 1979.
7. MUELLER, T.J. and BATILL, S.M. "Experimental Studies of Separation on a Two-Dimensional Airfoil at Low Reynolds Numbers", AIAA Journal, Vol. 20, No. 4, pp 457-463, April 1982.

8. KOKKALIS, A. "An Investigation into the Wake Flow Behind Circular Cylinders Fitted with Slat Devices", M.Sc. Dissertation, Glasgow University, APRIL 1983
9. McGBEE, R.J. and BEASLEY, W.D. "Low Speed Aerodynamic Characteristics of a 17-percent Thick Airfoil Section Designed for General Aviation Applications", NASA-TN D-7428, December 1973
10. MUELLER, T.J. "Low Reynolds Number Vehicles", AGARD-AG-288.
11. MUELLER, T.J. and BATILL, S.M. "Visualisation of Transition in the Flow over an Airfoil Using the Smoke-Wire Technique", AIAA Journal, Vol. 19, No. 3, pp 340-345, March 1981.
12. SELIG, M.S. "The Design of Airfoils at Low Reynolds Numbers" AIAA paper 85-0074.
13. MUELLER, T.J. "The Influence of Laminar Separation and Transition on Low Reynolds Number Airfoil Hysteresis", AIAA 84-1617
14. MUELLER, T.J., CONIGLIARO, P.E. and JANSEN, B.J. "The Influence of Free-Stream Disturbances on Low Reynolds Number Airfoil Experiments", Experiments in Fluids, Vol. I, pp 3-14, 1983.
15. RICHARDS, E.J. and BURSTALL, F.H. "The China-Clay Method of Indicating Transition", Reports and Memoranda No. 2126, Aug 1945.

16. POPE, A. and HARPER, J.J. "Low Speed Wind Tunnel Testing", John Wiley & Sons Book Company, 1966.
17. KELLING, F.H. "Experimental Investigation of a High-Lift Low-Drag Aerofoil", Glasgow University, Aeronautics Department, Report No. 6802, September 1968.
18. KOKKODIS, G. Departmental report in progress, Glasgow University, Aeronautics Department. "COLLECTED DATA FOR LOW REYNOLDS NUMBER PERFORMANCE ON A GA(W)-1 AEROFOIL".
19. KOKKODIS, G. Departmental report in progress, Glasgow University, Aeronautics Department. "COLLECTED DATA FOR LOW REYNOLDS NUMBER PERFORMANCE ON A NACA-0015 AEROFOIL".
20. ARENA, A.V. and MUELLER, T.J. "On the Laminar Separation, Transition and Turbulent Reattachment of Low Reynolds Number Flows Near the Leading Edge of Airfoils", AIAA paper 79-0004.
21. McMASTERS, J.H., NORDVIK, R.H., HENDERSON, M.L. and SANDVIG, J.H. "Two Airfoil Sections Designed for Low Reynolds Number", Technical Soaring, Vol. VI, No. 4.
22. WARD, J.W. "Behaviour and Effects of Laminar Separation Bubbles on Airfoils in Incompressible Flow", Journal of the Royal Aeronautical Society, Vol. 67, pp 783-789, December 1963.
23. MEYER, J.R. and FALABELLA, G.J. "An Investigation of the Experimental Aerodynamic Loading on a Model Helicopter Rotor Blade", NACA TN 2953, MAY 1953

24. YOUNG, A.D. and HORTON, H.P. "Some Results of Investigations of Separation Bubbles", AGARD Conference Proceedings, Part I, No. 4, pp 779-813.
25. RENDER, P.H. "An Experimental Investigation into the Effects of Modifying the Trailing Edge Geometry of a Wortmann FX63-137 Aerofoil". *CONFERENCE ON R.P.V's, LONDON, 1983*
26. GAULT, D.E. "An experimental Investigation of Regions of Separated Laminar Flow", NACA Technical Note No. 3505, September 1955.
27. SQUIRE, L.C. and MALTBY, R.L. "The Surface Oil Flow Technique", AGARDograph 70, Part I, pp 1-75.
28. GASTER, M. "The Structure and Behaviour of Laminar Separation Bubbles", AGARD Conference Proceedings, Part II, No. 4, pp 813-855, May 1966.
29. MCGREGOR, I. "Regions of Localised Boundary Layer Separation and Their Role in the Nose Stalling of Airfoils", Ph.D. Thesis, Queen Mary College, London, June 1954.
30. INGER, G.R. "A Theoretical Study of Spanwise-Periodic 3-D Disturbances in the Wake of a Slightly Stalled Wing at Low Reynolds Numbers". *CONFERENCE ON AERODYNAMICS AT LOW REYNOLDS NUMBERS ($10^4 < Re < 10^6$) LONDON OCT 1986*

31. ALTHAUS, D. "Drag Measurements on Airfoils;" Paper presented to the SVII OSTIV Congress, Paderborn, FRG, (1981).
32. McCULLOUGH, G.B. and GAULT, D.E. "Examples of Three Representative Types of Airfoil Stall at Low Speed", NACA Technical Note 2502, September 1951.
33. NELSON, R.C. "The Influence of Airfoil Roughness on the Performance of Flight Vehicles at Low Reynolds Numbers", AIAA Paper 84-0540.
34. LAING, S. "Wind Tunnel Testing of Airfoil Sections", Final year project, University of Glasgow, April 1984.
35. SPALDING, D.J. "Wind Tunnel Testing of Airfoil Sections", Final year project, University of Glasgow, March 1985.
36. LUNDE, K. "Wind Tunnel Testing of Airfoil Sections" Final year project, University of Glasgow, April 1983.

TABLE 1

NASA GA(W)-1 AIRFOIL COORDINATES
[c = 30cm]

x/c	(z/c) upper	(z/c) lower
0.0	0.0	0.0
.002	.01300	-.00974
.005	.02035	-.01444
.0125	.03069	-.02052
.025	.04165	-.02691
.0375	.01974	-.03191
.05	.05600	-.03569
.075	.06561	-.04209
.100	.07309	-.04700
.125	.07909	-.05087
.150	.08413	-.05426
.175	.08848	-.05700
.20	.09209	-.05826
.25	.09778	-.06265
.30	.10169	-.06448
.35	.10409	-.06517
.40	.10500	-.06483
.45	.10456	-.06344
.50	.10269	-.06091
.55	.09917	-.05683
.575	.09374	-.05396
.60	.09374	-.05061
.625	.09013	-.04678
.65	.08604	-.04265
.675	.08144	-.03830
.700	.07639	-.03383
.725	.07096	-.02930
.750	.06517	-.02461
.775	.05913	-.02030
.800	.06291	-.01587
.825	.04644	-.01191
.850	.03983	-.00852
.875	.03313	-.00565
.900	.02639	-.00352
.925	.01965	-.00248
.950	.01287	-.00257
.975	.00604	-.00396
1.000	-.00074	-.00783

TABLE 2

NACA 0015 AIRFOIL COORDINATES
[c = 30cm]

x/c	(z/c) _{upper}	(z/c) _{lower}
0.00	0.00	0.00
0.005	0.01526	-0.01526
0.01	0.02129	-0.02129
0.03	0.0355	-0.0355
0.04	0.04033	-0.04033
0.049	0.04443	-0.04443
0.0699	0.0510	-0.0510
0.08	0.0538	-0.0538
0.089	0.0563	-0.0563
0.0999	0.05853	-0.05853
0.125	0.06316	-0.06316
0.175	0.0696	-0.0696
0.225	0.07323	-0.07323
0.2749	0.07483	-0.07483
0.325	0.07484	-0.07484
0.375	0.07356	-0.07356
0.4249	0.07123	-0.07123
0.475	0.0680	-0.0680
0.525	0.0641	-0.0641
0.575	0.0595	-0.0595
0.625	0.0544	-0.0544
0.6749	0.04876	-0.04876
0.7249	0.0427	-0.0427
0.775	0.03616	-0.03616
0.825	0.02926	-0.02926
0.875	0.0219	-0.0219
0.925	0.01413	-0.01413
0.975	0.00586	-0.00586
1.00	0.00156	-0.0156

TABLE 3

NASA GA(W)-1 AIRFOIL ORIFICE LOCATIONS

Upper Surface

x/c
0.00000
0.00033
0.00116
0.00153
0.01037
0.01662
0.02281
0.03079
0.03843
0.04648
0.05280
0.06078
0.06876
0.07933
0.08672
0.0933
0.10281
0.15747
0.26434
0.3159
0.369

Upper Surface

x/c
0.419
0.4739
0.52876
0.5828
0.6357
0.68717
0.74004
0.78971
0.84431
0.85289
0.86240
0.87969
0.88840
0.89665
0.90563
0.92192
0.930704262
0.936822504
0.954512203
0.975793
1.00

Lower Surface

x/c
0.01037
0.01702
0.02414
0.03617
0.04402
0.05473
0.06670
0.07754
0.08851
0.13519
0.24193
0.39722
0.5509
0.69961
0.84744
0.96741
0.98071
1.000

TABLE 4

NACA 0015 AIRFOIL ORIFICE LOCATIONS

Upper Surface	Upper Surface	Lower Surface
x/c	x/c	x/c
0.00	0.4936	0.002
0.0005	0.5330	0.009
0.007	0.5745	0.0184
0.0172	0.6156	0.0276
0.0285	0.6547	0.0427
0.0387	0.6935	0.052
0.049	0.7125	0.062
0.05786	0.7345	0.0712
0.06953	0.7515	0.0835
0.0812	0.7747	0.09
0.09	0.7912	0.195
0.1326	0.8145	0.297
0.173	0.8347	0.397
0.2122	0.8562	0.498
0.2536	0.8725	0.599
0.2926	0.8958	0.698
0.3326	0.9112	0.798
0.3714	0.9311	0.844
0.4126	0.9516	0.897
0.4527	0.9678	0.9413
	1.00	1.00

TABLE 5

COMBINATIONS OF REYNOLDS NUMBERS AND INCIDENCES TESTED FOR THE NASA GA(W)-1 AEROFOIL SECTION

REYNOLDS NUMBER

α	Re	5×10^4	1×10^5	1.5×10^5	2×10^5	2.5×10^5	3×10^5	3.5×10^5	4×10^5	4.5×10^5	5×10^5
0°	*	*	*	*	*	*	*	*	*	*	*
2°	*	*	*	*	*	*	*	*	*	*	*
4°	*	*	*	*	*	*	*	*	*	*	*
6°	*	*	*	*	*	*	*	*	*	*	*
8°	*	*	*	*	*	*	*	*	*	*	*
10°	*	*	*	*	*	*	*	*	*	*	*
12°	*	*	*	*	*	*	*	*	*	*	*
13°	*	*	*	*	*	*	*	*	*	*	*
14°	*	*	*	*	*	*	*	*	*	*	*
15°	*	*	*	*	*	*	*	*	*	*	*
16°	*	*	*	*	*	*	*	*	*	*	*
18°	*	*	*	*	*	*	*	*	*	*	*
20°	*	*	*	*	*	*	*	*	*	*	*
22°	*	*	*	*	*	*	*	*	*	*	*

α (DEGREES)

TABLE 6

COMBINATIONS OF REYNOLDS NUMBERS AND INCIDENTS TESTED FOR THE NACA-0015 AEROFOIL SECTION

REYNOLDS NUMBER

Re	5x10 ⁴	1x10 ⁵	1.5x10 ⁵	2x10 ⁵	2.5x10 ⁵	3x10 ⁵	3.5x10 ⁵	4x10 ⁵	4.5x10 ⁵	5x10 ⁵
0°	*	*	*	*	*	*	*	*	*	*
1°	*	*	*	*	*	*	*	*	*	*
2°	*	*	*	*	*	*	*	*	*	*
3°	*	*	*	*	*	*	*	*	*	*
4°	*	*	*	*	*	*	*	*	*	*
5°	*	*	*	*	*	*	*	*	*	*
6°	*	*	*	*	*	*	*	*	*	*
7°	*	*	*	*	*	*	*	*	*	*
8°	*	*	*	*	*	*	*	*	*	*
9°	*	*	*	*	*	*	*	*	*	*
10°	*	*	*	*	*	*	*	*	*	*
10.5°										
11°	*	*	*	*	*	*	*	*	*	*
11.5°										
12°	*	*	*	*	*	*	*	*	*	*
12.5°										
13°	*	*	*	*	*	*	*	*	*	*
13.5°										
14°	*	*	*	*	*	*	*	*	*	*
16°	*	*	*	*	*	*	*	*	*	*
18°	*	*	*	*	*	*	*	*	*	*
20°	*	*	*	*	*	*	*	*	*	*
22°	*	*	*	*	*	*	*	*	*	*

α (DEGREES)

TABLE 7

OIL FLOW VISUALISATION TESTS PERFORMED ON THE NASA GA(W)-1 AND NACA 0015 AEROFOIL SECTIONS

NASA GA(W)-1

REYNOLDS NUMBER

α	Re	1.5x10 ⁵	2x10 ⁵	2.5x10 ⁵	3x10 ⁵	3.5x10 ⁵	4x10 ⁵	4.5x10 ⁵	5x10 ⁵
	0°	*	*	*	*	*	*	*	*
	3°	*	*	*	*	*	*	*	*
	6°	*	*	*	*	*	*	*	*
	12°	*	*	*	*	*	*	*	*
	16°	*	*	*	*	*	*	*	*

α (DEGREES)

NACA 0015

REYNOLDS NUMBER

α	Re	1.5x10 ⁵	2x10 ⁵	2.5x10 ⁵	3x10 ⁵	3.5x10 ⁵	4x10 ⁵	4.5x10 ⁵	5x10 ⁵
	0°	*	*	*	*	*	*	*	*
	3°	*	*	*	*	*	*	*	*
	6°	*	*	*	*	*	*	*	*
	9°	*	*	*	*	*	*	*	*
	10°	*							
	11°		*						
	12°			*					
	12.5°				*	*	*	*	*
	13°	*	*	*	*	*	*	*	*
	13.5°								*
	14°						*	*	*

α (DEGREES)

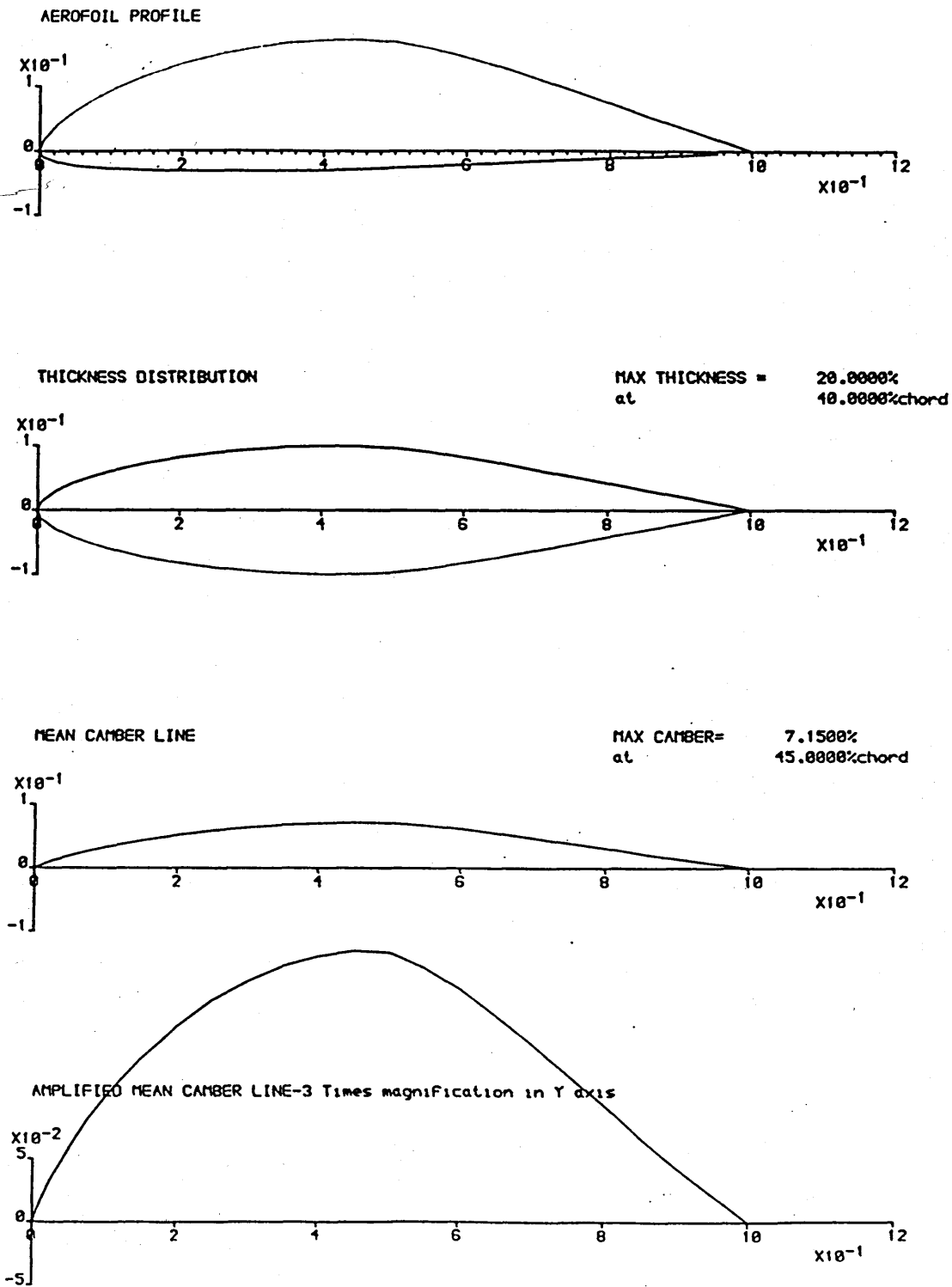


Fig. 2.1 GU25-5(11)8 AEROFOIL PROFILE, THICKNESS DISTRIBUTION AND CAMBER LINE

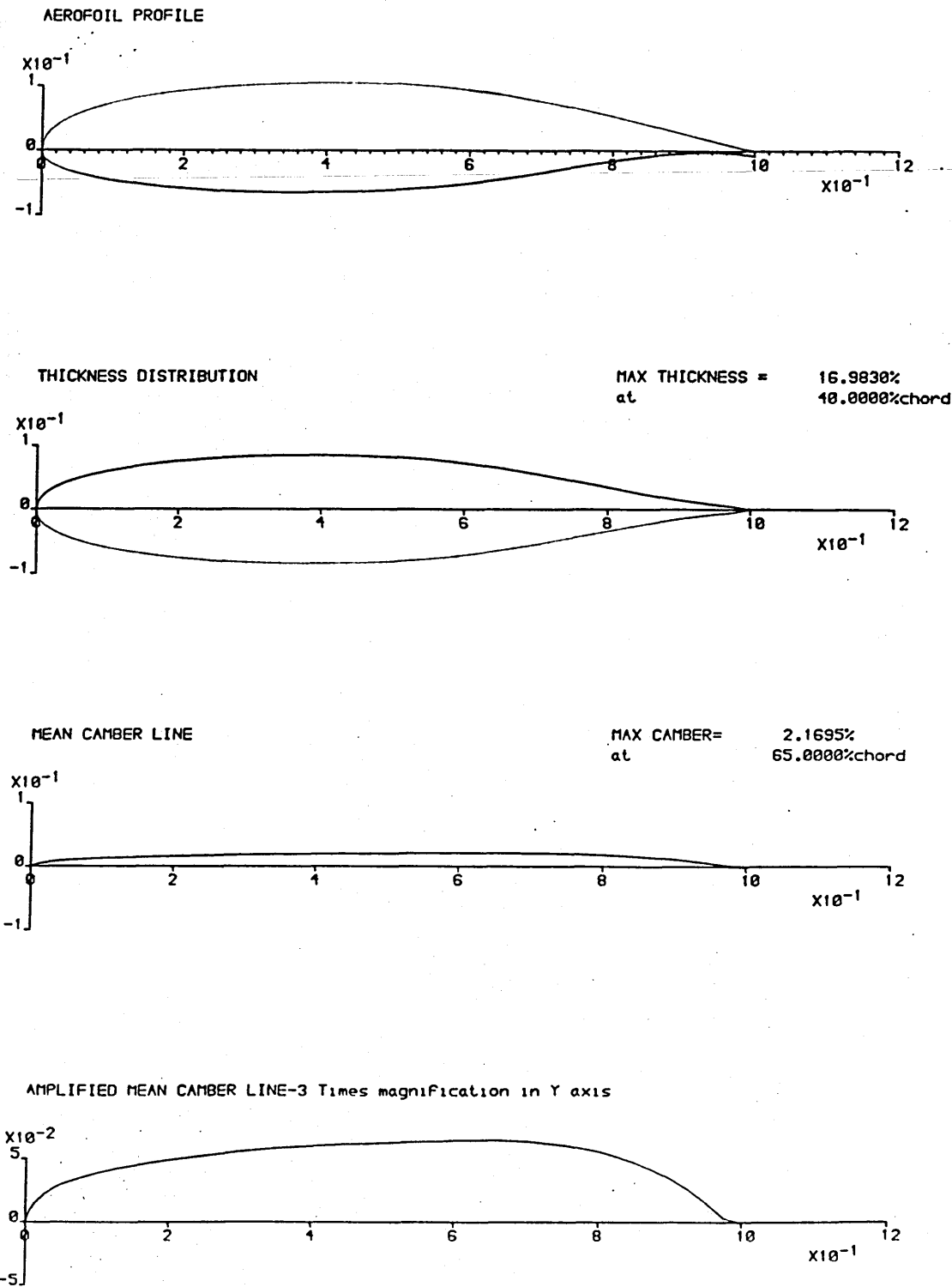
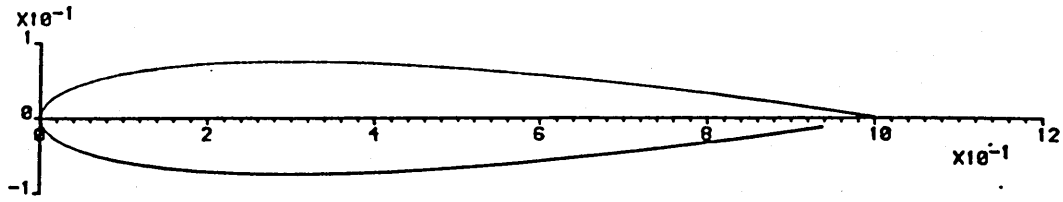


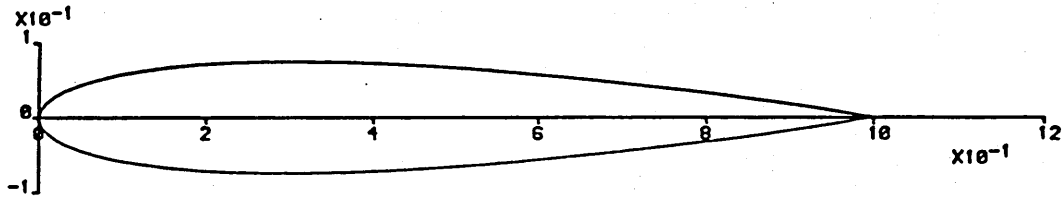
Fig. 2.2 NASA GA(W)-1 AEROFOIL PROFILE, THICKNESS DISTRIBUTION AND CAMBER LINE

AEROFOIL PROFILE

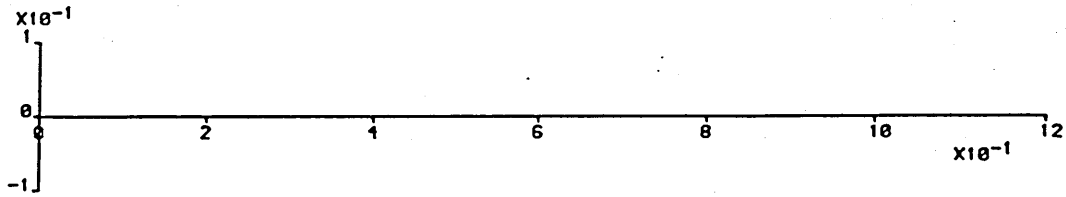


THICKNESS DISTRIBUTION

MAX THICKNESS = 14.998%
at 31.5153%chord



MEAN CAMBER LINE



AMPLIFIED MEAN CAMBER LINE-3 Times magnification in Y axis

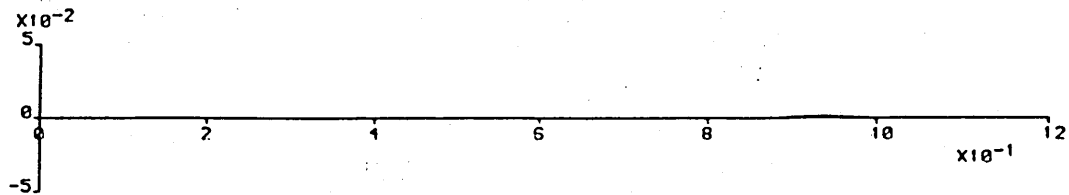


Fig. 2.3 NACA-0015 AEROFOIL PROFILE, THICKNESS DISTRIBUTION AND CAMBER LINE

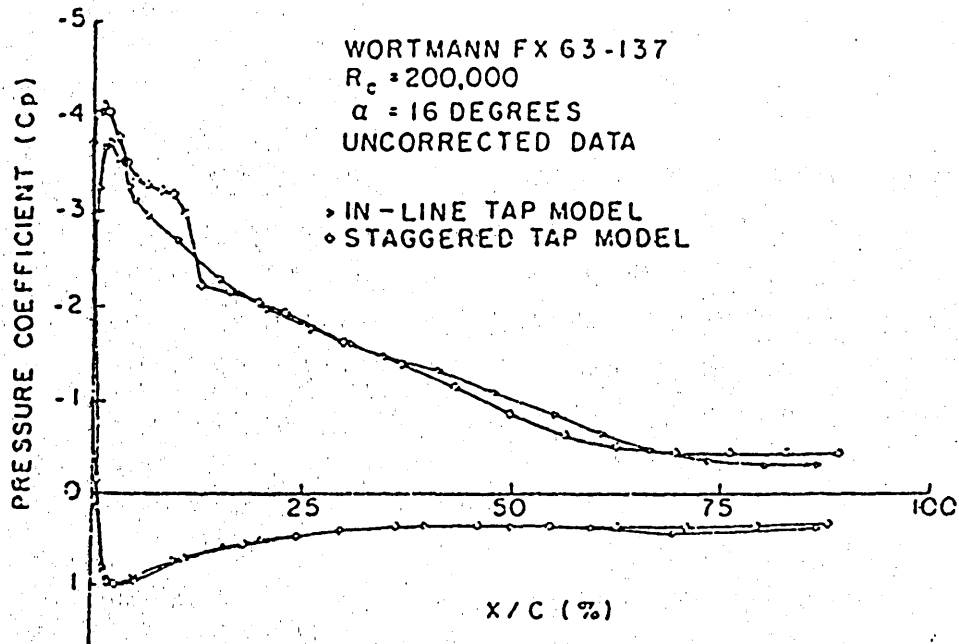


Fig. 2.4. PRESSURE COEFFICIENT VERSUS X/C OF THE WORTMANN FX 63-137 AIRFOIL MODEL SHOWING THE INFLUENCE OF PRESSURE TAP ORIENTATION (TAKEN FROM REF (10))

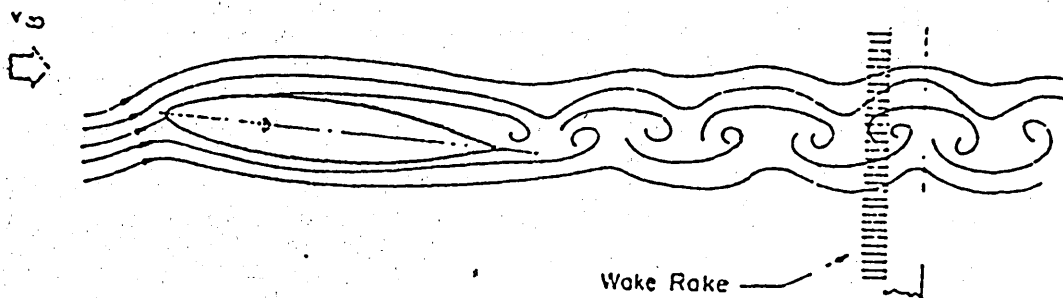


Fig. 2.5 UNSTEADY WAKE PRODUCED BEHIND A NACA 66₃-018 AIRFOIL AT 6° ANGLE OF ATTACK AND $RE=40,000$ (TAKEN FROM REF (11))

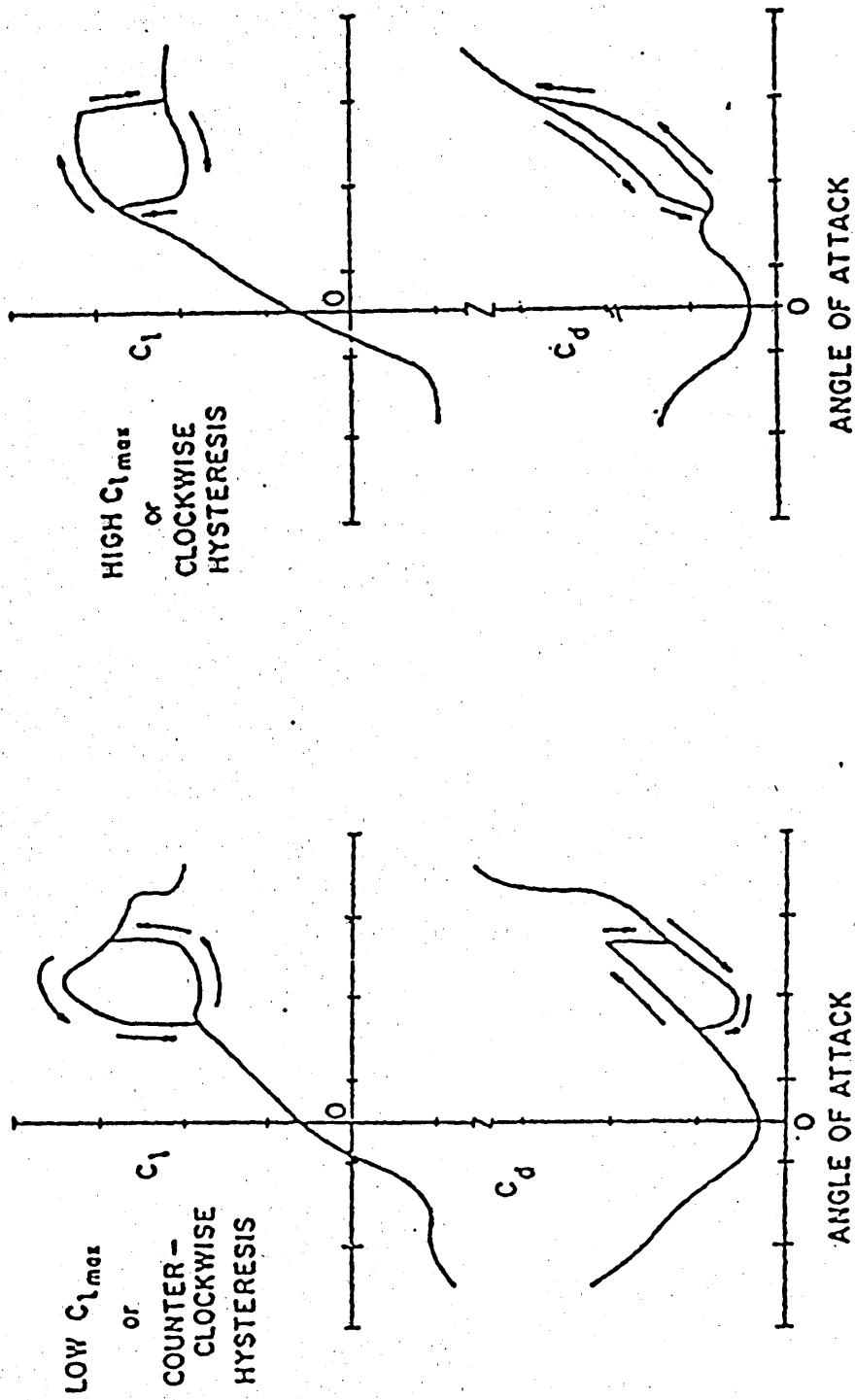


Fig. 2.6 AIRFOIL SECTION LIFT AND DRAG COEFFICIENTS VERSUS ANGLE OF ATTACK SHOWING THE "LOW $C_{l,max}$ " OR "COUNTERCLOCKWISE HYSTERESIS"

AIRFOIL SECTION LIFT AND DRAG COEFFICIENTS VERSUS ANGLE OF ATTACK SHOWING THE "HIGH $C_{l,max}$ " OR "CLOCKWISE HYSTERESIS"

(TAKEN FROM REF (12,13))

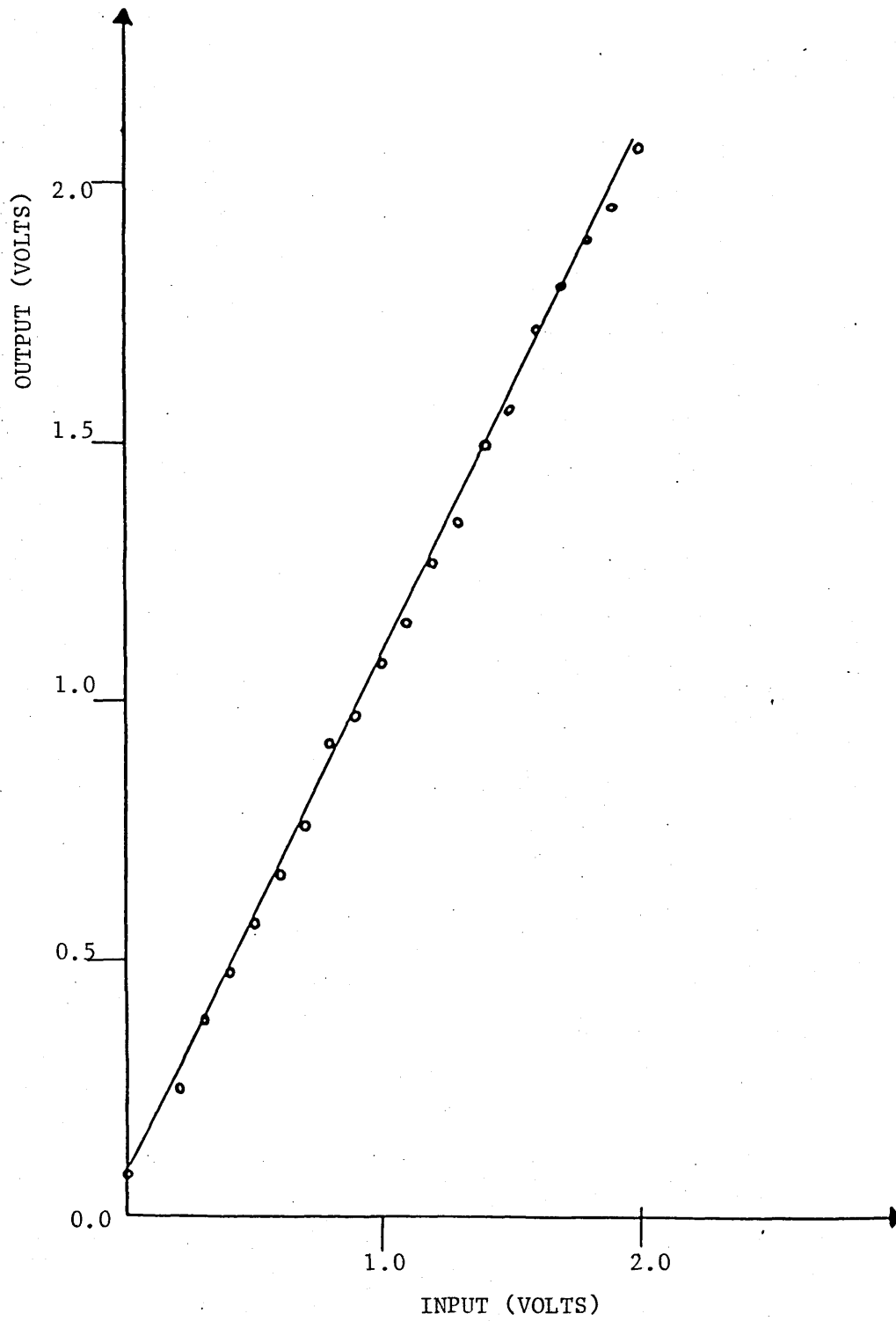


Fig. 2.7 VARIATION OF OUTPUT WITH INPUT VOLTAGE OF THE A/D CONVERTOR

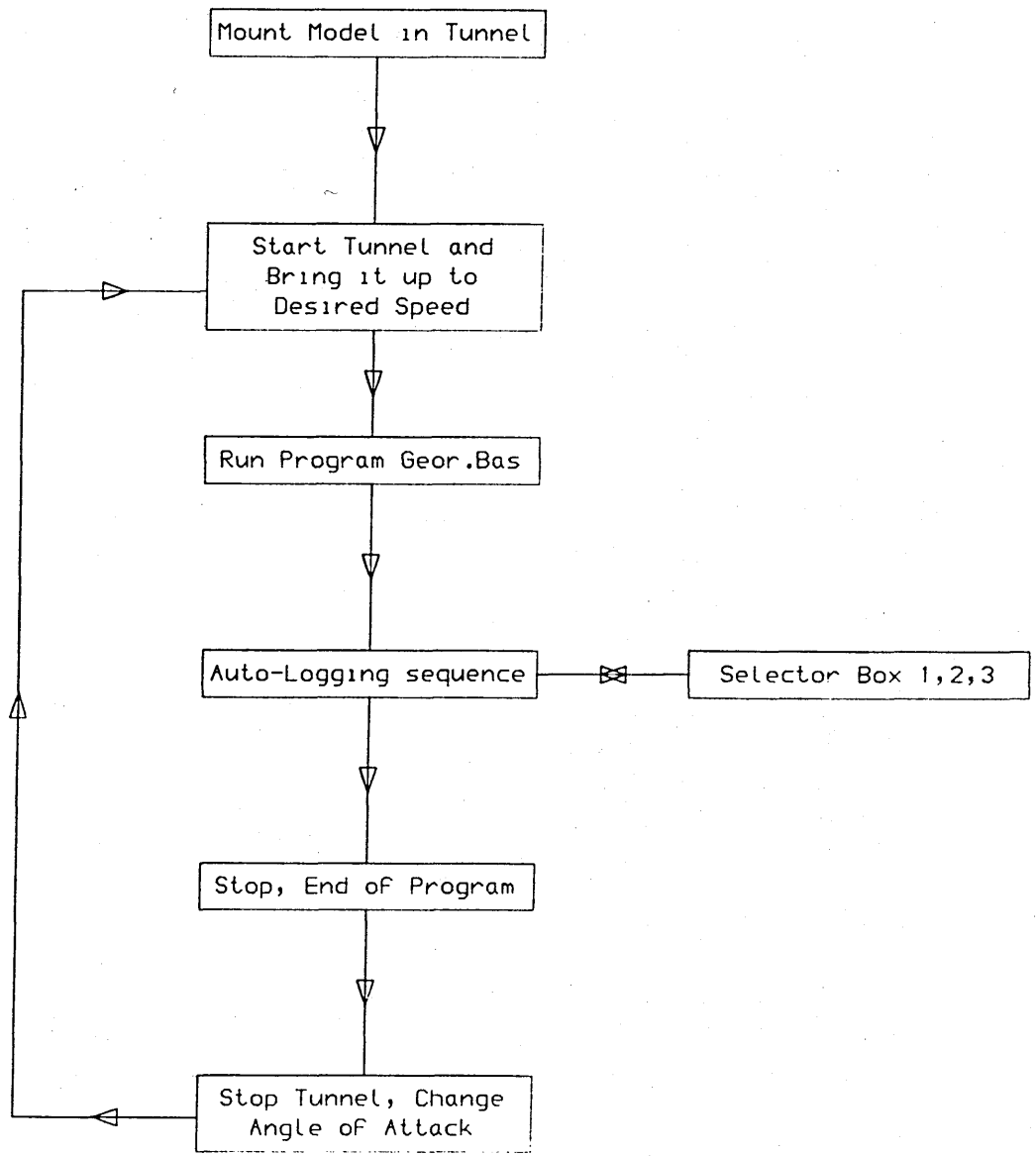


Fig. 2.8 BLOCK DIAGRAM OF THE EXPERIMENTAL PROCEDURE

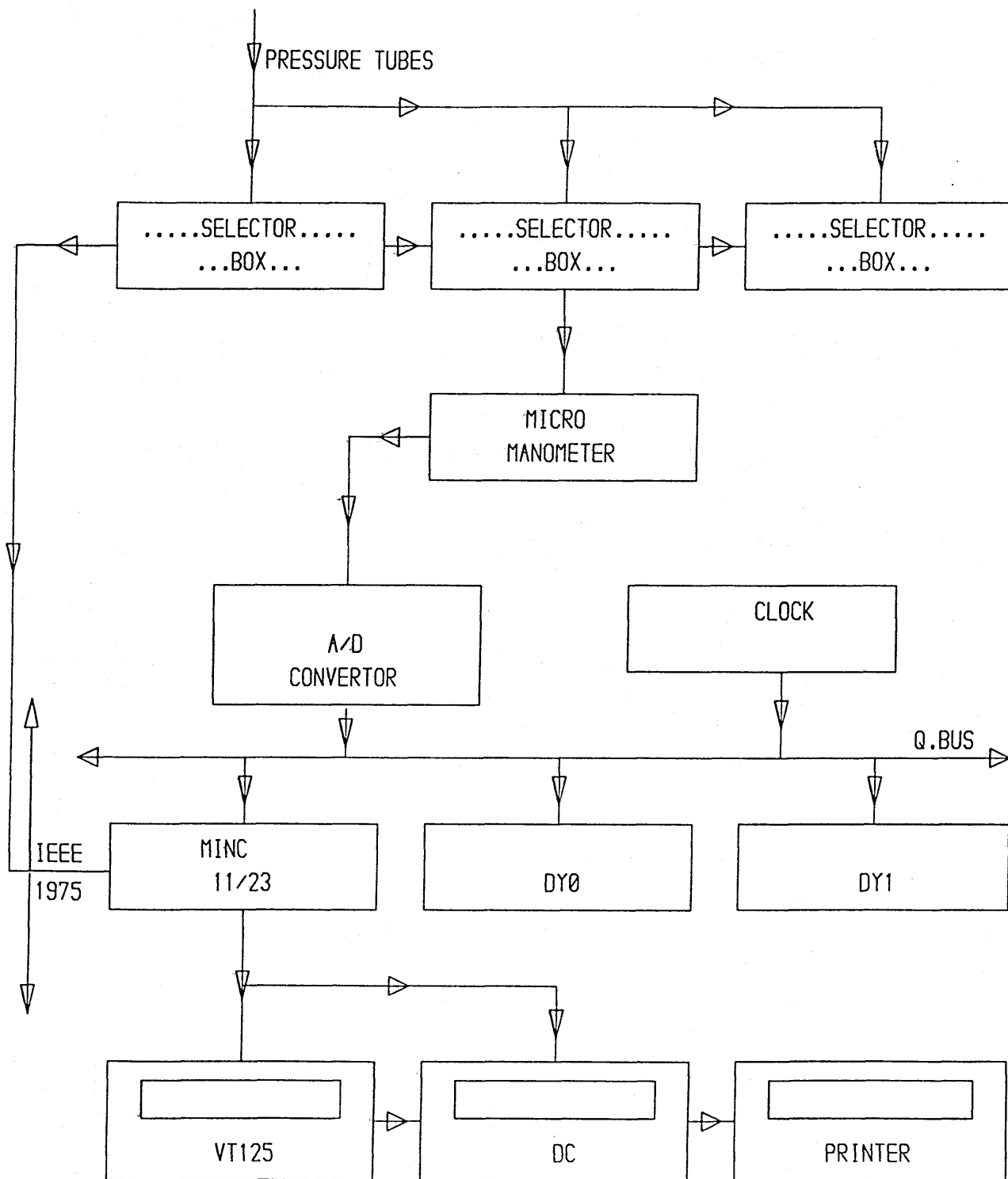


Fig. 2.9 SCHEMATIC OF INSTRUMENTATION USED FOR DATA ACQUISITION

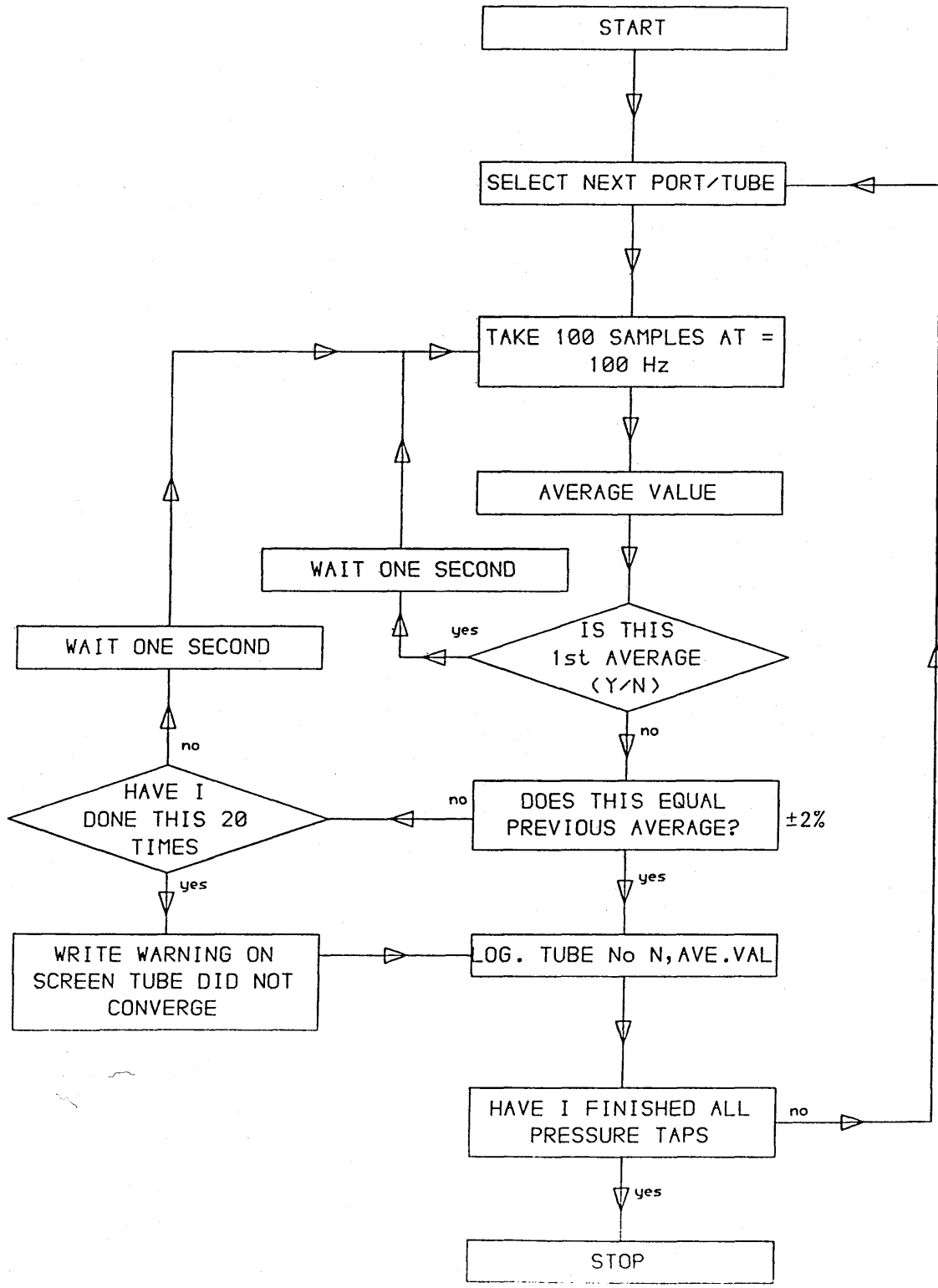
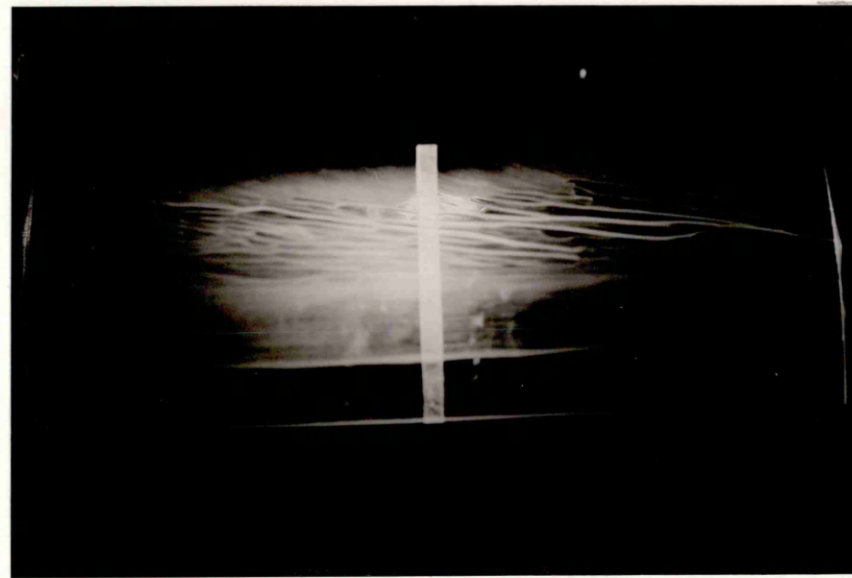
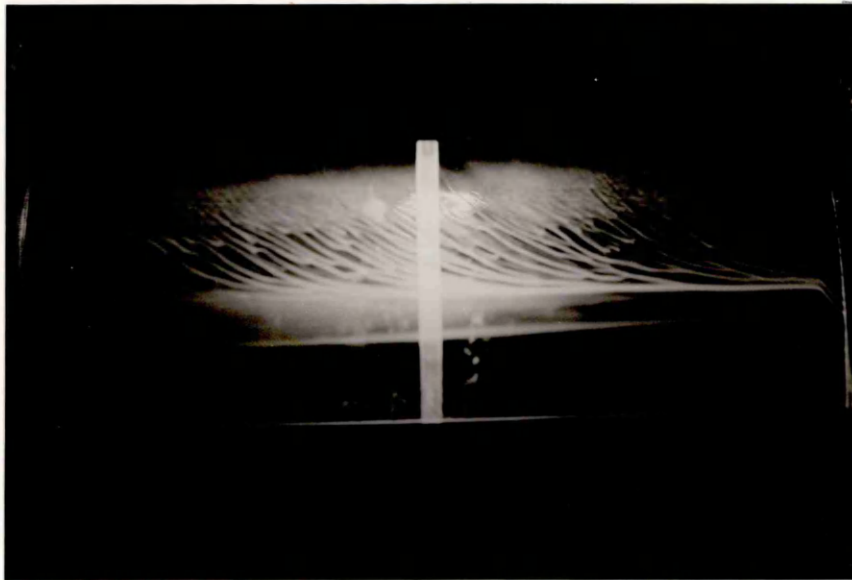


Fig. 2.10 FLOW CHART DIAGRAM OF LOGGING SEQUENCE



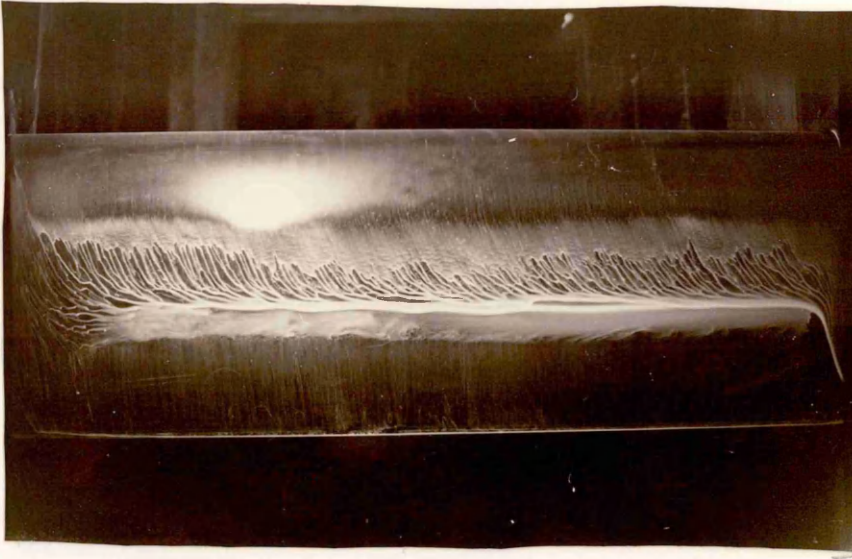
Re ≈ 150,000

(a)



Re ≈ 300,000

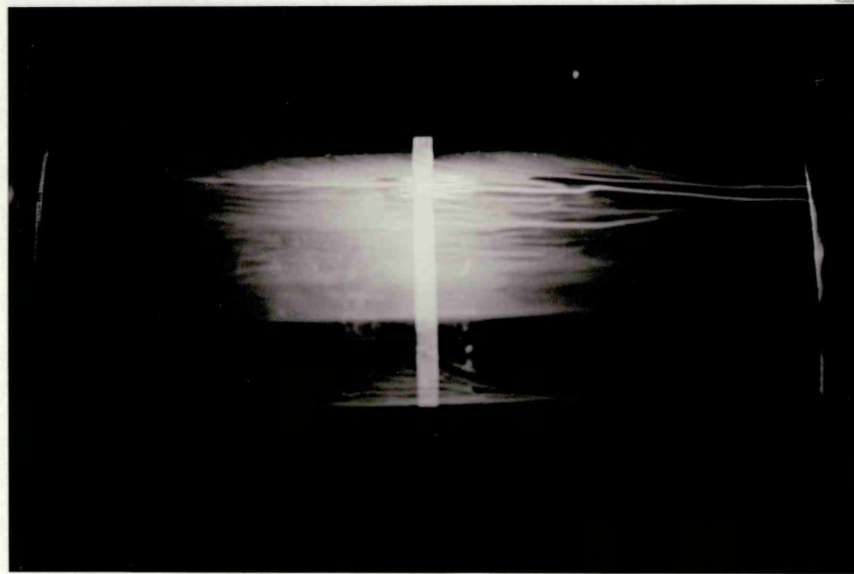
(b)



Re ≈ 500,000

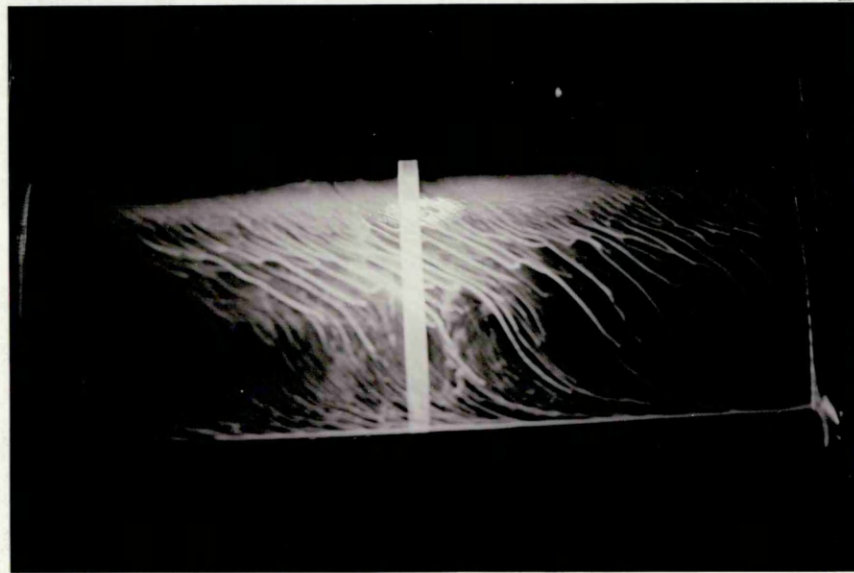
(c)

Fig. 3.1 FLOW VISUALISATION OF THE NASA GA(W)-1 SECTION AT 0.6° DEGREES AT VARIOUS REYNOLDS NUMBERS



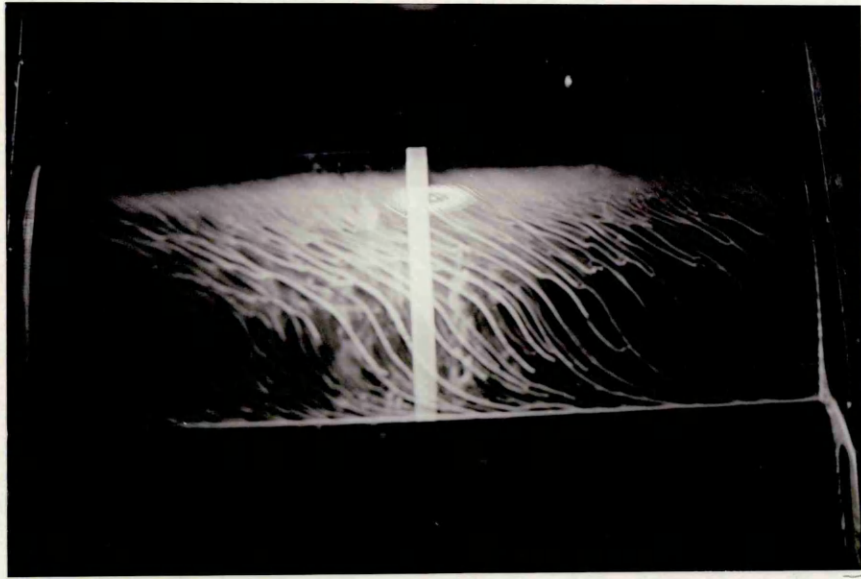
Re \approx 150,000

(a)



Re \approx 300,000

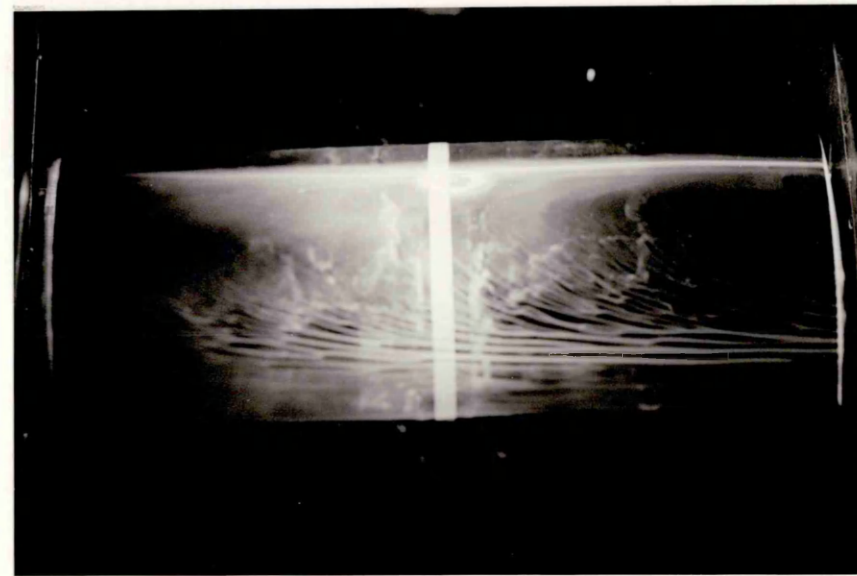
(b)



Re \approx 350,000

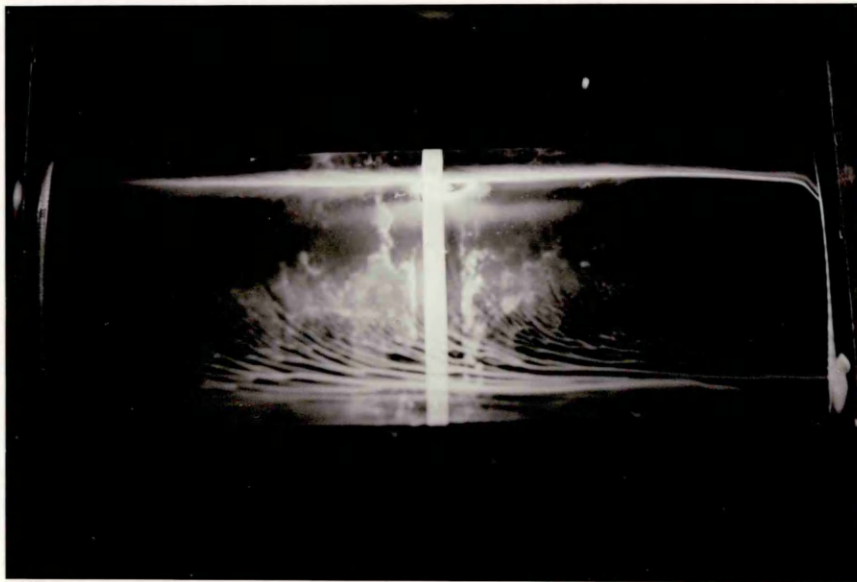
(c)

Fig. 3.2 FLOW VISUALISATION OF THE NASA GA(W)-1 SECTION AT 3.6° DEGREES AT VARIOUS REYNOLDS NUMBERS



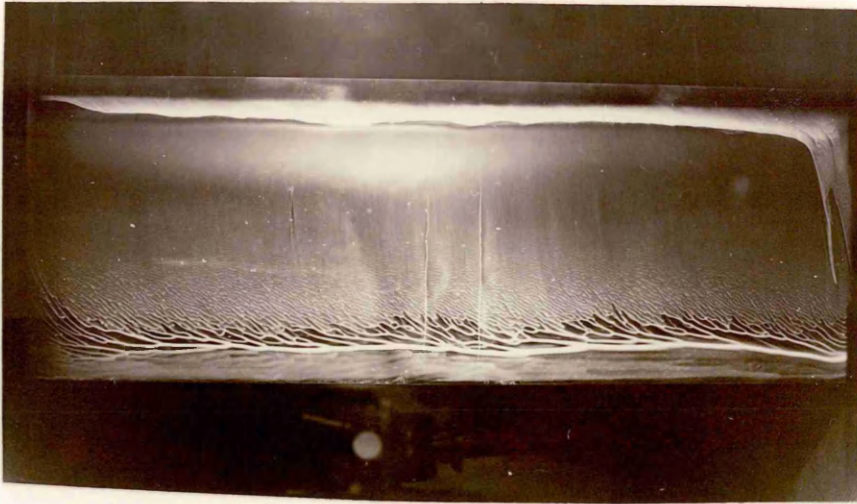
Re \approx 150,000

(a)



Re \approx 250,000

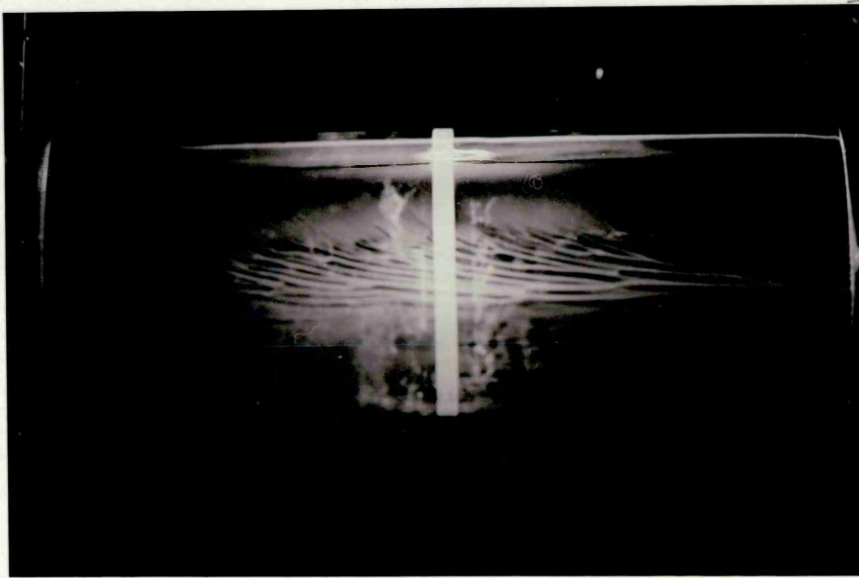
(b)



Re \approx 500,000

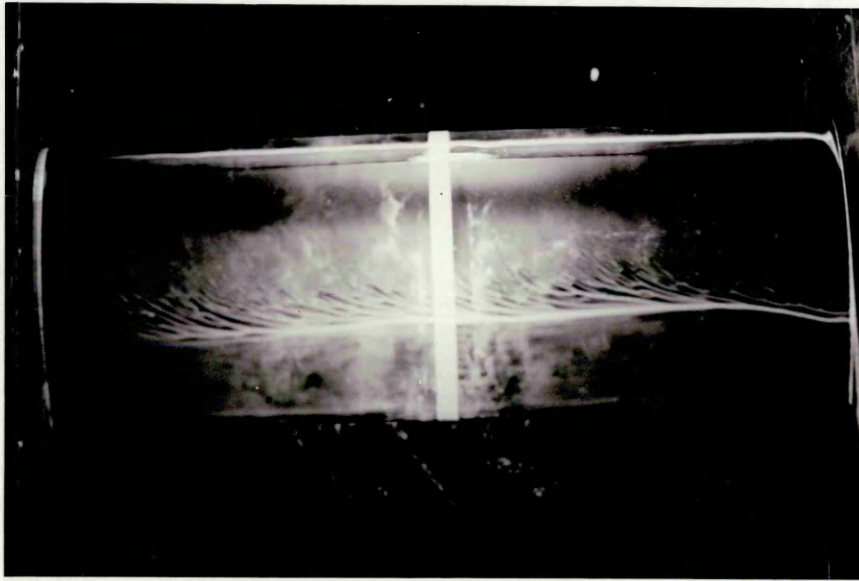
(c)

Fig. 3.3 FLOW VISUALISATION OF THE NASA GA(w)-1 SECTION AT 6.6° DEGREES AT VARIOUS REYNOLDS NUMBERS



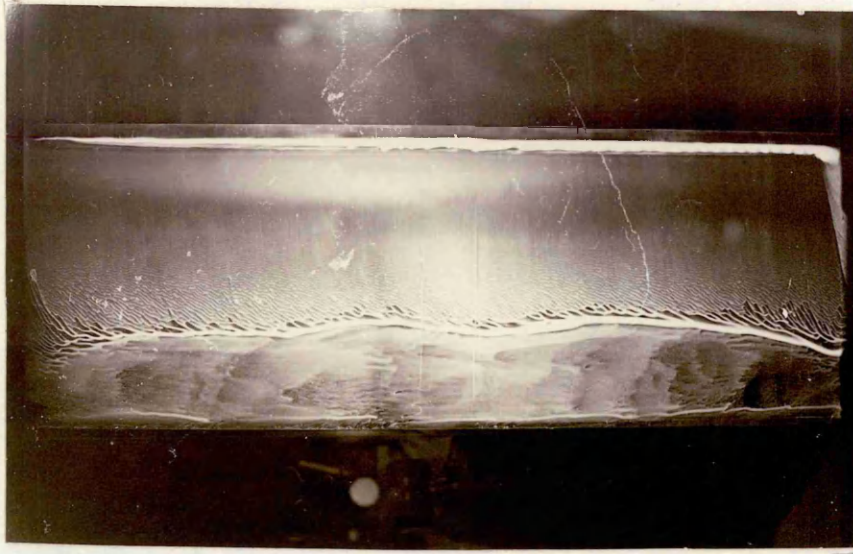
Re ≈ 150,000

(a)



Re ≈ 300,000

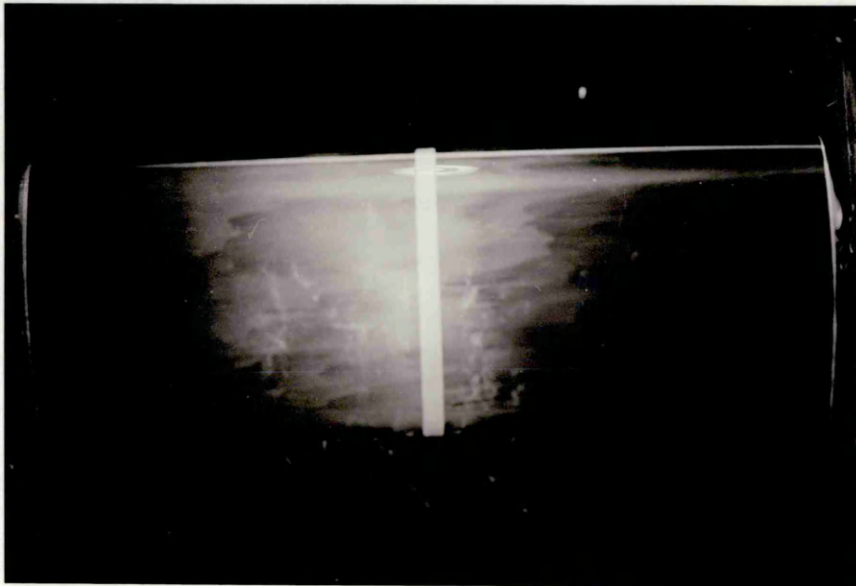
(b)



Re ≈ 500,000

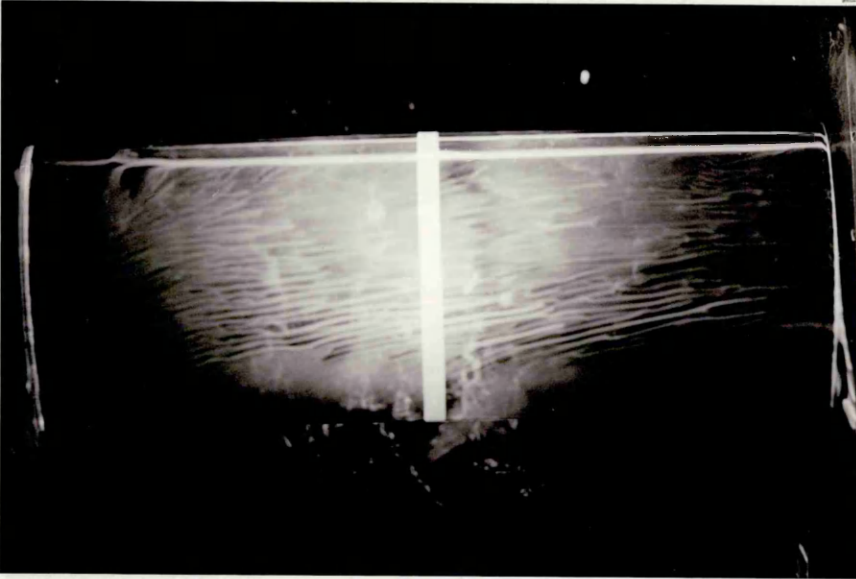
(c)

Fig. 3.4 FLOW VISUALISATION OF THE NASA GA(W)-1 SECTION AT 12.6° DEGREES AT VARIOUS REYNOLDS NUMBERS



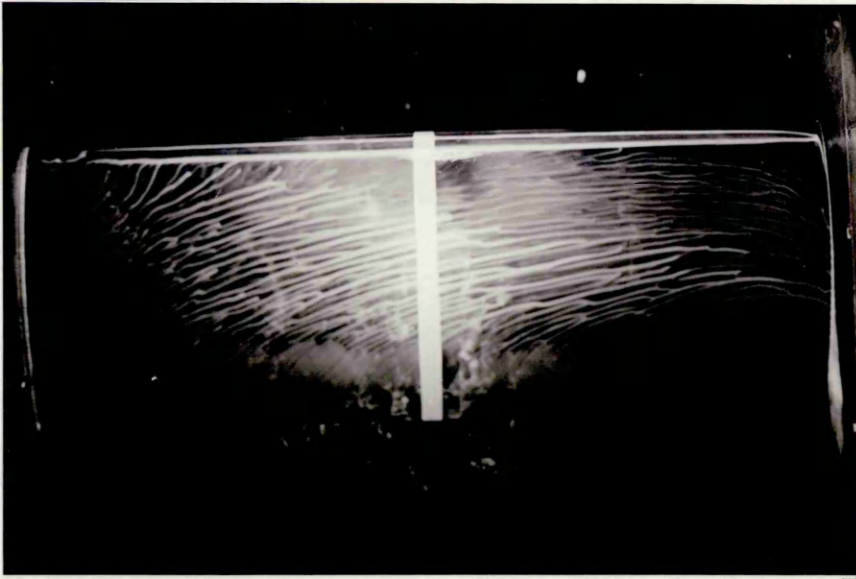
Re \approx 150,000

(a)



Re \approx 300,000

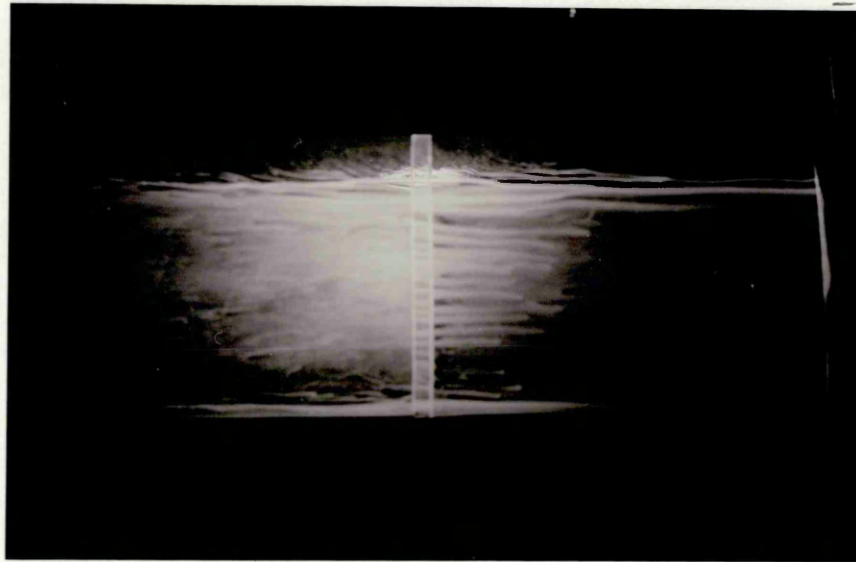
(b)



Re \approx 400,000

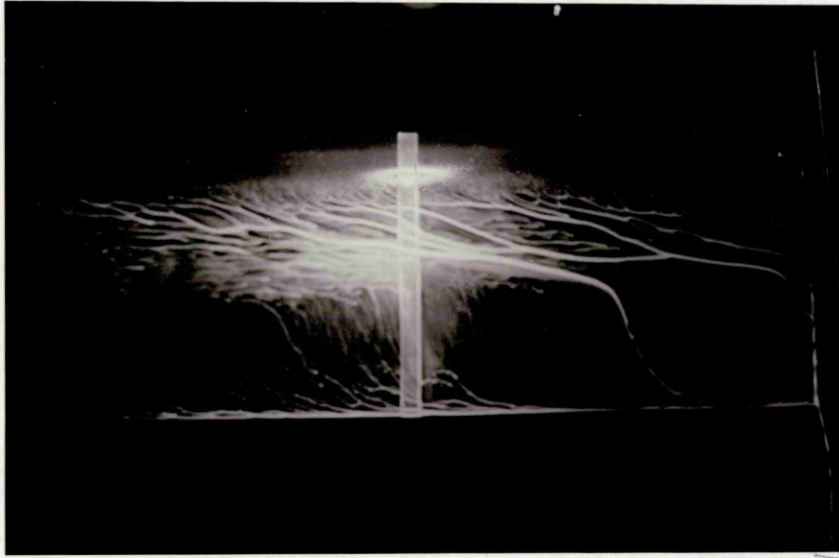
(c)

Fig. 3.5 FLOW VISUALISATION OF THE NASA GA(W)-1 SECTION AT 16.6° DEGREES AT VARIOUS REYNOLDS NUMBERS



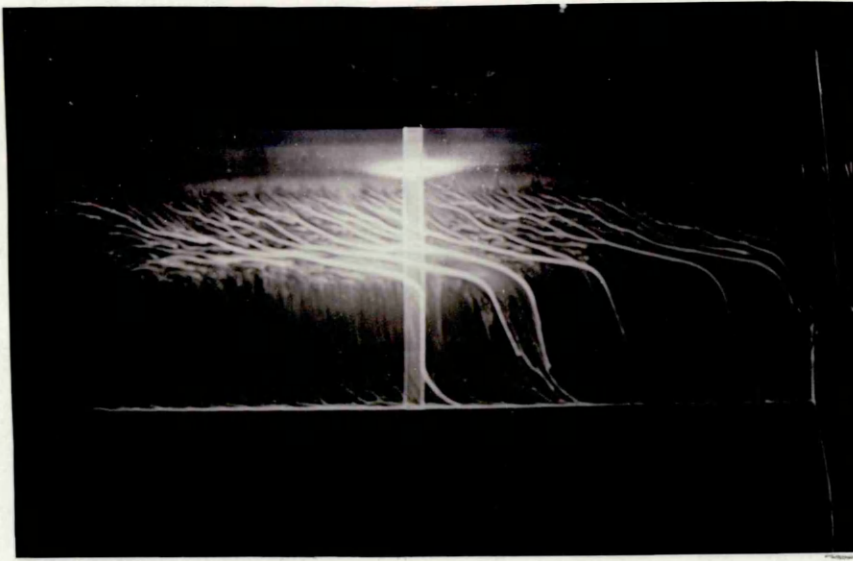
Re=150,000

(a)



Re=400,000

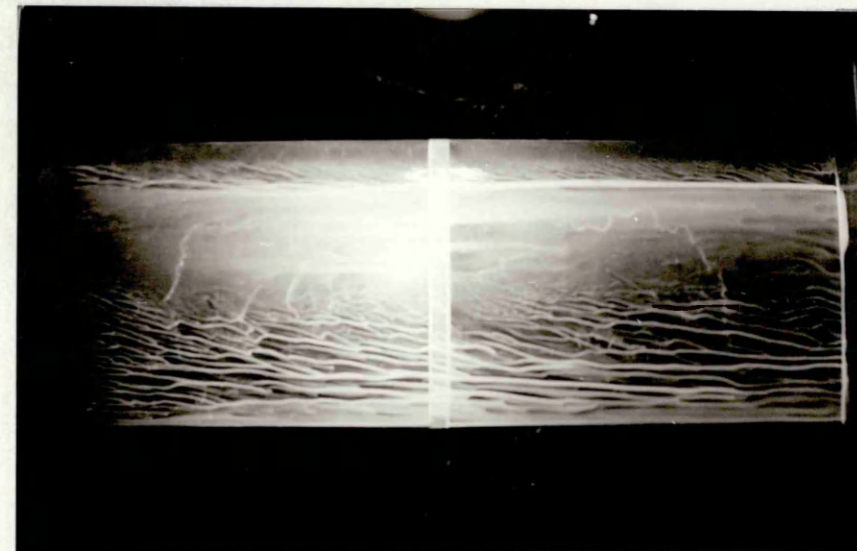
(b)



Re=500,000

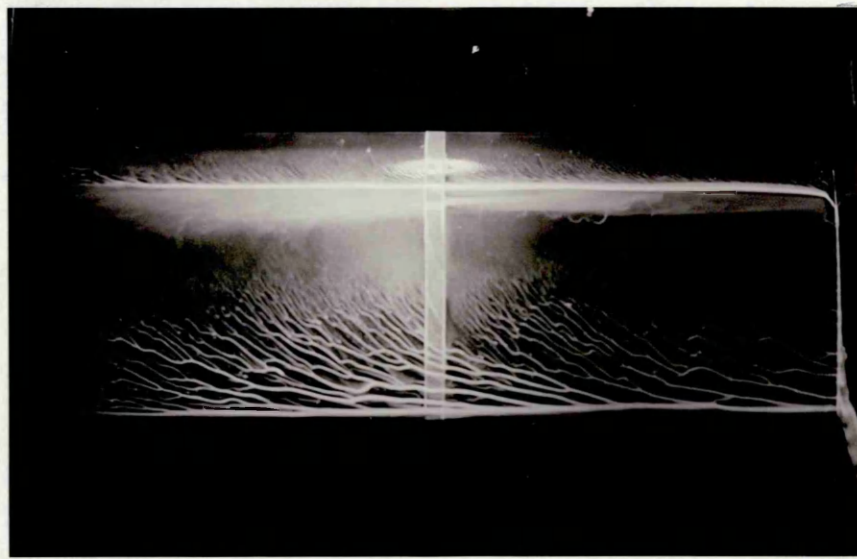
(c)

Fig. 3.6 FLOW VISUALISATION OF THE NACA-0015 SECTION AT 0.6° DEGREES AT VARIOUS REYNOLDS NUMBERS



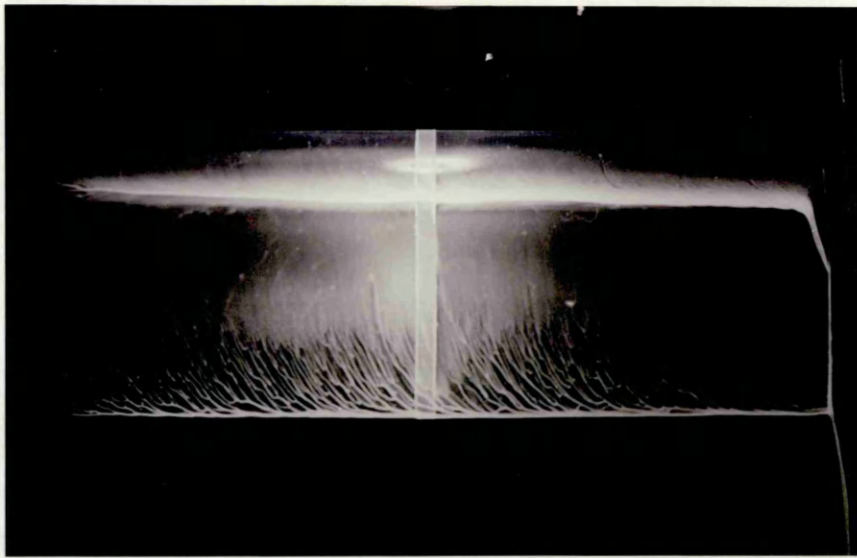
Re ≈ 150,000

(a)



Re ≈ 300,000

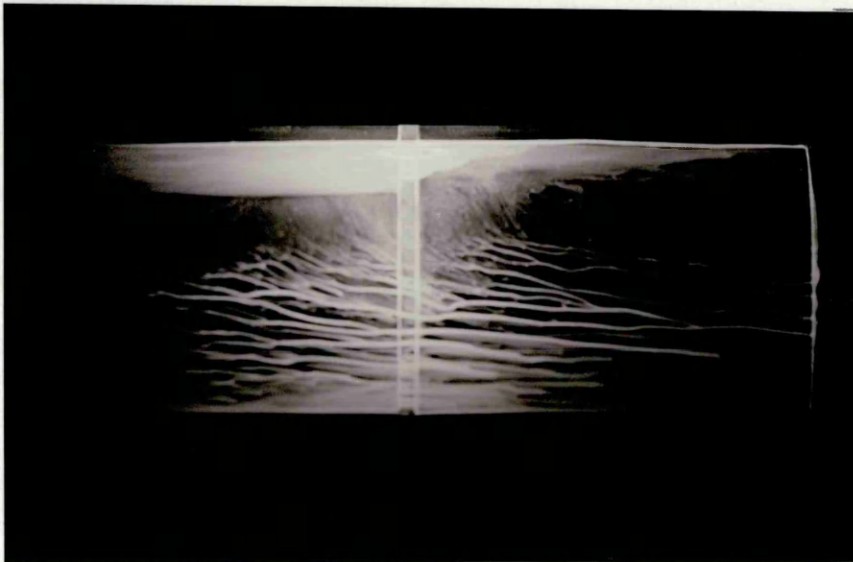
(b)



Re ≈ 500,000

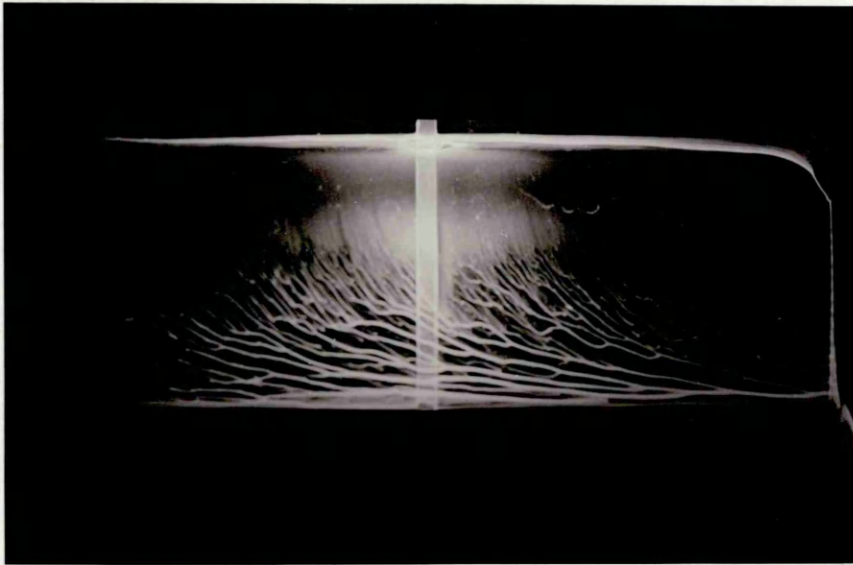
(c)

Fig. 3.7 FLOW VISUALISATION OF THE NACA-0015 SECTION AT 3.6° DEGREES AT VARIOUS REYNOLDS NUMBERS



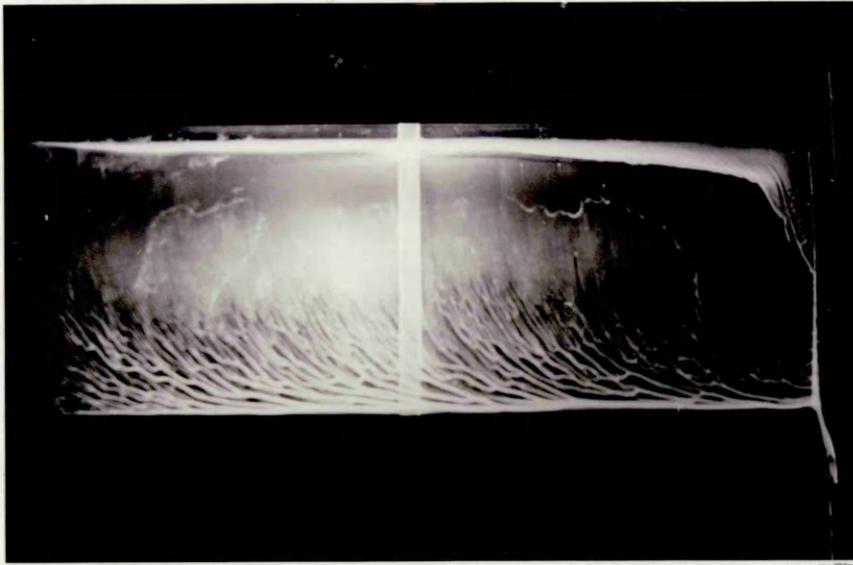
Re \approx 150,000

(a)



Re \approx 350,000

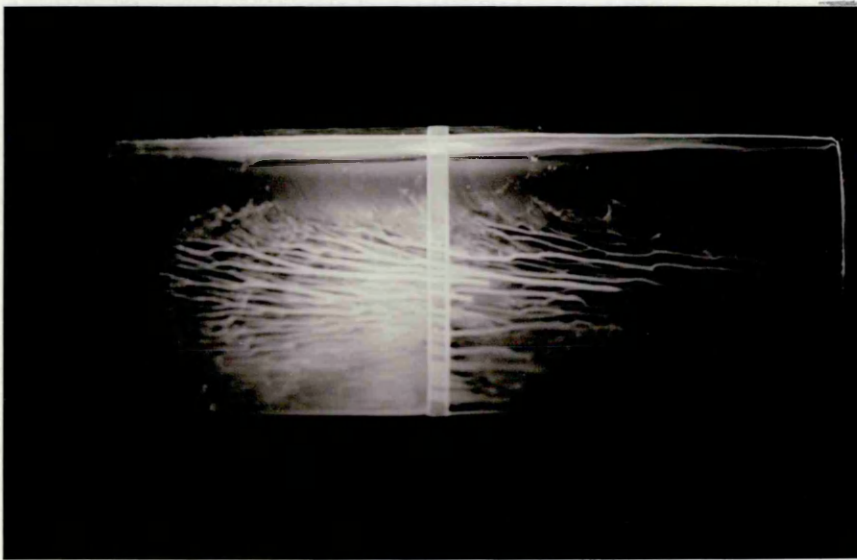
(b)



Re \approx 450,000

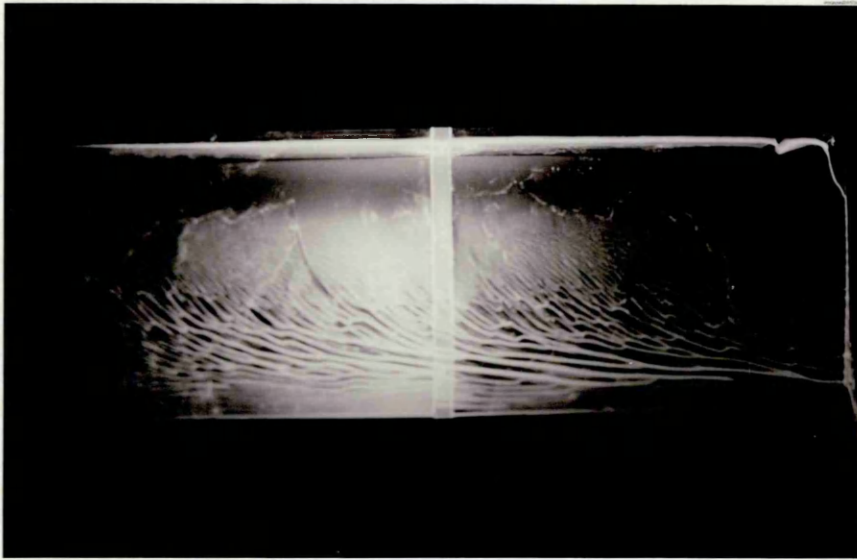
(c)

Fig. 3.8 FLOW VISUALISATION OF THE NACA-0015 SECTION AT 6.6° DEGREES AT VARIOUS REYNOLDS NUMBERS



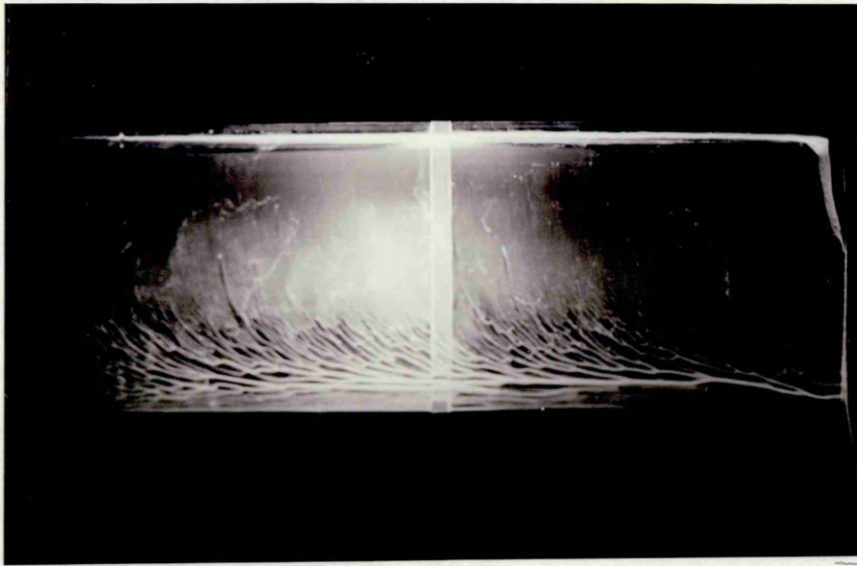
Re=150,000

(a)



Re=350,000

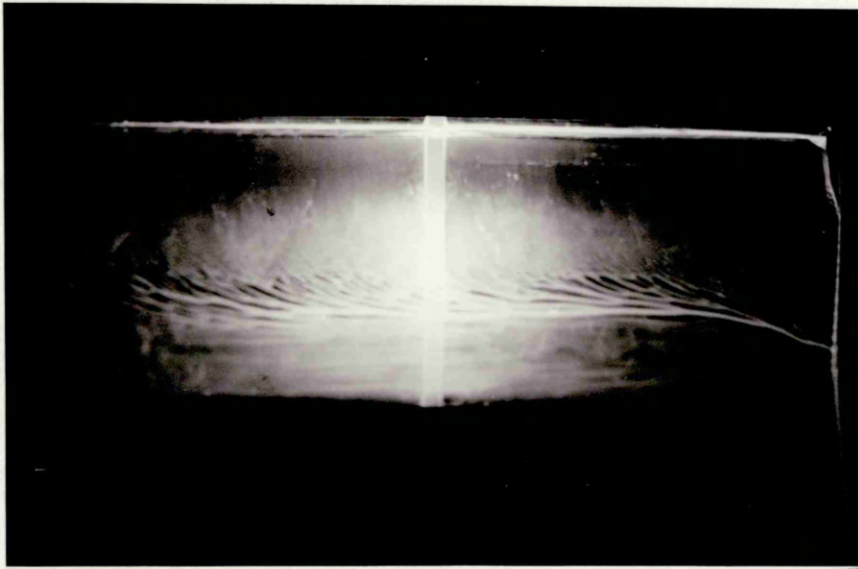
(b)



Re=500,000

(c)

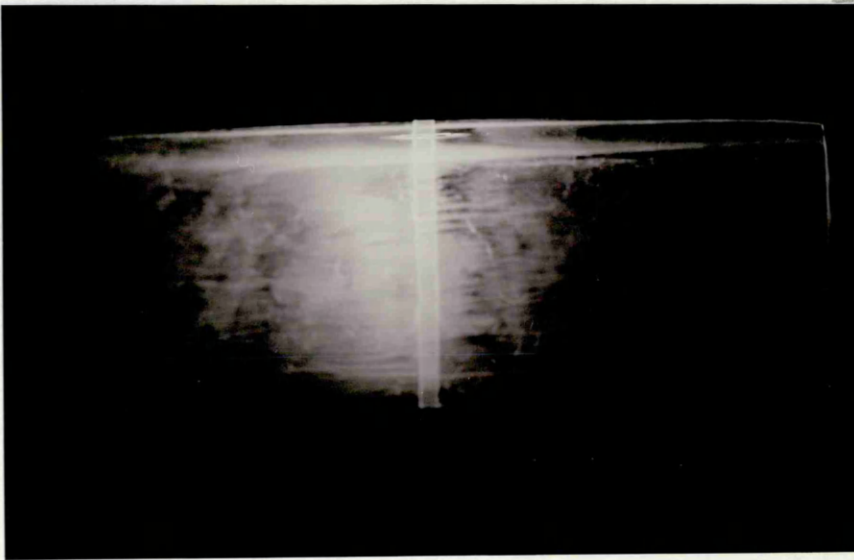
Fig. 3.9 FLOW VISUALISATION OF THE NACA-0015 SECTION AT 9.9° DEGREES AT VARIOUS REYNOLDS NUMBERS



$Re \approx 400,000$

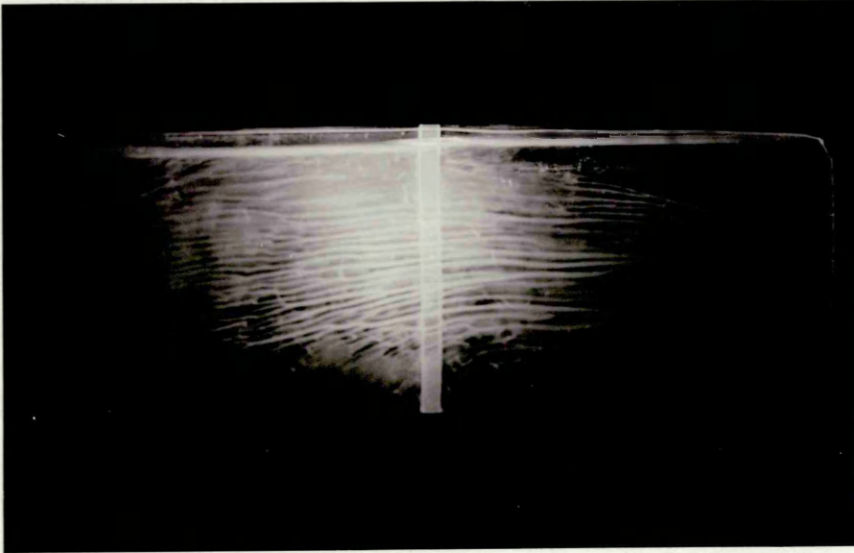
(d)

Fig. 3.10 FLOW VISUALISATION OF THE NACA-0015 SECTION AT 13.1° DEGREES AT VARIOUS REYNOLDS NUMBERS



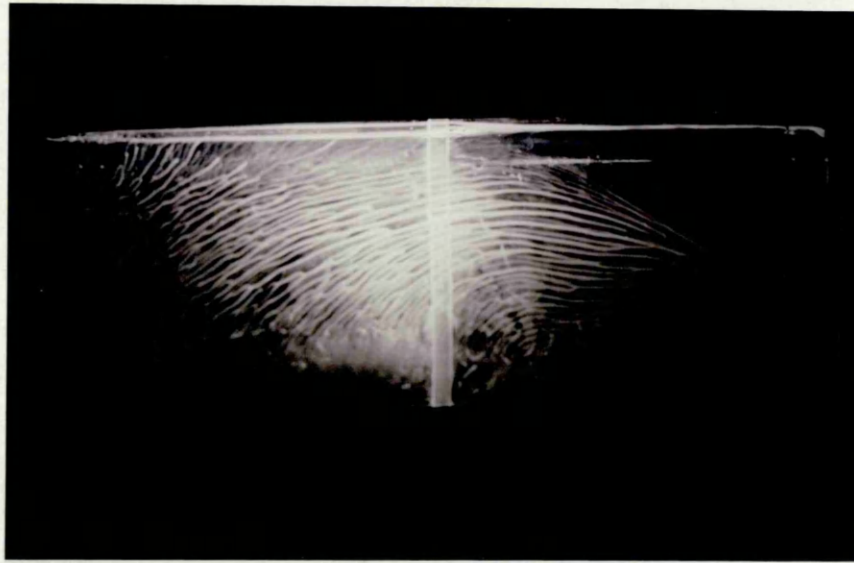
Re=150,000

(a)



Re=250,000

(b)



Re=450,000

(c)

Fig. 3.10 FLOW VISUALISATION OF THE NACA-0015 SECTION AT 13.6° DEGREES AT VARIOUS REYNOLDS NUMBERS

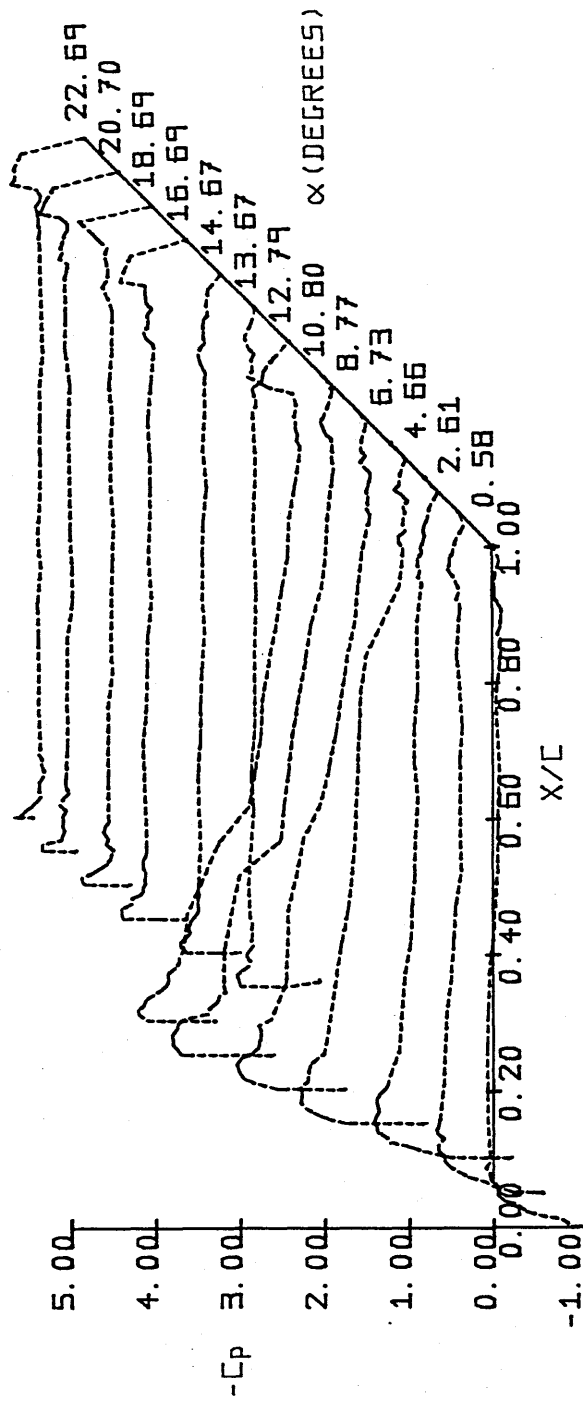


FIG.3.11 PRESSURE DISTRIBUTION FOR THE NASA GA(W)-1
($Re = 50320$.)

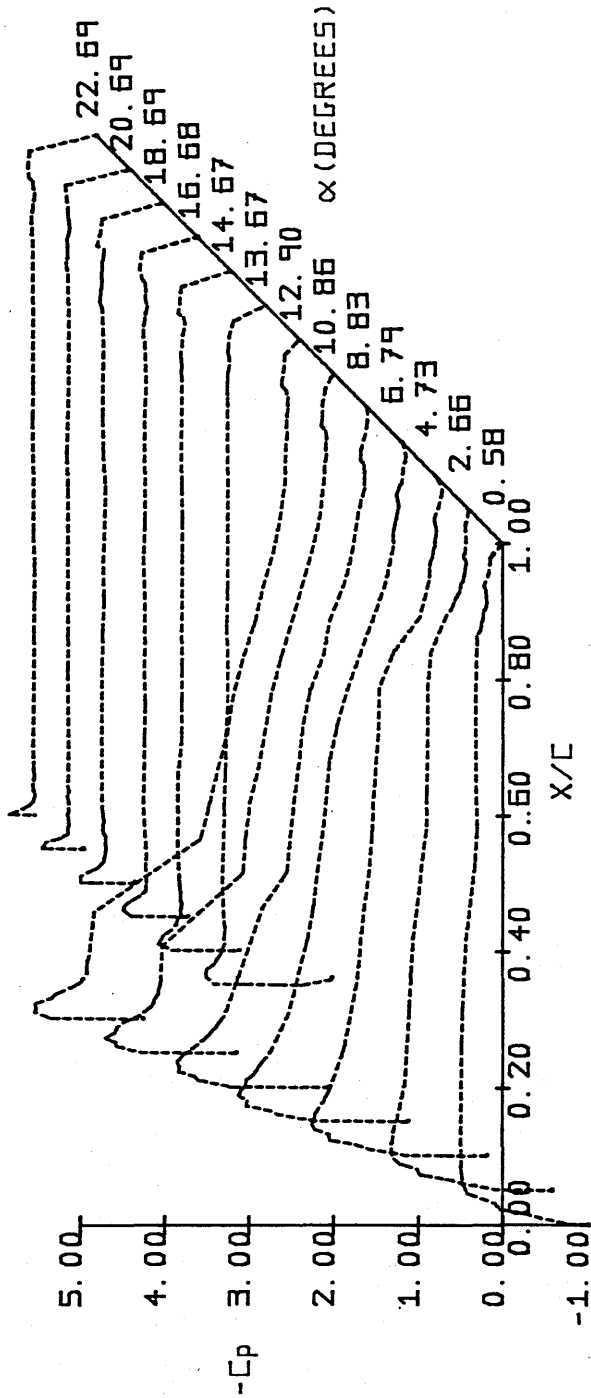


FIG.3.12 PRESSURE DISTRIBUTION FOR THE NASA GA(W)-1
 (Re = 100630.)

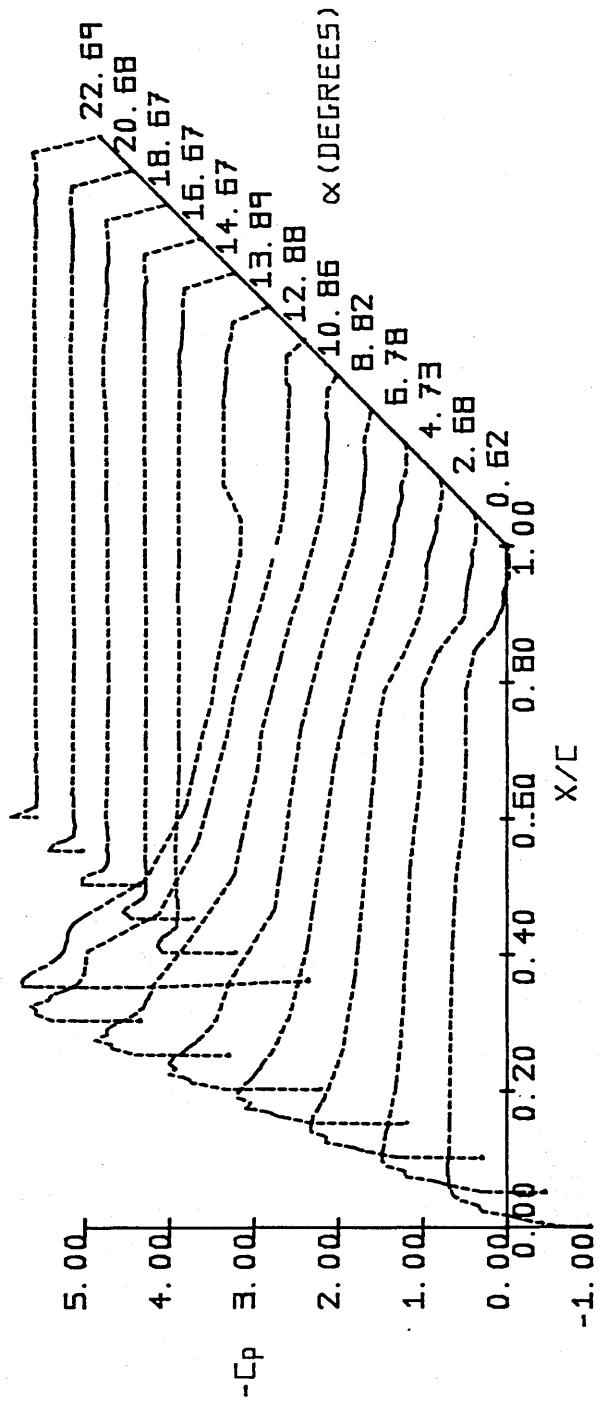


FIG.3. 13 PRESSURE DISTRIBUTION FOR THE NASA GA(W) -1
 (Re = 150950.)

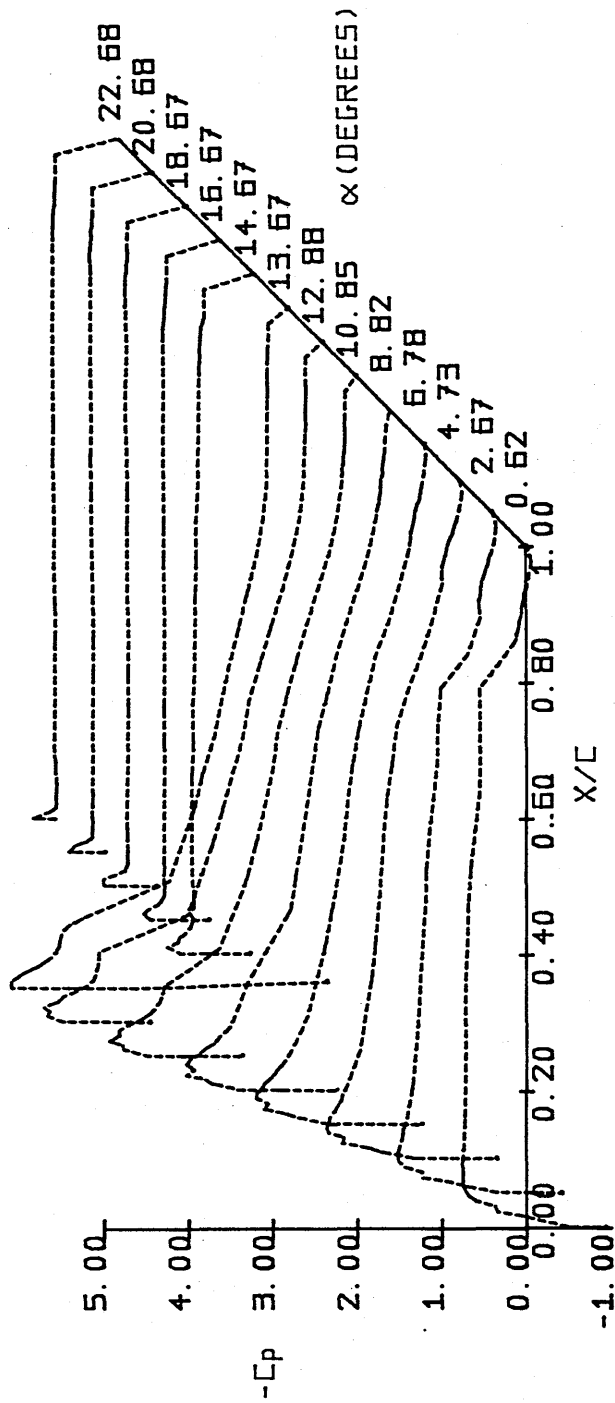


FIG.3.14 PRESSURE DISTRIBUTION FOR THE NASA GA(W)-1
($Re = 201250$.)

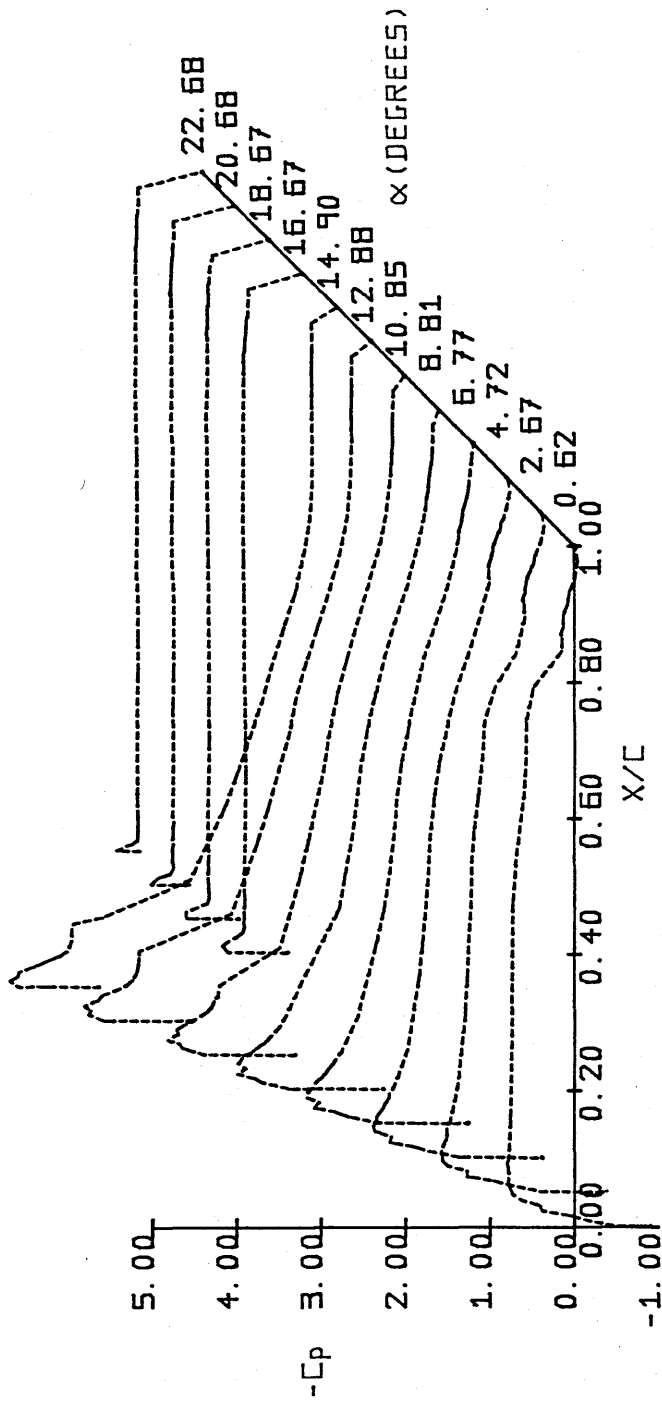


FIG.3. 15 PRESSURE DISTRIBUTION FOR THE NASA GA(W)-1
 (Re = 251575.)

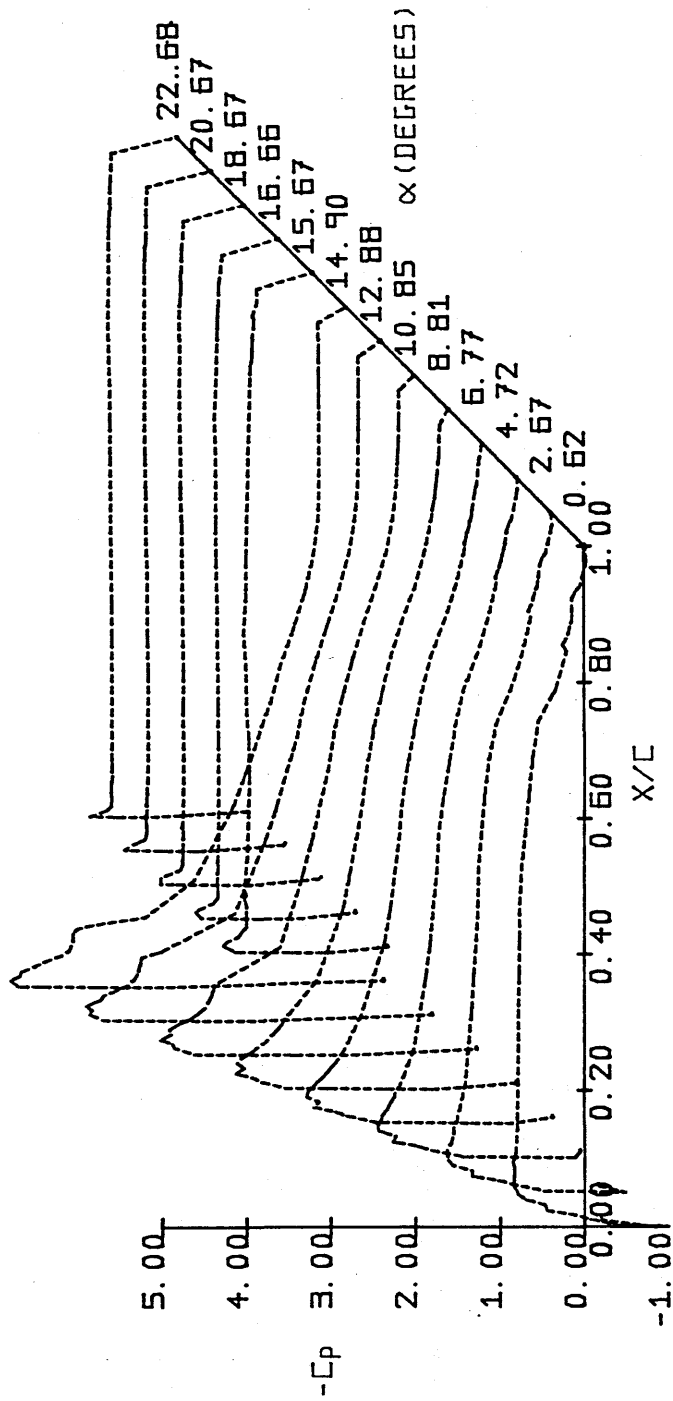


FIG.3.16 PRESSURE DISTRIBUTION FOR THE NASA GA(W)-1
 (Re = 302000.)

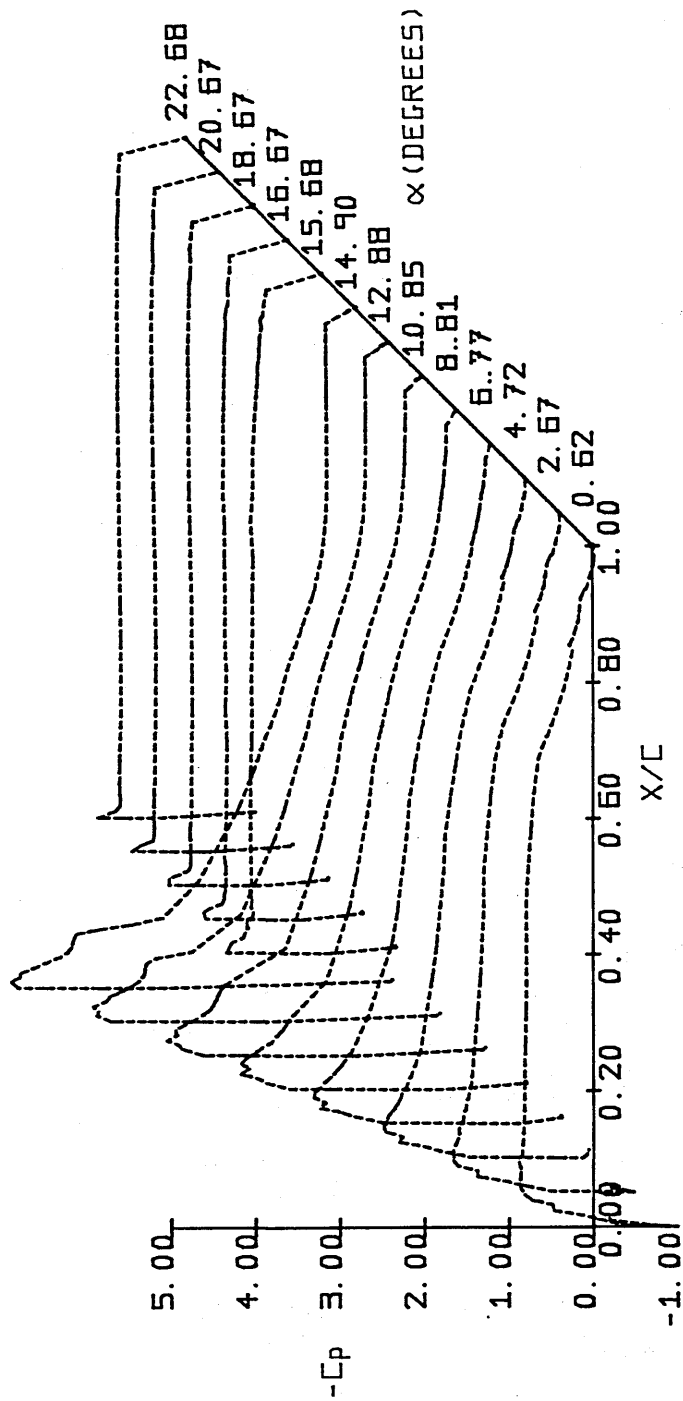


FIG.3.17 PRESSURE DISTRIBUTION FOR THE NASA GA(W)-1
 (Re = 352200.)

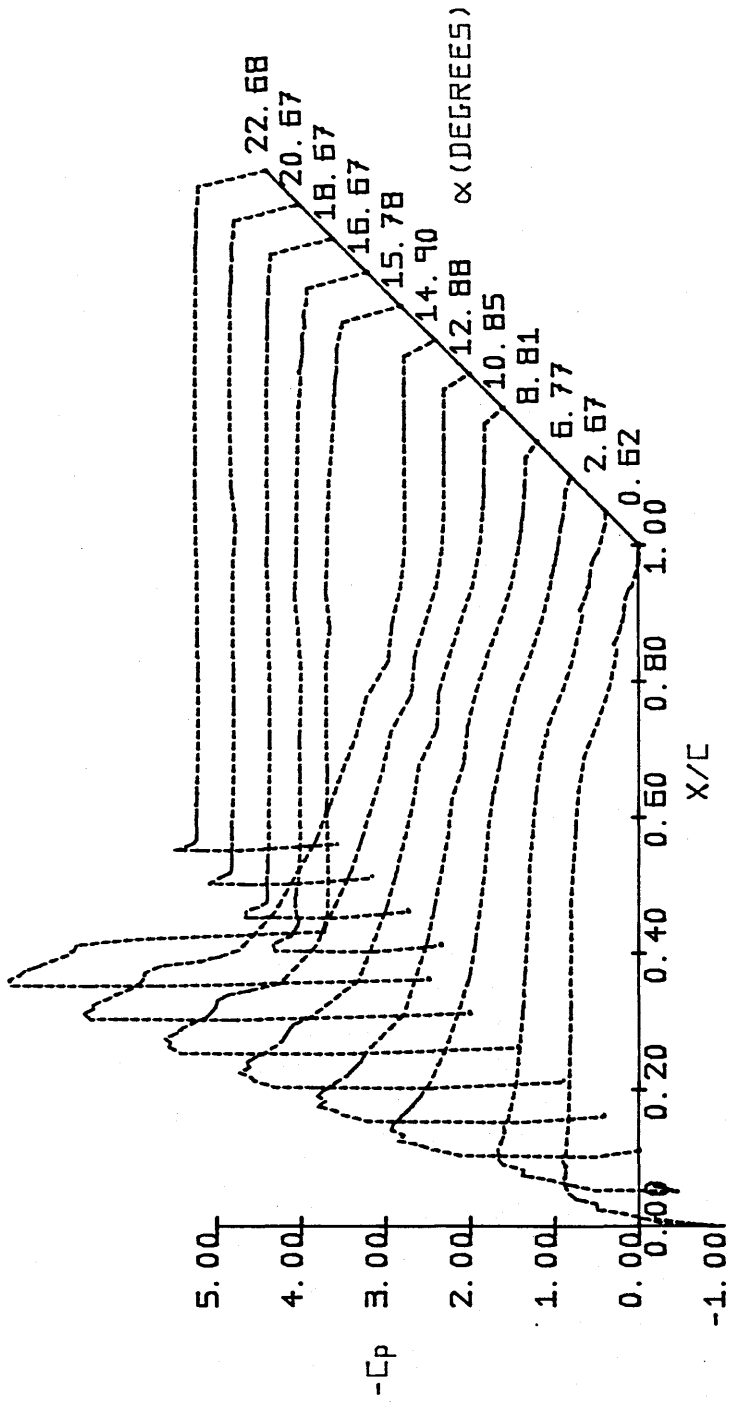


FIG.3.18 PRESSURE DISTRIBUTION FOR THE NASA GA(W)-1
 (Re = 402520.)

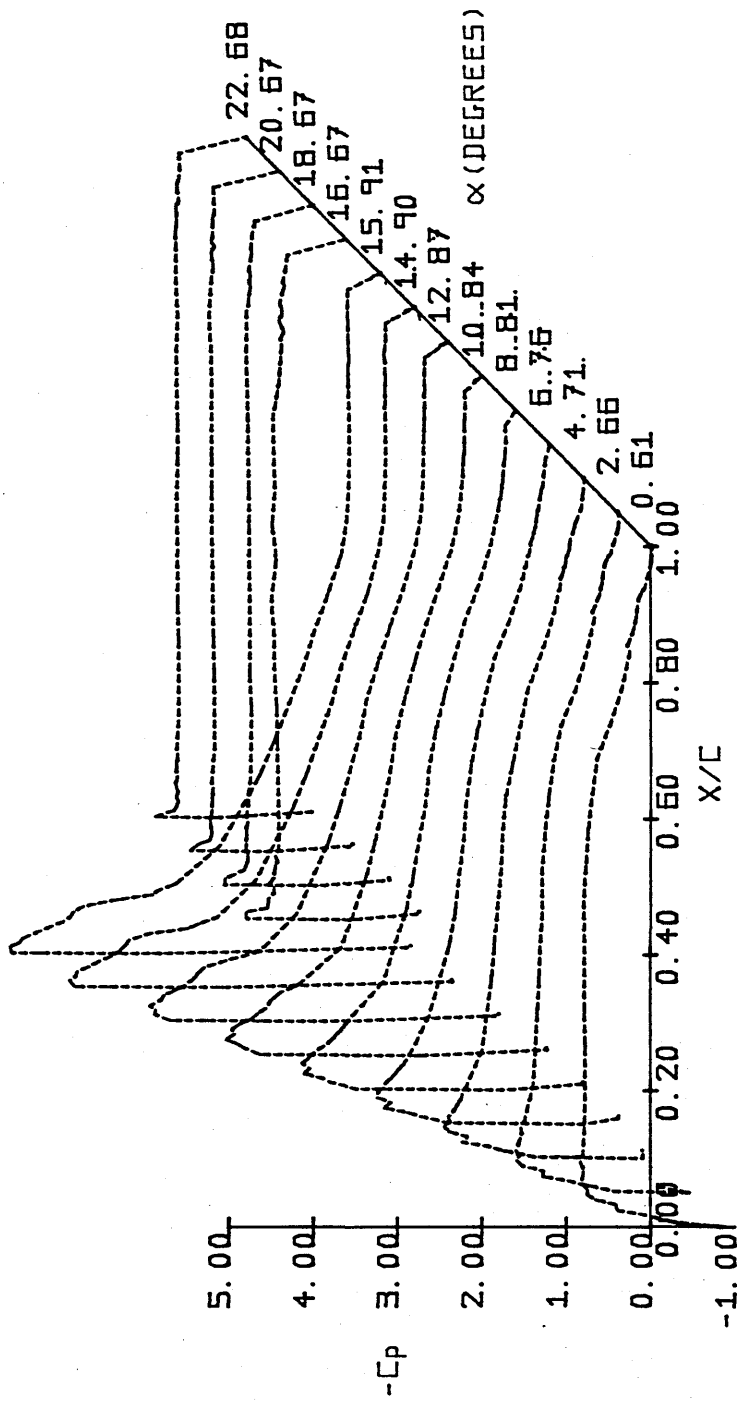


FIG.3.19 PRESSURE DISTRIBUTION FOR THE NASA GA(W)-1
 (Re = 452835.)

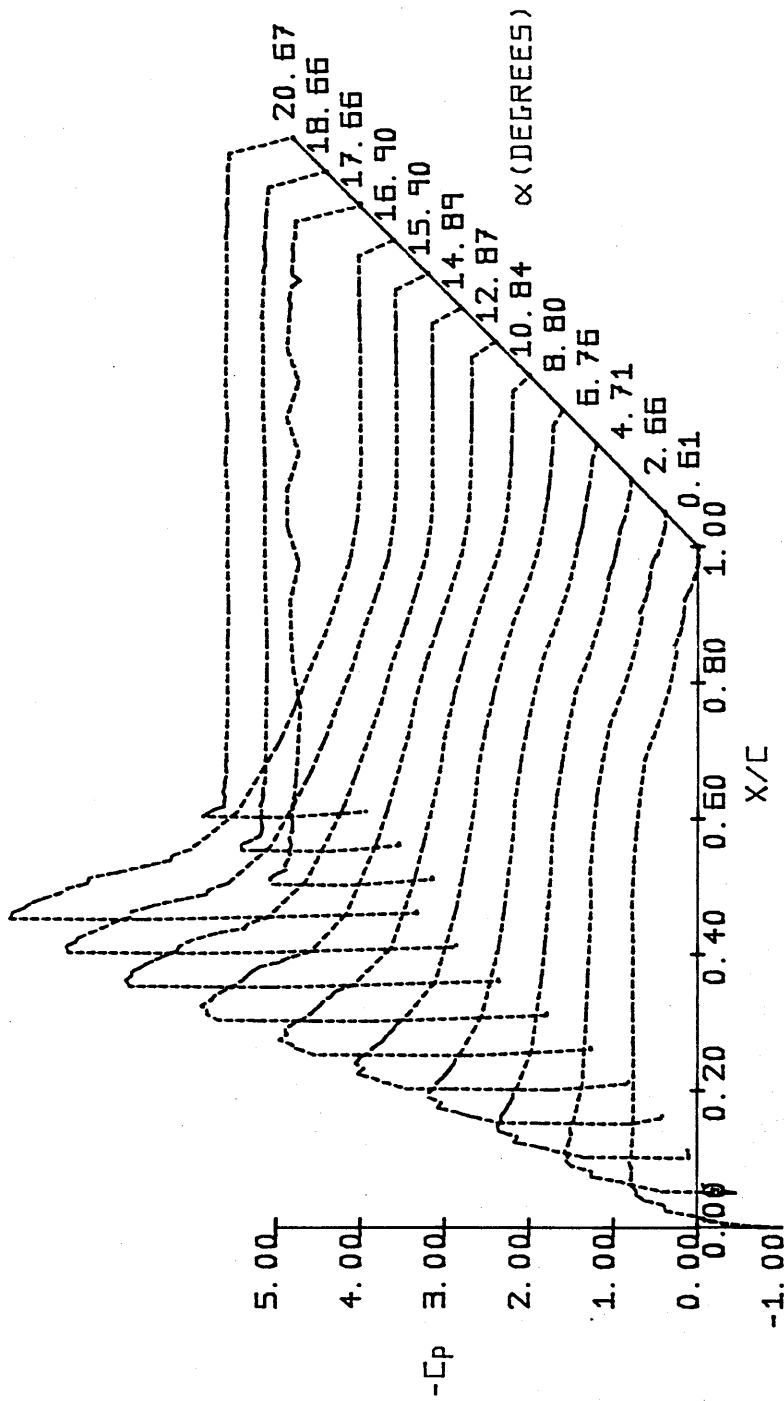


FIG.3.20 PRESSURE DISTRIBUTION FOR THE NASA GA(W)-1
(Re = 503150.)

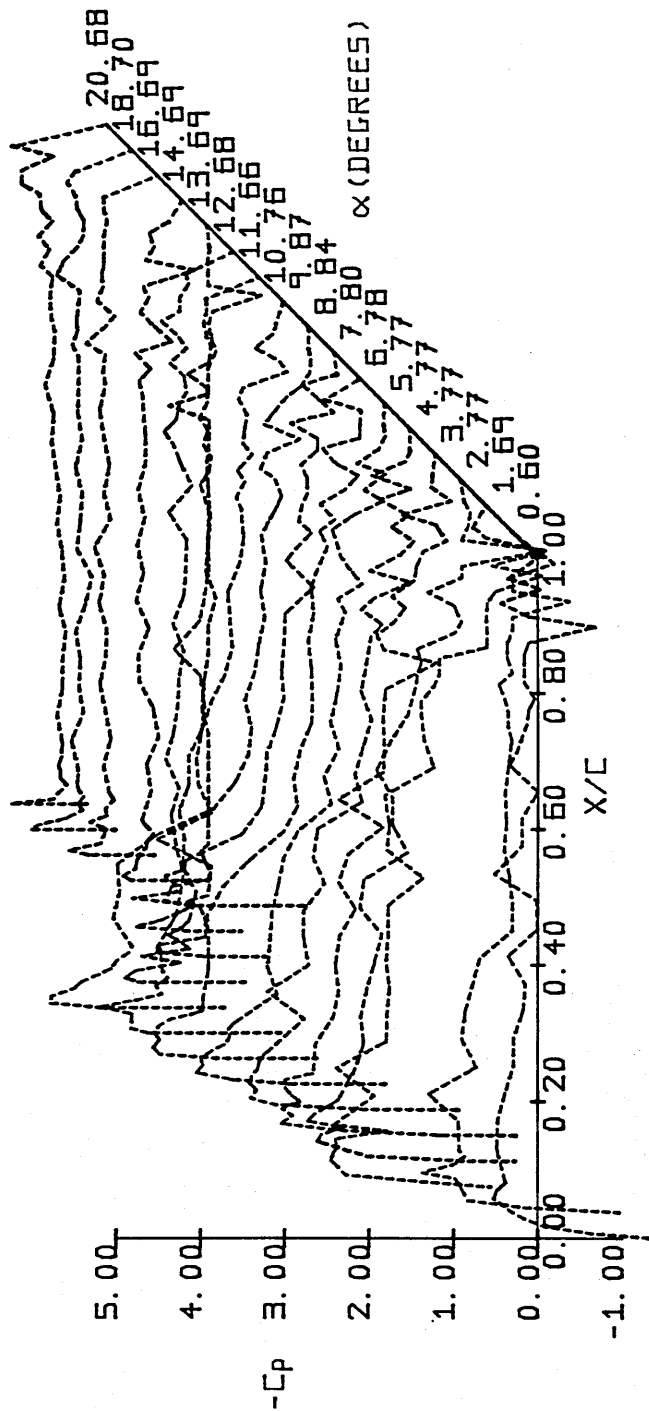


FIG.3.21 PRESSURE DISTRIBUTION FOR THE NACA-0015
(Re = 50280.)

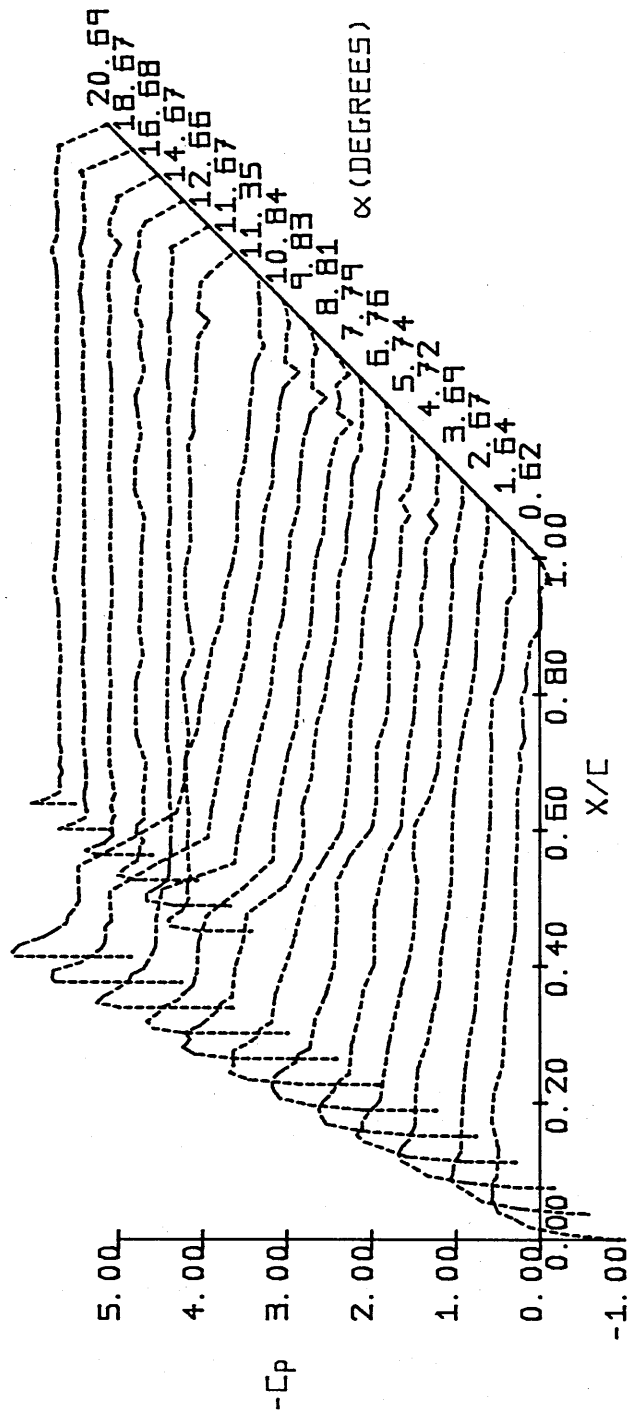


FIG.3.22 PRESSURE DISTRIBUTION FOR THE NACA-0015
 (Re = 100556.)

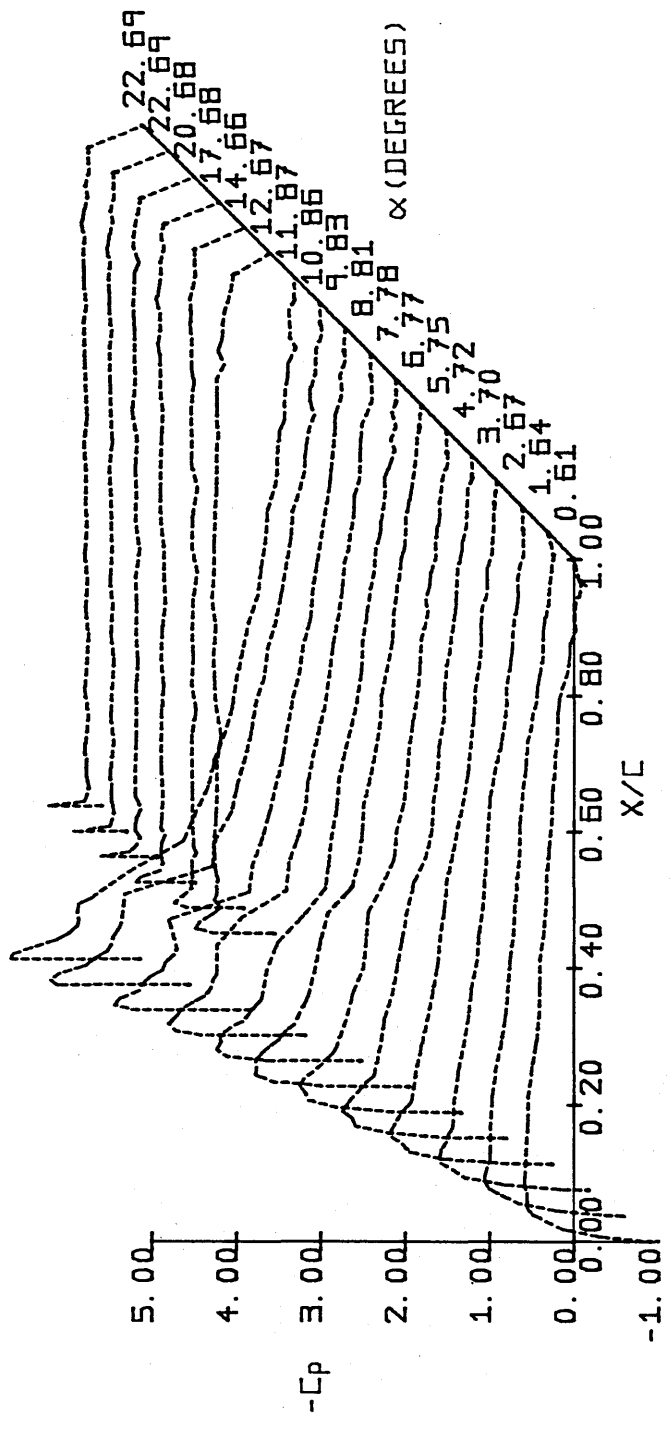


FIG.3.23 PRESSURE DISTRIBUTION FOR THE NACA-0015
($Re = 150835$.)

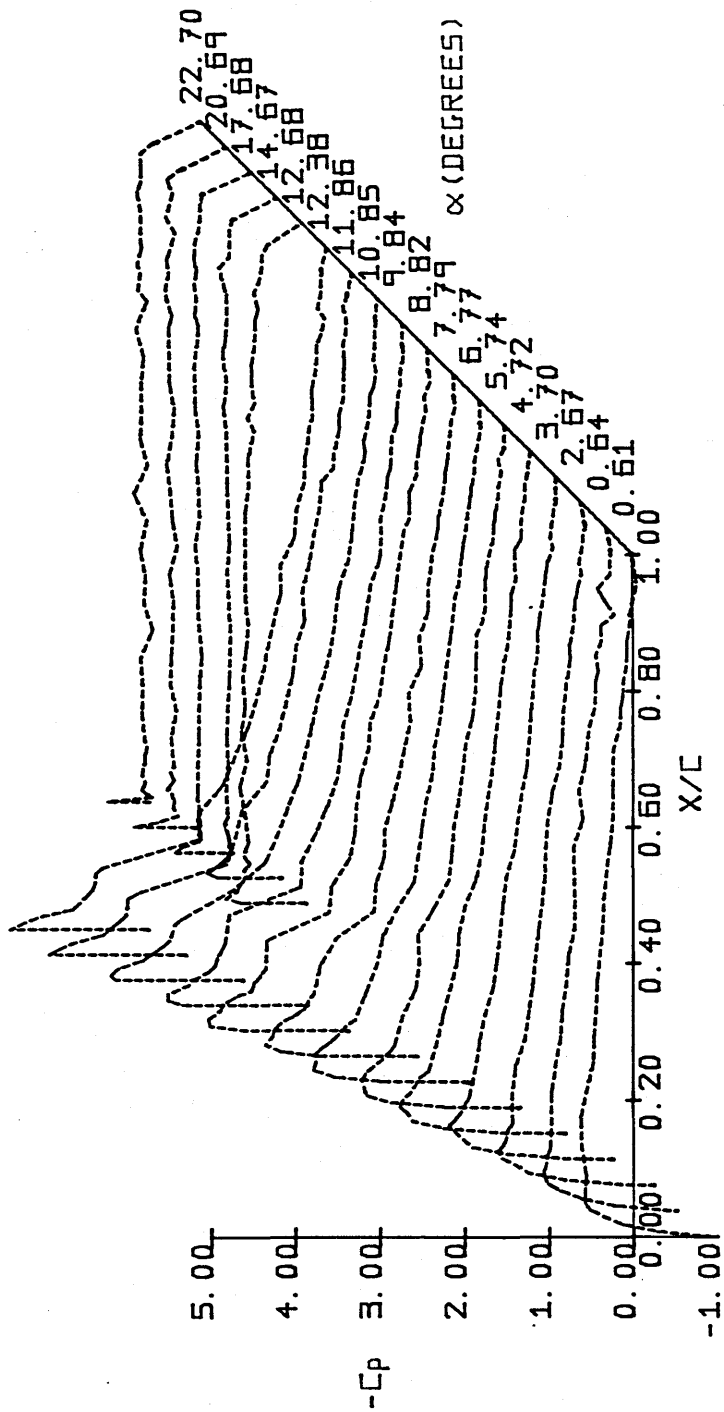


FIG.3.24 PRESSURE DISTRIBUTION FOR THE NACA-0015
($Re = 201113.$)

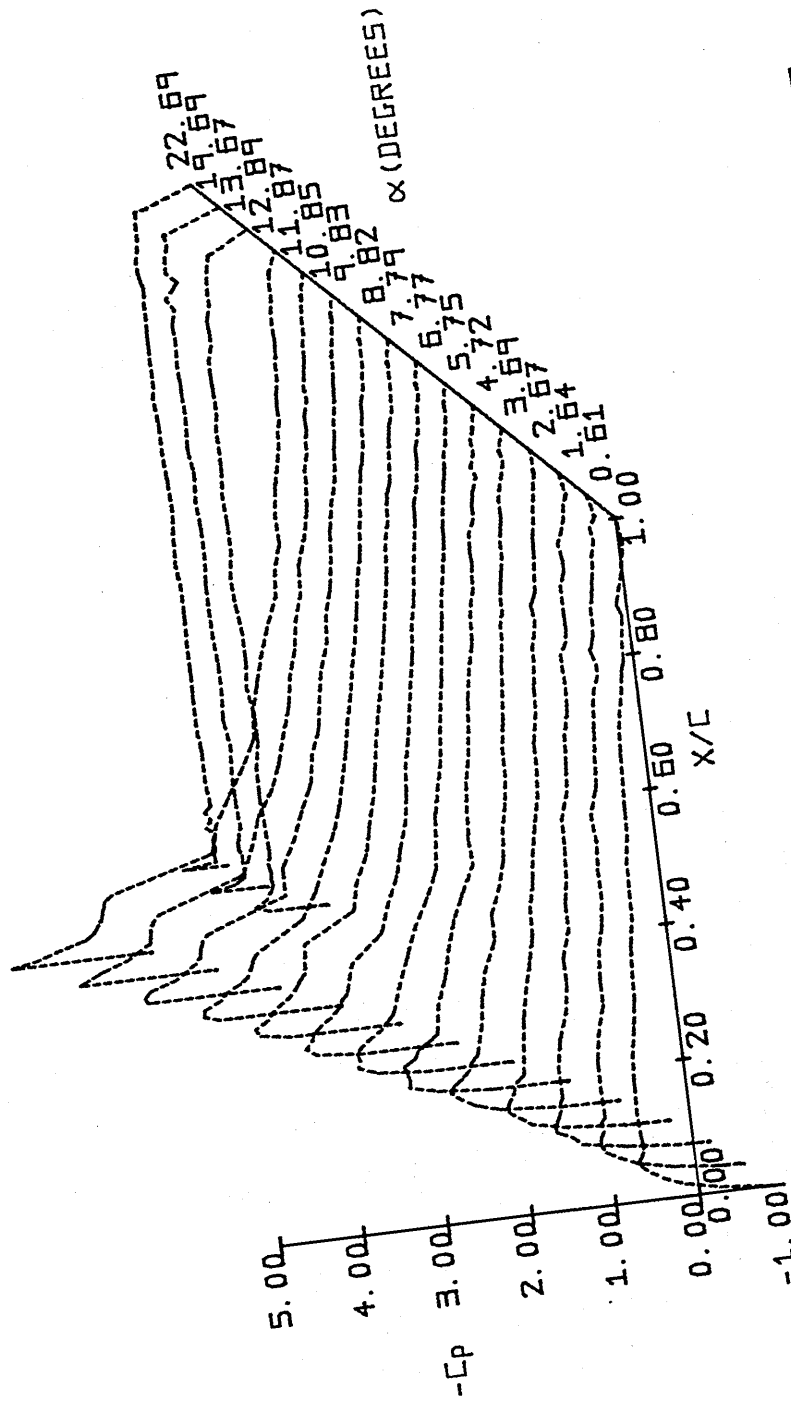


FIG. 3. 25 PRESSURE DISTRIBUTION FOR THE NACA-0015
($Re = 251390.$)

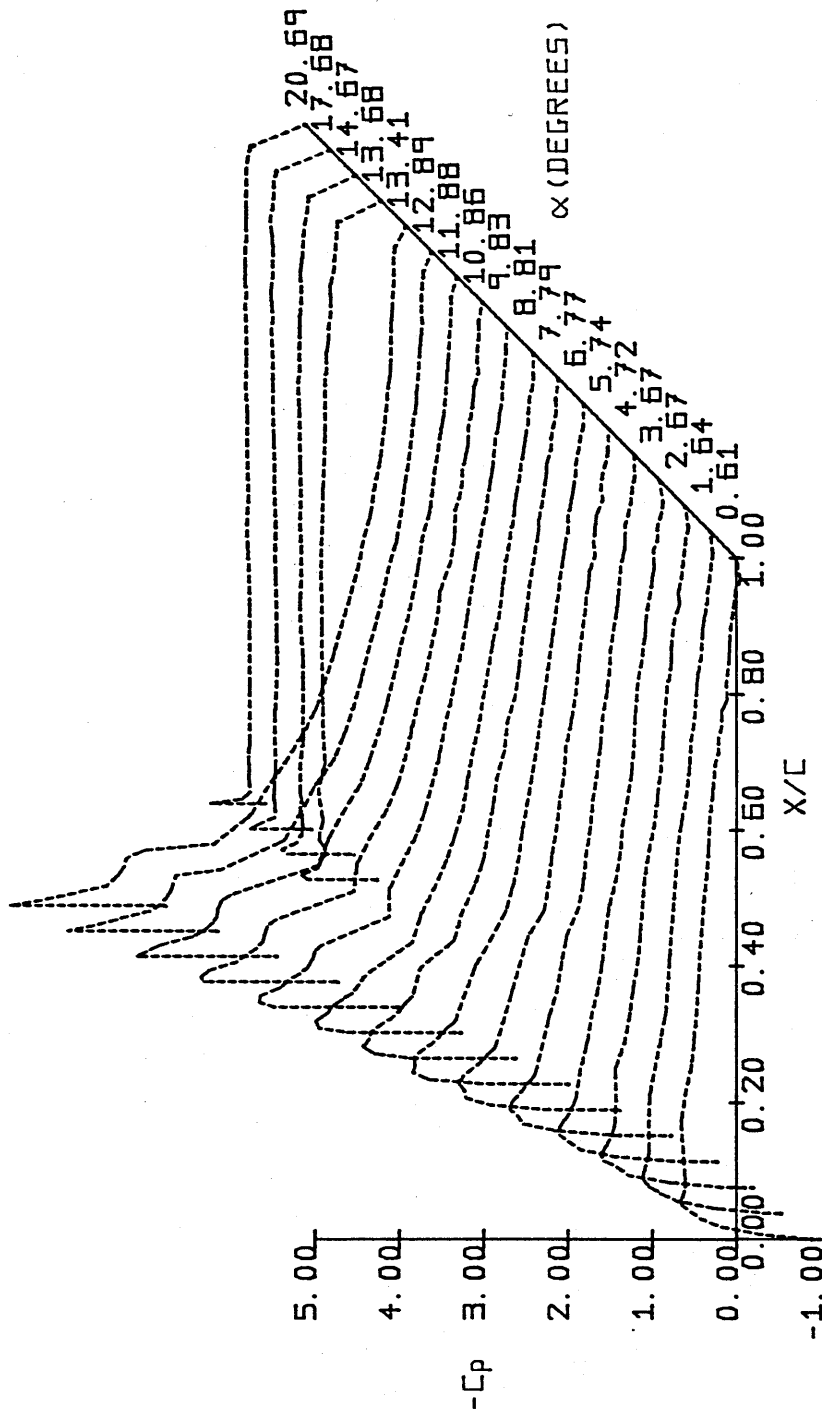


FIG.3.26 PRESSURE DISTRIBUTION FOR THE NACA-0015
($Re = 301670.$)

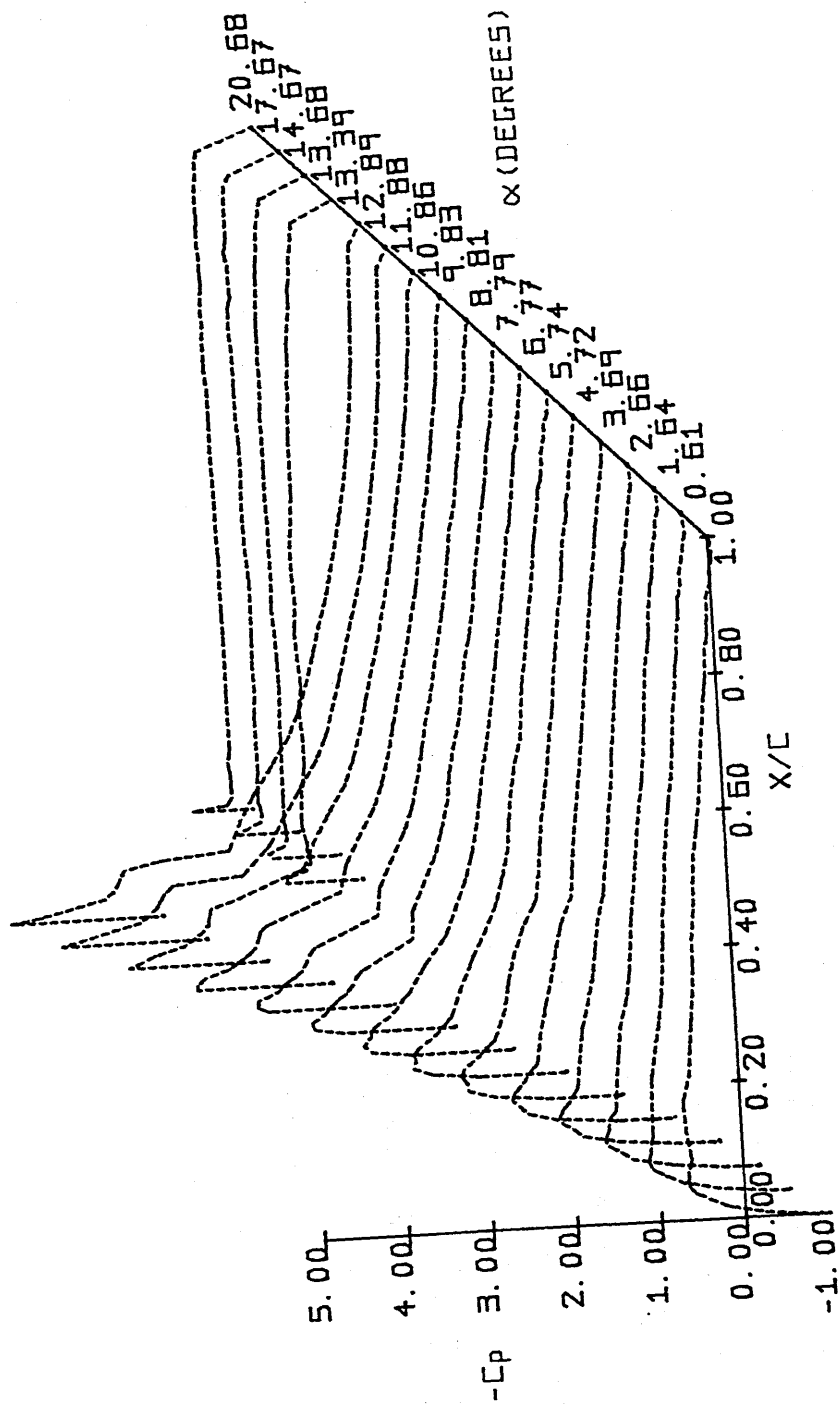


FIG.3.27 PRESSURE DISTRIBUTION FOR THE NACA-0015
($Re = 351950.$)

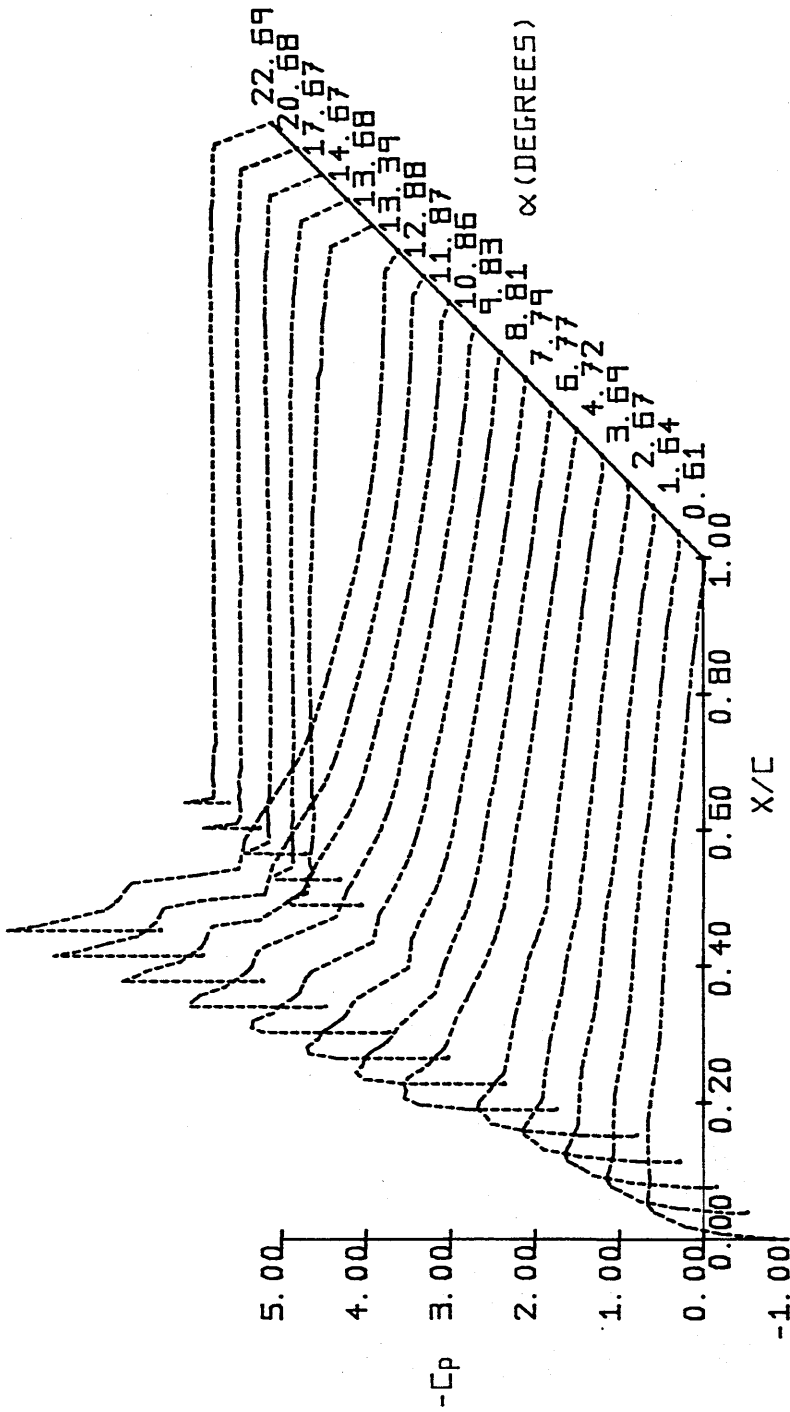


FIG.3.28 PRESSURE DISTRIBUTION FOR THE NACA-0015
(Re = 402230.)

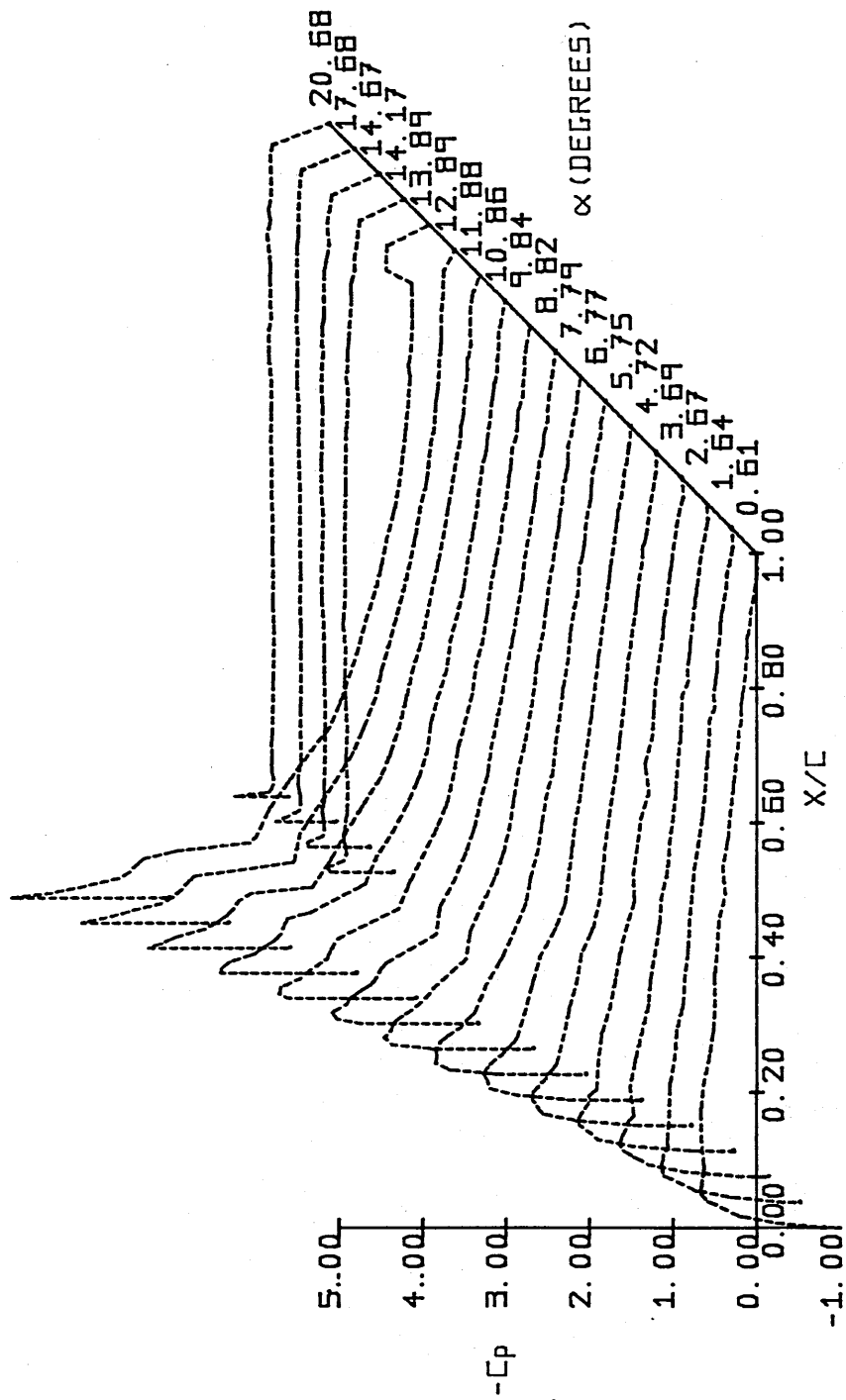


FIG.3.29 PRESSURE DISTRIBUTION FOR THE NACA-0015
(Re = 452500.)

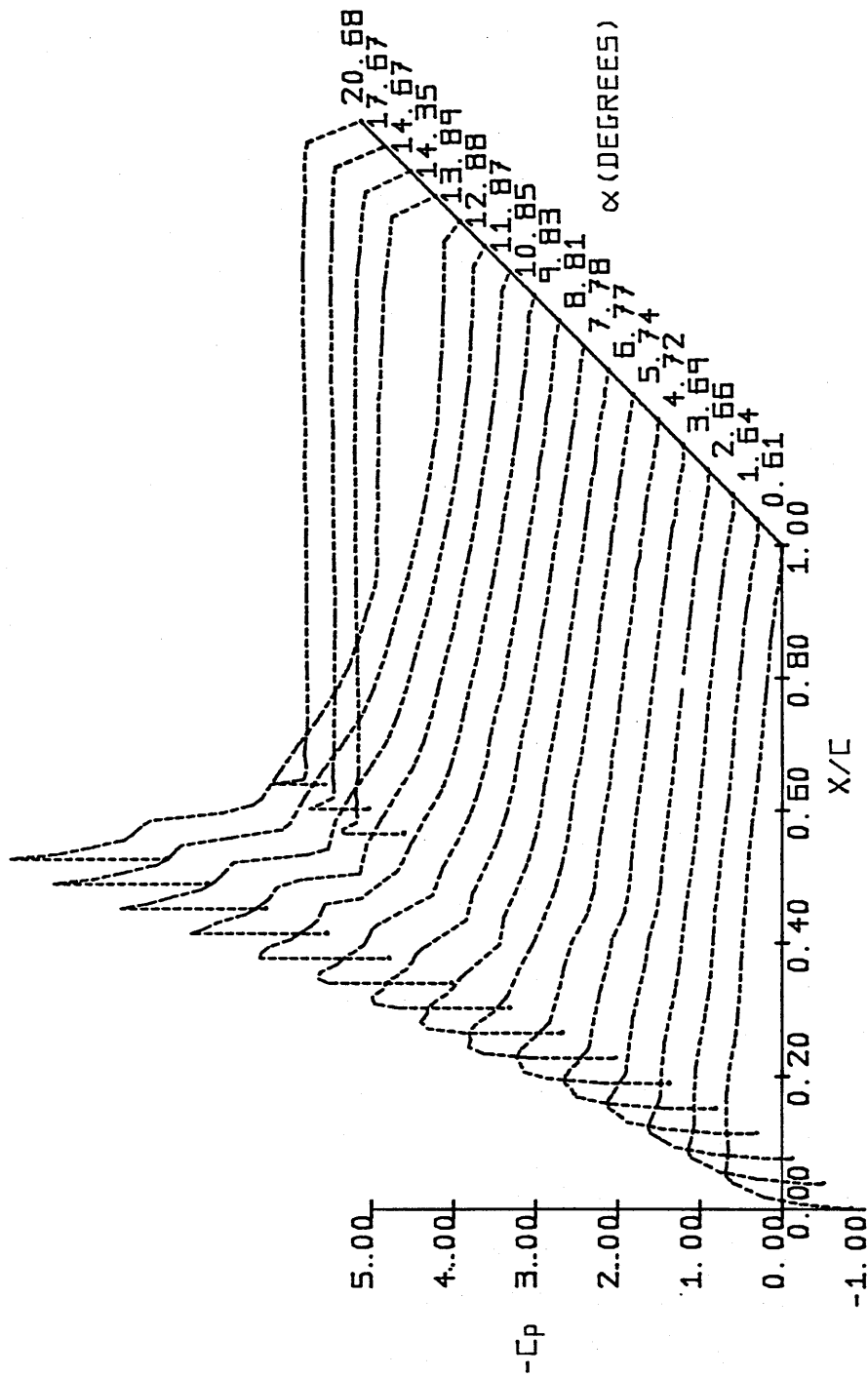
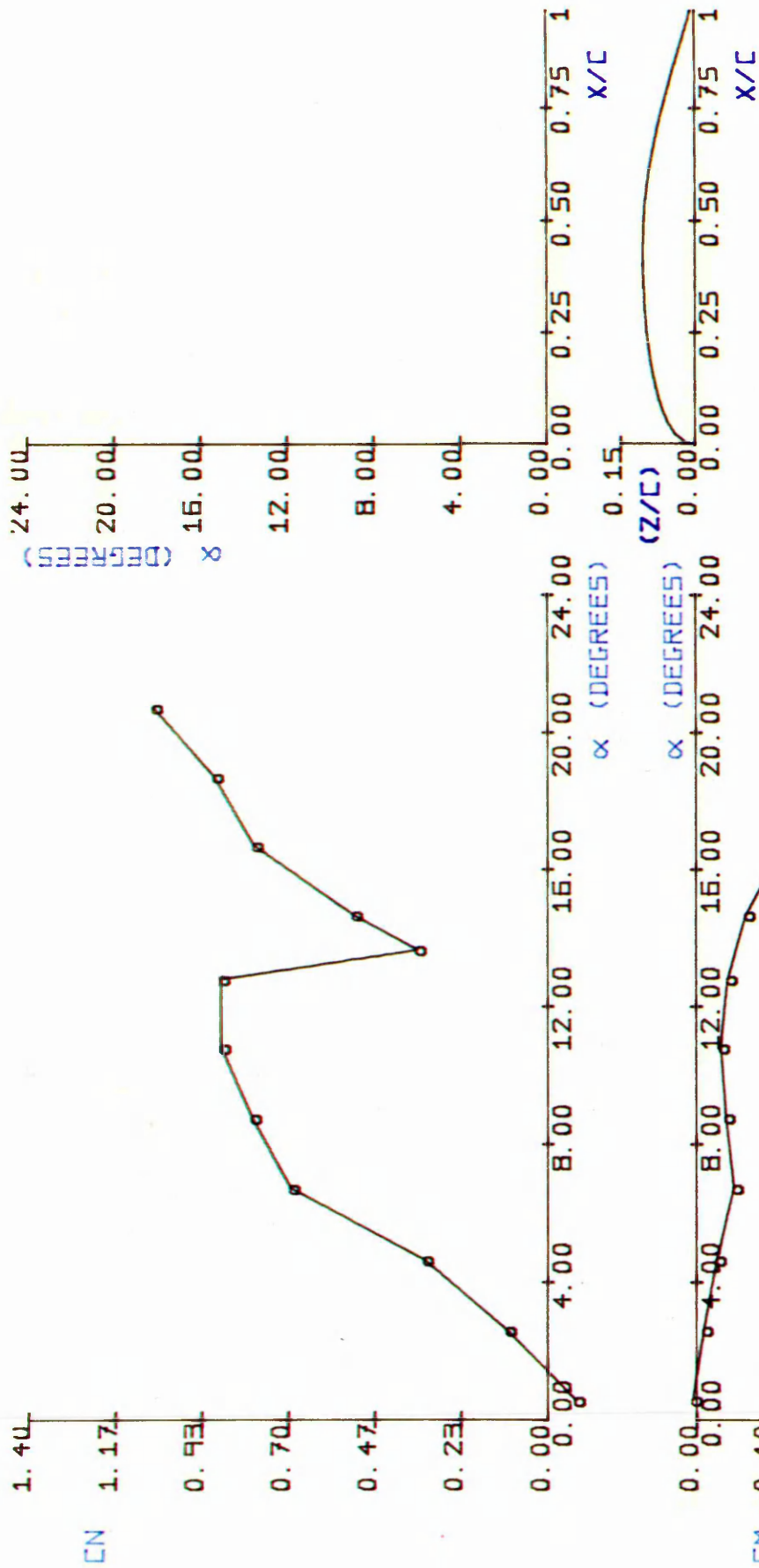
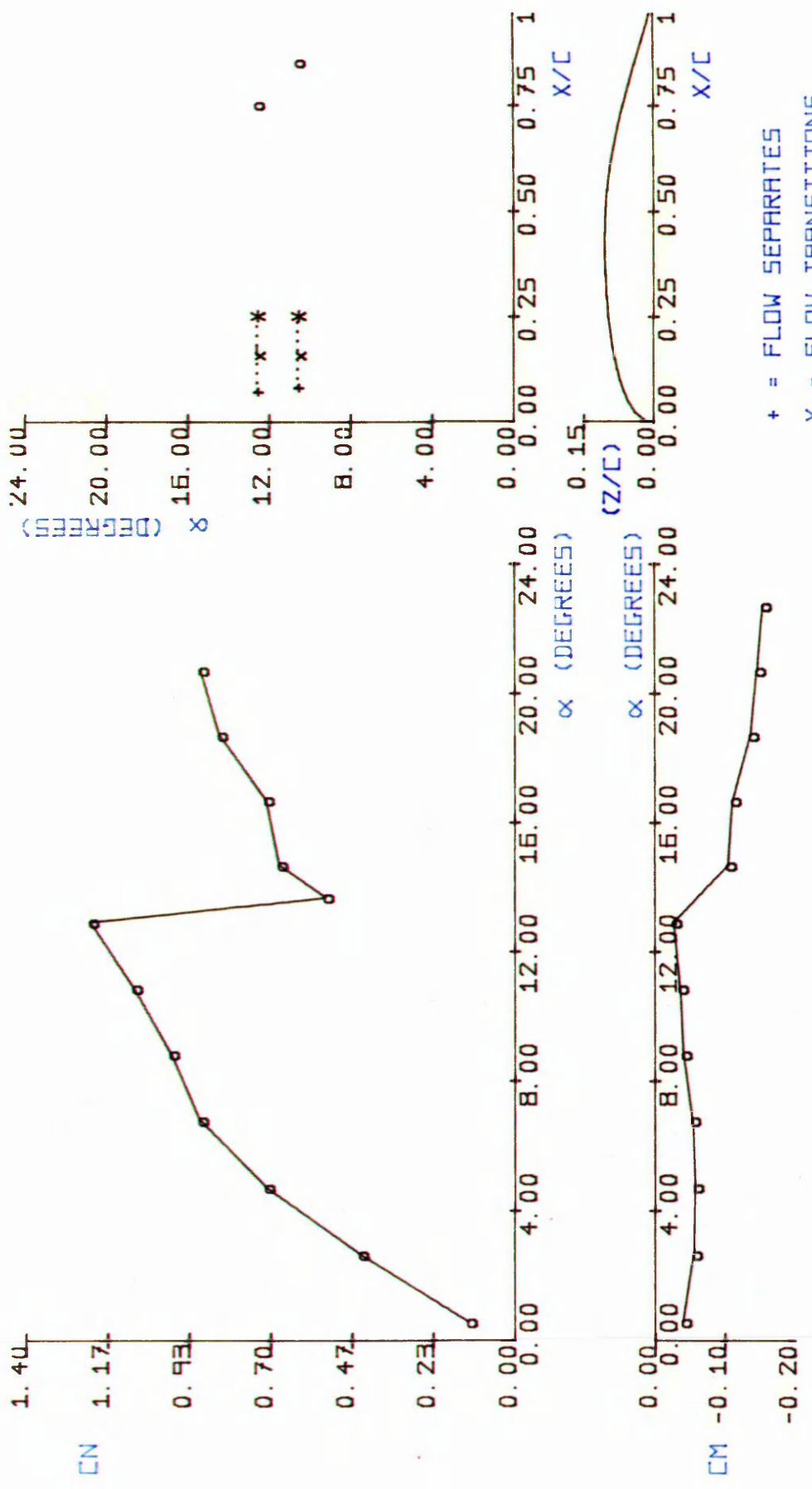


FIG.3.30 PRESSURE DISTRIBUTION FOR THE NACA-0015
($Re = 502784$.)



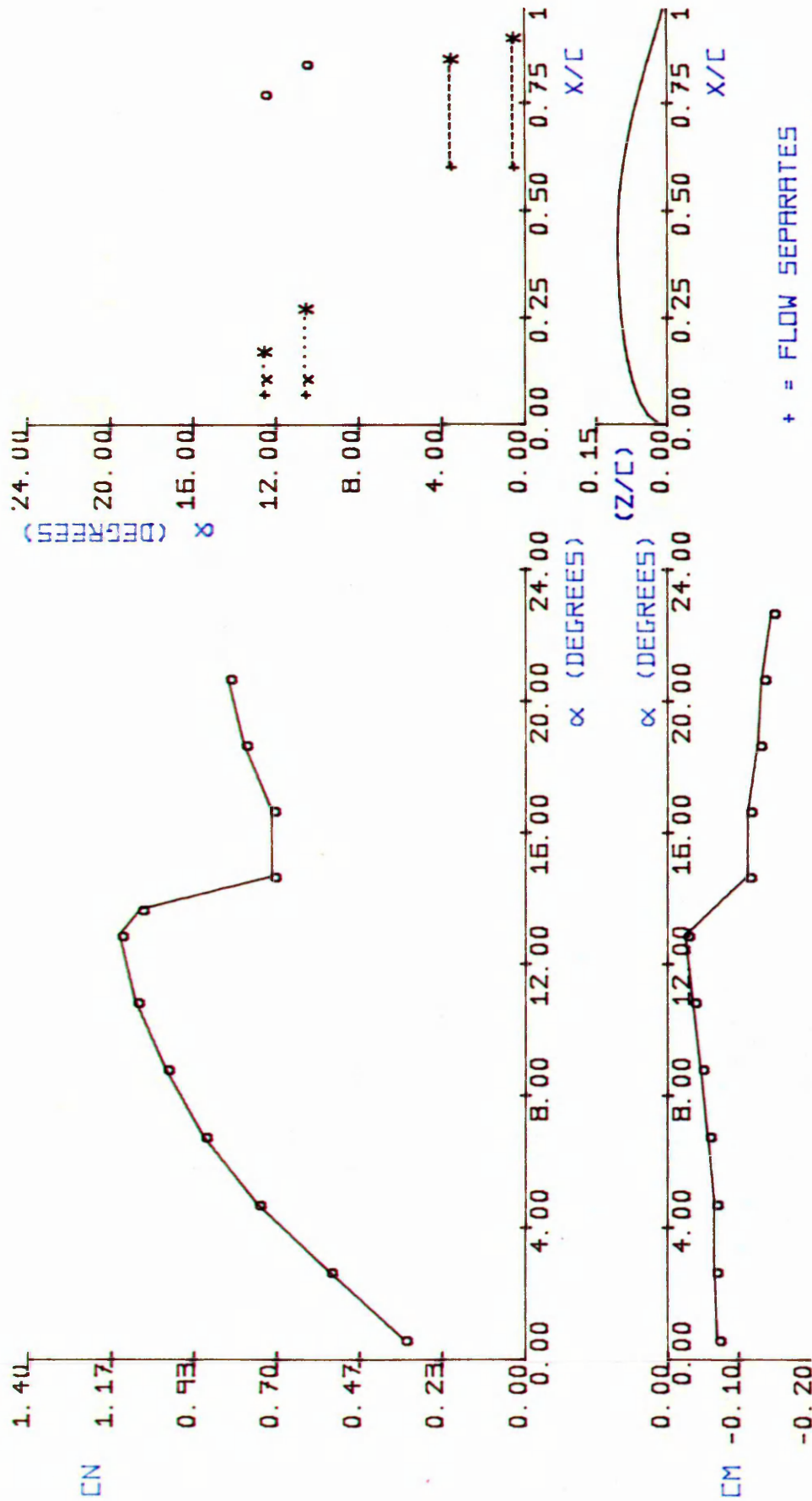
- + = FLOW SEPARATES
- X = FLOW TRANSITIONS
- * = FLOW REATTACHES
- o = FLOW SEPARATES
- = LONG BUBBLE REGION
- ... = SHORT BUBBLE REGION

FIG.3.31 AERODYNAMIC CHARACTERISTICS OF THE NASA GA(W)-1 AIRFOIL
(Re = 50320.)



+ = FLOW SEPARATES
 X = FLOW TRANSITIONS
 * = FLOW REATTACHES
 O = FLOW SEPARATES
 ---- = LONG BUBBLE REGION
 ... = SHORT BUBBLE REGION

FIG.3.32 AERODYNAMIC CHARACTERISTICS OF THE
 NASA GA(W)-1 AEROFOIL
 ($Re = 100630$.)



+ = FLOW SEPARATES
X = FLOW TRANSITIONS
* = FLOW REATTACHES
O = FLOW SEPARATES
----- = LONG BUBBLE REGION
... = SHORT BUBBLE REGION

FIG.3.33 AERODYNAMIC CHARACTERISTICS OF THE NASA GA(W)-1 AEROFOIL
(Re = 150950.)

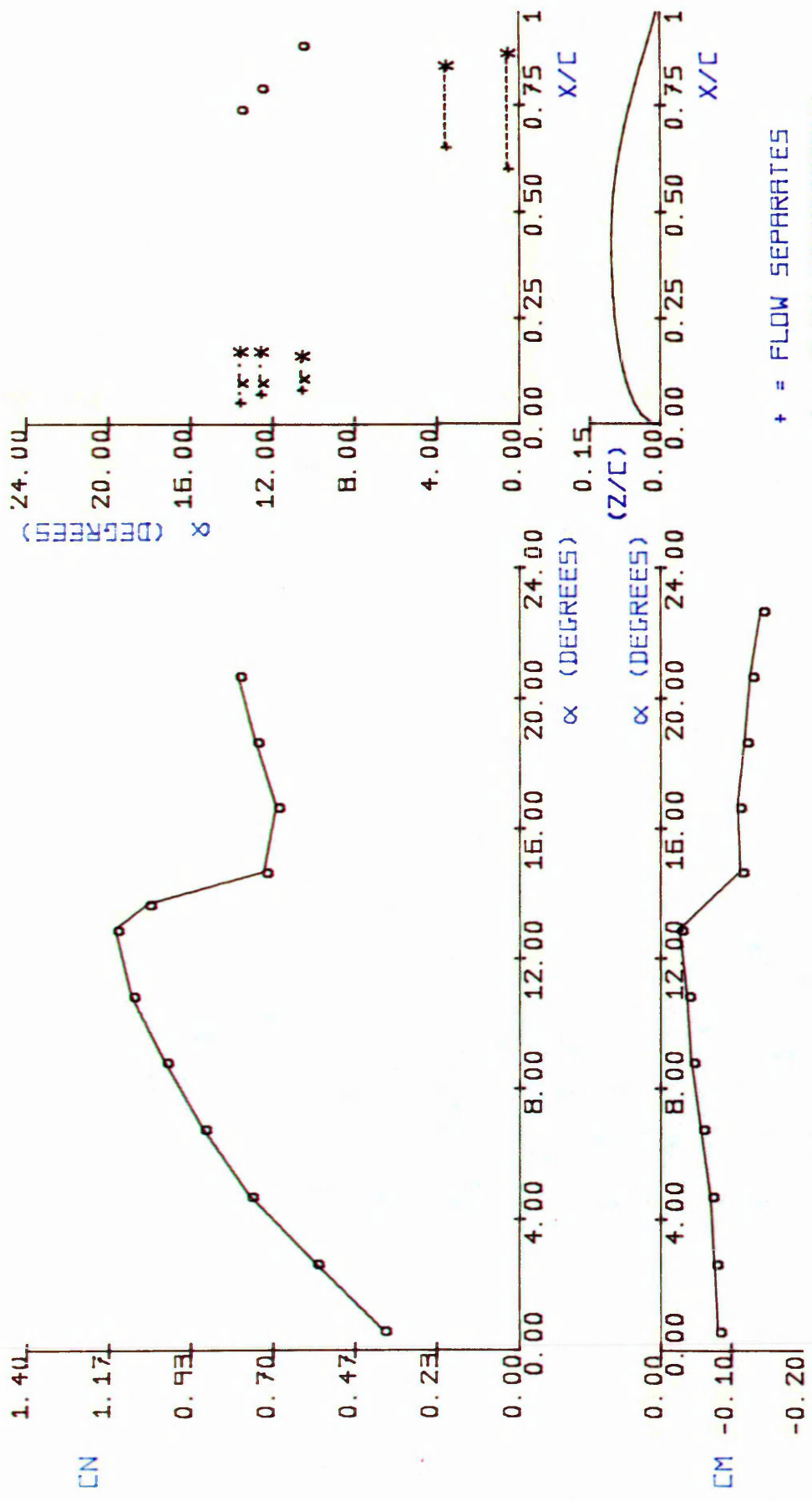
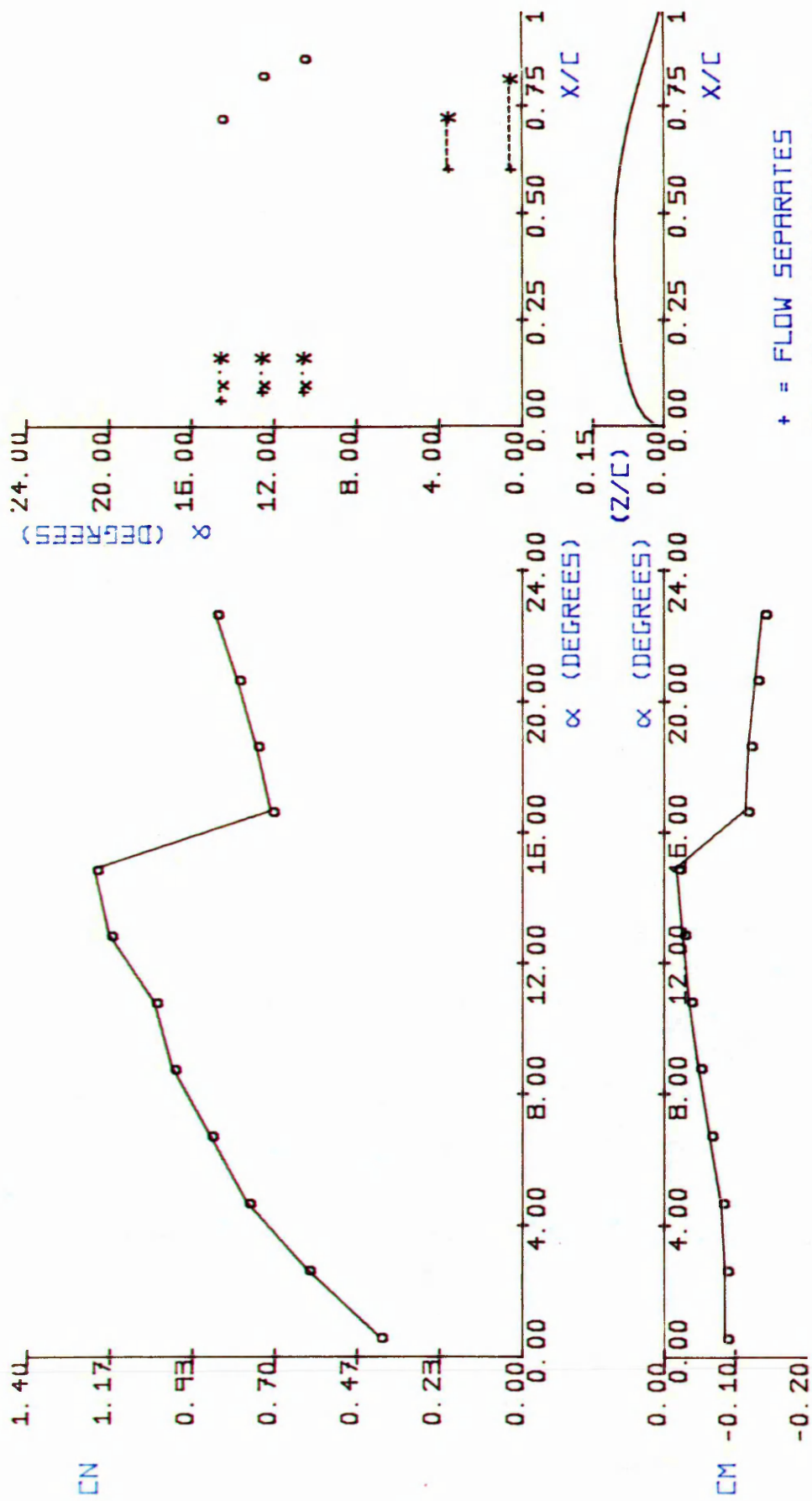


FIG.3.34 AERODYNAMIC CHARACTERISTICS OF THE NASA GA(W)-1 AEROFOIL
 (Re = 201260.)



+ = FLOW SEPARATES
 X = FLOW TRANSITIONS
 * = FLOW REATTACHES
 O = FLOW SEPARATES
 ---- = LONG BUBBLE REGION
 ... = SHORT BUBBLE REGION

FIG.3.35 AERODYNAMIC CHARACTERISTICS OF THE NASA GA(W)-1 AERDFOIL
 (Re = 251575.)

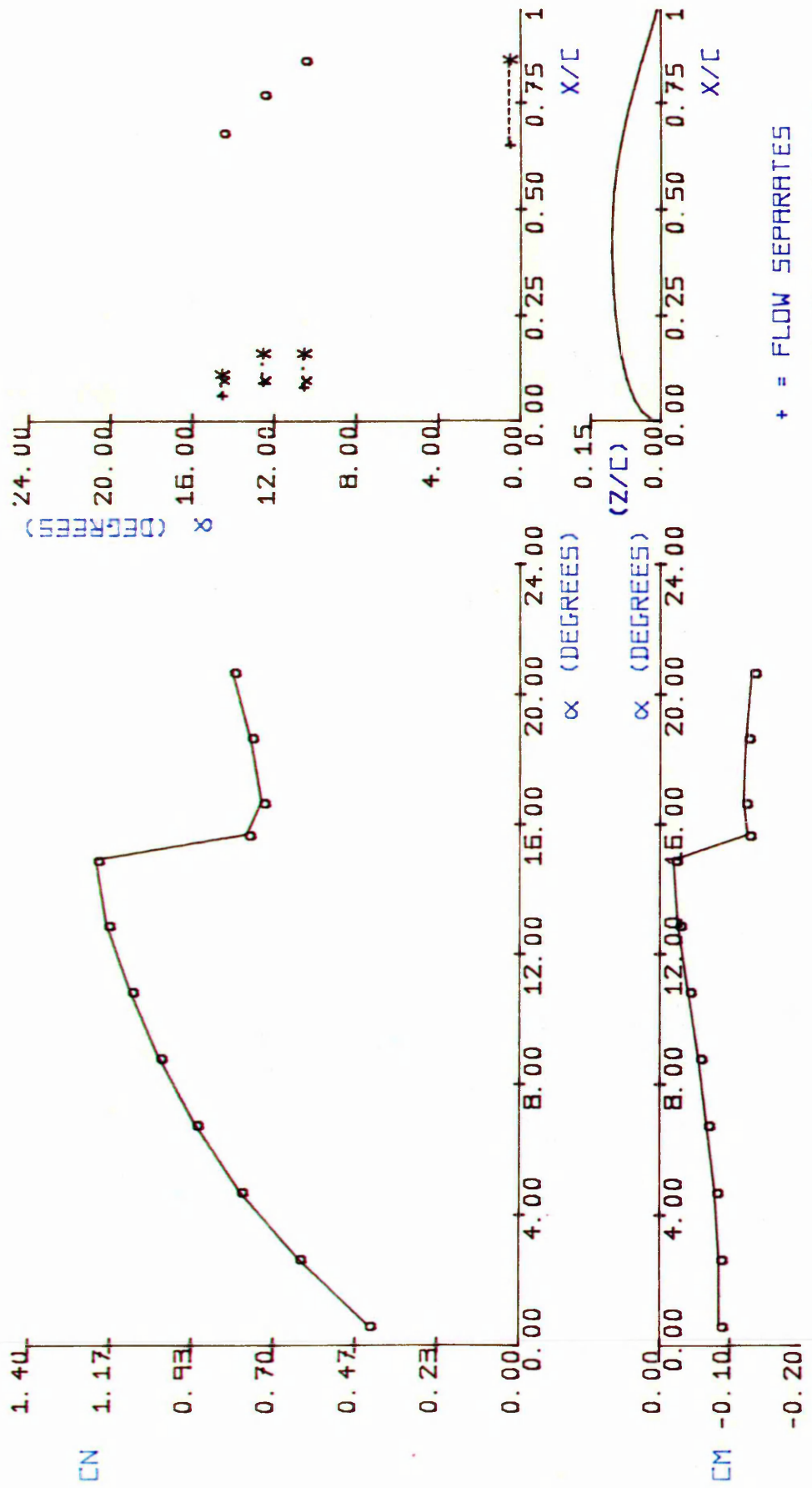


FIG.3.36 AERODYNAMIC CHARACTERISTICS OF THE
 NASA GA(W)-1 AEROFOIL
 (Re = 302000.)

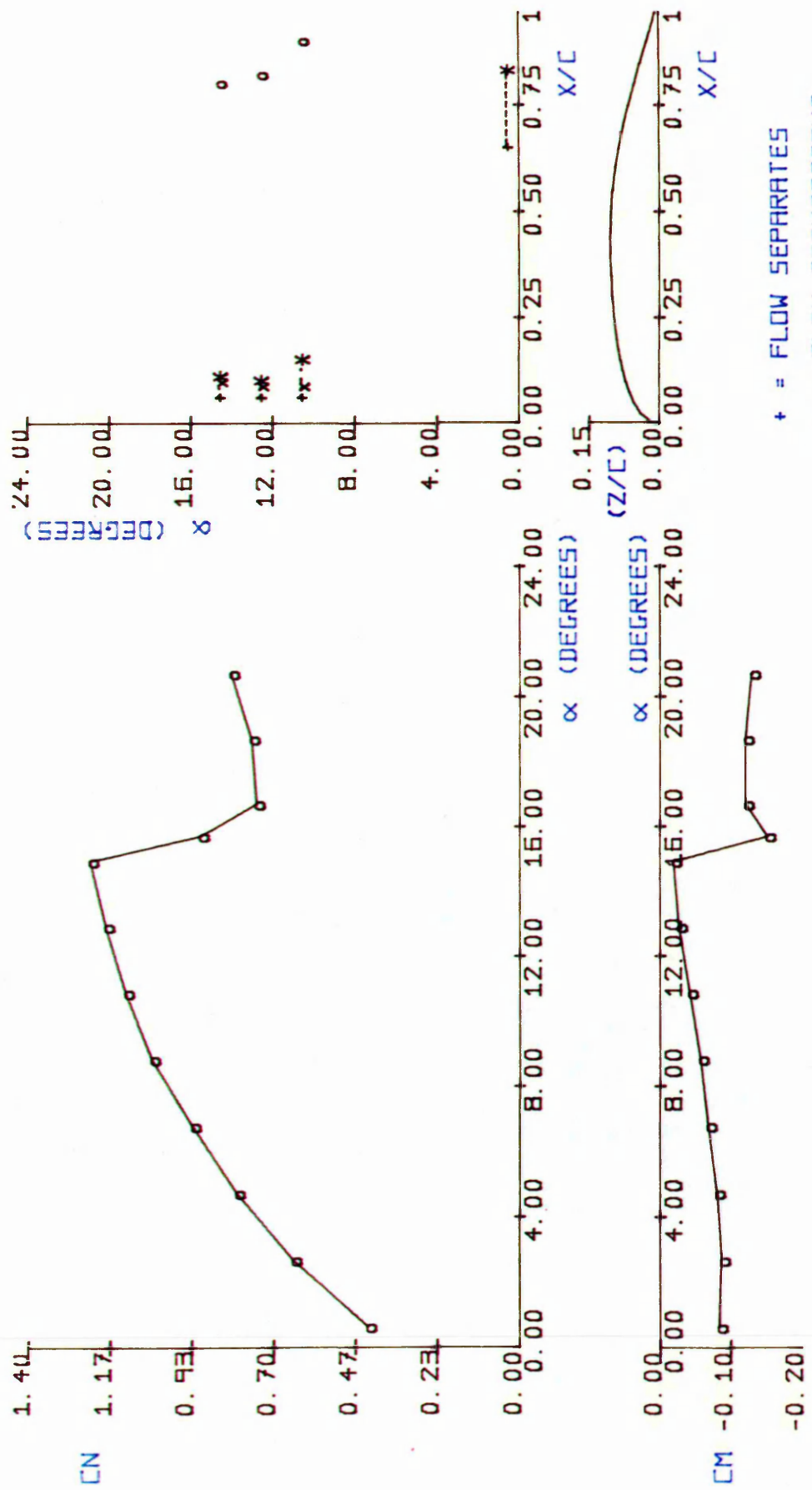
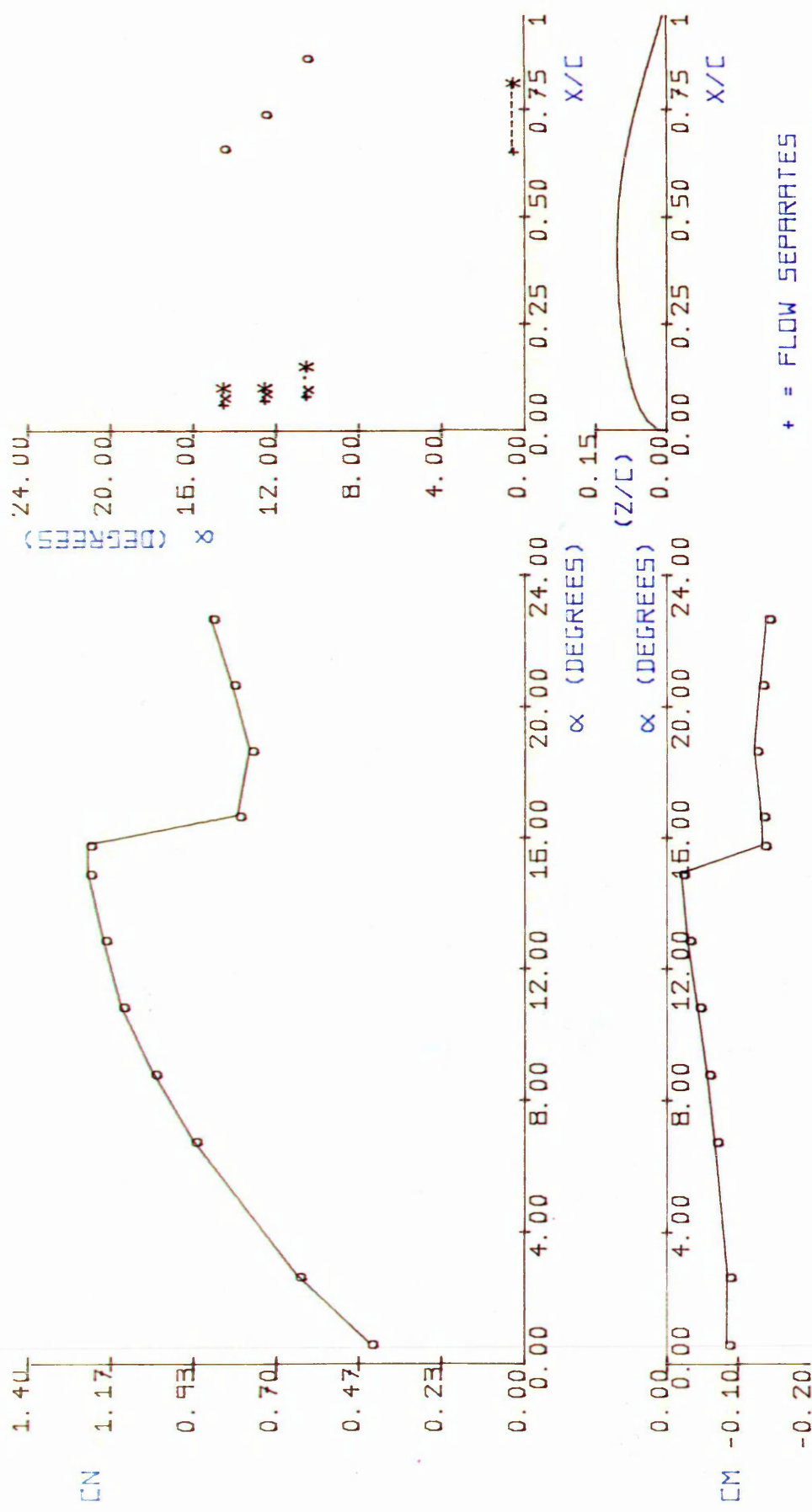
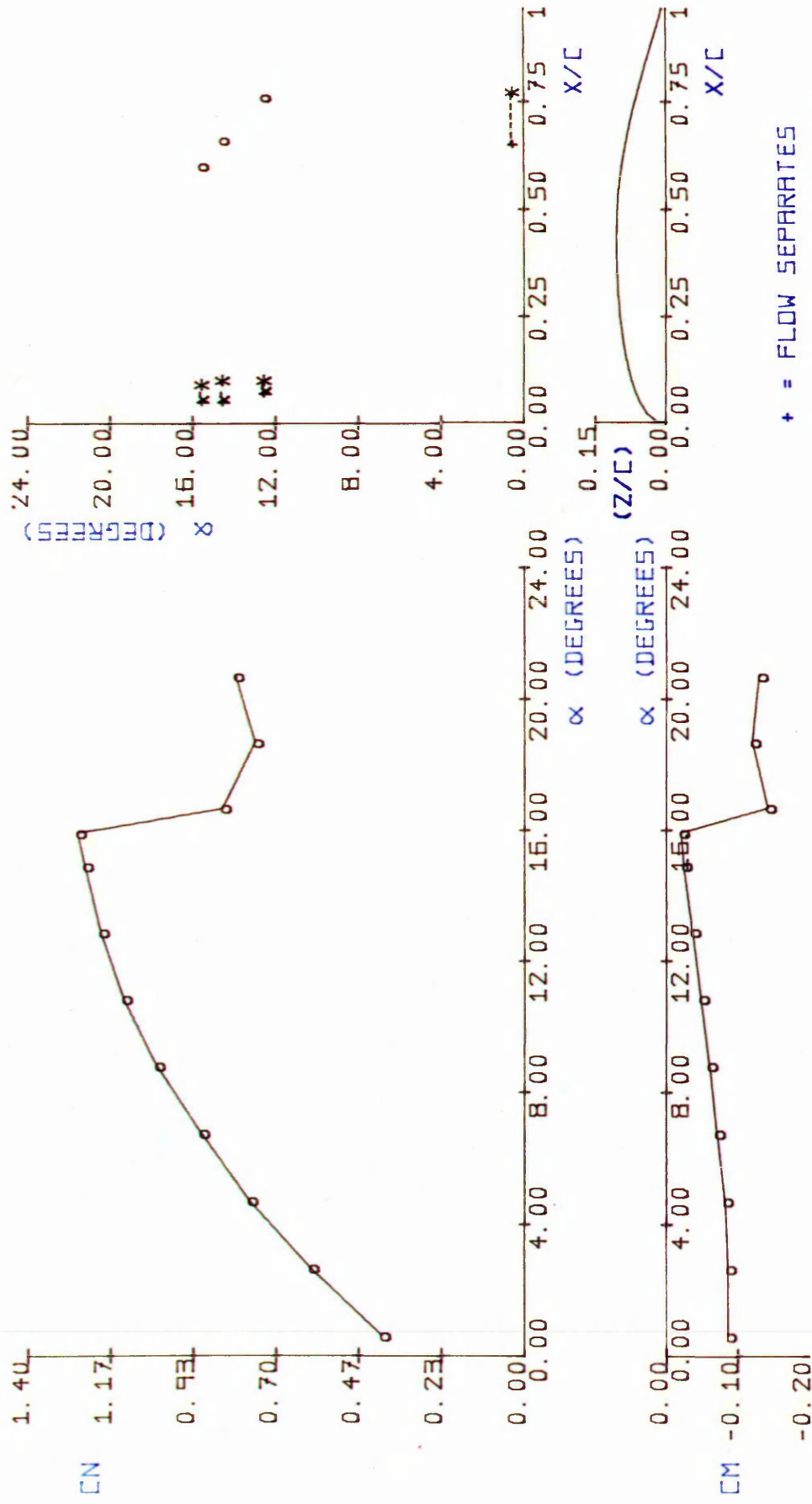


FIG.3.37 AERODYNAMIC CHARACTERISTICS OF THE
 NASA GA(W)-1 AEROFOIL
 ($Re = 352200$.)



- + = FLOW SEPARATES
- x = FLOW TRANSITIONS
- * = FLOW REATTACHES
- o = FLOW SEPARATES
- = LONG BUBBLE REGION
- ... = SHORT BUBBLE REGION

FIG. 3. 38 AERODYNAMIC CHARACTERISTICS OF THE
 NASA GA(W)-1 AEROFOIL.
 (Re = 402520.)



- + = FLOW SEPARATES
- x = FLOW TRANSITIONS
- * = FLOW REATTACHES
- o = FLOW SEPARATES
- = LONG BUBBLE REGION
- ... = SHORT BUBBLE REGION

FIG.3.39 AERODYNAMIC CHARACTERISTICS OF THE
 NASA GA(W)-1 AEROFOIL
 (Re = 452835.)

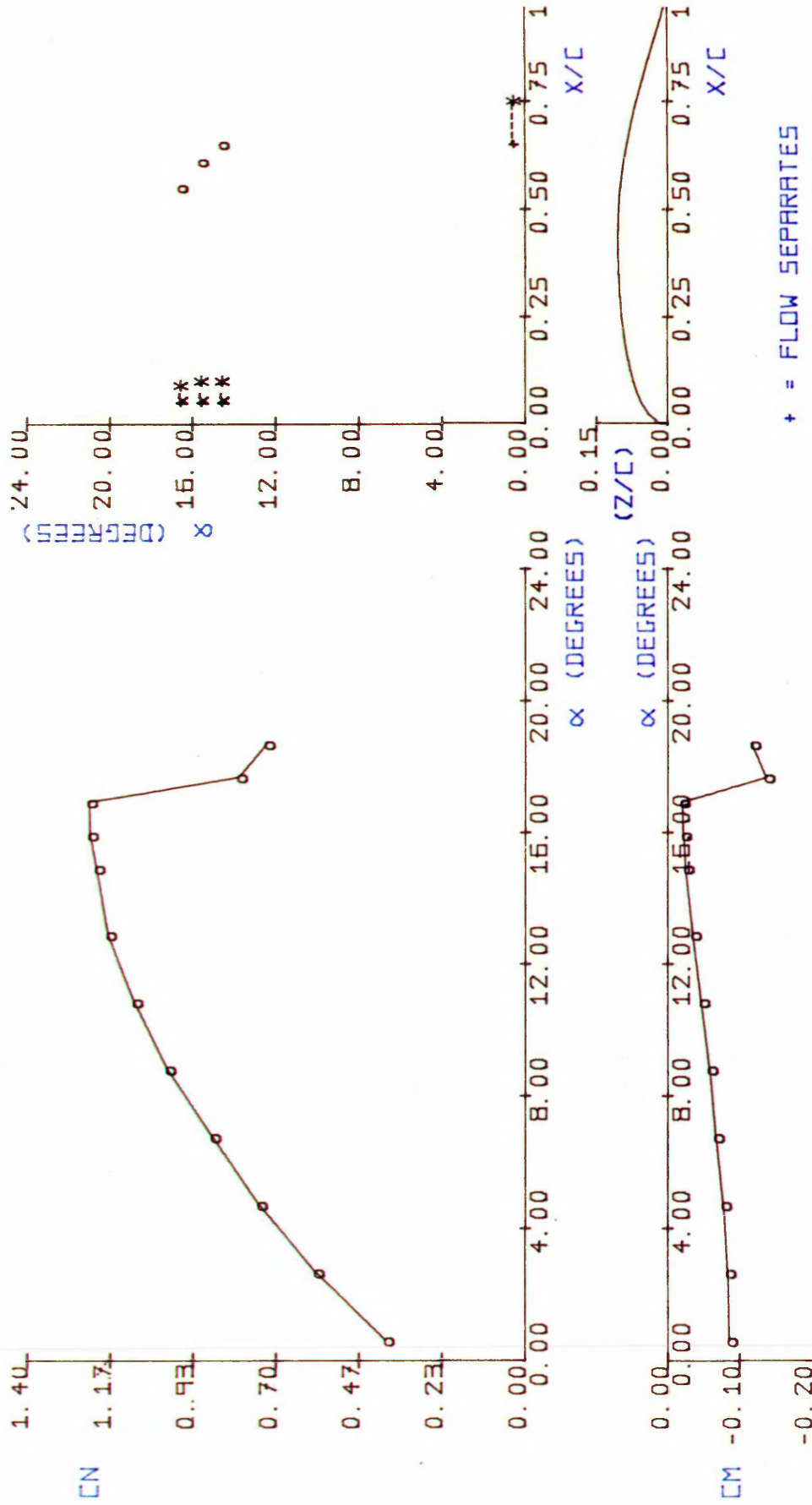


FIG.3.40 AERODYNAMIC CHARACTERISTICS OF THE
 NASA GA(W)-1 AEROFOIL
 ($Re = 503150.$)

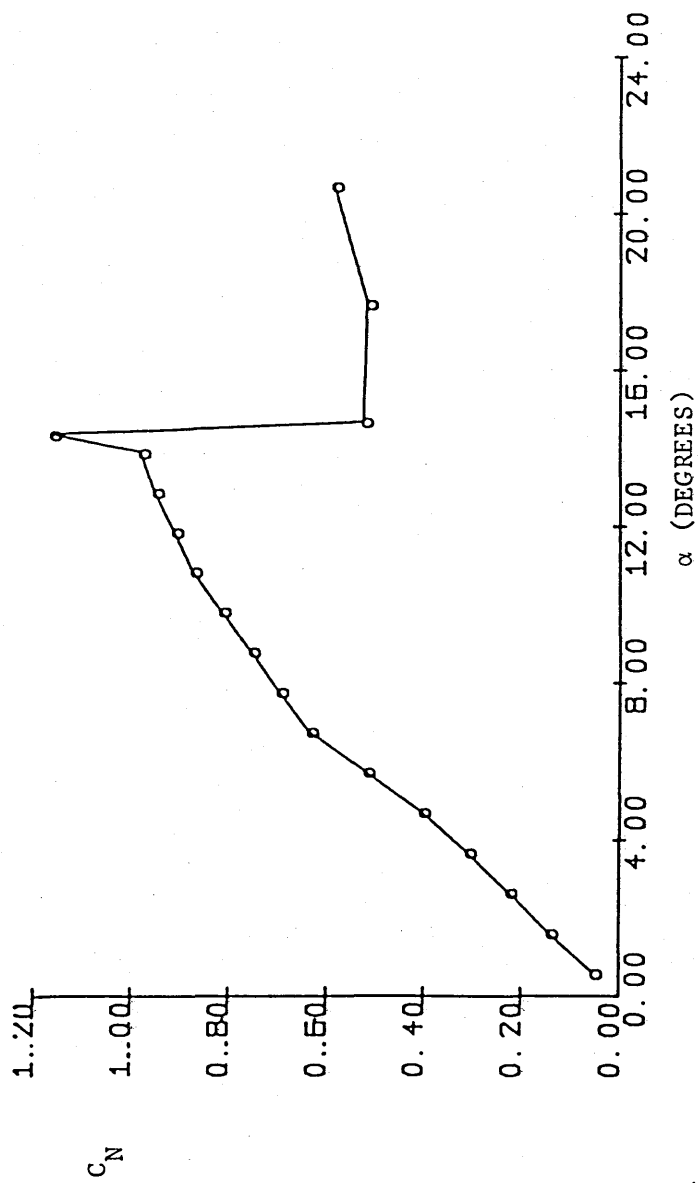
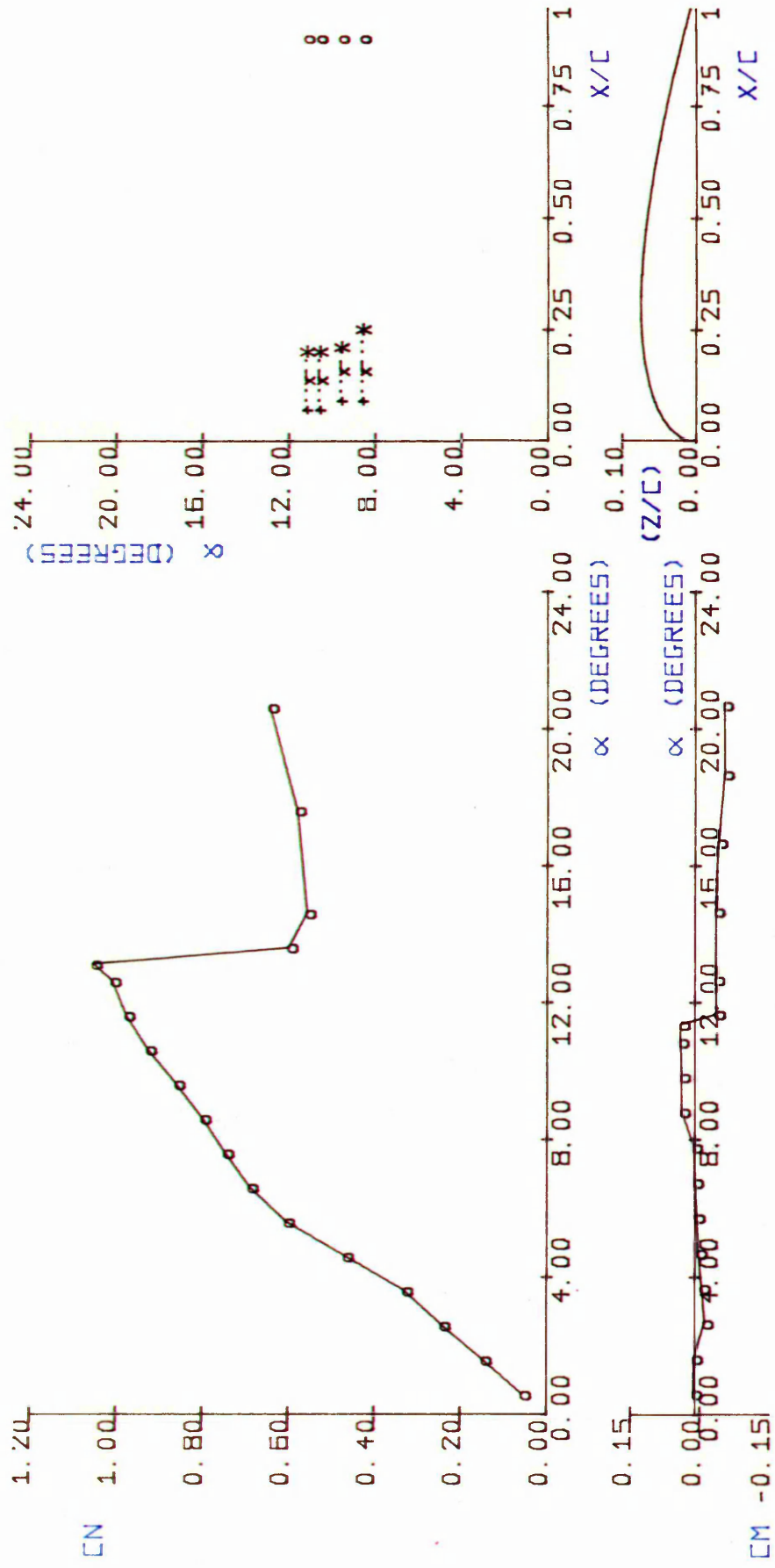
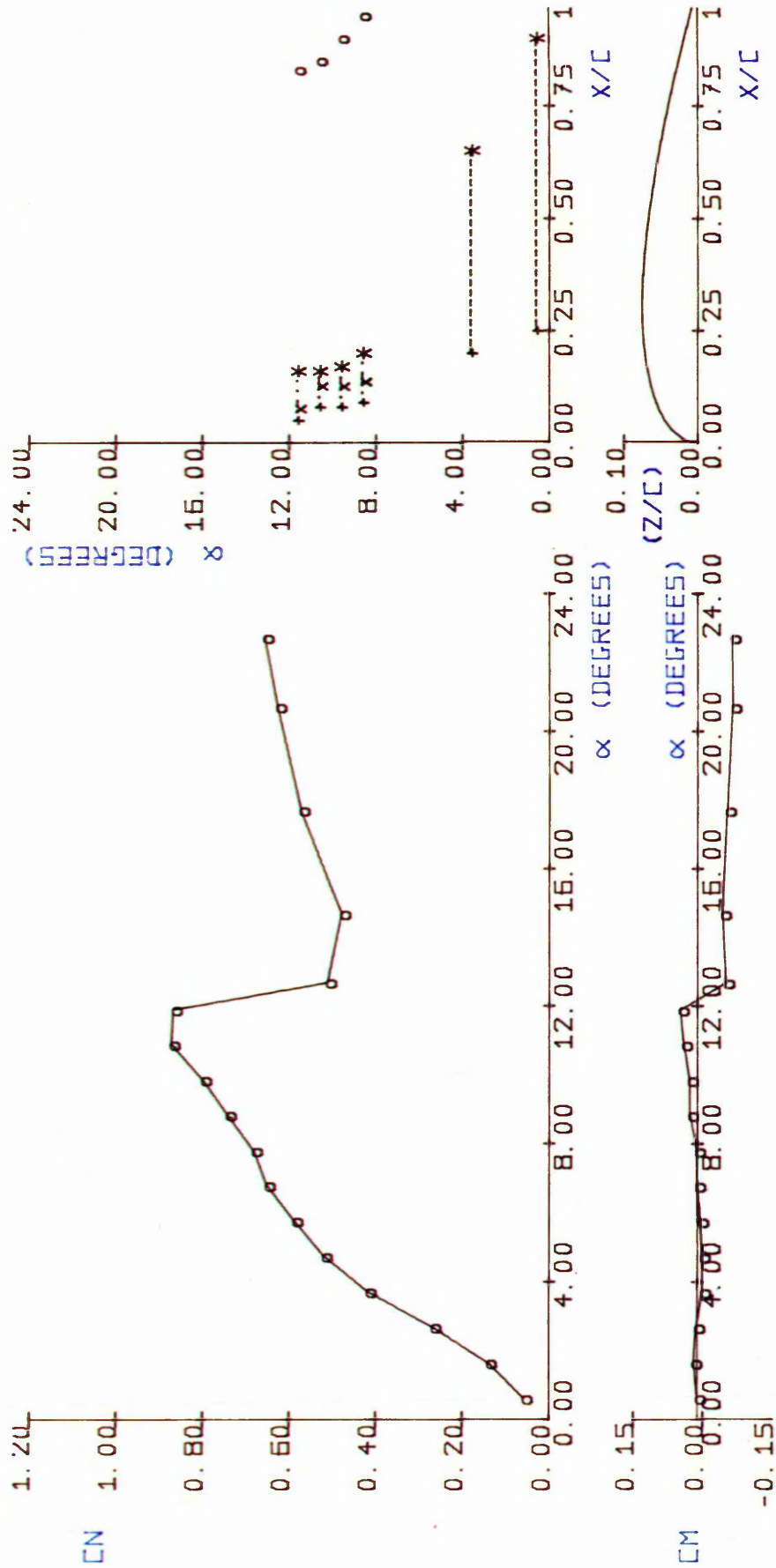


Fig. 3.41 VARIATION OF NORMAL FORCE COEFFICIENT WITH INCIDENCE
 AT A REYNOLDS NUMBER OF 500,000
 NACA-0015 AIRFOIL



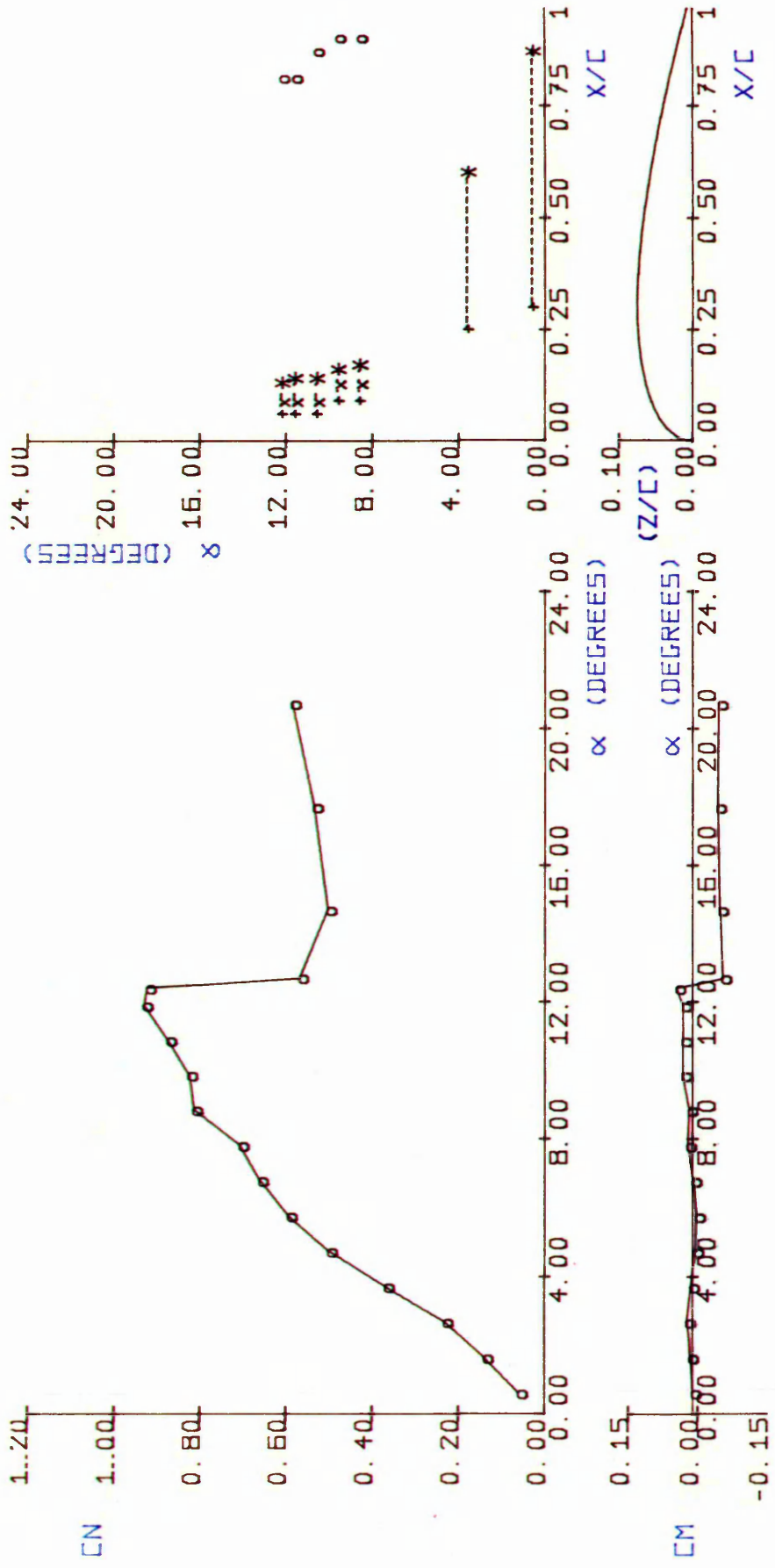
- + = FLOW SEPARATES
- x = FLOW TRANSITIONS
- * = FLOW REATTACHES
- o = FLOW SEPARATES
- = LONG BUBBLE REGION
- ... = SHORT BUBBLE REGION

FIG.3.42 AERODYNAMIC CHARACTERISTICS OF THE
 NACA-0015 AEROFOIL
 ($Re = 100556$.)



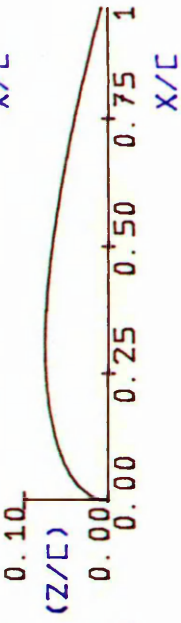
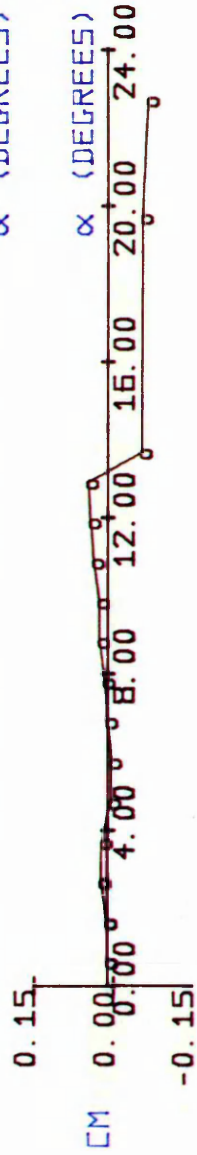
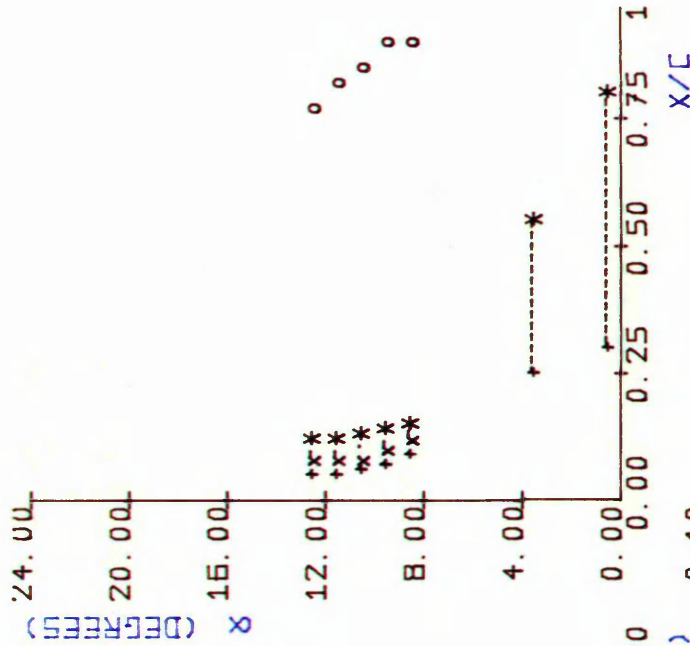
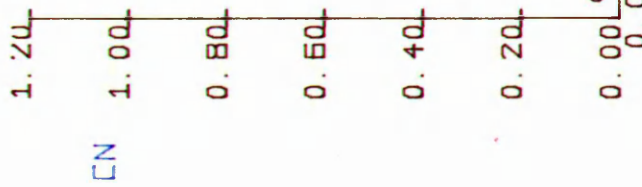
- + = FLOW SEPARATES
- x = FLOW TRANSITIONS
- * = FLOW REATTACHES
- o = FLOW SEPARATES
- = LONG BUBBLE REGION
- ... = SHORT BUBBLE REGION

FIG.3.43 AERODYNAMIC CHARACTERISTICS OF THE
 NACA-0015 AEROFOIL
 (Re = 150835.)



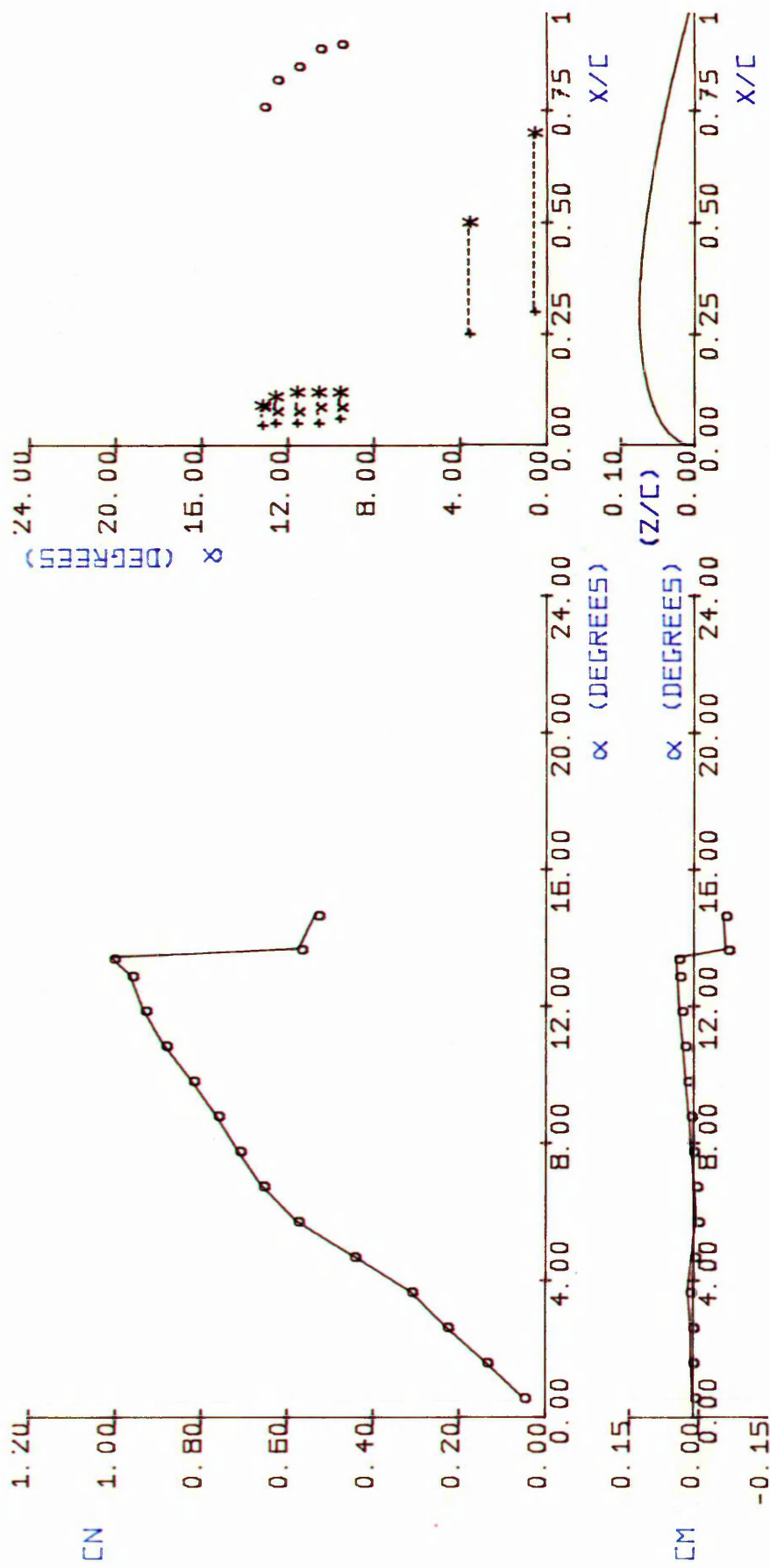
- + = FLOW SEPARATES
- x = FLOW TRANSITIONS
- * = FLOW REATTACHES
- o = FLOW SEPARATES
- = LONG BUBBLE REGION
- ... = SHORT BUBBLE REGION

FIG. 3. 44 AERODYNAMIC CHARACTERISTICS OF THE
 NACA-0015 AEROFoil
 (Re = 201113.)



- + = FLOW SEPARATES
- x = FLOW TRANSITIONS
- * = FLOW REATTACHES
- o = FLOW SEPARATES
- = LONG BUBBLE REGION
- ... = SHORT BUBBLE REGION

FIG.3. 45 AERODYNAMIC CHARACTERISTICS OF THE
 NACA-0015 AEROFoil
 (Re = 251390.)



+ = FLOW SEPARATES
 x = FLOW TRANSITIONS
 * = FLOW REATTACHES
 o = FLOW SEPARATES
 ---- = LONG BUBBLE REGION
 ... = SHORT BUBBLE REGION

FIG.3. 46 AERODYNAMIC CHARACTERISTICS OF THE
 NACA-0015 AEROFOIL
 ($Re = 301670.$)

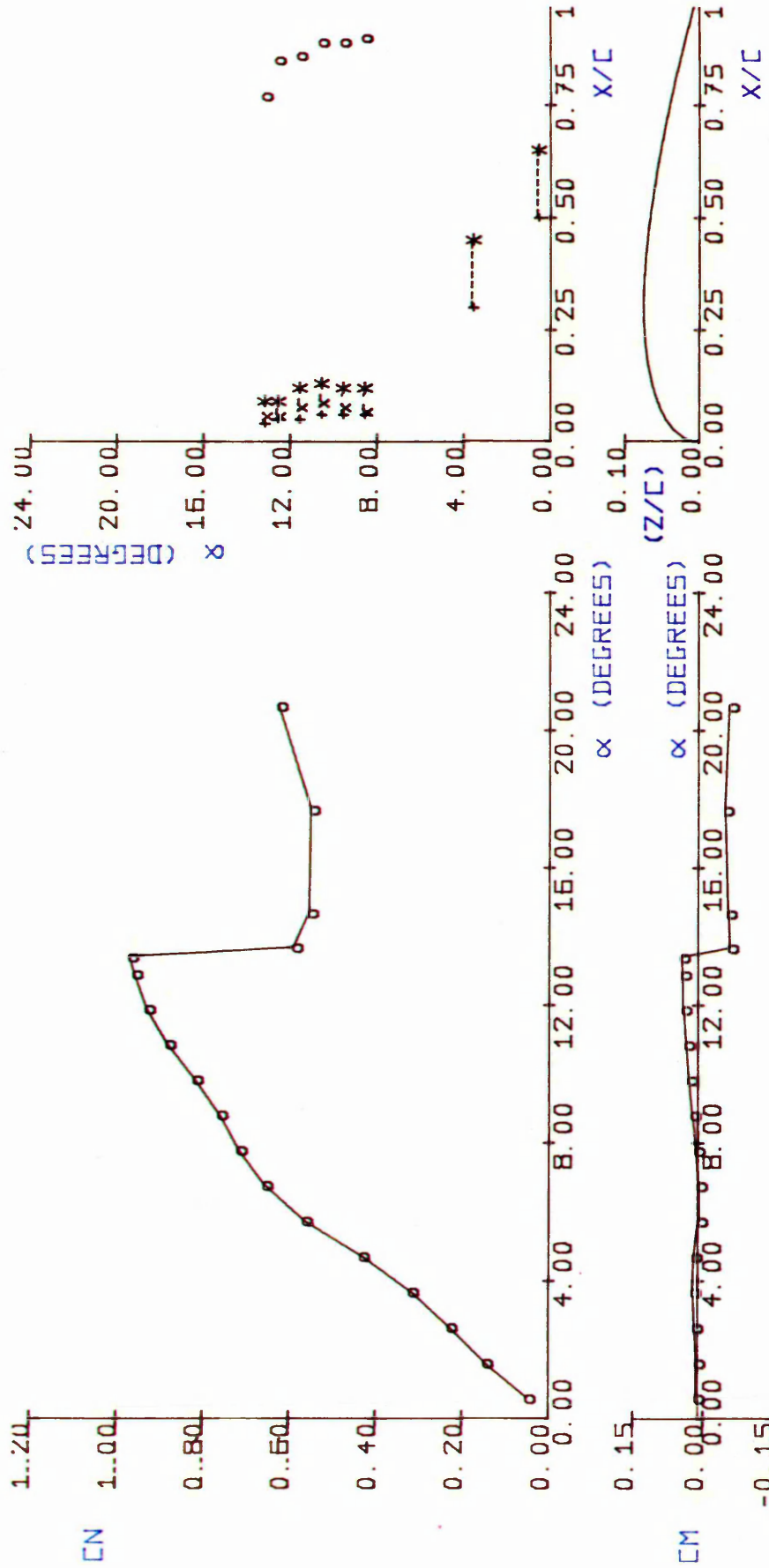
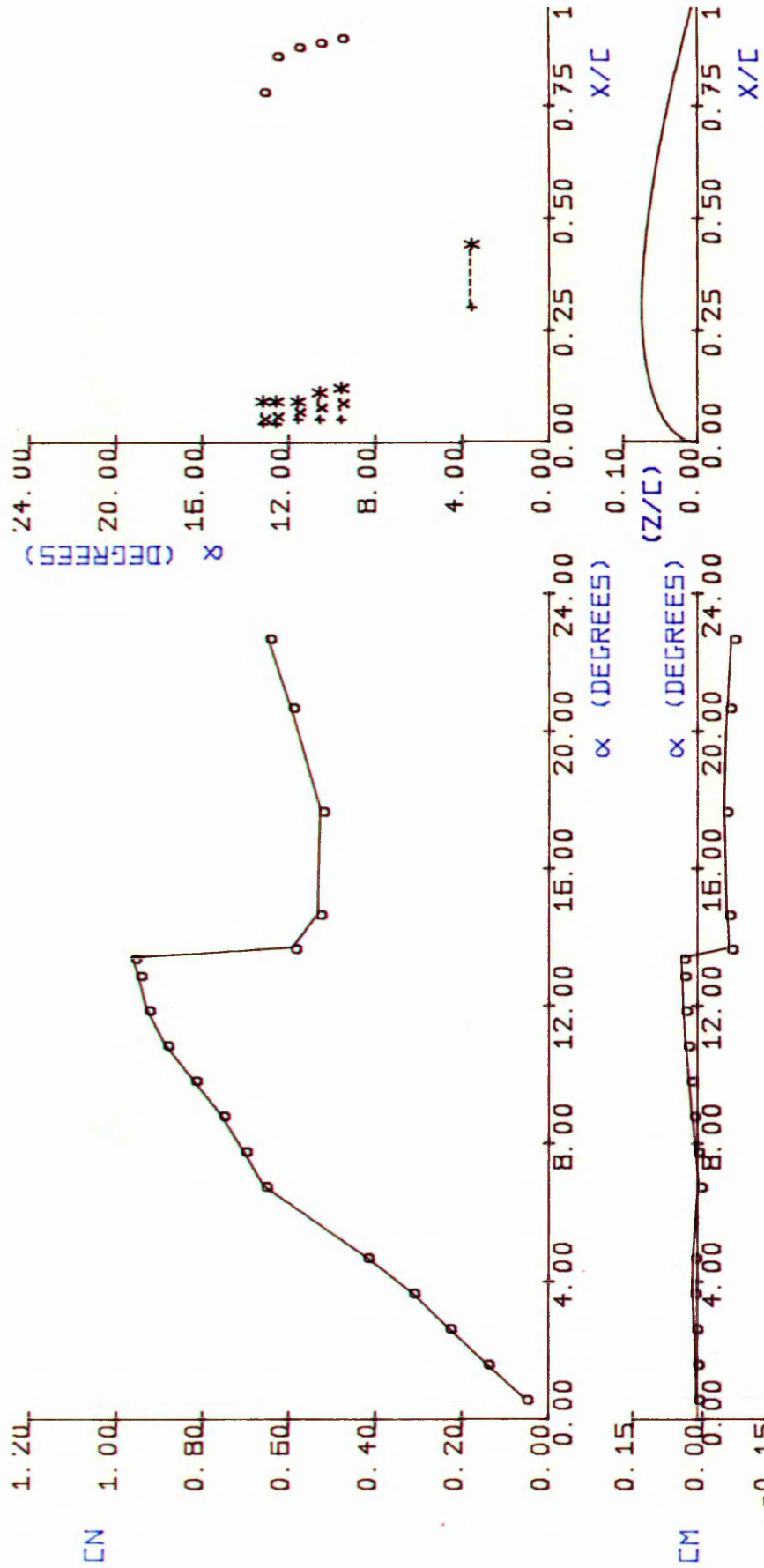
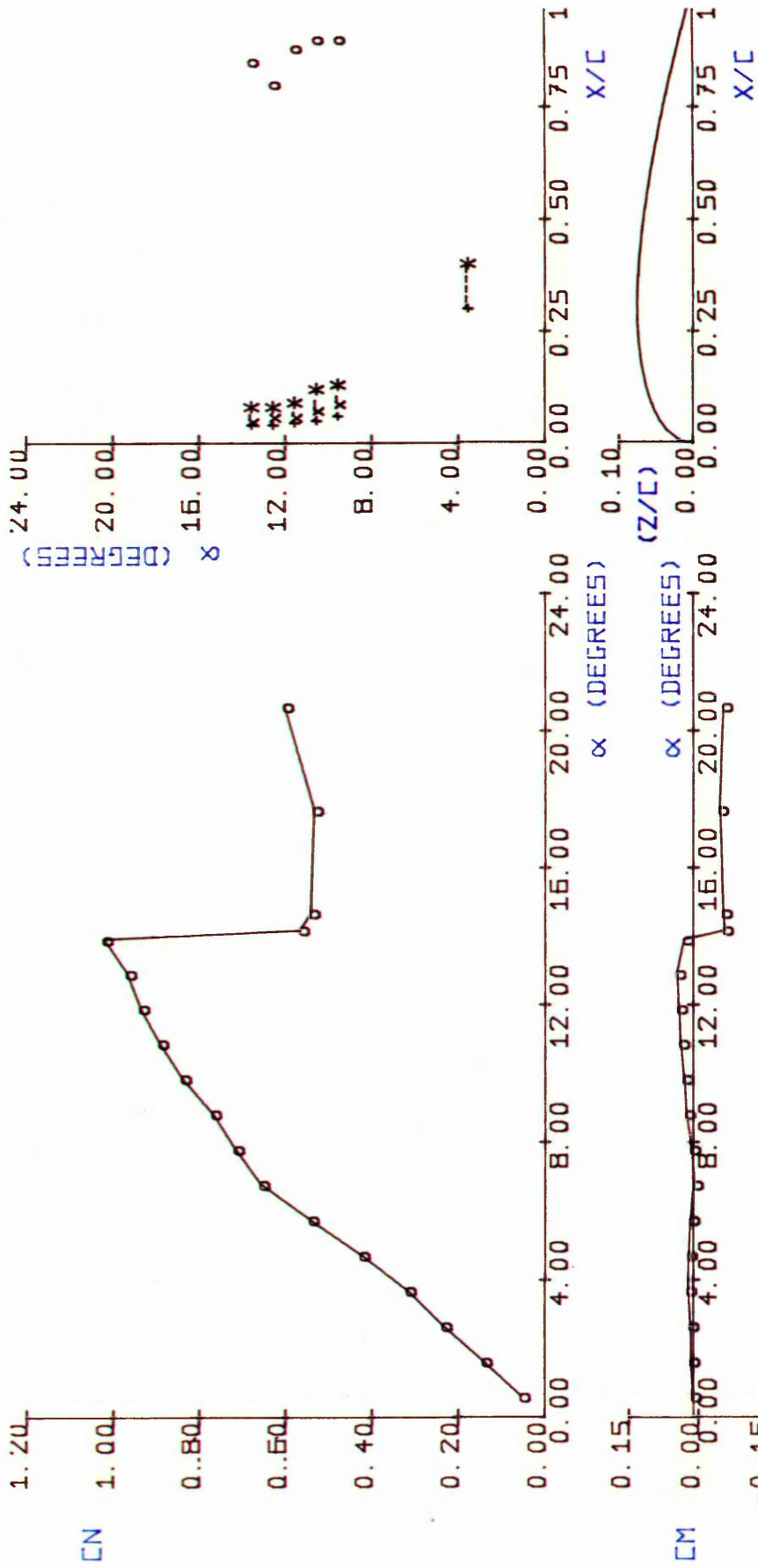


FIG.3. 47 AERODYNAMIC CHARACTERISTICS OF THE
 NACA-0015 AEROFOIL
 ($Re = 351950.$)



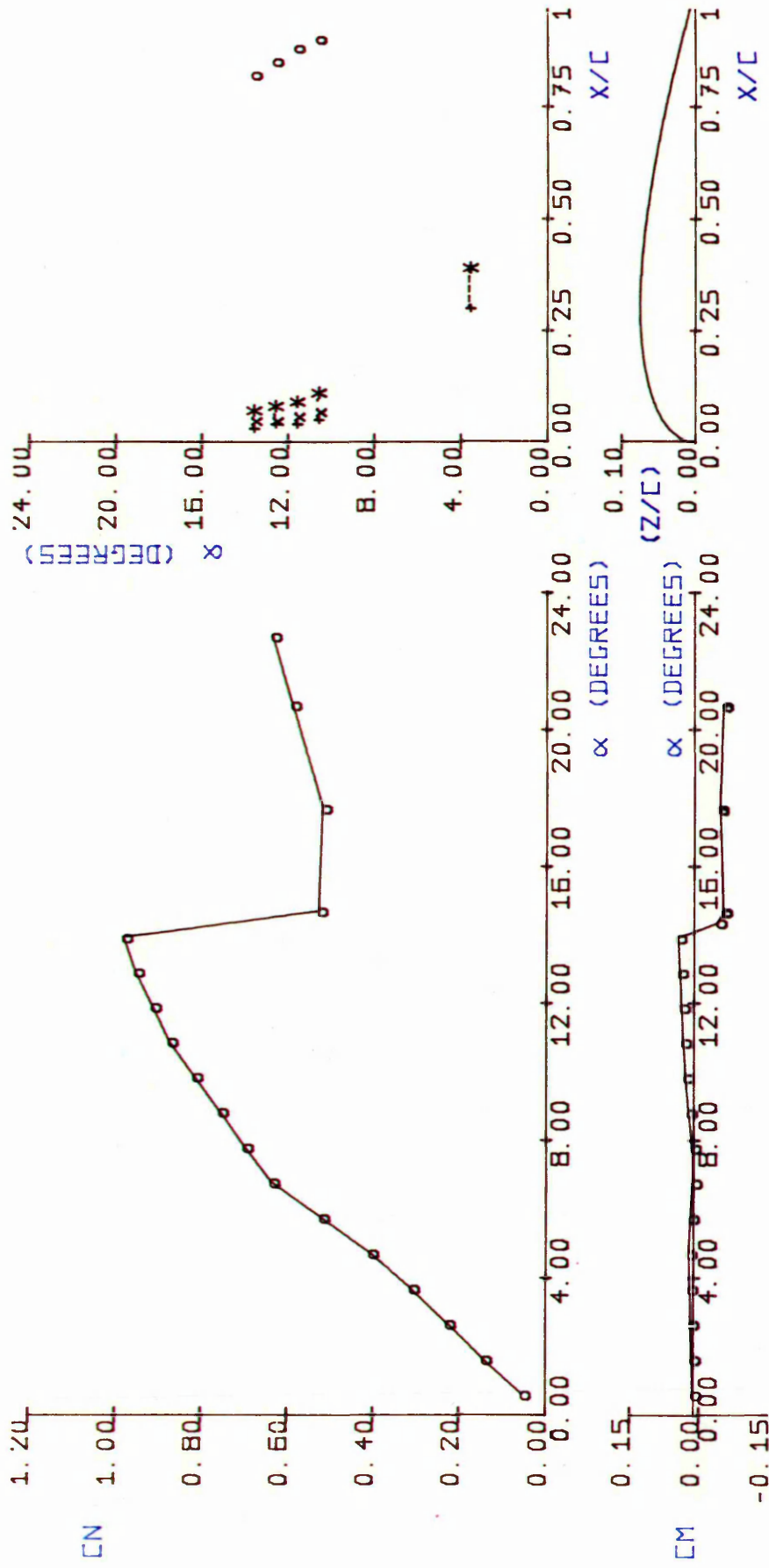
- + = FLOW SEPARATES
- x = FLOW TRANSITIONS
- * = FLOW REATTACHES
- o = FLOW SEPARATES
- = LONG BUBBLE REGION
- ... = SHORT BUBBLE REGION

FIG.3. 48 AERODYNAMIC CHARACTERISTICS OF THE
 NACA-0015 AEROFOIL
 (Re = 402230.)



- + = FLOW SEPARATES
- x = FLOW TRANSITIONS
- * = FLOW REATTACHES
- o = FLOW SEPARATES
- = LONG BUBBLE REGION
- ... = SHORT BUBBLE REGION

FIG.3.49 AERODYNAMIC CHARACTERISTICS OF THE
 NACA-0015 AEROFOIL
 (Re = 452500.)



- + = FLOW SEPARATES
- x = FLOW TRANSITIONS
- * = FLOW REATTACHES
- o = FLOW SEPARATES
- = LONG BUBBLE REGION
- ... = SHORT BUBBLE REGION

FIG.3.50 AERODYNAMIC CHARACTERISTICS OF THE
 NACA-0015 AEROFOIL
 (Re = 502784.)

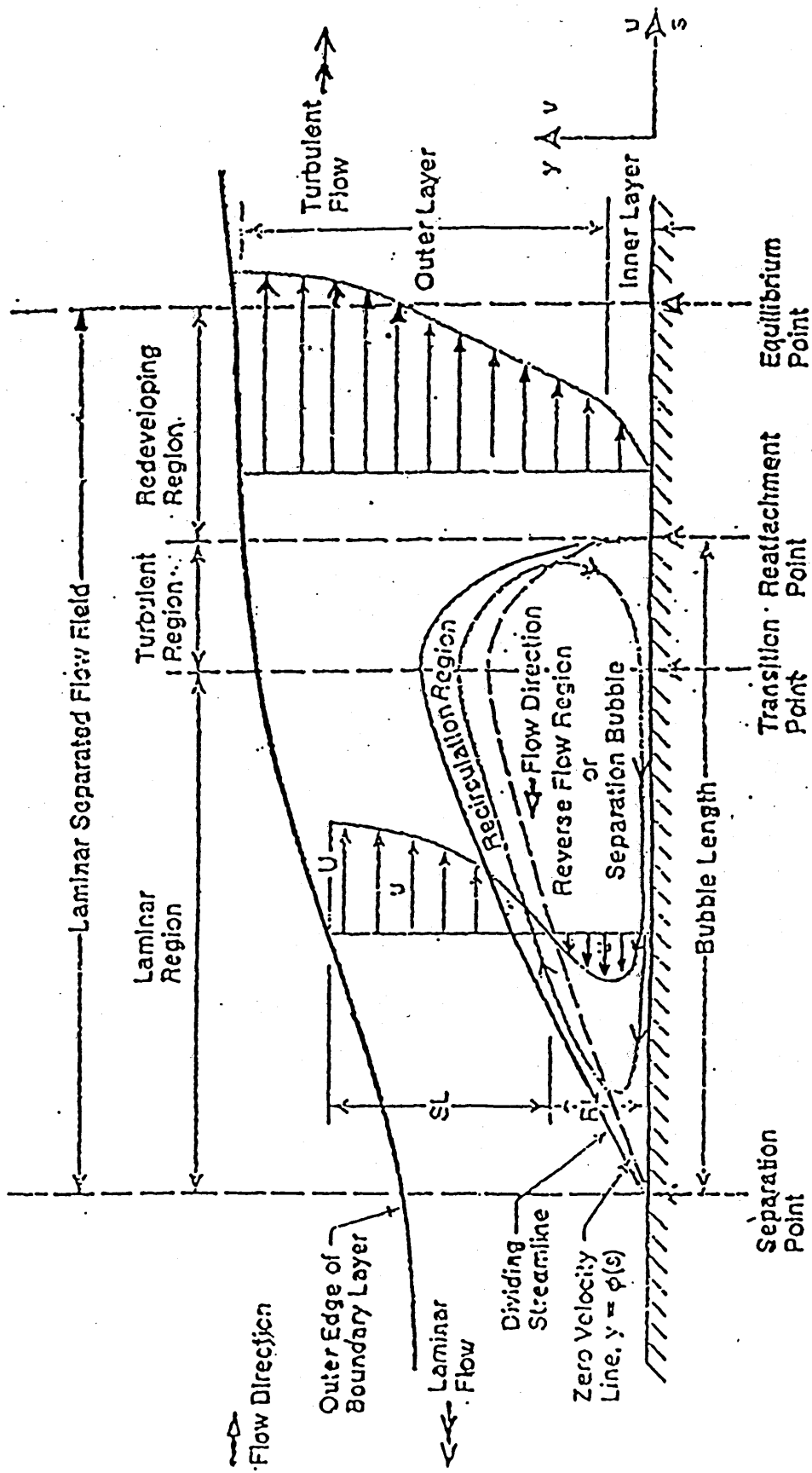


Fig. 4.1 SCHEMATIC DIAGRAM OF A LAMINAR SEPARATION BUBBLE

(TAKEN FROM REF (5))

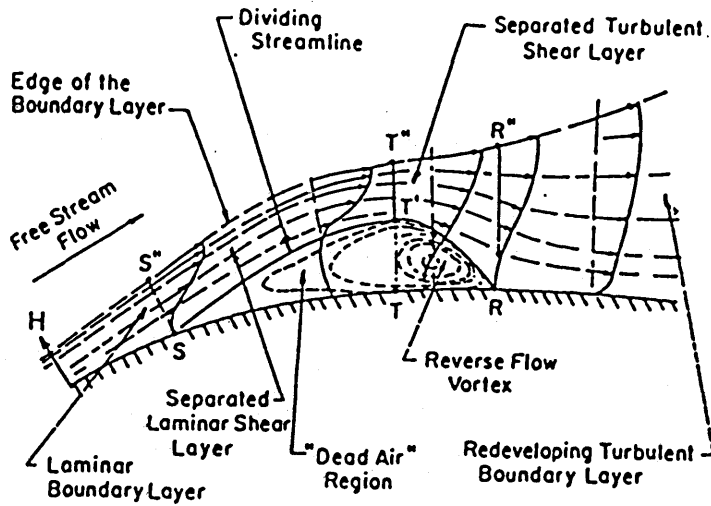


Fig. 4.2a SCHEMATIC OF A LAMINAR SEPARATION BUBBLE
(TAKEN FROM REF (37))

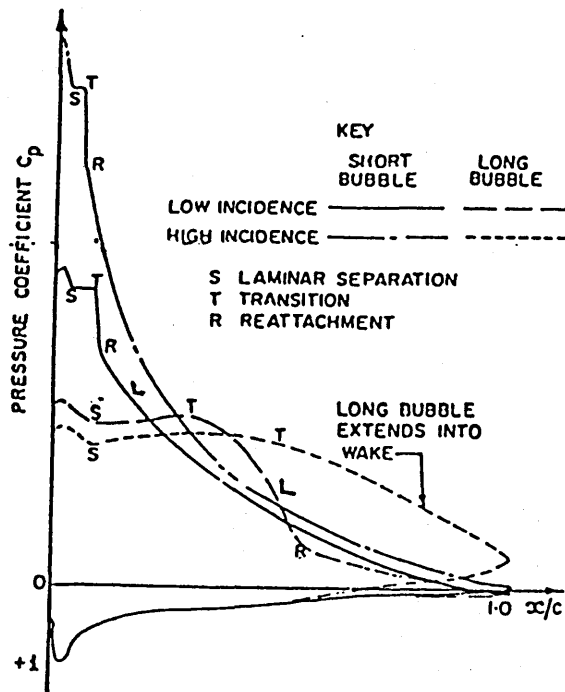


Fig. 4.2b EFFECT OF LONG AND SHORT SEPARATION BUBBLES ON THE PRESSURE DISTRIBUTION OVER AN AIRFOIL AT HIGH REYNOLDS NUMBER
(TAKEN FROM REF (22))

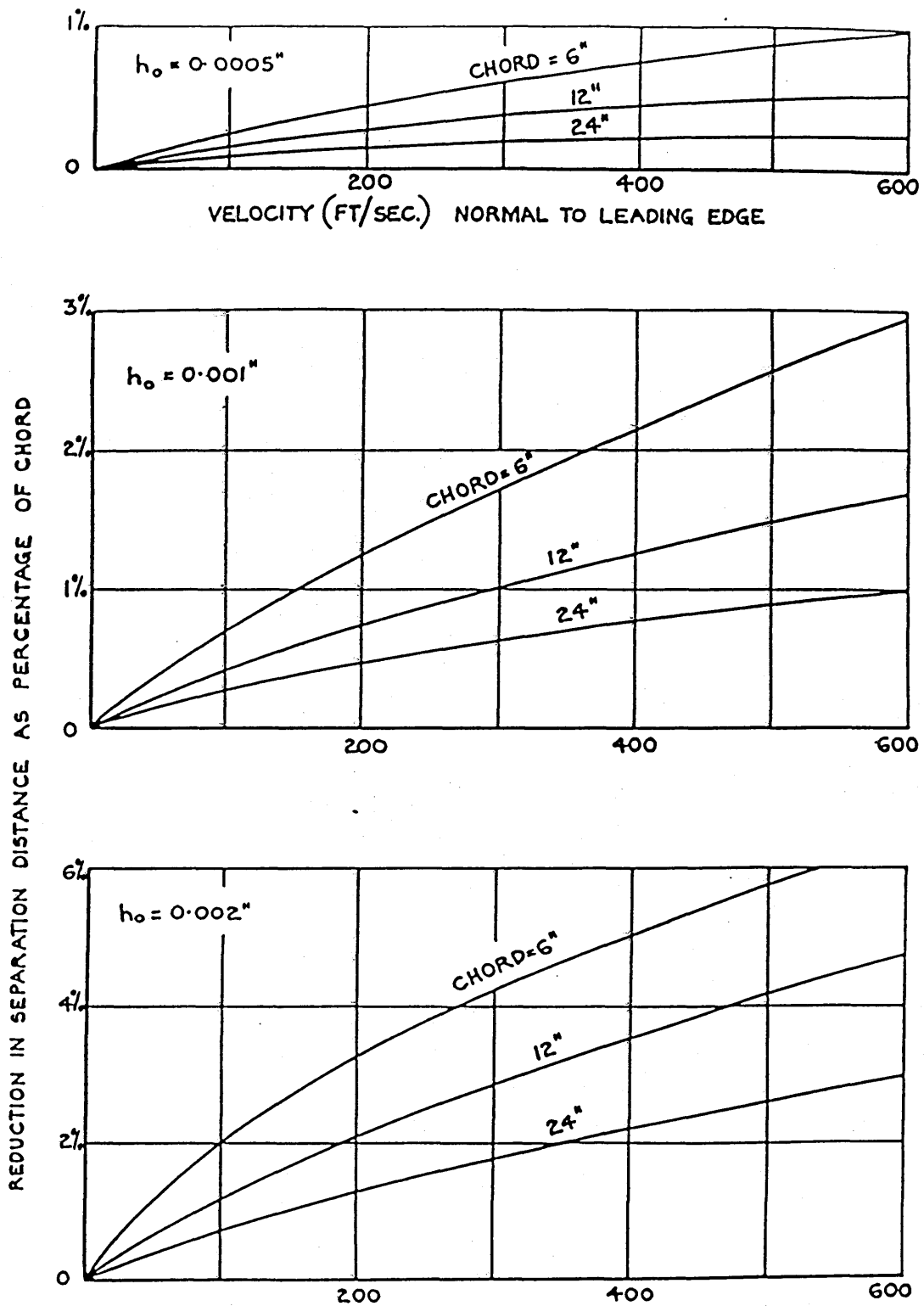


Fig. 4.3 PERCENTAGE REDUCTION IN APPARENT SEPARATION DISTANCE FOR DIFFERENT OIL SHEET THICKNESSES (h_o) AND AIRFOIL CHORDS WITH SPEED (TAKEN FROM REF (27))

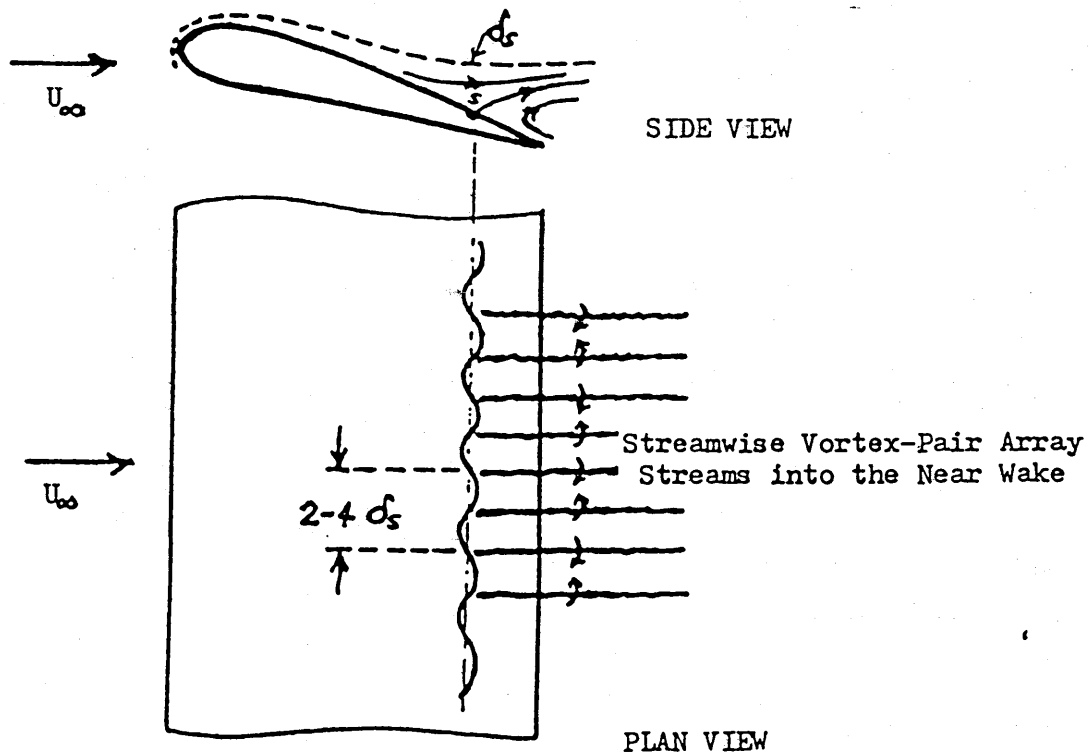


Fig. 4.4 SCHEMATIC OF A SEPARATION - DISTURBANCE
 VORTICES ON A WING
 (TAKEN FROM REF (30))

CM 1 80-140K/25

R_c	A/\ln	βc_m	\bar{C}_D	ΔC_D	%
3.0	3.0	0.0	0.0066	5.7	-4.4
2.0	3.0	0.0	0.0068	14.2	-9.3
1.0	3.0	0.0	0.0074	18.0	-13.4
1.0	3.0	0.0	0.0084	13.0	-10.9

FX 78-K-140

$\alpha = 3^\circ$

$Re_c = 2.5 \times 10^6$

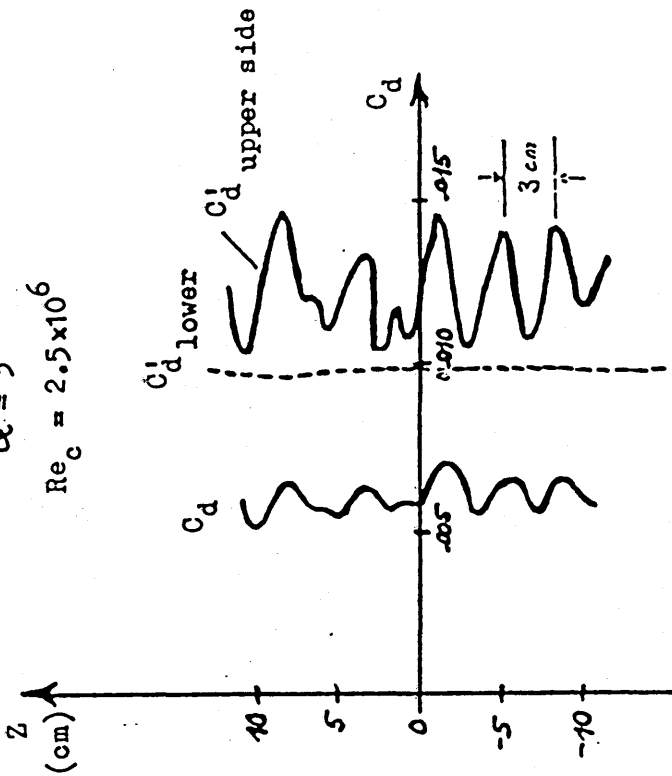
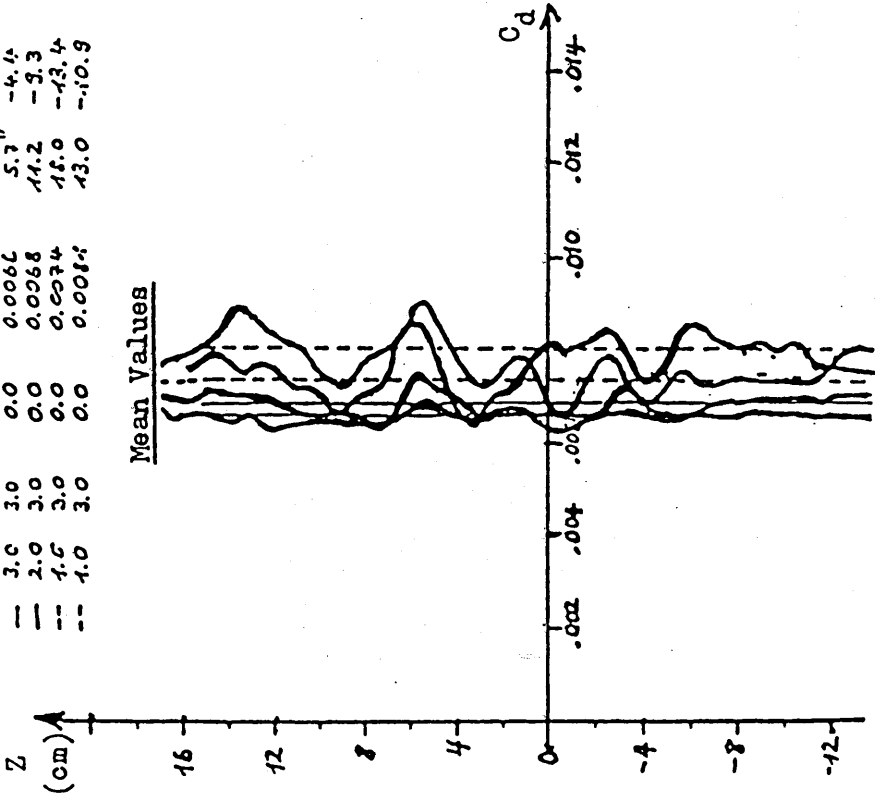
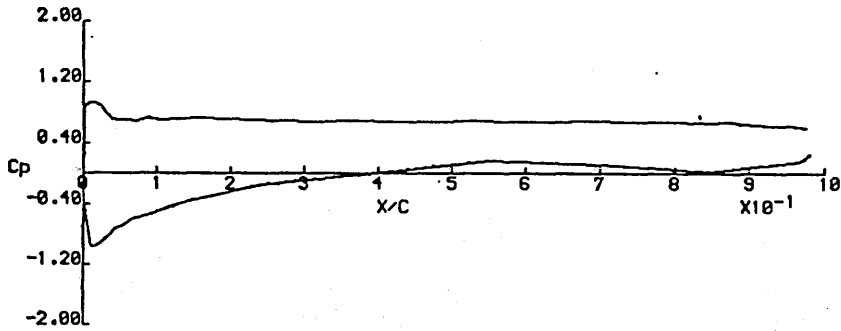
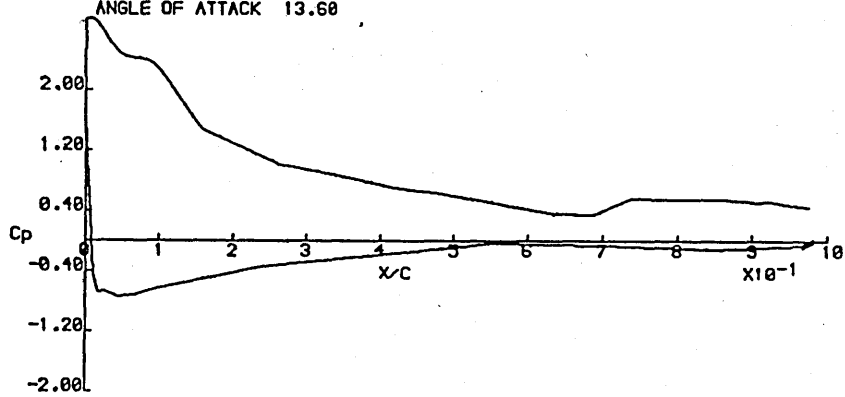


Fig. 4.5 INFLUENCE OF PERIODIC NEAR WAKE STRUCTURE ON SPANWISE DRAG VARIATION
(TAKEN FROM REF (31))

ANGLE OF ATTACK 14.67



ANGLE OF ATTACK 13.60



ANGLE OF ATTACK 12.88

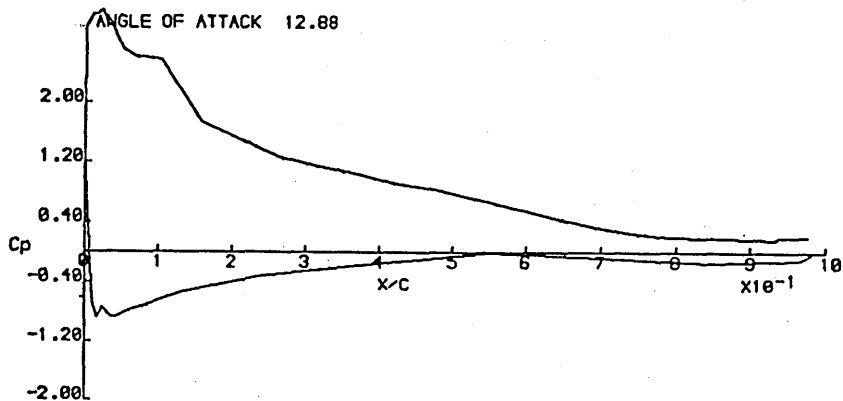


Fig. 4.6 VARIATION OF PRESSURE COEFFICIENT (C_p) WITH POSITION ALONG THE CHORD (x/c) AT VARIOUS INCIDENCES. NASA GA(W)-1 AIRFOIL. ($Re \approx 150,000$)

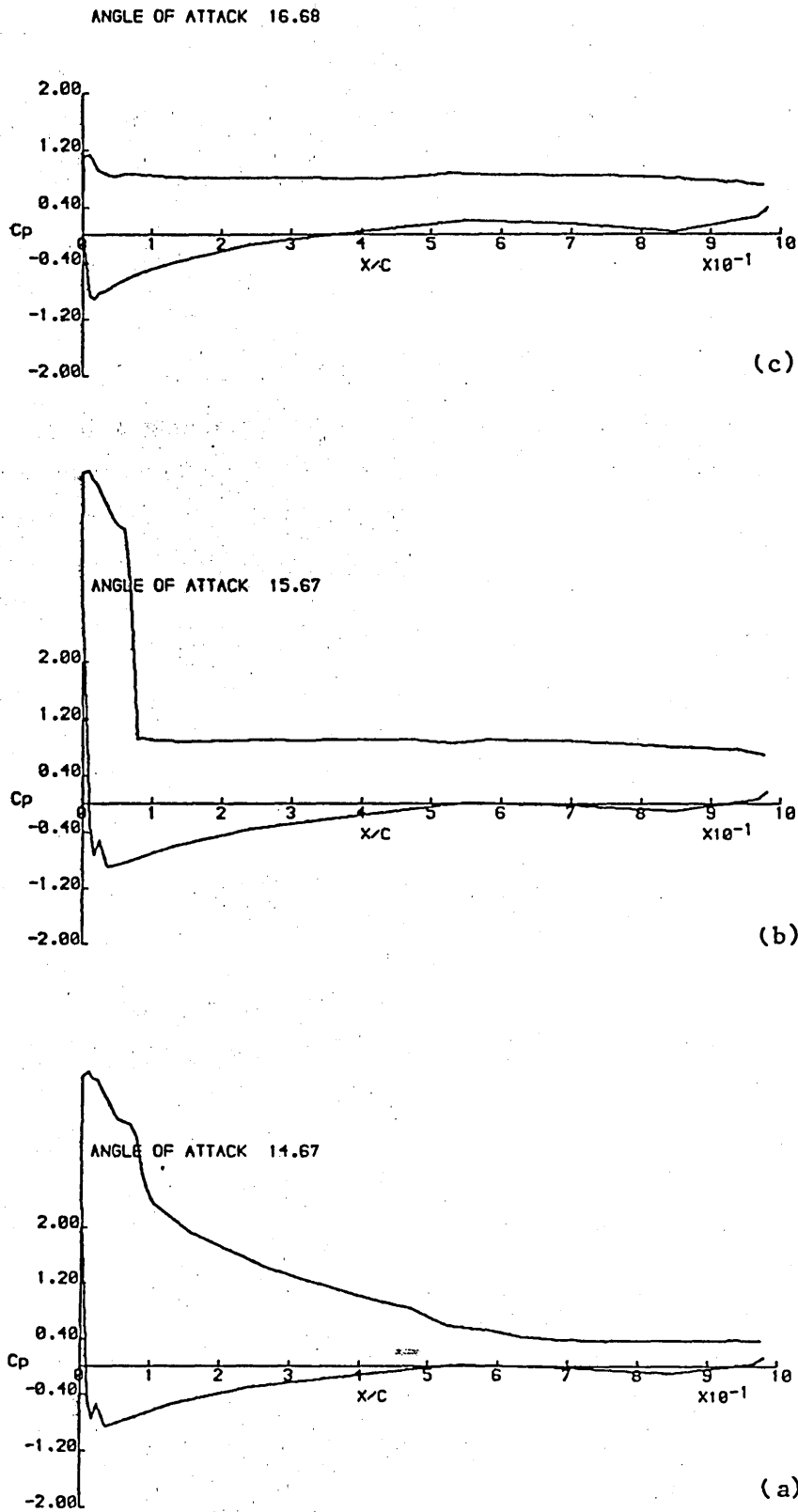


Fig. 4.7 VARIATION OF THE PRESSURE COEFFICIENT WITH POSITION ALONG THE CHORD (x/c) AT VARIOUS DEGREES. NASA GA(W)-1 AIRFOIL ($Re \approx 400,000$)

ANGLE OF ATTACK 14.67

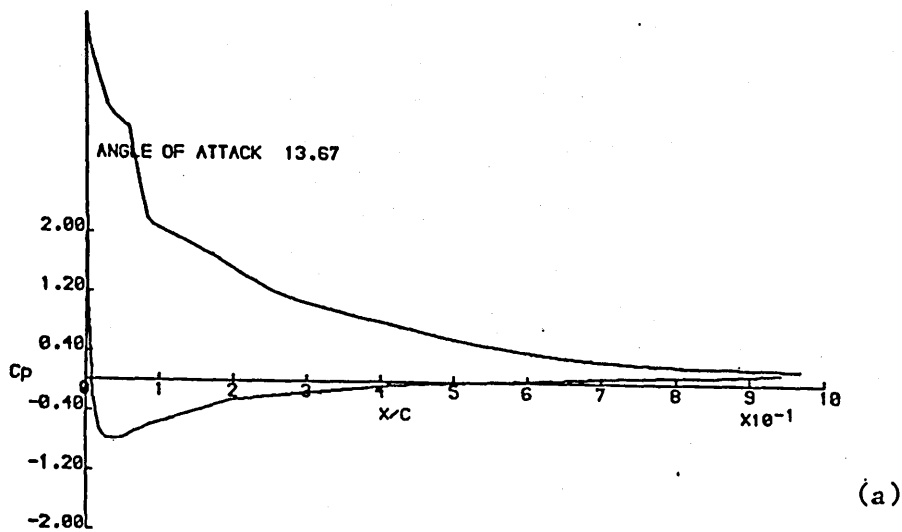
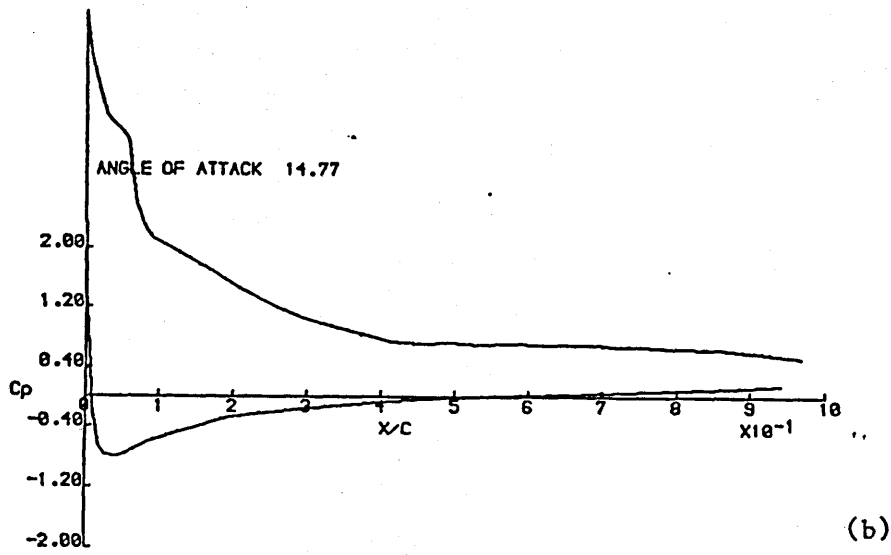
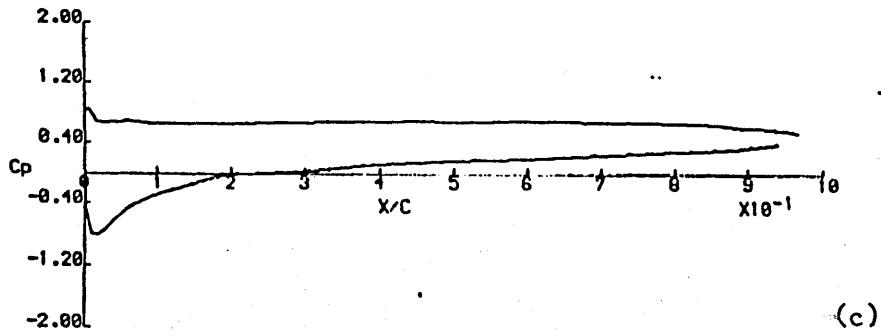


Fig 4.8 VARIATION OF PRESSURE COEFFICIENT WITH POSITION ALONG THE CHORD (x/c) AT VARIOUS INCIDENCES. NACA-0015 AIRFOIL. ($Re \approx 500,000$)

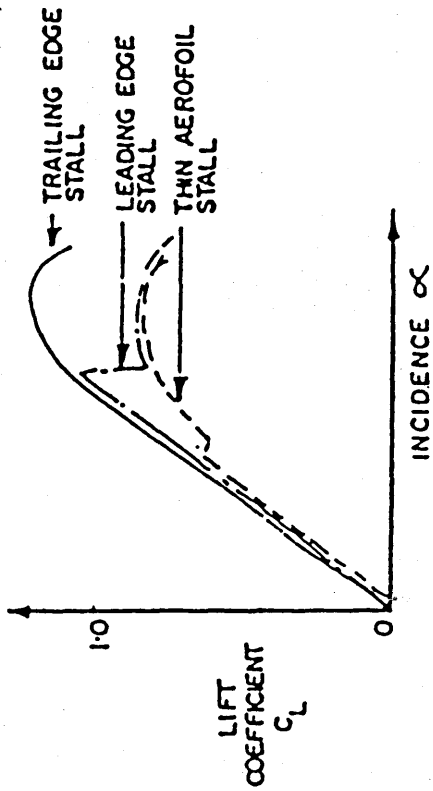


Fig. 4.9a THREE PRINCIPLE TYPES OF STALL
(TAKEN FROM REF (22))

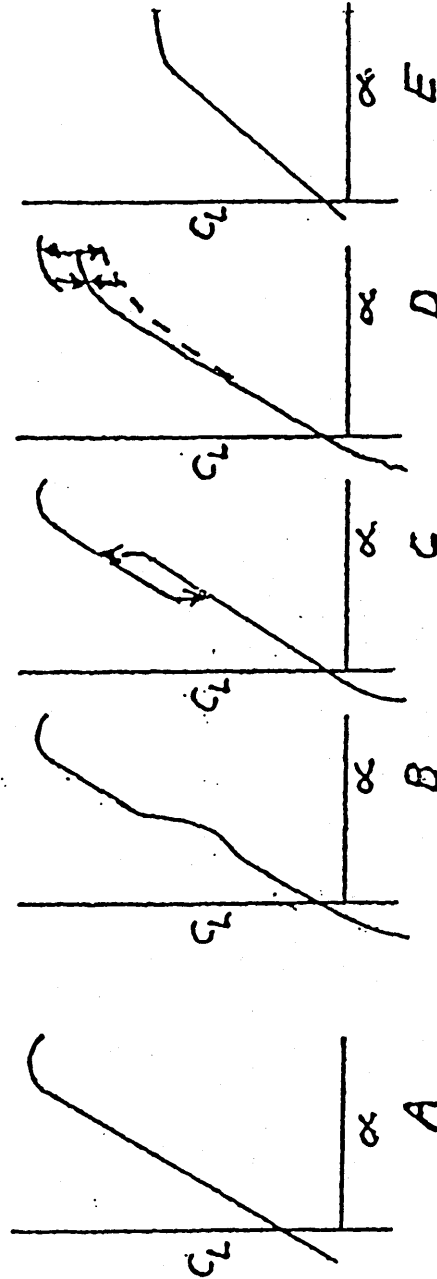


Fig. 4.9b LIFT COEFFICIENT (c_L) VERSUS INCIDENCE (α) FORMS
(TAKEN FROM REF (5))

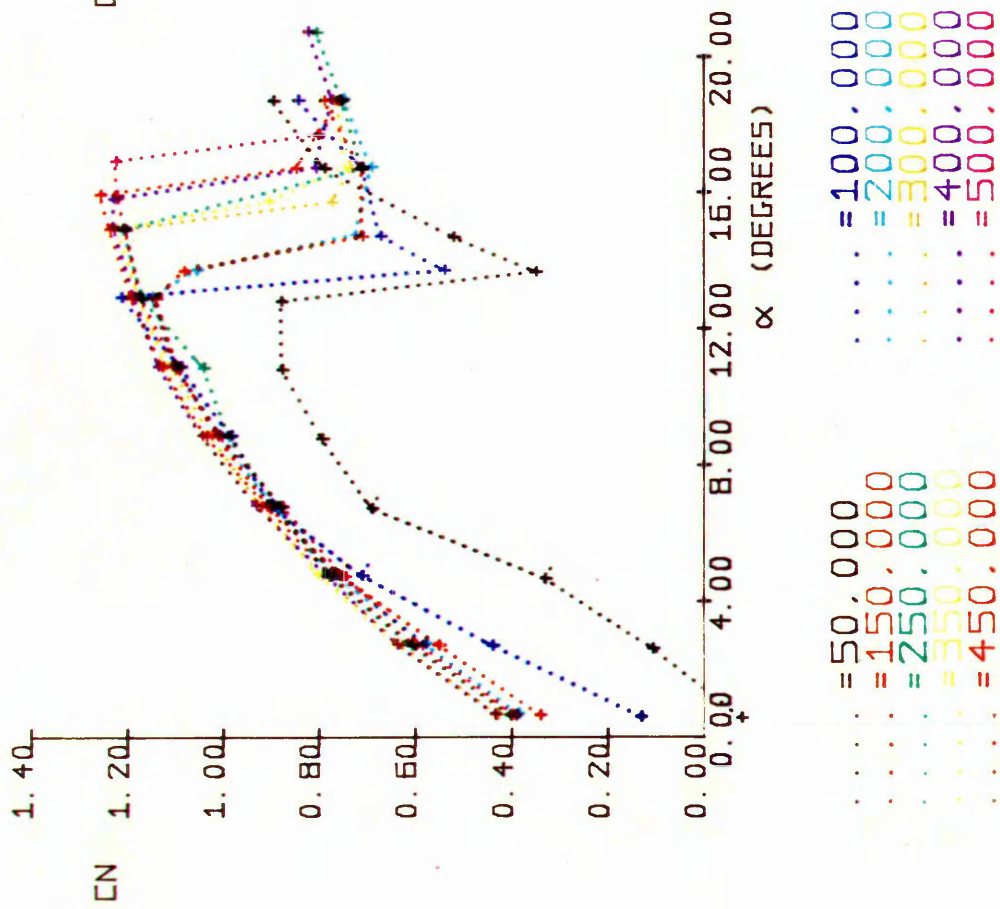


Fig. 4.10a VARIATION OF NORMAL FORCE COEFFICIENT (CN) WITH INCIDENCE (α) AT VARIOUS REYNOLDS NUMBERS, GA(ω)-1 AEROFOIL

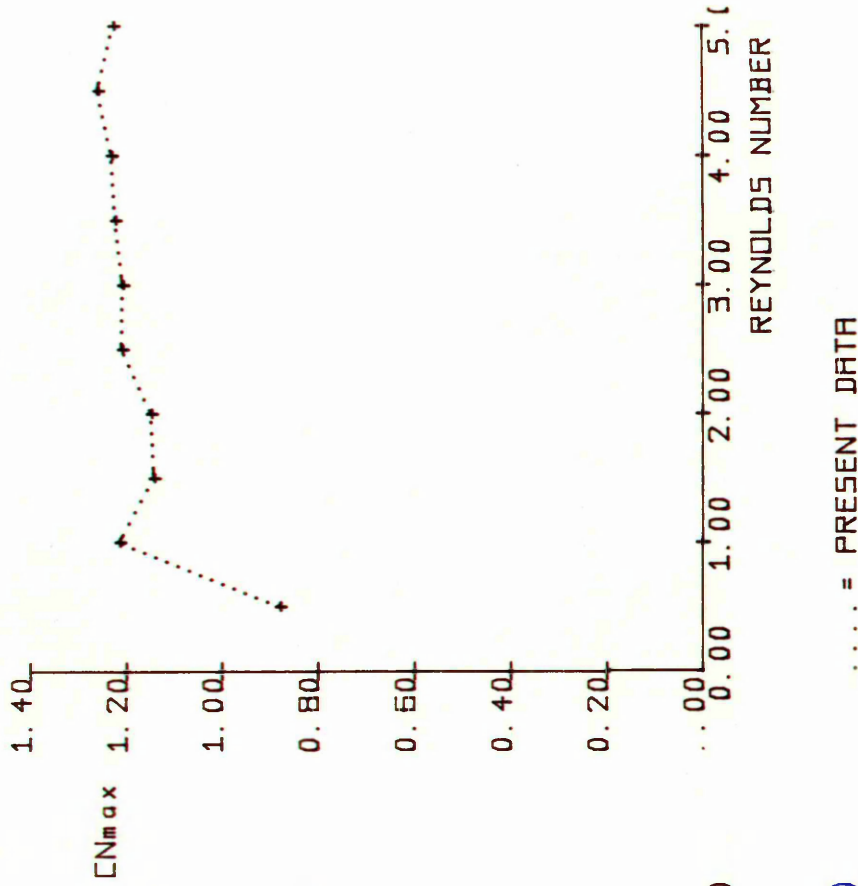


Fig. 4.10b VARIATION OF MAXIMUM NORMAL FORCE COEFFICIENT (CNmax) WITH REYNOLDS NUMBER, GA(ω)-1 AEROFOIL

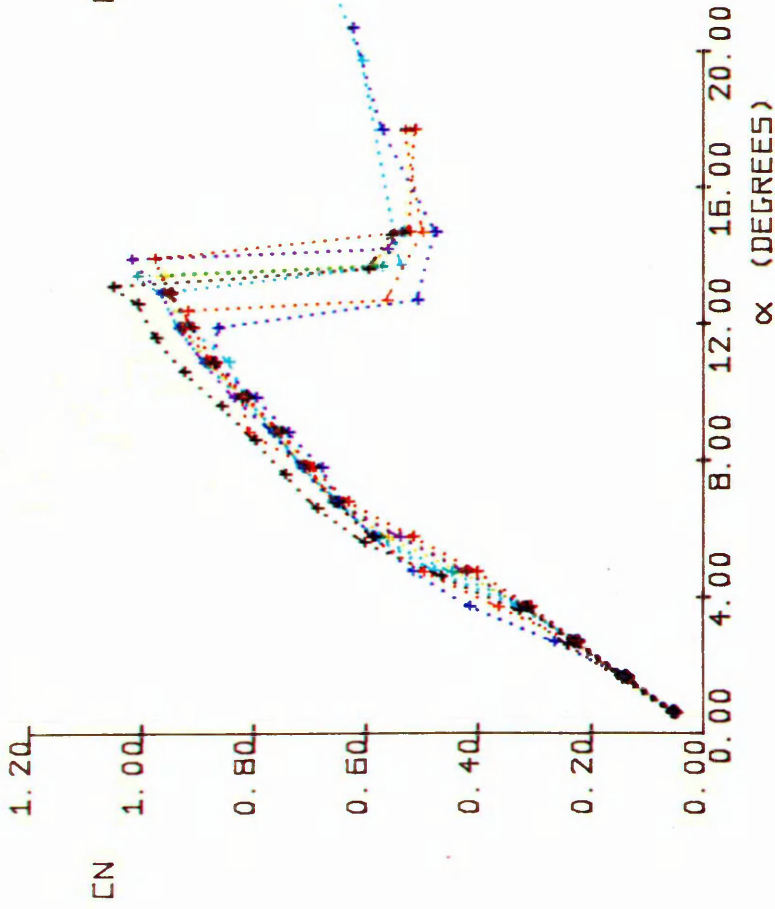


Fig. 4.11a VARIATION OF NORMAL FORCE COEFFICIENT (CN) WITH INCIDENCE (α) AT VARIOUS REYNOLDS NUMBERS. NACA-0015 AEROFOIL

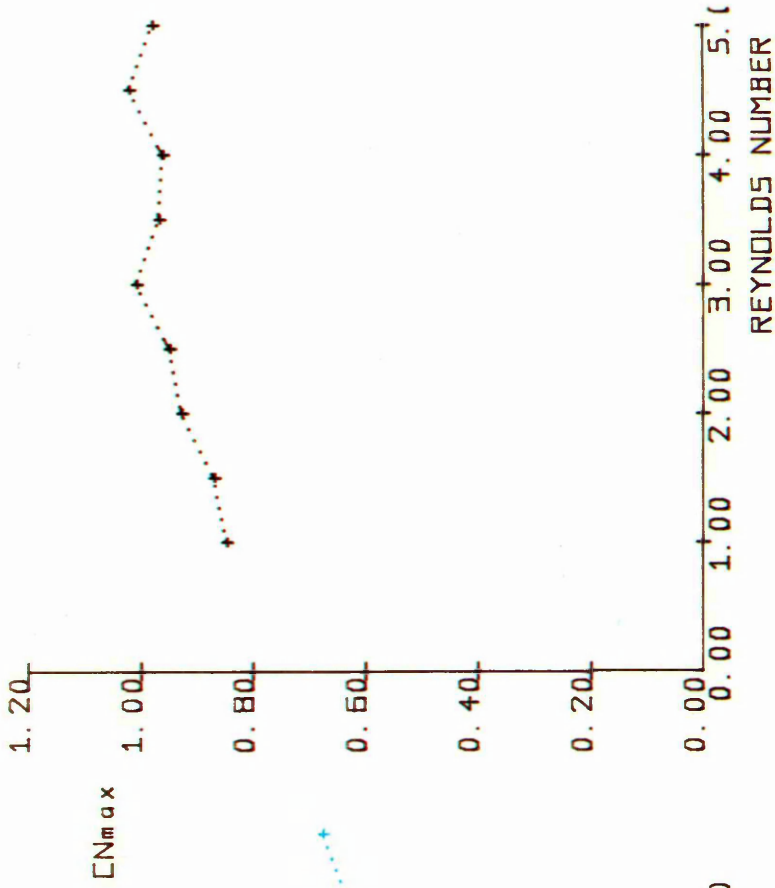
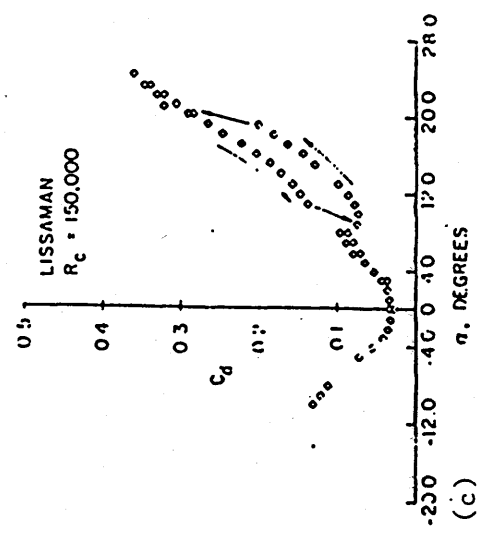
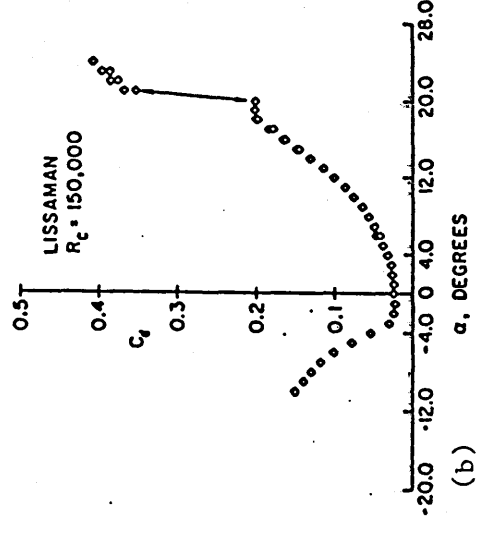
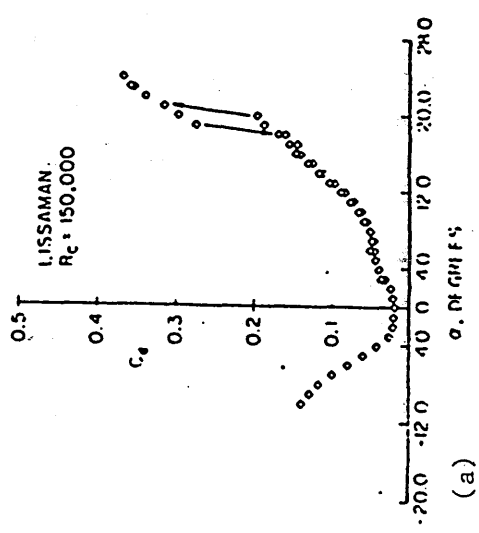
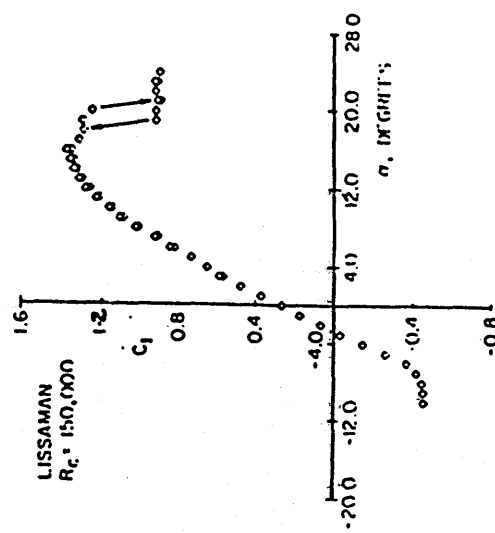
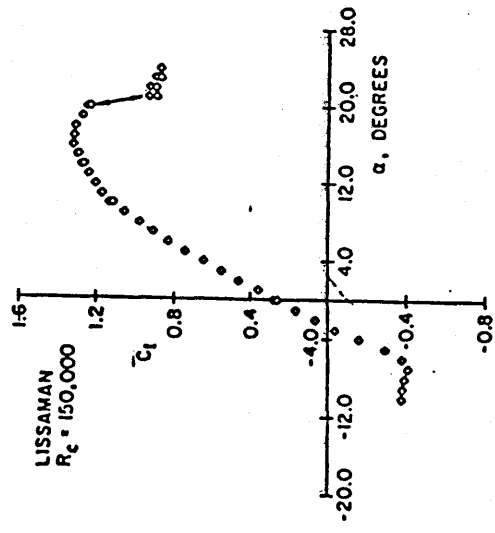
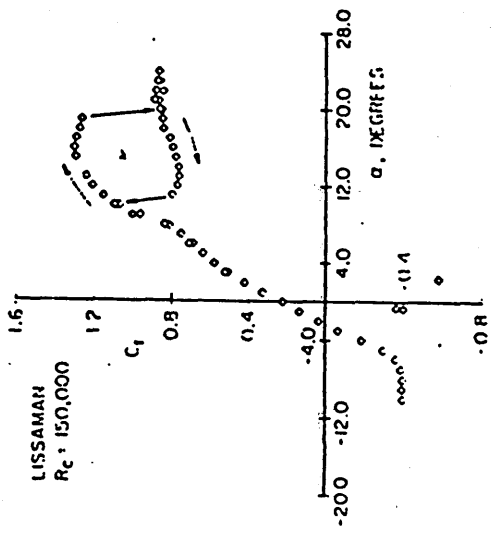
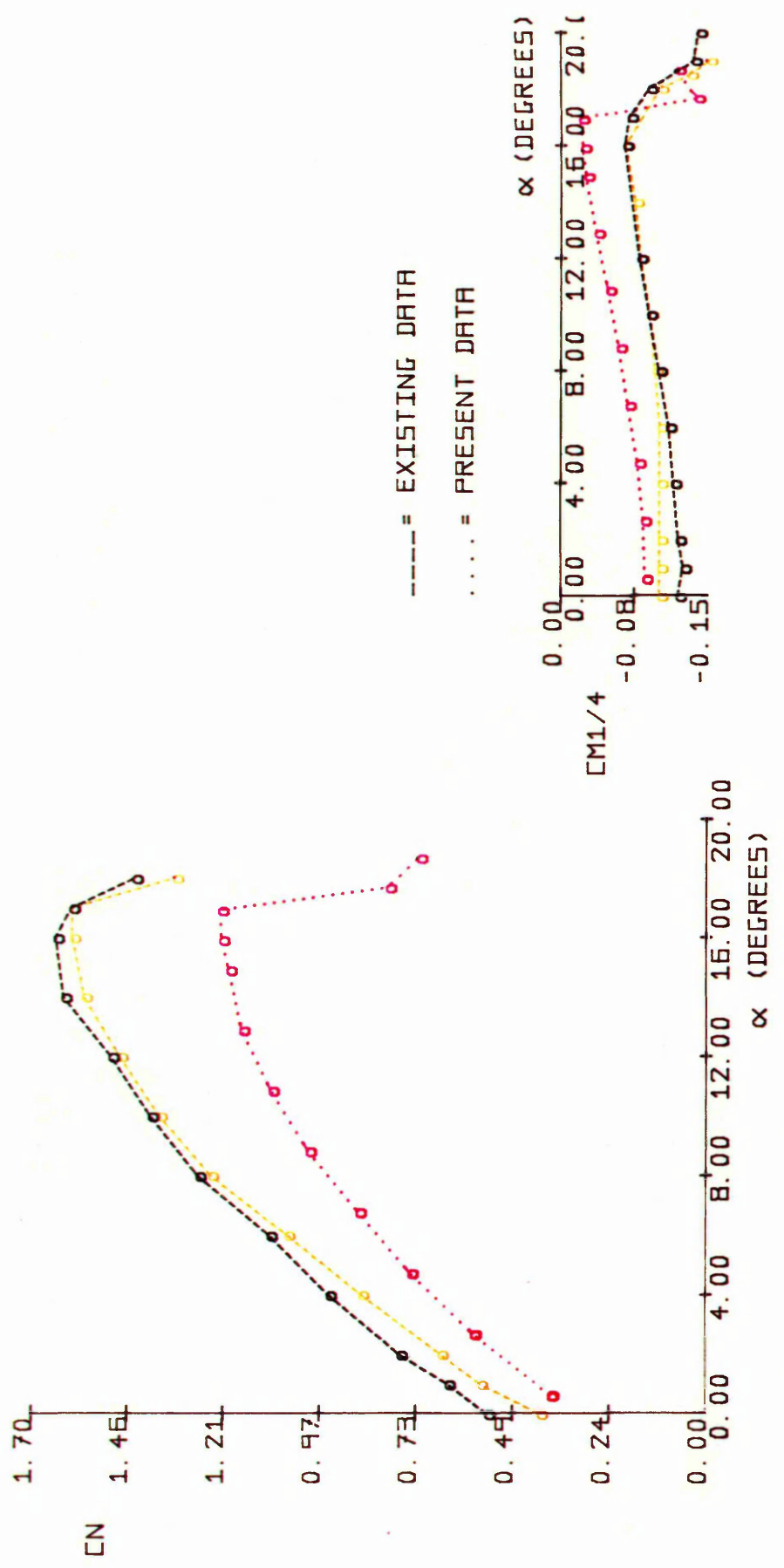


Fig. 4.11b VARIATION OF MAXIMUM NORMAL FORCE COEFFICIENT (C_{Nmax}) WITH REYNOLDS NUMBER. NACA-0015 AEROFOIL



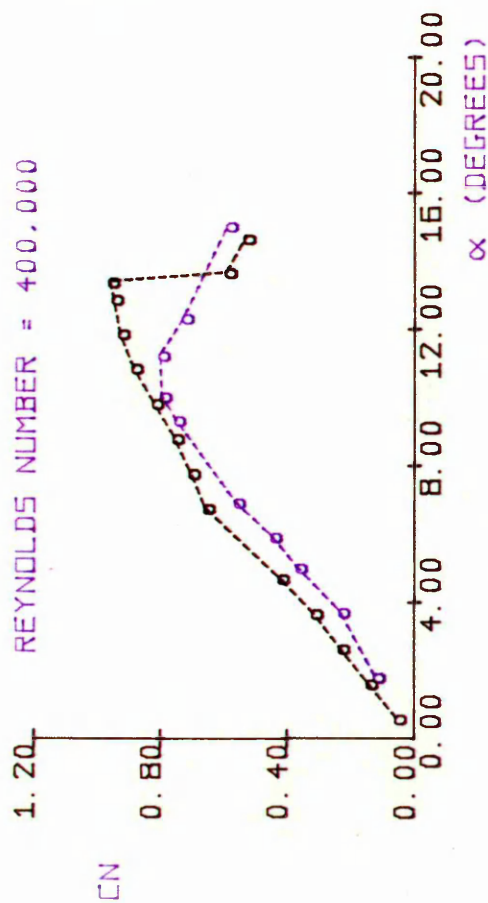
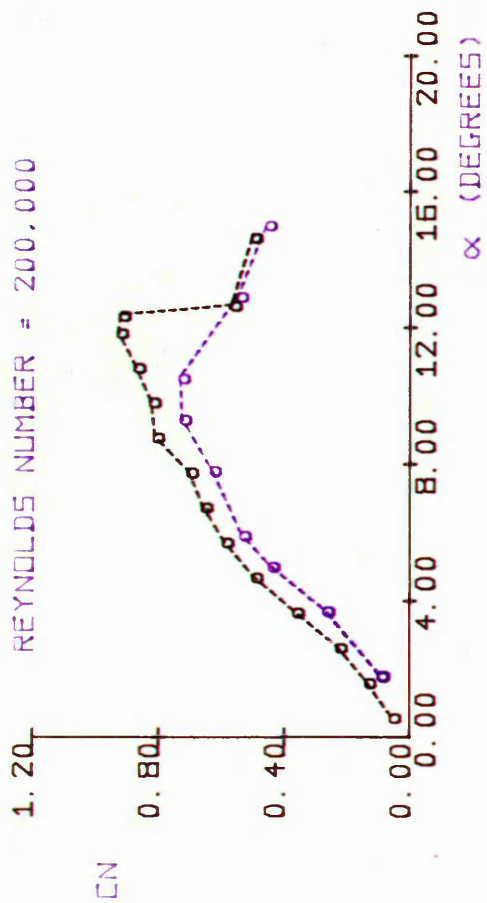
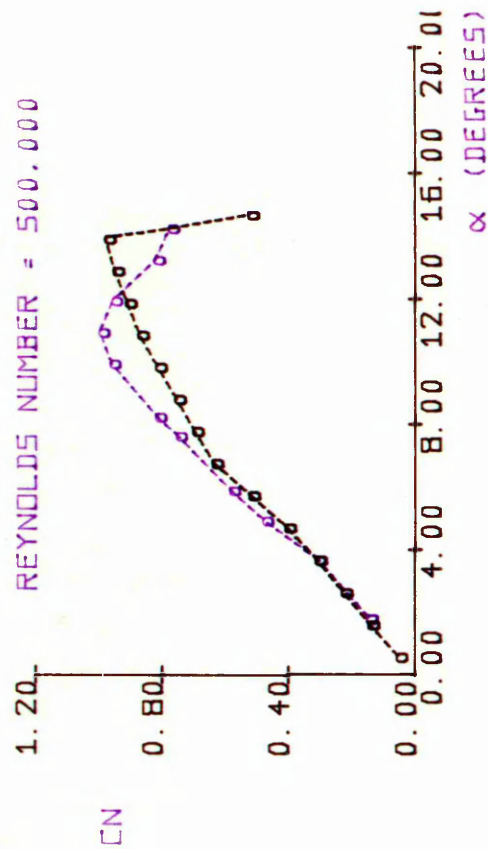
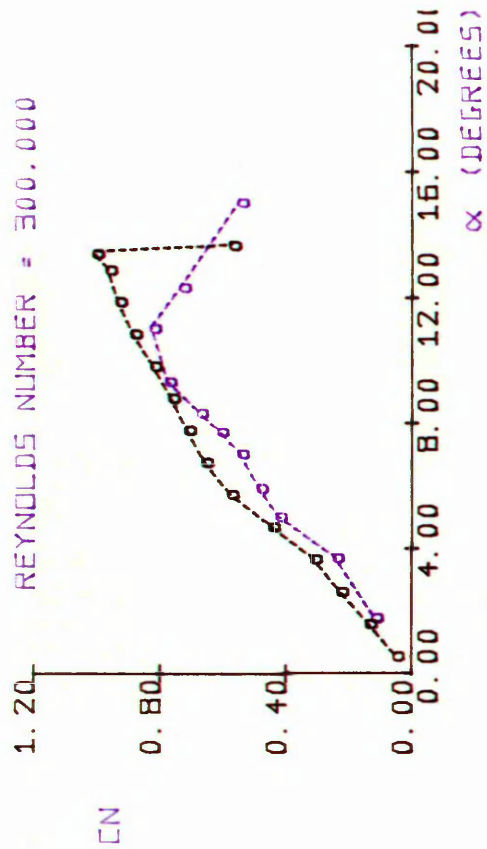
- 4.12a LIFT (C_L) AND DRAG (C_D) COEFFICIENT VERSUS ANGLE OF ATTACK (α) OF THE SMOOTH LISSAMAN AIRFOIL WITH NO SCREEN OR FLOW RESTRICTOR
- 4.12b LIFT (C_L) AND DRAG (C_D) COEFFICIENT VERSUS ANGLE OF ATTACK (α) OF THE SMOOTH LISSAMAN AIRFOIL WITH NO SCREEN AND ONE FLOW RESTRICTOR
- 4.12c LIFT (C_L) AND DRAG (C_D) COEFFICIENT VERSUS ANGLE OF ATTACK (α) OF THE SMOOTH LISSAMAN AIRFOIL WITH ONE 7.09 MESHES/CM SCREEN AND NO FLOW RESTRICTOR

(TAKEN FROM REF (14))



--- = 2.000.000 SMOOTH AIRFOIL
 - - - = 2.000.000 ROUGHNESS LOCATED AT 0.08c
 = 500.000 SMOOTH AIRFOIL

Fig. 4.13 COMPARISON OF THE NASA GA(w)-1 AIRFOIL AERODYNAMIC CHARACTERISTICS WITH EXISTING DATA



- o o o = PRESENT DATA
- o o o = EXISTING DATA

Fig. 4.14 COMPARISON OF THE NACA-0015 AIRFOIL AERODYNAMIC CHARACTERISTICS WITH EXISTING DATA

Fig. 4.15 VARIATION OF LIFT COEFFICIENT (C_L) WITH INCIDENCE AT VARIOUS REYNOLDS NUMBERS (TAKEN FROM REF (34))

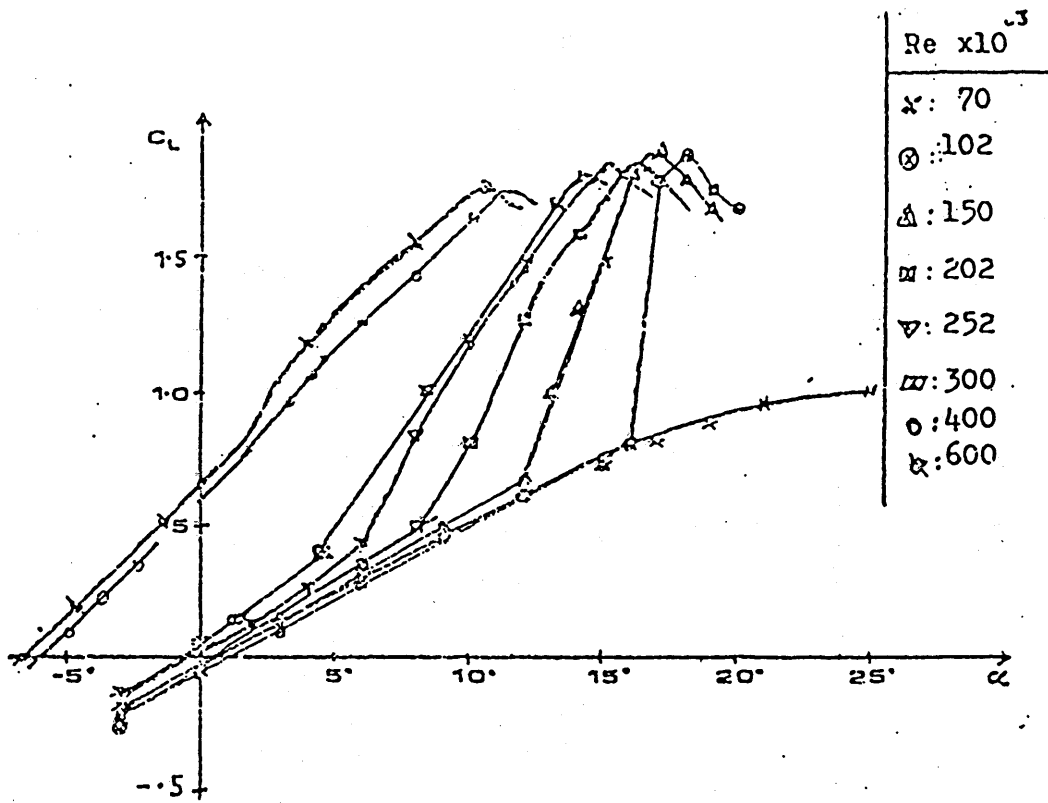
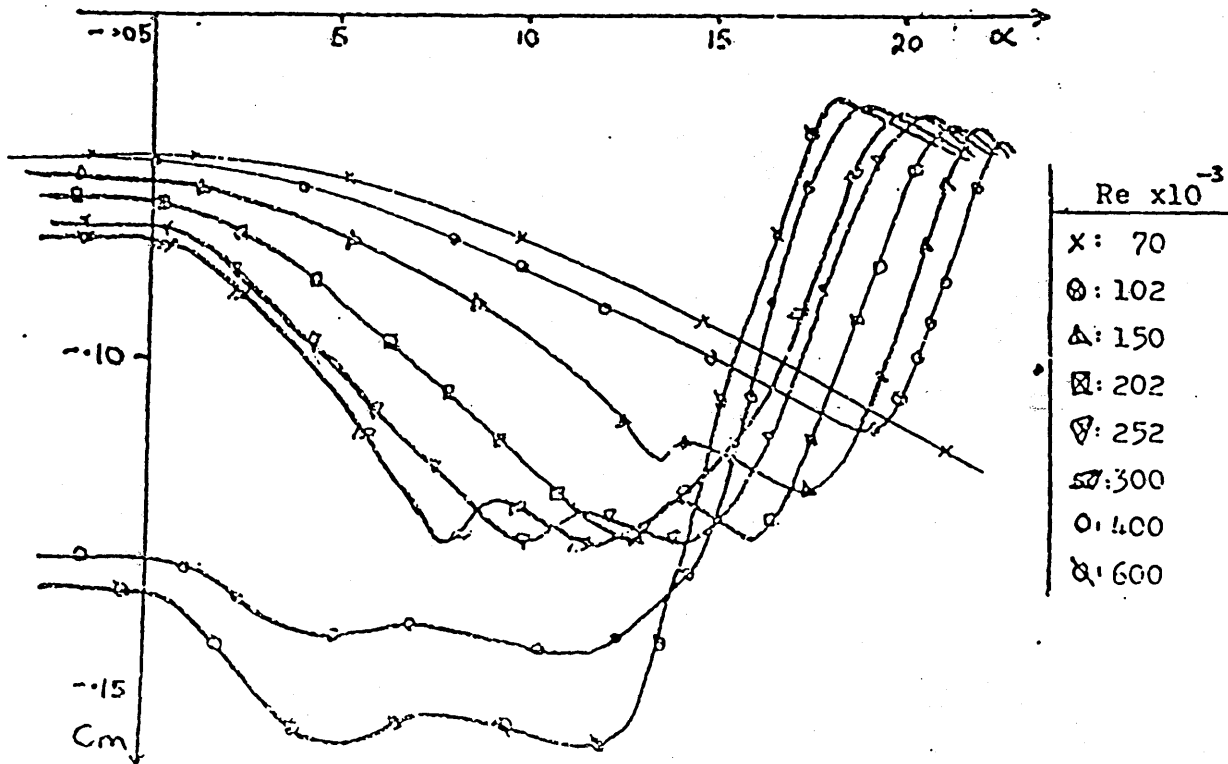


Fig. 4.16: Variation of pitching moment coefficient (C_m) with incidence at various Reynolds numbers. (TAKEN FROM REF (34))



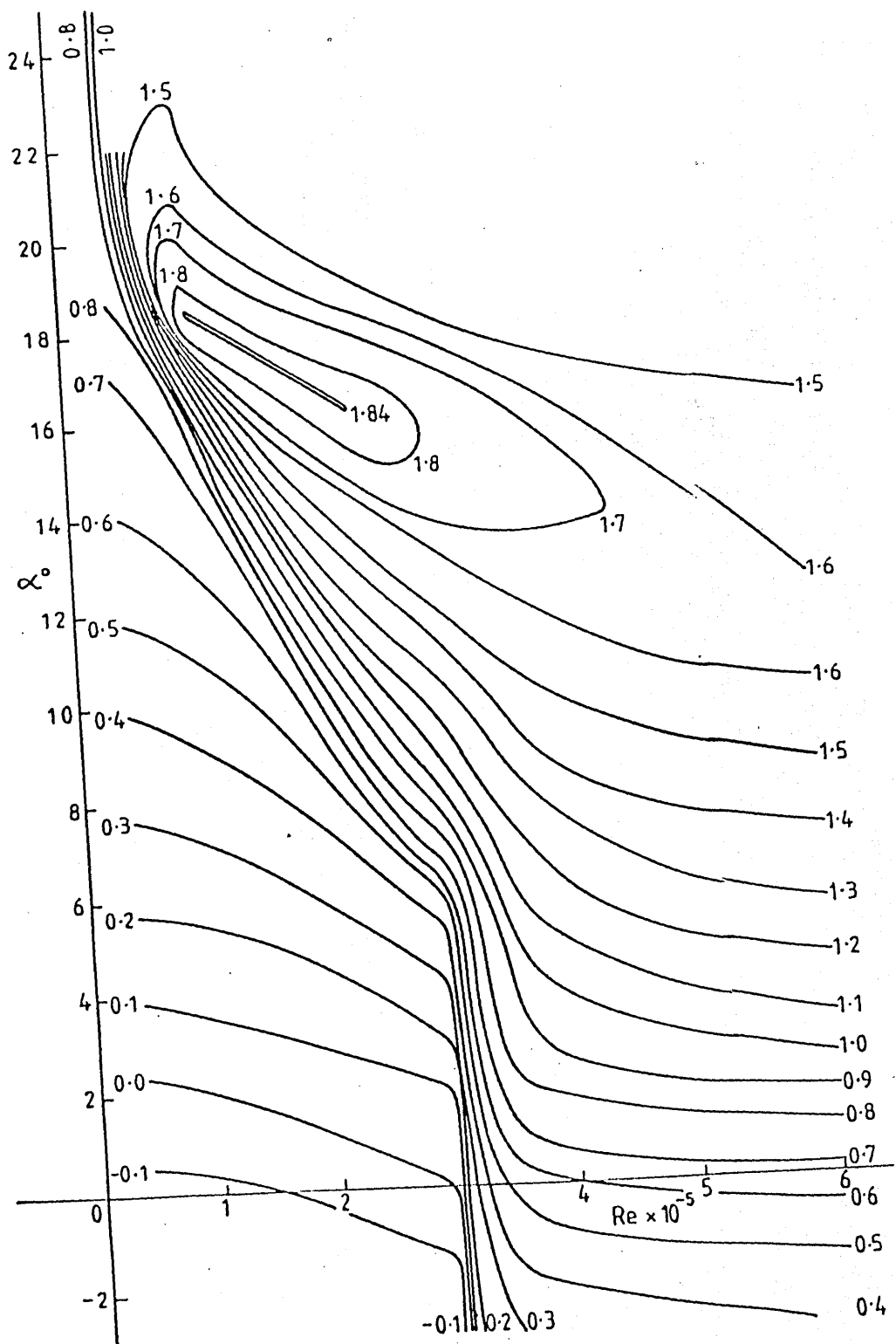
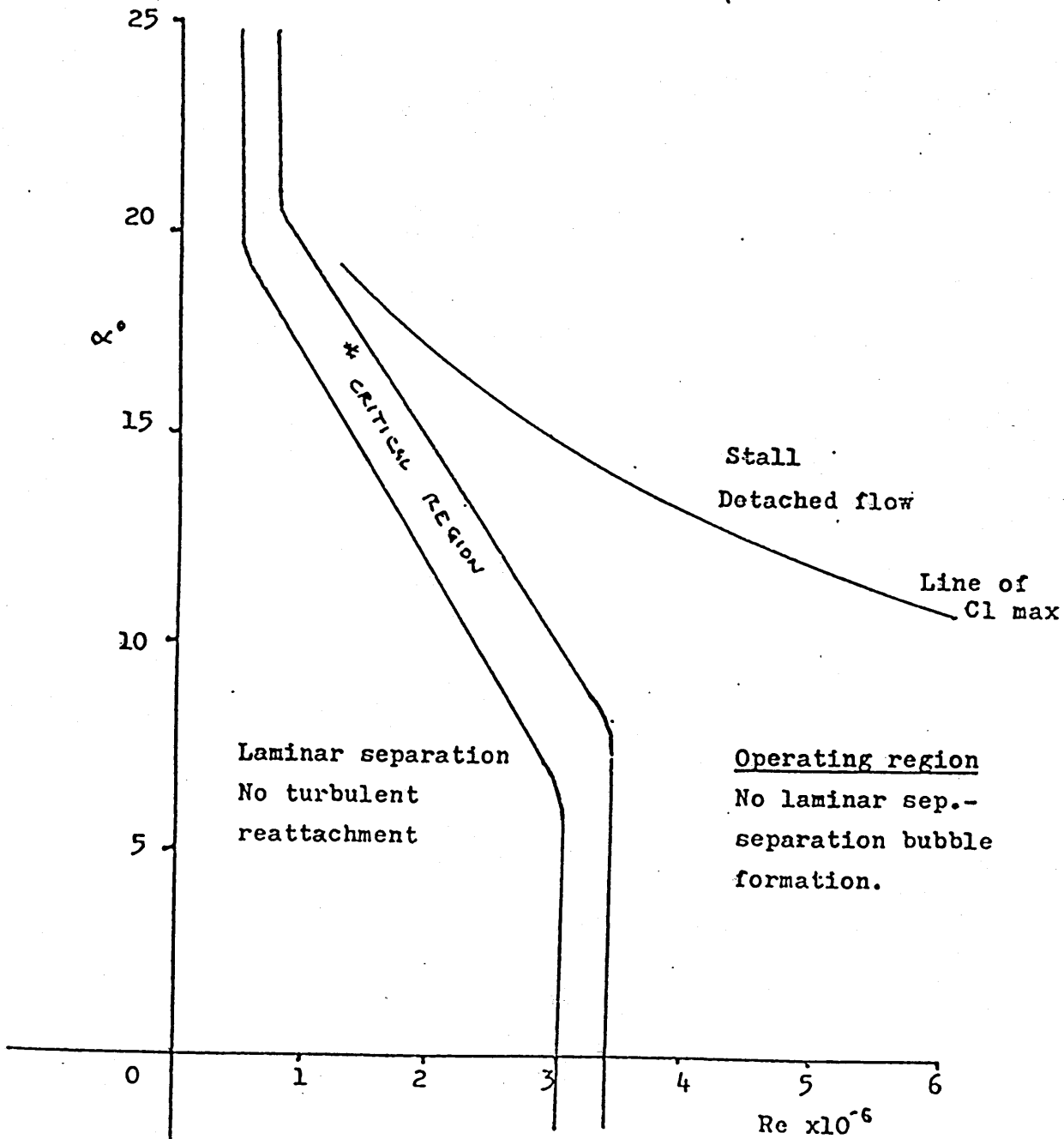


Fig. 4.17 CONTOURS OF LIFT COEFFICIENT AGAINST A BASE OF INCIDENCE AND REYNOLDS NUMBER GU25-5(11)8 AIRFOIL

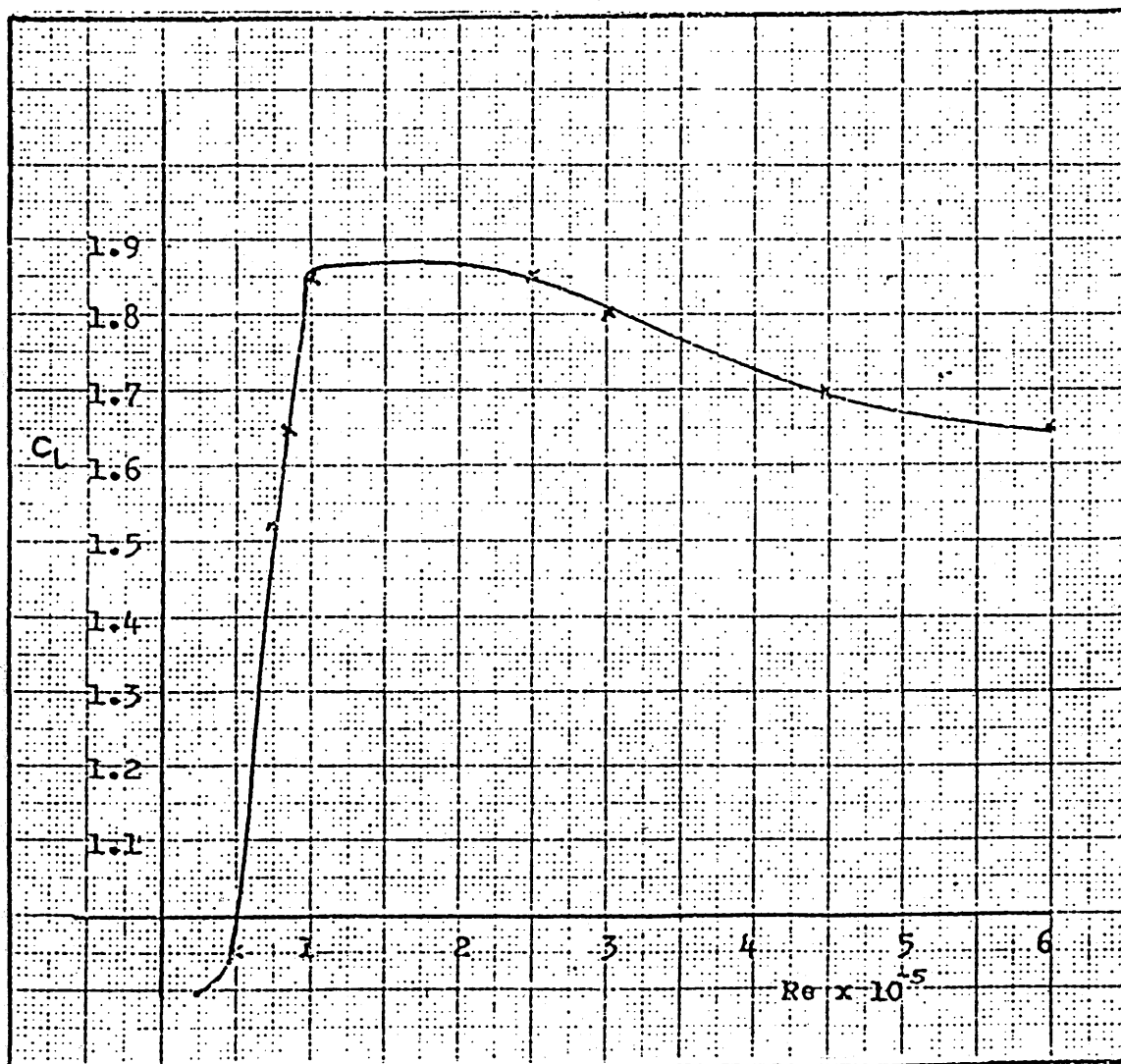
(TAKEN FROM REF (34))

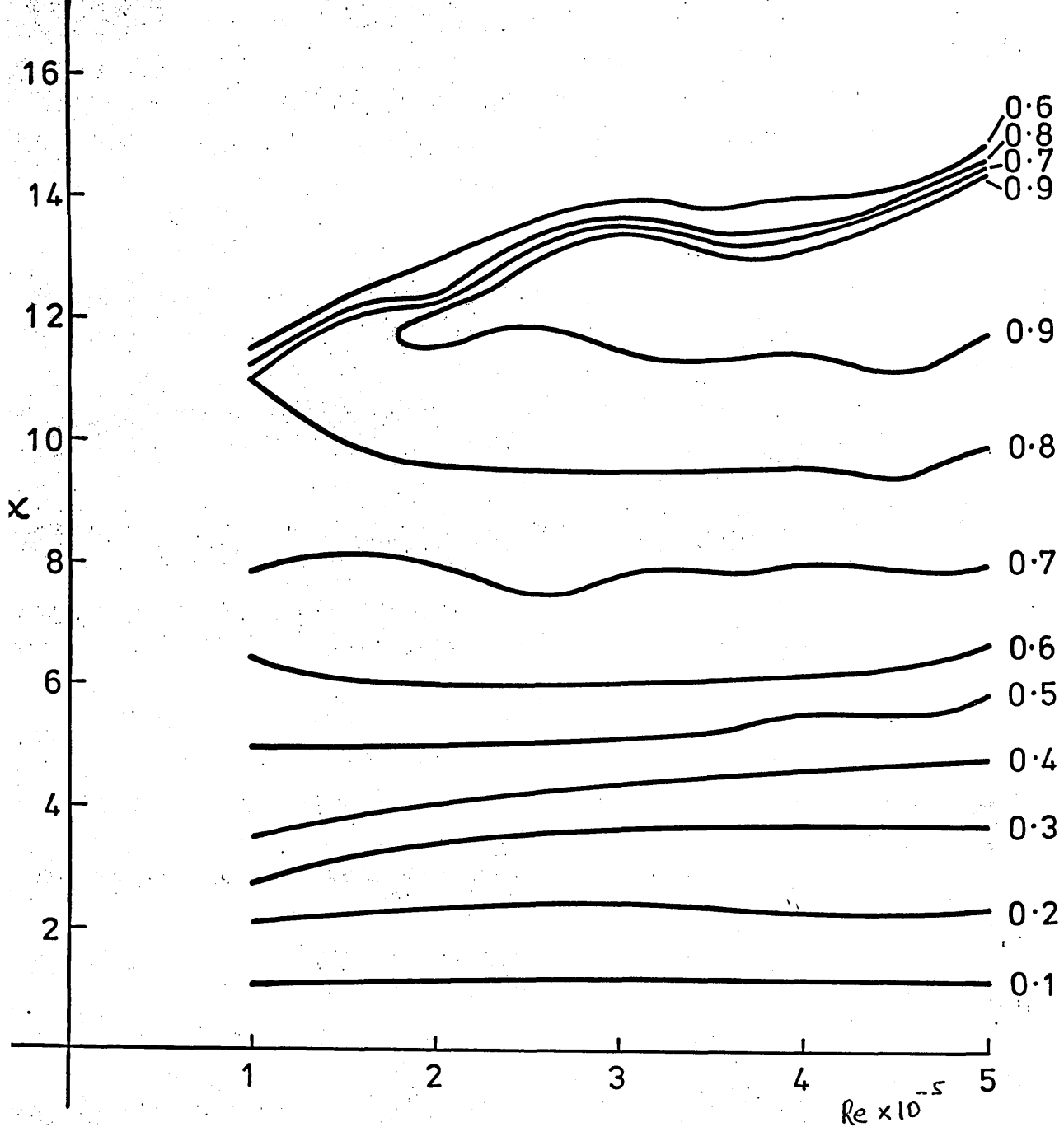
Figure 4.18: Graph detailing flow characteristics in the region covered by the contour charts. (TAKEN FROM REF (34))



* Critical region : Laminar separation with turbulent reattachment. Separation bubble forming.

Figure 4.19: C_l max. versus Reynolds number. GU25-5(11)8 Aerofoil.





REYNOLDS NUMBER

Fig. 4.20 CONTOURS OF LIFT COEFFICIENT AGAINST A BASE OF INCIDENCE AND REYNOLDS NUMBER
NACA-0015 AIRFOIL

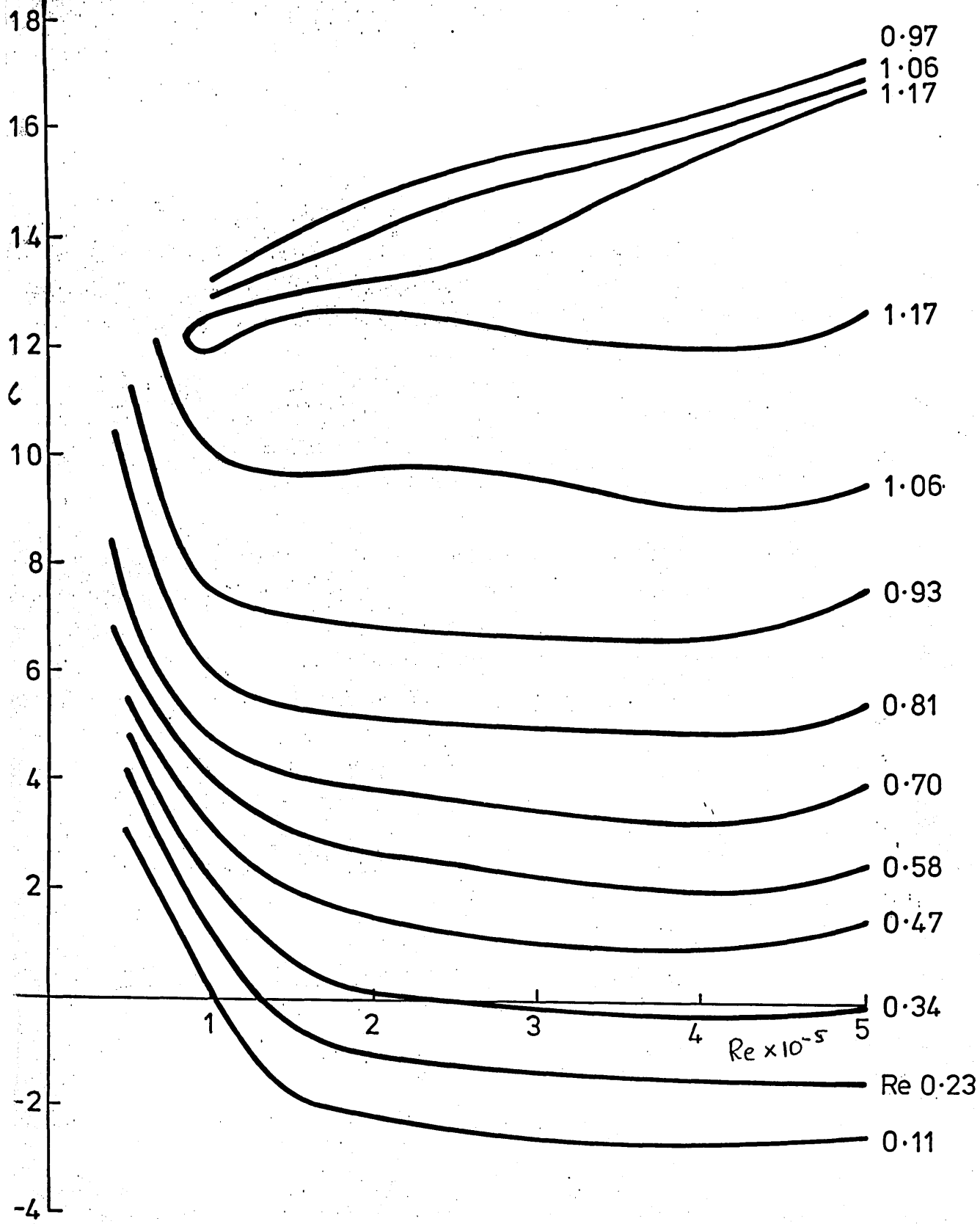


Fig. 4.21 CONTOURS OF LIFT COEFFICIENT AGAINST A BASE OF INCIDENCE AND REYNOLDS NUMBER
 NASA GA(W)-1 AIRFOIL

